Université de Montréal

USE OF HYDROGEN BONDS TO CONTROL MOLECULAR AGGREGATION: SELF-ASSEMBLY OF THREE-DIMENSIONAL NETWORKS WITH LARGE CHAMBERS

par

Dan Su

Département de Chimie

Faculté des arts et des sciences

Thèse présentée à la Faculté des études supérieures

en vue de l'obtention du grade de

Philosophiæ Doctor (Ph. D.)

en chimie

Mai, 1995

© Dan Su, 1995

QD
3
U54
1996
V.014

Name DAN SU

Dissertation Abstracts International is arranged by broad, general subject categories. Please select the one subject which most nearly describes the content of your dissertation. Enter the corresponding four-digit code in the spaces provided.

ORGANIC CHEMISTRY
SUBJECT TERM

0490
SUBJECT CODE

U·M·I

Subject Categories

THE HUMANITIES AND SOCIAL SCIENCES

COMMUNICATIONS AND THE ARTS
Architecture 0729
Art History 0377
Cinema 0900
Dance 0378
Fine Arts 0357
Information Science 0723
Journalism 0391
Library Science 0399
Mass Communications 0708
Music 0413
Speech Communication 0459
Theater 0465

EDUCATION
General 0515
Administration 0514
Adult and Continuing 0516
Agricultural 0517
Art 0273
Bilingual and Multicultural 0282
Business 0688
Community College 0275
Curriculum and Instruction 0727
Early Childhood 0518
Elementary 0524
Finance 0277
Guidance and Counseling 0519
Health 0680
Higher 0745
History of 0520
Home Economics 0278
Industrial 0521
Language and Literature 0279
Mathematics 0280
Music 0522
Philosophy of 0998
Physical 0523
Psychology 0525
Reading 0535
Religious 0527
Sciences 0714
Secondary 0533
Social Sciences 0534
Sociology of 0340
Special 0529
Teacher Training 0530
Technology 0710
Tests and Measurements 0288
Vocational 0747

LANGUAGE, LITERATURE AND LINGUISTICS
Language
- General 0679
- Ancient 0289
- Linguistics 0290
- Modern 0291

Literature
- General 0401
- Classical 0294
- Comparative 0295
- Medieval 0297
- Modern 0298
- African 0316
- American 0591
- Asian 0305
- Canadian (English) 0352
- Canadian (French) 0355
- English 0593
- Germanic 0311
- Latin American 0312
- Middle Eastern 0315
- Romance 0313
- Slavic and East European 0314

PHILOSOPHY, RELIGION AND THEOLOGY
Philosophy 0422
Religion
- General 0318
- Biblical Studies 0321
- Clergy 0319
- History of 0320
- Philosophy of 0322

Theology 0469

SOCIAL SCIENCES
American Studies 0323
Anthropology
- Archaeology 0324
- Cultural 0326
- Physical 0327

Business Administration
- General 0310
- Accounting 0272
- Banking 0770
- Management 0454
- Marketing 0338

Canadian Studies 0385
Economics
- General 0501
- Agricultural 0503
- Commerce-Business 0505
- Finance 0508
- History 0509
- Labor 0510
- Theory 0511

Folklore 0358
Geography 0366
Gerontology 0351
History
- General 0578
- Ancient 0579
- Medieval 0581
- Modern 0582
- Black 0328
- African 0331
- Asia, Australia and Oceania 0332
- Canadian 0334
- European 0335
- Latin American 0336
- Middle Eastern 0333
- United States 0337

History of Science 0585
Law 0398
Political Science
- General 0615
- International Law and Relations 0616
- Public Administration 0617

Recreation 0814
Social Work 0452
Sociology
- General 0626
- Criminology and Penology ... 0627
- Demography 0938
- Ethnic and Racial Studies 0631
- Individual and Family Studies 0628
- Industrial and Labor Relations 0629
- Public and Social Welfare 0630
- Social Structure and Development 0700
- Theory and Methods 0344

Transportation 0709
Urban and Regional Planning 0999
Women's Studies 0453

THE SCIENCES AND ENGINEERING

BIOLOGICAL SCIENCES
Agriculture
- General 0473
- Agronomy 0285
- Animal Culture and Nutrition 0475
- Animal Pathology 0476
- Food Science and Technology 0359
- Forestry and Wildlife 0478
- Plant Culture 0479
- Plant Pathology 0480
- Plant Physiology 0817
- Range Management 0777
- Wood Technology 0746

Biology
- General 0306
- Anatomy 0287
- Biostatistics 0308
- Botany 0309
- Cell 0379
- Ecology 0329
- Entomology 0353
- Genetics 0369
- Limnology 0793
- Microbiology 0410
- Molecular 0307
- Neuroscience 0317
- Oceanography 0416
- Physiology 0433
- Radiation 0821
- Veterinary Science 0778
- Zoology 0472

Biophysics
- General 0786
- Medical 0760

EARTH SCIENCES
Biogeochemistry 0425
Geochemistry 0996
Geodesy 0370
Geology 0372
Geophysics 0373
Hydrology 0388
Mineralogy 0411
Paleobotany 0345
Paleoecology 0426
Paleontology 0418
Paleozoology 0985
Palynology 0427
Physical Geography 0368
Physical Oceanography 0415

HEALTH AND ENVIRONMENTAL SCIENCES
Environmental Sciences 0768
Health Sciences
- General 0566
- Audiology 0300
- Chemotherapy 0992
- Dentistry 0567
- Education 0350
- Hospital Management 0769
- Human Development 0758
- Immunology 0982
- Medicine and Surgery 0564
- Mental Health 0347
- Nursing 0569
- Nutrition 0570
- Obstetrics and Gynecology .. 0380
- Occupational Health and Therapy 0354
- Ophthalmology 0381
- Pathology 0571
- Pharmacology 0419
- Pharmacy 0572
- Physical Therapy 0382
- Public Health 0573
- Radiology 0574
- Recreation 0575
- Speech Pathology 0460
- Toxicology 0383

Home Economics 0386

PHYSICAL SCIENCES
Pure Sciences
Chemistry
- General 0485
- Agricultural 0749
- Analytical 0486
- Biochemistry 0487
- Inorganic 0488
- Nuclear 0738
- Organic 0490
- Pharmaceutical 0491
- Physical 0494
- Polymer 0495
- Radiation 0754

Mathematics 0405
Physics
- General 0605
- Acoustics 0986
- Astronomy and Astrophysics 0606
- Atmospheric Science 0608
- Atomic 0748
- Electronics and Electricity 0607
- Elementary Particles and High Energy 0798
- Fluid and Plasma 0759
- Molecular 0609
- Nuclear 0610
- Optics 0752
- Radiation 0756
- Solid State 0611

Statistics 0463

Applied Sciences
Applied Mechanics 0346
Computer Science 0984
Engineering
- General 0537
- Aerospace 0538
- Agricultural 0539
- Automotive 0540
- Biomedical 0541
- Chemical 0542
- Civil 0543
- Electronics and Electrical 0544
- Heat and Thermodynamics ... 0348
- Hydraulic 0545
- Industrial 0546
- Marine 0547
- Materials Science 0794
- Mechanical 0548
- Metallurgy 0743
- Mining 0551
- Nuclear 0552
- Packaging 0549
- Petroleum 0765
- Sanitary and Municipal 0554
- System Science 0790

Geotechnology 0428
Operations Research 0796
Plastics Technology 0795
Textile Technology 0994

PSYCHOLOGY
General 0621
Behavioral 0384
Clinical 0622
Developmental 0620
Experimental 0623
Industrial 0624
Personality 0625
Physiological 0989
Psychobiology 0349
Psychometrics 0632
Social 0451

Name DAN SU

Dissertation Abstracts International is arranged by broad, general subject categories. Please select the one subject which most nearly describes the content of your dissertation. Enter the corresponding four-digit code in the spaces provided.

ORGANIC CHEMISTRY
SUBJECT TERM

0490
SUBJECT CODE

U·M·I

Subject Categories

THE HUMANITIES AND SOCIAL SCIENCES

COMMUNICATIONS AND THE ARTS
Architecture 0729
Art History 0377
Cinema 0900
Dance 0378
Fine Arts 0357
Information Science 0723
Journalism 0391
Library Science 0399
Mass Communications 0708
Music 0413
Speech Communication 0459
Theater 0465

EDUCATION
General 0515
Administration 0514
Adult and Continuing 0516
Agricultural 0517
Art 0273
Bilingual and Multicultural 0282
Business 0688
Community College 0275
Curriculum and Instruction 0727
Early Childhood 0518
Elementary 0524
Finance 0277
Guidance and Counseling 0519
Health 0680
Higher 0745
History of 0520
Home Economics 0278
Industrial 0521
Language and Literature 0279
Mathematics 0280
Music 0522
Philosophy of 0998
Physical 0523
Psychology 0525
Reading 0535
Religious 0527
Sciences 0714
Secondary 0533
Social Sciences 0534
Sociology of 0340
Special 0529
Teacher Training 0530
Technology 0710
Tests and Measurements 0288
Vocational 0747

LANGUAGE, LITERATURE AND LINGUISTICS
Language
- General 0679
- Ancient 0289
- Linguistics 0290
- Modern 0291

Literature
- General 0401
- Classical 0294
- Comparative 0295
- Medieval 0297
- Modern 0298
- African 0316
- American 0591
- Asian 0305
- Canadian (English) 0352
- Canadian (French) 0355
- English 0593
- Germanic 0311
- Latin American 0312
- Middle Eastern 0315
- Romance 0313
- Slavic and East European 0314

PHILOSOPHY, RELIGION AND THEOLOGY
Philosophy 0422
Religion
- General 0318
- Biblical Studies 0321
- Clergy 0319
- History of 0320
- Philosophy of 0322

Theology 0469

SOCIAL SCIENCES
American Studies 0323
Anthropology
- Archaeology 0324
- Cultural 0326
- Physical 0327

Business Administration
- General 0310
- Accounting 0272
- Banking 0770
- Management 0454
- Marketing 0338

Canadian Studies 0385
Economics
- General 0501
- Agricultural 0503
- Commerce-Business 0505
- Finance 0508
- History 0509
- Labor 0510
- Theory 0511

Folklore 0358
Geography 0366
Gerontology 0351
History
- General 0578
- Ancient 0579
- Medieval 0581
- Modern 0582
- Black 0328
- African 0331
- Asia, Australia and Oceania 0332
- Canadian 0334
- European 0335
- Latin American 0336
- Middle Eastern 0333
- United States 0337

History of Science 0585
Law 0398
Political Science
- General 0615
- International Law and Relations 0616
- Public Administration 0617

Recreation 0814
Social Work 0452
Sociology
- General 0626
- Criminology and Penology ... 0627
- Demography 0938
- Ethnic and Racial Studies 0631
- Individual and Family Studies 0628
- Industrial and Labor Relations 0629
- Public and Social Welfare 0630
- Social Structure and Development 0700
- Theory and Methods 0344

Transportation 0709
Urban and Regional Planning 0999
Women's Studies 0453

THE SCIENCES AND ENGINEERING

BIOLOGICAL SCIENCES
Agriculture
- General 0473
- Agronomy 0285
- Animal Culture and Nutrition 0475
- Animal Pathology 0476
- Food Science and Technology 0359
- Forestry and Wildlife 0478
- Plant Culture 0479
- Plant Pathology 0480
- Plant Physiology 0817
- Range Management 0777
- Wood Technology 0746

Biology
- General 0306
- Anatomy 0287
- Biostatistics 0308
- Botany 0309
- Cell 0379
- Ecology 0329
- Entomology 0353
- Genetics 0369
- Limnology 0793
- Microbiology 0410
- Molecular 0307
- Neuroscience 0317
- Oceanography 0416
- Physiology 0433
- Radiation 0821
- Veterinary Science 0778
- Zoology 0472

Biophysics
- General 0786
- Medical 0760

EARTH SCIENCES
Biogeochemistry 0425
Geochemistry 0996
Geodesy 0370
Geology 0372
Geophysics 0373
Hydrology 0388
Mineralogy 0411
Paleobotany 0345
Paleoecology 0426
Paleontology 0418
Paleozoology 0985
Palynology 0427
Physical Geography 0368
Physical Oceanography 0415

HEALTH AND ENVIRONMENTAL SCIENCES
Environmental Sciences 0768
Health Sciences
- General 0566
- Audiology 0300
- Chemotherapy 0992
- Dentistry 0567
- Education 0350
- Hospital Management 0769
- Human Development 0758
- Immunology 0982
- Medicine and Surgery 0564
- Mental Health 0347
- Nursing 0569
- Nutrition 0570
- Obstetrics and Gynecology .. 0380
- Occupational Health and Therapy 0354
- Ophthalmology 0381
- Pathology 0571
- Pharmacology 0419
- Pharmacy 0572
- Physical Therapy 0382
- Public Health 0573
- Radiology 0574
- Recreation 0575
- Speech Pathology 0460
- Toxicology 0383

Home Economics 0386

PHYSICAL SCIENCES
Pure Sciences
Chemistry
- General 0485
- Agricultural 0749
- Analytical 0486
- Biochemistry 0487
- Inorganic 0488
- Nuclear 0738
- Organic 0490
- Pharmaceutical 0491
- Physical 0494
- Polymer 0495
- Radiation 0754

Mathematics 0405
Physics
- General 0605
- Acoustics 0986
- Astronomy and Astrophysics 0606
- Atmospheric Science 0608
- Atomic 0748
- Electronics and Electricity 0607
- Elementary Particles and High Energy 0798
- Fluid and Plasma 0759
- Molecular 0609
- Nuclear 0610
- Optics 0752
- Radiation 0756
- Solid State 0611

Statistics 0463

Applied Sciences
Applied Mechanics 0346
Computer Science 0984
Engineering
- General 0537
- Aerospace 0538
- Agricultural 0539
- Automotive 0540
- Biomedical 0541
- Chemical 0542
- Civil 0543
- Electronics and Electrical 0544
- Heat and Thermodynamics ... 0348
- Hydraulic 0545
- Industrial 0546
- Marine 0547
- Materials Science 0794
- Mechanical 0548
- Metallurgy 0743
- Mining 0551
- Nuclear 0552
- Packaging 0549
- Petroleum 0765
- Sanitary and Municipal 0554
- System Science 0790

Geotechnology 0428
Operations Research 0796
Plastics Technology 0795
Textile Technology 0994

PSYCHOLOGY
General 0621
Behavioral 0384
Clinical 0622
Developmental 0620
Experimental 0623
Industrial 0624
Personality 0625
Physiological 0989
Psychobiology 0349
Psychometrics 0632
Social 0451

Université de Montréal

Faculté des études supérieures

Cette thèse intitulée

Use of Hydrogen Bonds to Control Molecular Aggregation: Self-Assembly of Three-Dimesional Networks with Large Chambers

Présentée par:

Dan Su

a été évaluée par un jury composé des personnes suivantes:

[redacted] président rapporteur

[redacted] directeur de recherche

[redacted] membre du jury

[redacted] examinateur externe

Thèse acceptée le: 22 mars 1996

Dedicated to my father (1912-1989) and my mother, for their eternal love and understanding.

谨以本文告慰父亲在天之灵。并献给远在北京的母亲，
以感谢母亲永恒的理解和爱。

Abstract

Hydrogen bonding is used extensively in nature and plays a critical role in all the chemistry of life. It is a selective, directional and strongly attractive noncovalent interaction which can induce self-assembly by causing molecular aggregation. *Tectons* are defined as molecules whose interactions are dominated by specific attractive forces that induce the assembly of aggregates with controlled geometries. *Molecular tectonics* is the art and science of supramolecular construction using tectonic subunits. Intermolecular hydrogen bonds offer a particularly effective force for promoting controlled tectonic aggregation, and tectons which are able to participate in extensive networks of hydrogen bonds can be constructed by the simple expedient of attaching multiple 2-pyridone subunits to carefully chosen molecular frameworks. This thesis describes the design and synthesis of tectons that incorporate four tetrahedrally oriented 2-pyridone subunits so that they are predisposed to generate diamondoid networks or related three-dimensional lattices. As expected, we have found that such tetrahedral tectons can associate by hydrogen bonding to form diamondoid networks with large cavities. The large internal volumes defined by the networks are filled by a combination of independent interpenetrating diamond networks and enclathrated guest molecules. We have also found that tetrahedral tectons with different sizes and shapes may generate three-dimensional hydrogen-bonded networks not based on diamondoid lattices. These results indicate that clever application of the strategy of molecular tectonics can be employed as a routine crystal-engineering method to build a wide range of ordered three-dimensional organic networks with some of the desirable properties of zeolites and related inorganic materials, including high structural integrity, potentially large void volumes, and adjustable microporosity.

Résumé

La liaison hydrogène est omniprésente dans la nature et joue un rôle capital dans la chimie de la matière vivante. Cette interaction non covalente, sélective, forte et directionnelle peut induire l'auto-assemblage de molécules. Les tectones sont définies comme étant des molécules dont les interactions sont dominées par des forces attractives spécifiques qui induisent la formation d'agrégats de géométrie contrôlée. La tectonique moléculaire est l'art et la science de la construction de supramolécules en utilisant des sous-unités tectoniques. Les liens hydrogène intermoléculaires présentent une force particulièrement efficace pour promouvoir la formation d'agrégats tectoniques et de telles tectones pouvant participer dans un vaste réseau de liens hydrogène peuvent être synthétisée simplement en ajoutant des sous-unités 2-pyridones sur une molécule support appropriée. Cette thèse décrit la conception et la synthèse de tectones comprenant quatre sous-unités 2-pyridones orientées suivant un tétraèdre de telle sorte qu'elles sont prédisposées à générer un réseau diamantoïde ou de géométrie comparable. Nous avons mis en évidence que de telles tectones tétraédriques peuvent s'associer par des liaisons hydrogène pour former un réseau diamantoïde contenant de larges cavités. Ces cavités générées par le réseau sont comblées par un entrelacement de réseaux diamantoïdes indépendants et autres molécules hôtes. Nous avons aussi mis en évidence que des tectones tétraédrique de différentes grandeurs peuvent engendrer des réseaux tridimensionnels autre que diamantoïdes. Ces résultats laissent entrevoir que l'application astucieuse de la tectonique moléculaire peut être employée à l'élaboration de molécules organiques dont l'assemblage tridimensionnel offrirait les propriétés remarquables des zéolites et autre substances inorganiques semblables comme la microporosité, la présence de cavités et la stabilité structurelle.

Acknowledgments

I would like to take this opportunity to express my sincerest respect and gratitude to Professor James D. Wuest, my research supervisor, for his enthusiastic and very rigorous attitude to science; for his building up of a harmonious atmosphere that is suitable for research in the lab; and for his guidance, encouragement, understanding, patience and financial support throughout this work.

I am grateful to all my colleagues, for their helpfulness and kindness during my work, and for their helpful suggestions and discussions about chemistry.

I would like to thank Dr. Michel Simard, for his effort in resolving the crystal structures which are contained herein, as well as for helpful discussions and comments.

Finally, my sincere thanks are extended to my sister, Ms. Shanshan Wang, who is always there ready to support, to listen, to share either sadness or happiness.

Table of Contents

Dedication i

Abstract ii

Résumé iii

Acknowledgments iv

Table of Contents v

List of Abbreviations viii

List of Figures x

List of Schemes xix

List of Tables xxii

Chapter 1:

INTRODUCTION 1

Chapter 2:

INITIAL DESIGN OF AN ORGANIC TECTON ABLE TO GENERATE DIAMONDOID NETWORKS 20

2.1 Design and synthesis of tecton **I** 20

2.2 Prediction of the crystal structure of tecton **I** 22

2.3 The crystal structure of tecton **I** revealed by X-ray crystallographic analysis 26

2.4 The crystal structure of tecton **I**•8 CH_3CH_2COOH 29

2.5 The crystal structure of tecton **I**•2 $CH_3CH_2CH_2COOH$ 47

2.6 Crystallization of tecton **I** from other carboxylic acids 69

Chapter 3:

TECTONS WITH AMPLIFIED INTERTECTONIC ADHESION ... 73

3.1 Design and synthesis of tectons **II-III** 74

3.2 Design and synthesis of tectons **IV-V** 81

Chapter 4:

FUNCTIONALIZED TECTONS 94

Chapter 5:

TECTONS WITH MODIFIED ARCHITECTURAL FEATURES .. 102

5.1 Isomers of tecton **I** which are able to define longer intertectonic distances and may generate diamondoid networks with more open channels 103

5.2 Design and synthesis of large tectons which may be able to generate diamondoid networks with more open channels because of lengthened intertectonic distances 112

5.3 Tectons with geometries resistant to close packing 125

5.3.1 Design and synthesis of tecton **XVII** 125

5.3.2 Crystal structure of tecton **XVII** 126

5.4 Design and synthesis of smaller tectons which may be able to construct contracted diamondoid networks because of shorter intertectonic distances 140

5.5 Crystal structure of tecton **XVIII** 145

5.5.1 Comparison of characteristic structural features of different tectonic aggregates 147

5.5.2 The low degree of interpenetration of 5 152

5.5.3 Interpenetration in the crystal of tecton **XVIII** 156

Chapter 6:

CONCLUSIONS 165

Chapter 7:

EXPERIMENTAL SECTION 168

References 228

Appendix 234

Appendix 1: Crystallographic report for tecton **I**•8$CH_3CH_2CO_2H$ 234

Appendix 2: Crystallographic report for tecton **I**•2$CH_3CH_2CH_2CO_2H$ 249

Appendix 3: Crystallographic report for tecton **XVII**•4DMF 270

Appendix 4: Crystallographic report for tecton **XVIII**•4DMF 292

List of Abbreviations

Å	Ångstrom
Ac	acetyl
aq	aqueous
Bn	benzyl
Bu	butyl
$BTMAICl_2$	benzyltrimethylammonium dichloroiodate
$BTEAICl_2$	benzyltriethylammonium dichloroiodate
°C	degree centigrade
cm	centimeter
DMF	N,N-dimethylformamide
DMSO	dimethyl sulfoxide
EI	electron impact
Et	ethyl
FAB	fast atom bombardment
HRMS	high resolution mass spectrum
IR	infrared
LDA	lithium diisopropylamide
Me	methyl
m/z	mass per unit charge
ml	milliliter
mmol	millimole
mp	melting point
N_3Et_2	3,3-diethyltriazenyl
NMR	nuclear magnetic resonance

Ph	phenyl
$TBABr_3$	tetrabutylammonium tribromide
iPr	iso-propyl
TFA	trifluoroacetic acid
THF	tetrahydrofuran
TMS	trimethylsilyl
TMSI	iodotrimethylsilane
δ	chemical shift in ppm relative to Me_4Si in NMR spectra

List of Figures

Figure 1. Ureylenedicarboxylic acids, designed and synthesized by Fowler, Lauher and co-workers. 5

Figure 2. A β-network formed by the two-dimensional array of self-complementary hydrogen-bonded ureylenedicarboxylic acids. 5

Figure 3. Schematic representation of the hydrogen-bonded strand **9** and the cyclic hexameric motif **10** formed by self-assembly of the self-complementary components **5-8.** 7

Figure 4. Schematic representation of the hydrogen-bonded ribbon-like species **13a** and **b** formed by homo-association of the self-complementary components **11** and **12** and cyclic hexamer motif **14** formed by their hetero-association. 8

Figure 5. Common hydrogen-bonding pattern for secondary diamides 9

Figure 6. Stronger bidentate hydrogen-bonding motif between secondary diamides and second subunits. 10

Figure 7. First subunits -- Bis(2-aminopyridine) derivatives of different aryl diacids 11

Figure 8. Second subunits -- Aliphatic dicarboxylic acids. 11

Figure 9. Effect of component length on slip angle. 12

Figure 10. Tectons designed and synthesized by Ducharme and Wuest. 16

Figure 11. Tectons constructed by joining two pyridone rings with different rigid spacers. 16

Figure 12. Ermer's tectons **33-38.** 25

Figure 13. ORTEP drawing of part of the diamondoid network present in crystals of

tecton **I**•8 $CH_3CH_2CO_2H$. The tetrahedral centers of the ten tectons shown in the drawing define a slightly distorted adamantane, shown on top. Non-hydrogen atoms are represented by ellipsoids corresponding to 50% probability. Propionic acid and all hydrogen atoms are omitted for clarity. 27

Figure 14 ORTEP drawing of part of the diamondoid network present in crystals of tecton **I**•2 $CH_3CH_2CH_2CO_2H$. The tetrahedral centers of the ten tectons shown in the drawing define a distorted adamantane, shown on top . Non-hydrogen atoms are represented by ellipsoids corresponding to 50% probability. Butyric acid and all hydrogen atoms are omitted for clarity .. 28

Figure 15. Complete adduct **39** viewed down the **c** axis. Non-hydrogen atoms are represented by ellipsoids corresponding to 50% probability. Hydrogen atoms are represented by spheres of arbitrary size. 30

Figure 16. The asymmetric unit present in crystals of tecton **I**•8 $CH_3CH_2CO_2H$. Non-hydrogen atoms are represented by ellipsoids corresponding to 50% probability, and hydrogen atoms by spheres of arbitrary size. 31

Figure 17. ORTEP view of the packing arrangement of tecton **I**•8 $CH_3CH_2CO_2H$ along the **c** axis. Non-hydrogen atoms are represented by ellipsoids corresponding to 50% probability, and hydrogen atoms by spheres of arbitrary size. 32

Figure 18. Top view of the intertectonic π-stacking observed in the crystal structure of tecton **I**•8 $CH_3CH_2CO_2H$. Only the asymmetric unit of two neighboring tectons **I**•8 $CH_3CH_2CO_2H$ is shown. Non-hydrogen atoms are represented by ellipsoids corresponding to 50% probability, and hydrogen atoms by spheres of arbitrary size. 34

Figure 19. Side view of the intertectonic π-stacking observed in the crystal structure of

tecton **I**•8 $CH_3CH_2CO_2H$. Only the asymmetric unit of two neighboring tectons **I**•8 $CH_3CH_2CO_2H$ is shown. Non-hydrogen atoms are represented by ellipsoids corresponding to 50% probability, and hydrogen atoms by spheres of arbitrary size. 35

Figure 20. The asymmetric unit present in crystals of tecton **I**•8 $CH_3CH_2CO_2H$, showing the center of the pyridone ring defined in the crystal structure. Non-hydrogen atoms are represented by ellipsoids corresponding to 50% probability, and hydrogen atoms by spheres of arbitrary size. 36

Figure 21. Side view of the intertectonic π-stacking observed in the crystal structure of tecton **I**•8 $CH_3CH_2CO_2H$. Only the asymmetric unit of two neighboring tectons **I**•8 $CH_3CH_2CO_2H$ is shown. Non-hydrogen atoms are represented by ellipsoids corresponding to 50% probability, and hydrogen atoms by spheres of arbitrary size. 37

Figure 22. Top view of the intertectonic π-stacking observed in the crystal structure of tecton **I**•8 $CH_3CH_2CO_2H$, showing the centre-to-centre offset along the dipole orientation of the carbonyl group of pyridone. Propionic acid is omitted for clarity. 38

Figure 23. View of the superadamantane framework of tecton **I**•8 $CH_3CH_2CO_2H$ cut out of one diamondoid lattice induced by p-stacked tectons whose tetrahedral core structures are represented by solid sticks. 39

Figure 24. Schematic view of the six interpenetrating diamondoid networks present in tecton **I**•8 $CH_3CH_2CO_2H$, each represented by one superadamantane framework . They interpenetrate each other along the **c** axis translational-equivalently. Only the central carbon atoms of tecton **I** are shown. The interconnecting rods symbolize the π-stacked asymmetric units of two neighboring tectons as shown in Figure 22. 40

Figure 25. View of a π-stacked superadamantane unit of a diamondoid lattice of tecton **I**•8 $CH_3CH_2CO_2H$ down the **c** axis. Propionic acid is omitted for clarity. 41

Figure 26. Schematic stereoview of a π-stacked superadamantane unit of the diamondoid lattice of tecton **I**•8 $CH_3CH_2CO_2H$ down the **c** axis, in which the core structure of tecton **I** is represented by four tetrahedrally oriented solid sticks for clarity. 42

Figure 27. View down the **c** axis of an individual four-sided channel present in the diamondoid lattices of tecton **I**•8 $CH_3CH_2CO_2H$. 44

Figure 28. Space-filling stereoview (down the **c** axis) of an individual four-sided channel present in the diamondoid lattices of tecton **I**•8 $CH_3CH_2CO_2H$. 45

Figure 29. ORTEP view of tecton **I**•2 $CH_3CH_2CH_2CO_2H$ viewed down the **b** axis showing the numbering scheme. Non-hydrogen atoms are represented by ellipsoids corresponding to 50% probability. Hydrogen atoms are represented by spheres of arbitrary size. 49

Figure 30. A diamondoid lattice showing its three dimensional indices. 50

Figure 31. Projection (down the **c** axis) of an individual superadamantane cut out of a diamondoid lattice in tecton **I**•8 $CH_3CH_2CO_2H$. Only the central carbon atoms of tecton **I** are shown. The interconnecting rods symbolize the intertectonic hydrogen bonding. The labels ***a*** and ***b*** represent the dimensions of the distorted diamondoid lattice, and **a**, **b**, and **c** represent the crystallographic axes. 52

Figure 32. Projection (down the **b** axis) of an individual superadamantane cut out of a diamondoid lattice in tecton **I**•2 $CH_3CH_2CH_2CO_2H$. Only the central carbon atoms of tecton **I** are shown. The interconnecting rods symbolize the intertectonic hydrogen bonding. The labels ***a*** and ***b*** represent the

dimensions of the distorted diamondoid lattice, and **a**, **b**, and **c** represent the crystallographic axes. 53

Figure 33. Schematic illustration of the translational equivalence of the five interpenetrating diamondoid lattices in the crystals of tecton **34**, i.e., of the relationship between the translational vector **b** and the diamondoid lattice geometry. The view shows a projection down the crystallographic **c** axis. 55

Figure 34. An individual superadamantane cut out of the diamondoid lattice formed by tecton **I**•2 $CH_3CH_2CH_2CO_2H$. Only the central carbon atoms of tecton **I** are shown. The interconnecting rods symbolize the intertectonic hydrogen bonding. The labels **a** , **b** and **c** represent the dimensions of the distorted diamondoid lattice, while **a**, **b** and **c** represent the crystallographic axes. 56

Figure 35. View of the crystal structure of tecton **I**•2 $CH_3CH_2CH_2CO_2H$ showing a second distorted diamondoid lattice (represented with small spheres and white solid sticks) interlaced into the first one (represented with small spheres and black solid sticks). The two networks are related by shifting along the crystallographic **b** axis by a distance corresponding to the value of the cell edge (7.350 Å). The label **c** represents the longest index of the distorted diamondoid lattice. 57

Figure 36. Seven interpenetrating diamondoid networks in the crystal of tecton **I**•2 $CH_3CH_2CH_2CO_2H$ are merged into each other by translating them along the **b** axis by a distance of 7.350 Å. 58

Figure 37. Top view of the stacking of tecton **I**•2 $CH_3CH_2CH_2CO_2H$ down the **b** axis. Non-hydrogen atoms are represented by ellipsoids corresponding to 50% probability. Hydrogen atoms are represented by spheres of arbitrary size. 59

Figure 38. Side view of tectonic stacking in crystals of tecton **I**•2 $CH_3CH_2CH_2CO_2H$ along the **b** axis. Non-hydrogen atoms are represented by ellipsoids corresponding to 50% probability. Hydrogen atoms are represented by spheres of arbitrary size. 60

Figure 39. The relationship between an individual hydrogen-bonded diamondoid lattice and the stacking of molecules of tecton **I**. The diamondoid lattice is represented by small spheres and black solid sticks. Non-hydrogen atoms are represented by ellipsoids corresponding to 50% probability. Hydrogen atoms are represented by spheres of arbitrary size. 61

Figure 40. View along the **b** axis of crystals of tecton **I**•2 $CH_3CH_2CH_2CO_2H$ showing cross sections of the channels containing parallel columns of butyric acid. 63

Figure 41. ORTEP view along the **b** axis of the packing arrangement of tecton **I**•2 $CH_3CH_2CH_2CO_2H$. Non-hydrogen atoms are represented by ellipsoids corresponding to 50% probability, and hydrogen atoms by spheres of arbitrary size. Arbitrary spheres are used for the butyric acid moiety. .. 64

Figure 42. View along the **b** axis in crystals of tecton **I**•2 $CH_3CH_2CH_2CO_2H$ showing cross sections of the channels. Butyric acid is omitted for clarity. 66

Figure 43. View (down the **b** axis) of an individual four-sided channel cut out from diamondoid lattices in crystals of tecton **I**•2 $CH_3CH_2CH_2CO_2H$. 67

Figure 44. Space-filling view (down the **b** axis) of an individual four-sided channel cut out from diamondoid lattices with diameter 8.1 Å x 3.5 Å. .. 68

Figure 45. Tectons **II-V** designed to interact with amplified stickiness. 74

Figure 46. Structures of substrates cited in Table 9. 96

Figure 47. Tectons designed and synthesized with modified architectural features ..109

Figure 48. ORTEP views along the **b** axis of the packing arrangements in crystals of tectons **XVII** (a) and **I**•2 $CH_3CH_2CH_2CO_2H$ (b). Non-hydrogen atoms are represented by ellipsoids corresponding to 50% probability, and hydrogen atoms by spheres of arbitrary size. Arbitrary spheres are used for the butyric acid moiety. 130

Figure 49. ORTEP view of tecton **XVII** along the **b** axis with the numbering scheme adopted. Non-hydrogen atoms are represented by ellipsoids corresponding to 40% probability. Hydrogen atoms are represented by spheres of arbitrary size. 133

Figure 50. Top view of the stacking of tecton **XVII** down the **b** axis. Non-hydrogen atoms are represented by ellipsoids corresponding to 50% probability. Hydrogen atoms are represented by spheres of arbitrary size. 135

Figure 51. Top view of the single intertectonic hydrogen bonding observed in the crystal structure of tecton **XVII**. Only the asymmetric unit of neighboring tectons **XVII** is shown. Non-hydrogen atoms are represented by ellipsoids corresponding to 50% probability, and hydrogen atoms are represented by spheres of arbitrary size. 136

Figure 52. Side view of hydrogen-bonded tectons **XVII** stacking along the **b** axis by sitting on top of each other. Non-hydrogen atoms are represented by ellipsoids corresponding to 50% probability, and hydrogen atoms by spheres of arbitrary size. 137

Figure 53. View (down the **b** axis) of an individual four-sided channel cut out of the layer networks in crystals of tecton **XVII**. 138

Figure 54. Space-filling view (down the **b** axis) of an individual four-sided channel cut out of the layer networks with diameter 14 Å x 4 Å. 139

Figure 55. ORTEP views along the **b** axis of the packing arrangement in the unit cell of (a) tecton **XVIII**•4 DMF (disordered molecules of DMF are omitted for

clarity) and (b) **I**•2 $CH_3CH_2CH_2CO_2H$. Non-hydrogen atoms are represented by ellipsoids corresponding to 50% probability, and hydrogen atoms by spheres of arbitrary size. 149

Figure 56. View of a tetrahedral molecular aggregate constructed from five hydrogen-bonded molecules of tecton **XVIII** down the **c** axis. Non-hydrogen atoms are represented by ellipsoids corresponding to 50% probability, and hydrogen atoms by spheres of arbitrary size. 150

Figure 57. View of a tetrahedral molecular aggregate constructed from five hydrogen-bonded molecules of tecton **XVIII** down the **a** or **b** axis. Non-hydrogen atoms are represented by ellipsoids corresponding to 50% probability, and hydrogen atoms by spheres of arbitrary size. 151

Figure 58. ORTEP drawing of part of the diamondoid network present in crystals of tecton **XVIII**•4 DMF. The tetrahedral centers of the ten tectons shown in the drawing define a slightly distorted adamantane, shown on top. Non-hydrogen atoms are represented by ellipsoids corresponding to 50% probability. Disordered molecules of DMF are omitted for clarity. 153

Figure 59. View of the superadamantane framework of tecton **XVIII**•4 DMF cut out of one diamondoid lattice induced by hydrogen-bonded tectons whose tetrahedral core structures are represented by solid sticks. 154

Figure 60. View down the **a** or **b** axis of an individual diamondoid lattice cut out of the networks formed by tecton **XVIII** (a), and its view down the **c** axis (b). Only the central carbon atoms of tecton **XVIII** are shown. The interconnecting rods symbolize the intertectonic hydrogen bonding. ... 157

Figure 61. Five interpenetrating diamondoid lattices in the crystal of tecton **XVIII**•4DMF are interwoven by translating them along the **a** or **b** axis by a distance of 11.52 Å viewed along the **c** axis. 158

Figure 62. Channels defined by the diamondoid networks viewed along the **b** axis in the crystal of tecton **XVIII**. 159

Figure 63. Channels defined by the diamondoid networks viewed along the **b** axis in the crystal of tecton **XVIII**. 160

Figure 64. View (down the **b** axis) of two adjacent four-sided channels constructed from four hydrogen-bonded tectons **XVIII**, which are cut out of diamondoid lattices in the crystal of tecton **XVIII**•4DMF. 161

Figure 65. View (down the **b** axis) of an individual four-sided channel cut out of diamondoid networks in the crystal of tecton **XVIII**•4DMF. 162

Figure 66. Space-filling view (down the **b** axis) of an individual four-sided channel cut out of diamondoid networks in the crystal of tecton **XVIII**•4DMF with diameter 6.0 Å x 4.7 Å. 163

List of Schemes

Scheme 1 18
Scheme 2 21
Scheme 3 21
Scheme 4 23
Scheme 5 75
Scheme 6 76
Scheme 7 77
Scheme 8 77
Scheme 9 78
Scheme 10 78
Scheme 11 79
Scheme 12 80
Scheme 13 82
Scheme 14 83
Scheme 15 83
Scheme 16 84
Scheme 17 84
Scheme 18 85
Scheme 19 86
Scheme 20 87
Scheme 21 88
Scheme 22 89
Scheme 23 90
Scheme 24 91

Scheme 25 92
Scheme 26 97
Scheme 27 98
Scheme 28 99
Scheme 29 100
Scheme 30 104
Scheme 31 105
Scheme 32 106
Scheme 33 107
Scheme 34 110
Scheme 35 111
Scheme 36 113
Scheme 37 114
Scheme 38 115
Scheme 39 115
Scheme 40 116
Scheme 41 117
Scheme 42 118
Scheme 43 120
Scheme 44 120
Scheme 45 121
Scheme 46 122
Scheme 47 123
Scheme 48 125
Scheme 49 126
Scheme 50 127
Scheme 51 129

Scheme 52 142

Scheme 53 143

Scheme 54 144

Scheme 55 144

List of Tables

Table 1. Symmetry of crystal system and individual tectons 48

Table 2. Conformations existing in the crystal structures of I•8 $CH_3CH_2CO_2H$ and I•2 $CH_3CH_2CH_2CO_2H$ 50

Table 3. Relationship between the dimensional indices of diamondoid lattices and crystal systems 51

Table 4. Unit cell parameters of I•8$CH_3CH_2CO_2H$ and I•2$CH_3CH_2CH_2CO_2H$ and the dimensional indices of the distorted diamondoid lattices 54

Table 5. The physical properties of carboxylic acids and the number n of acid molecules enclathrated per molecule of tecton I 69

Table 6. X-ray determination of the structures of clathrates obtained by crystallizing tecton I from different carboxylic acids 70

Table 7. Comparison of the crystal data for tecton I•0.3 $CH_3CH_2CO_2H$ •0.6 $CH_3CH_2CH_2CO_2H$ with the data for tecton I•8 $CH_3CH_2CO_2H$ and I•2 $CH_3CH_2CH_2CO_2H$ 71

Table 8. The hydrogen bond energies (ΔH_D), corrected hydrogen bond energies (ΔH_{Dc}), and equilibrium distances (R_e) of monoamino-substituted 2-pyridone dimers, as calculated by the CNDO/2 method 95

Table 9. Association of hydroxypyridine-pyridones measured by vapor pressure osmometry 95

Table 10. Results of crystallization of tecton XII from carboxylic acids 119

Table 11. The degree of interpenetration and some geometric parameters for various diamondoid lattices estimated on the basis of the crystal structure of tecton I 124

Table 12. Conformational flexibility of tectonic molecules 128

Table 13. Comparison of the crystal data for tecton **XVII**•4DMF with the data for tecton **I**•2$CH_3CH_2CH_2CO_2H$ 131

Table 14. Crystal data for various tetraaryl compounds 132

Table 15. Torsion angles for the two sets of asymmetric units in a molecule of tecton **XVII** 134

Table 16. Energy contributions for straight-chain carboxylic acids (eV unit $cell^{-1}$) 141

Table 17. Crystal data of tecton **XVIII**•4 DMF compared with those of tecton **I**•2 $C_3H_7CO_2H$ and tetraphenylmethane 146

Table 18. The calculated densities of tectons 146

Table 19. The characteristic structural feature of tectons 148

Table 20. The dimensional indices of diamondoid lattices generated by tectons **I** and **XVIII** and extent of elongation 155

CHAPTER 1

INTRODUCTION

Hydrogen bonds are extensively used in nature to help accomplish a wide variety of critical and subtle tasks, such as the recognition and binding of selected molecules, the catalysis of key reactions, the storage, replication, and expression of genetic information, and the production of organized structural materials. The remarkable diversity and ingenuity of these natural processes challenge chemists to devise unnatural compounds that use hydrogen bonds to perform similar tasks, and to invent entirely new applications that take full advantage of the characteristic features of hydrogen bonds.

During recent decades, considerable effort has been devoted to the study of using hydrogen bonding as a tool or a synthetic vector for designing molecular aggregates and carrying out intermolecular synthesis in order to create new organic materials with specific physical and chemical properties. As a result of all these endeavors, "crystal engineering" and "supramolecular chemistry" have emerged as two major disciplines and are undergoing rapid development.

Crystal engineering is defined as the understanding of intermolecular interactions in the context of crystal packing and the utilization of such understanding in the design of new solids with desired physical and chemical properties. An organic crystal might be the most precise example of molecular recognition in the solid state since chemical processes blend with the laws of crystallography to generate a periodic molecular array. The almost perfect

alignment of molecules in an organic crystal results usually in highly predictable physical and chemical properties which in turn justifies efforts to control crystal engineering.

Supramolecular chemistry is the chemistry beyond the molecule and deals mostly with noncovalent chemical bonds. It is the designed chemistry of the intermolecular bond just as molecular chemistry is that of the covalent bond. The conceptual feature that distinguishes a supramolecular from a molecular species is not its size, but the possibility of splitting the species into molecular components that have an individual existence. In other words, supramolecular species are constructed by combining molecular building blocks in much the same way that molecules are obtained by the combination of atoms. One of the most important aspects of supramolecular chemistry is the design of systems undergoing self-organization, that is, systems capable of spontaneously generating a well-defined supramolecular architecture by self-assembling from their components under a given set of conditions. One of several approaches to self-assembling systems which have been pursued is the formation of ordered solid-state structures directed by molecular recognition. Accordingly, it is easy to see that both crystal engineering and supramolecular chemistry involve molecular recognition, while intermolecular interactions are the basis for it.

For the severe task of inducing the self-assembly of complex, predictable supramolecular aggregates, van der Waals interactions and many other intermolecular forces would appear inadequate because they are weak and nondirectional. However, hydrogen bonds more nearly resemble the covalent bonds which are the primary design elements in molecular chemistry. Specifically, hydrogen bonds are stable enough to ensure a high degree of association, are selective and directional enough to give predictable structural consequences, and occur frequently enough to be of practical interest. As a result of their strength, directionality and selectivity, hydrogen bonds can be expected under ideal circumstances to be able to determine the organization of aggregates with almost as much control as covalent bonds determine the structures of molecules.

It has therefore been recognized that hydrogen bonding is an indispensable tool for designing molecular aggregates[1]. As a result, it is very important to fully understand all aspects of hydrogen bonding, including not only the energy and geometry of individual hydrogen-bonding interactions but also the hydrogen-bonding preferences of individual functional groups. This will yield guidelines for the selectivity and patterns of molecular aggregates generated by hydrogen bonds, and hence will provide synthetic guidelines for designing new aggregate structures. If certain molecular building blocks tend to crystallize in specific energetically favorable arrangements, molecules containing these blocks can be encouraged to form aggregates with specific structural features. Extensive studies of solid-state structures of a wide range of molecular solids of this modular type have been carried out by several groups.

An early study by Schmidt and Leiserowitz[2b] has classified the structures of primary amides in terms of hydrogen-bond networks. The observed packing arrangements of primary amides were analyzed with the extension of the centrosymmetric dimer motif using glide planes, screw axes and translation symmetry elements. They argued that because the pattern of the amide hydrogen bond is well-known, the complicated and difficult question of intermolecular forces could be simplified to the simpler analysis of hydrogen-bond networks, and it was found that networks involving particular symmetry elements lead only to certain space groups and cell axis values. Later, Leiserowitz and Hagler and their co-workers[2] refined Schmidt's model and indicated that no structure is determined exclusively by electronic forces. In a series of papers, they described how Coulombic terms may be incorporated in the potential expression to calculate the energies of various hydrogen-bond motifs found in amide structures. They concluded that the actual crystal structures adopted result from a fine interplay of hydrogen bonding and van der Waals forces. Meanwhile, they indicated that it was noteworthy that the energy differences between observed and unobserved packing modes, which all have reasonable hydrogen bond patterns, may be as little as 1-2 kcal/mol. This means that not only thermodynamic

but kinetic factors play an important role in crystallization regulated by hydrogen bonding, and that polymorphism is likely to be ubiquitous in organic crystals and crystal engineering.

More recently, Etter and co-workers[3] have carried out very extensive studies of organic hydrogen-bonded solid-state structures. Their work has focused on the role of hydrogen bonds in the absence of preorganized and custom-designed cavities. They purposely chose systems where steric constraints are kept to a minimum and where the primary controlling feature of intermolecular association is the hydrogen-bond interaction. In this way the independent contributions of intermolecular hydrogen bonding to the structures of aggregates can be evaluated, and hydrogen-bond specificity and competitions can be studied. Consequently, a method for describing hydrogen-bond patterns was developed, and common features of these hydrogen-bonded aggregate structures were formulated as a set of rules which can be used as synthetic guidelines for designing new aggregate structures.

Even though there is still a long way to go in order to be able to predict the precise structure of an unknown material, and even though hydrogen bonding in molecular crystals is still at the stage of rationalization rather than prediction, several imaginative efforts have been made to use hydrogen bonding as a tool for creating specific structural features. Fowler and Lauher and co-workers[4] have successfully designed a molecular solid in which self-complementary functional groups participate in intermolecular hydrogen bonds and thereby direct molecules to self-associate to form supramolecular aggregates in a predicted way. The building blocks they designed and synthesized are a series of ureylenedicarboxylic acids **1** to **3** (Figure 1) which contain two functionalities, the carboxylic acid groups at each end of the molecules and the urea functional groups in the middle. These groups are combined in one molecular device so that a two-dimensional hydrogen-bonded array (β-network) can be formed, which is based upon two independent, self-complementary, one-dimensional hydrogen-bonded arrays (α-network) directed either

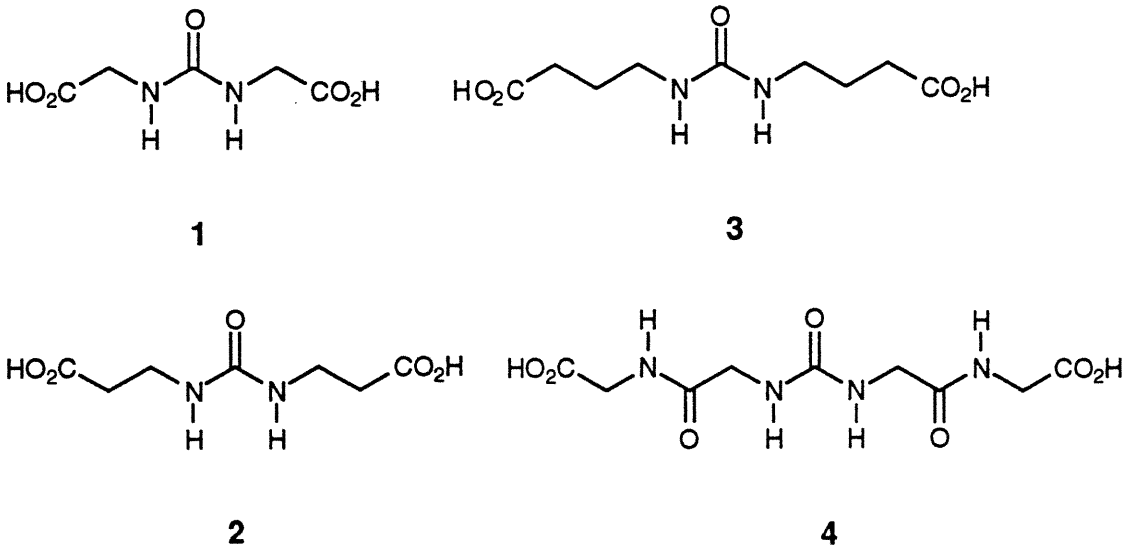

Figure 1. Ureylenedicarboxylic acids, designed and synthesized by Fowler, Lauher and co-workers[4].

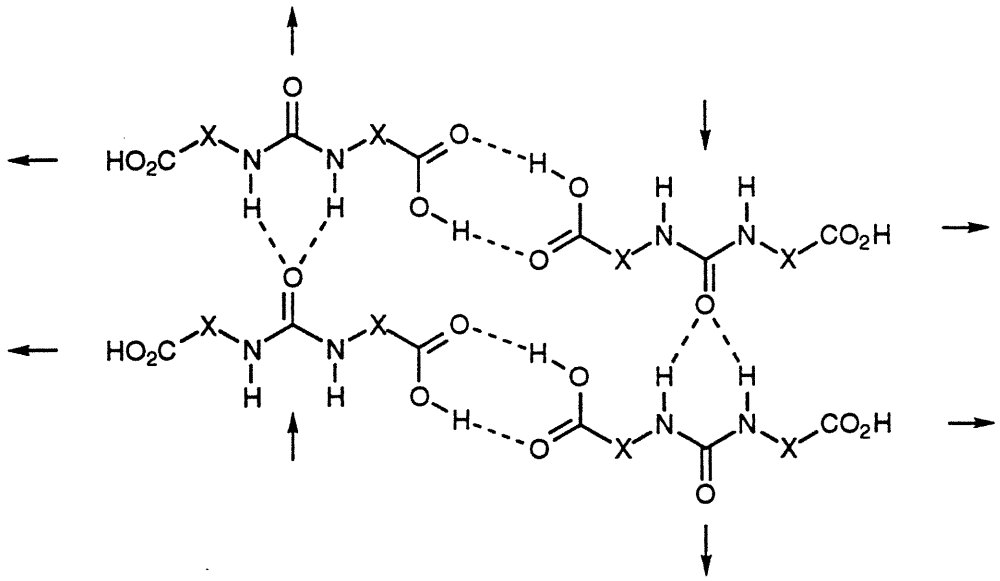

Figure 2. A β-network formed by the two-dimensional array of self-complementary hydrogen-bonded ureylenedicarboxylic acids[4].

by carboxylic acid groups or urea groups (Figure 2). Based on what was learned from these studies, a third functionality, in the form of two amide groups , was introduced into the molecules represented to form glycylglycine **4**. These new functionalities form additional hydrogen bonds to the next β-network layer and hence a three-dimensional network or so-called γ-network is built. Furthermore, they extended their studies to include an investigation of how crystal design strategies are affected by the laws of crystallography. They indicated that in a crystal all intermolecular interactions must conform to the laws of crystallography, which can be expressed in terms of symmetry relationships and group theory. They found that strategies based upon the application of complementary hydrogen bonding and the concept of correspondence of intermolecular interactions to specific crystallographic symmetry operators could be carried out successfully. In particular, β-networks were formed as predicted whenever symmetric disubstituted ureas with C_2 point group symmetry were used. However, unpredicted network structures were found in several cases when less symmetric disubstituted ureas were used. As a result, a design strategy for two-dimension layered molecular crystals has been formulated. This work improves upon previous strategies and makes a clever contribution to the engineering of organic solid materials.

Lehn and co-workers[6] have presented how to suitably design molecular components capable of self-assembling into supramolecular species with desired architectural and functional features. They employed 2,4,6-triaminopyrimidines **5** and **6** and barbituric acid derivatives **7** and **8** as complementary molecular components, each of which contains two identical recognition sites for generating the hetero-self-organized supramolecular strand **9** instead of the cyclic hexameric motif **10** based on intermolecular hydrogen bonding (Figure 3). In order to try to get a cyclic hexameric motif, they designed subunits **11** and **12** in which the symmetry possessed by **5-8** was broken (Figure 4). They expected that these modifications would make the subunits capable of only a single spatial relationship with neighboring subunits, in such a way that the hetero-association of **11** and

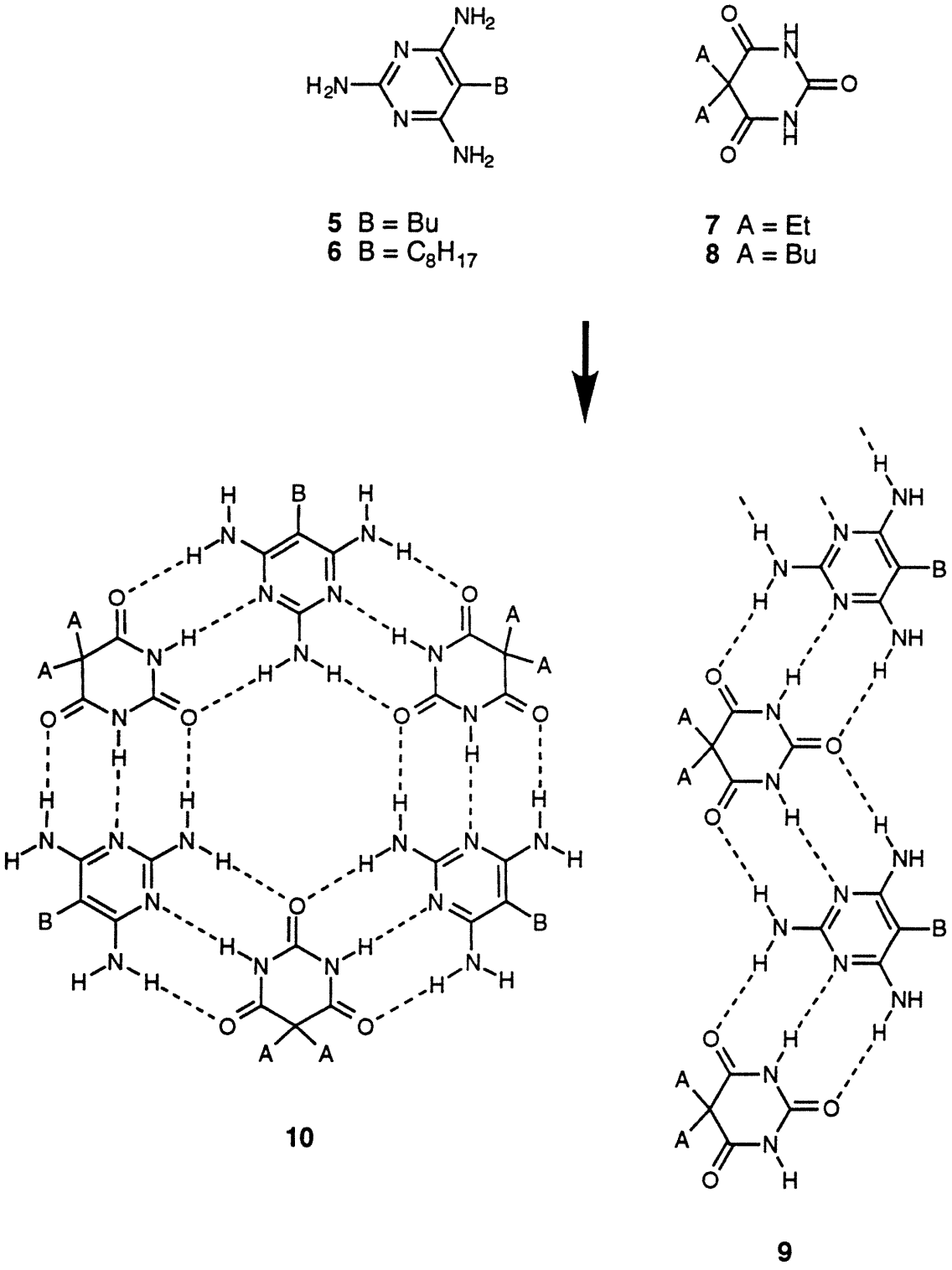

Figure 3. Schematic representation of the hydrogen -bonded strand **9** and the cyclic hexameric motif **10** formed by self-assembly of the self-complementary components **5-8**.

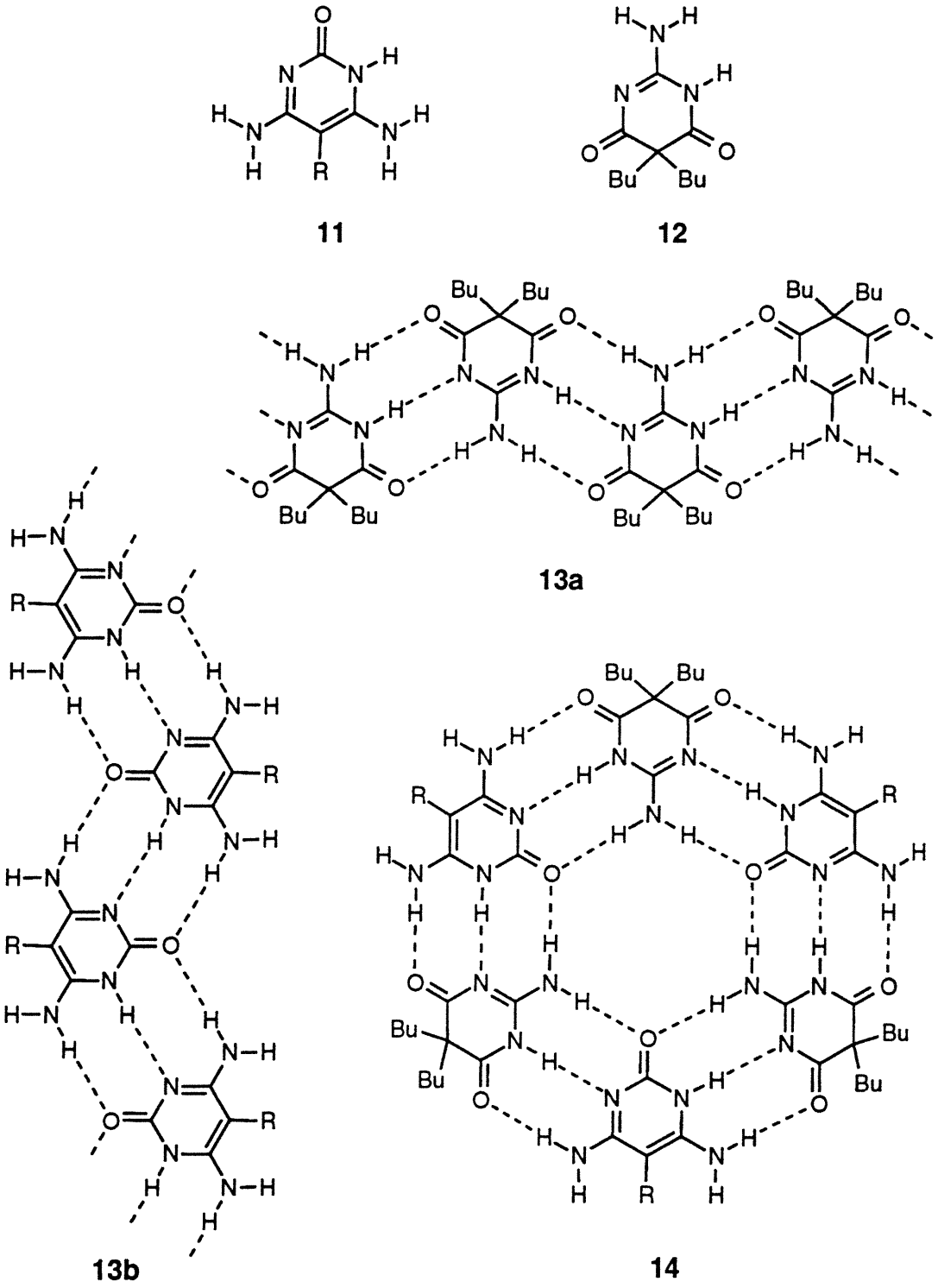

Figure 4. Schematic representation of the hydrogen-bonded ribbon-like species **13a** and **b** formed by homo-association of the self-complementary components **11** and **12** and cyclic hexamer motif **14** formed by their hetero-association.

12 could only lead to the geometric expression of a macrocyclic ring **14**. However, because the hydrogen-bonding preference for the hetero-association of **5** to **8** rather than their homo-association was destroyed as well when the symmetry was broken, only the self-association of either **11** or **12** occurred, giving ribbon polymers **13a** and **13b**. This phenomenon illustrates how important and subtle it is to design molecular components which are well-informed either in their geometry or their patterns of intermolecular interaction in supramolecular assemblies.

In related work, Whitesides and co-workers[5] have synthesized co-crystals of melamine derivatives and barbituric acids which contain extended hydrogen-bonded "tapes"[5a]. Later, they designed and synthesized three-dimensional supramolecular assemblies based on the pattern of hydrogen bonds present in the 1:1 complex between cyanuric acid and melamine[5b-f].

It is well-known that primary and secondary diamides containing either alkyl or aryl spacer groups frequently show hydrogen-bonding motifs based on an up/down translational arrangement of the amide groups (Figure 5). The result is an ordered array of

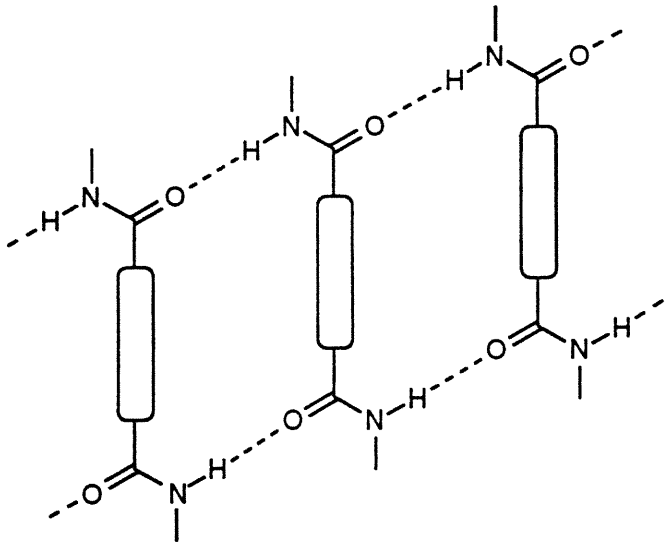

Figure 5. Common hydrogen-bonding pattern for secondary diamides[8].

single spacer units held in an α-network by predictable intermolecular interactions. Hamilton and co-workers[8] have been interested in extending the basic structures of these amides and in discovering ways to both alter the shape of the networks and to incorporate additional molecular subunits. They designed a polymeric complex in which a second subunit was interposed and linked to diamides by a stronger bidentate hydrogen-bonding

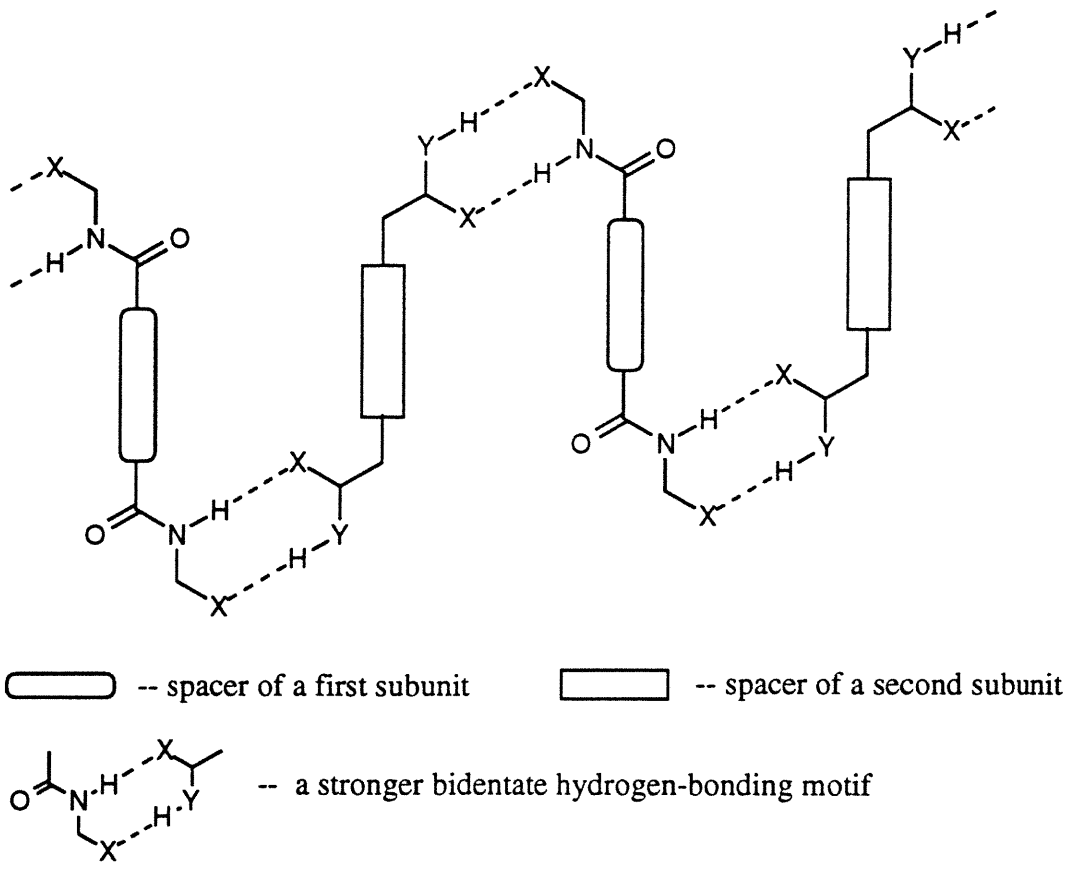

Figure 6. Stronger bidentate hydrogen-bonding motif between secondary diamides and second subunits[8].

motif as shown in Figure 6. According to the rules suggested by Etter[3b], which state that in the solid state the strongest hydrogen bond acceptor will bind to the strongest donor, the carboxylic acid and aminopyridine groups would be expected to hydrogen bond to each

other rather than form symmetrical dimers. Therefore a self-assembling system which consists of bis(2-amidopyridine) derivatives of different aryl diacids (Figure 7) and aliphatic dicarboxylic acids (Figure 8) was established. After exploring the structural and

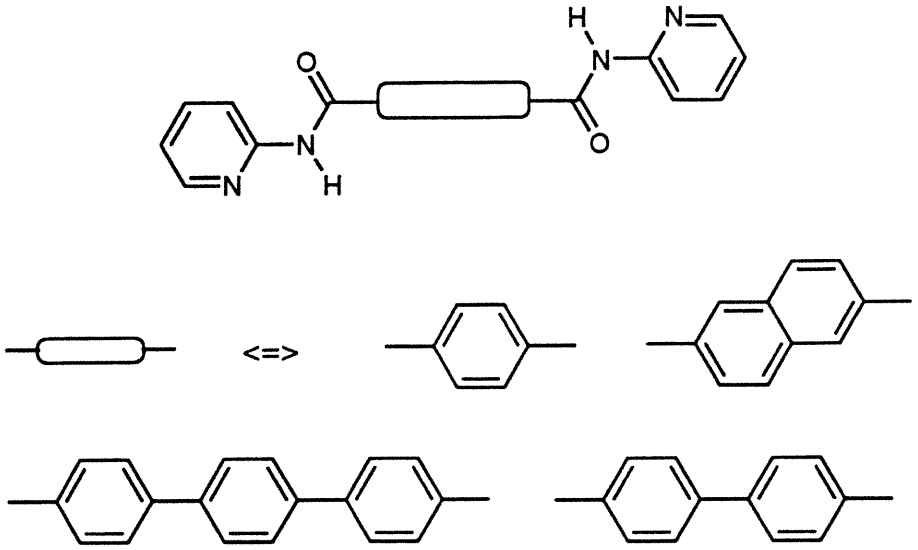

Figure 7. First subunits -- Bis(2-aminopyridine) derivatives of different aryl diacids.

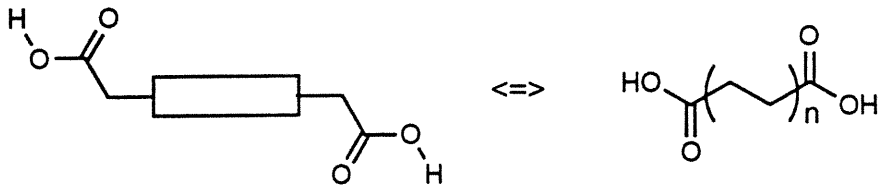

Figure 8. Second subunits -- Aliphatic dicarboxylic acids.

recognition properties of these bis(2-amidopyridines) with different spacer sizes in association with dicarboxylic acids of different lengths, Hamilton and co-workers discovered that recurring hydrogen-bonding networks form between aliphatic dicarboxylic

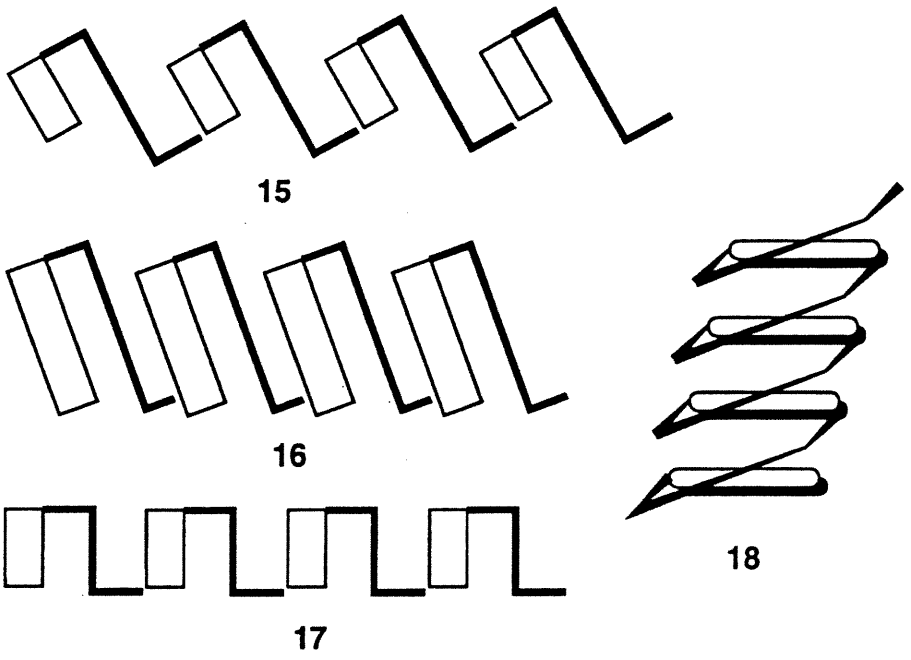

Figure 9. Effect of component length on slip angle

acids and bis(2-amidopyridine) derivatives, and the hydrogen-bonding motif is retained despite changes in the sizes of both molecular components. It was recognized that careful variation of the length of either the diacid or the diamide leads to predictable changes in the angular disposition of the different subunits (Figure 9, structures **15-17**). Later, they found[8c] that a simple aminopyridine subunit which has a proper conformation and spacer length can be introduced to interact with aliphatic dicarboxylic acids and self-assemble into an extended helical structure (Figure 9, structure **18**).

These examples focus on aggregation in the solid state, but considerable effort has been devoted to the study of molecular association in solution, especially for cases where the aggregate pattern that is formed involves only two species normally, where association constants are very high (10^4 M^{-1} or greater), and where the aggregates are stabilized primarily by topological features such as preorganized cavities[7].

Our own research has focused on what we call *molecular tectonics*[10]. A logical strategy for engineering an organic solid material could be based upon designing molecules

incorporating functional and architectural features in such a way that they are capable of self-assembling into supramolecular aggregates with well-defined and predictable structures. Obviously, such molecules must be cleverly constructed and "sticky" enough to participate in strong, specific intermolecular interactions. We call these sticky molecules *tectons*. This name is derived from the Greek word τεκτωη, which means "builder" and is the root of such words as architect. It is an appropriate name for molecules predisposed to associate in specific ways, because they serve as the fundamental building blocks for supramolecular construction. The observed crystal structures that they construct should be the result of compromises between the specific directional interactions and geometric information incorporated in the tectonic subunits. Wuest has defined *molecular tectonics* as the science and art of supramolecular construction using tectonic subunits[10b]. These special names are justified, because the high strength and predictable directionality of the intertectonic attractions sharply distinguish them from the weaker and more diffuse forces typically involved in other processes of self-assembly, including crystallization. In effect, the strategy of molecular tectonics promises to give chemists the elements of a molecular-scale construction set that can be used to build an infinite variety of predictably ordered structures. A principal advantage of this strategy is that the supramolecular aggregates are formed spontaneously by the self-association of sticky tectonic subunits, and the tedious bond-by-bond syntheses normally employed to build complex structures can be avoided.

A critical step in the study of molecular tectonics is to find a suitable intermolecular interaction that is able to regulate tectonic aggregation in a reliable and predictable way. Undoubtedly, hydrogen bonding is one of the best choices among the various intermolecular interactions, but there are many different types of hydrogen bonds. We need to select those that are not only simple but also likely to lead to aggregation with broad practical and theoretical significance. The specific choice of individual hydrogen-bond pattern for tectons is important because the aggregates they are going to construct must involve strong intermolecular hydrogen bonding. This means that the individual tectons are

expected to be able to form unusually strong, specific, and reliable hydrogen-bonding motifs. A particularly attractive motif is the cyclic hydrogen-bonding array defined by dimers of 2-pyridone and related heterocycles (eq.1).[9, 35-36] This motif is strong, well

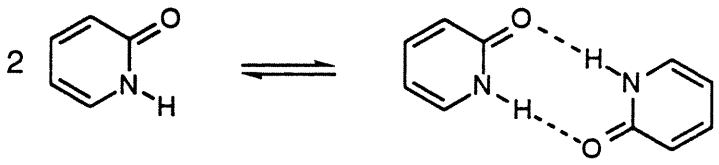

(1)

studied and dependable. Although pyridones exist in equilibrium with their hydroxypyridine tautomers, the more polar pyridone form normally predominates in solution and in the solid[10]. From this simple but cleverly chosen subunit, it has been possible to design and synthesize molecules that incorporate characteristic, well-defined patterns of hydrogen-bond donors and acceptors.

The routine prediction of structures of hydrogen-bonded crystals is still a difficult or even almost impossible task at the present time. To improve this situation, Ducharme and Wuest[10g] made a determined effort to amplify and regulate intertectonic adhesion in order to achieve stronger and more predictable intermolecular interaction. Although the hydrogen-bonding pattern defined by dimers of 2-pyridone and related heterocycles is strong, it nevertheless contains only two hydrogen bonds. For this reason, it cannot be expected that the self-assembling process of tectons which incorporate only single pyridone rings will be directed in a specific or predictable way, since two hydrogen bonds may not be able to override other interactions that may favor different modes of association. Fortunately, the strength of the basic pyridone dimer motif can be amplified easily by using spacers to link two or more 2-pyridones together in a rigid or flexible way. This is a very important idea, since it means that we do not need to make entirely new types of tectons to achieve stronger intermolecular attractions. Tectons incorporating two or more 2-pyridone rings rigidly linked by appropriate spacers should associate strongly, and the precise mode

of aggregation should depend critically on the pattern of hydrogen-bond donors and acceptors. Self-complementary asymmetric dipyridones **19** should be able to dimerize to

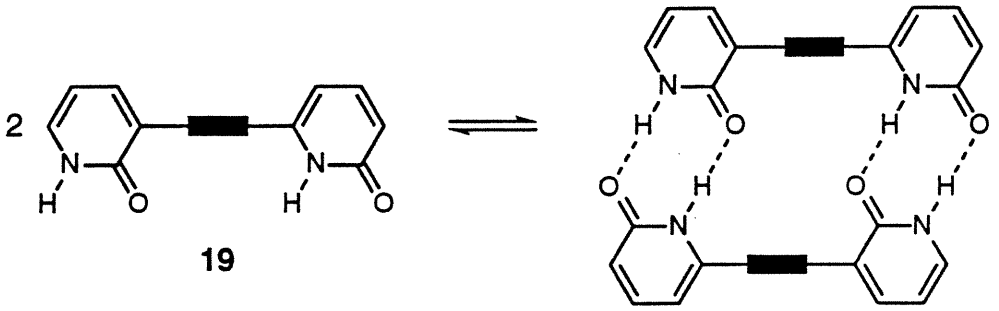

19 (2)

form an antiparallel duplex held together by four hydrogen bonds (eq. 2), whereas symmetric isomers **20** should be forced to polymerize to form linear oligomers (eq. 3). To test this hypothesis , Ducharme and Wuest designed and synthesized rigid acetylenic dipyridones **21** and **22** (shown in Figure 10), and they studied their associative behavior in

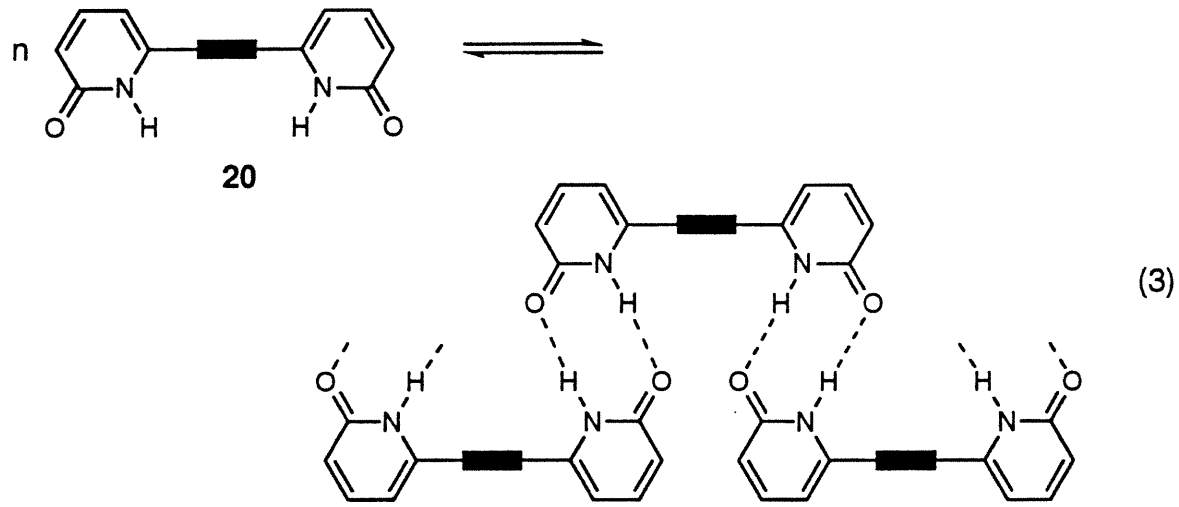

20 (3)

solution and in the solid. The results of their thermodynamic studies indicated that the behavior of symmetric dipyridone **22** is similar to that of 2-pyridone itself. In contrast, asymmetric dipyridone **21** is almost exclusively dimeric in chloroform (>90%) even at very low concentrations (3.6×10^{-4} M). Furthermore, X-ray crystallographic studies

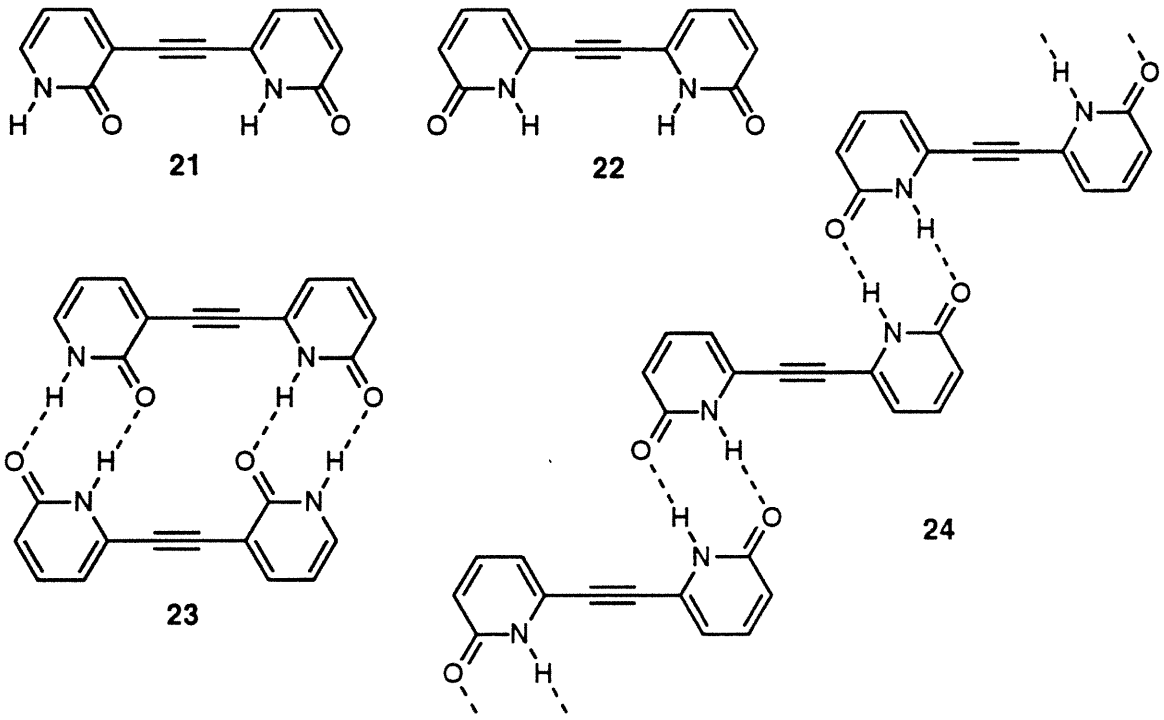

Figure 10. Tectons designed and synthesized by Ducharme and Wuest[10g].

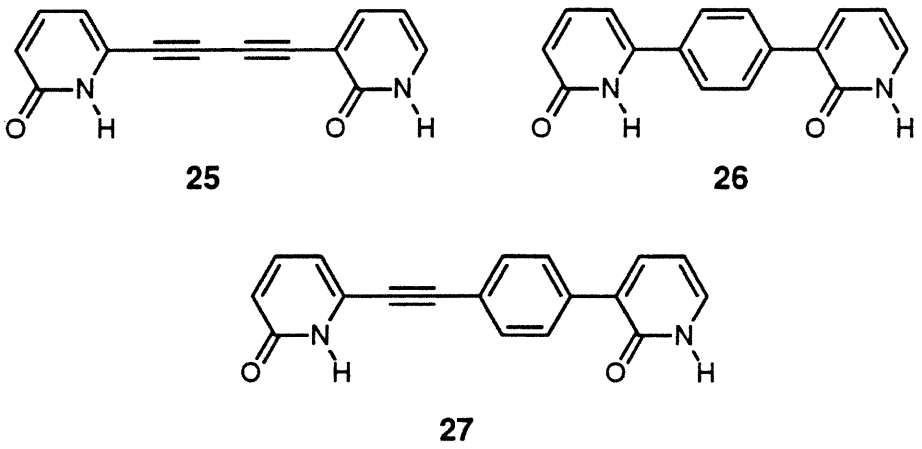

Figure 11. Tectons constructed by joining two pyridone rings with different rigid spacers.[10-12]

established that dipyridones **21** and **22** have different modes of aggregation in the solid state. As expected, asymmetric isomer **21** exists as discrete dimers **23**, while symmetric isomer **22** adopts polymeric motif **24**.

Accordingly, a wide variety of tectons with similar associative properties can be constructed by using different rigid spacers to join two pyridone rings together. For example, tectons **25**[10a], **26**[11] and **27**[12], which are all close relatives of self-complementary dipyridone **21**, have been synthesized, and they have similar strong tendencies to form duplexes by self-association (Figure 11).

Investigation of the tectons discussed above has confirmed that they have striking and predictable properties of recognition and self-association . Therefore they are qualified to serve as active functional features for creating molecular recognition patterns in molecules that make them capable of self-assembling into supramolecular aggregates. These features can be combined with appropriate architectures to create tectons from which predictable supramolecular architectures might be generated. This presents the challenge of creating complex tectons by attaching multiple sticky subunits to carefully chosen frameworks. Even though self-complementary dipyridones **21** and **25-27** can form antiparallel architectural duplexes strongly held by four hydrogen bonds, the networks that result are architecturally at a very primitive level[1c]. For example, the polymeric motif adopted by asymmetric dipyridone **22** can only self-assemble into essentially one-dimensional chains. It is not obvious that these dipyridones offer the chemist any dramatic new opportunities, because they closely resemble the simple pyridone subunits from which they are constructed. Fortunately, more complex tectons can be devised that yield more elaborate architectures of higher dimensionality. For example, hypothetical tecton **28** (Scheme 1) is created by using rigid arms to connect four sticky sites (•) to a tetrahedral core. Because of its well-defined tetrahedral geometry and the presence of four sticky sites, tecton **28** should be forced to self-associate to form the infinite diamondoid network **29** or another related three-dimensional lattice. This shows that molecular tectonics has the

potential of being a powerful and elegant strategy for the assembly of three-dimensional networks.

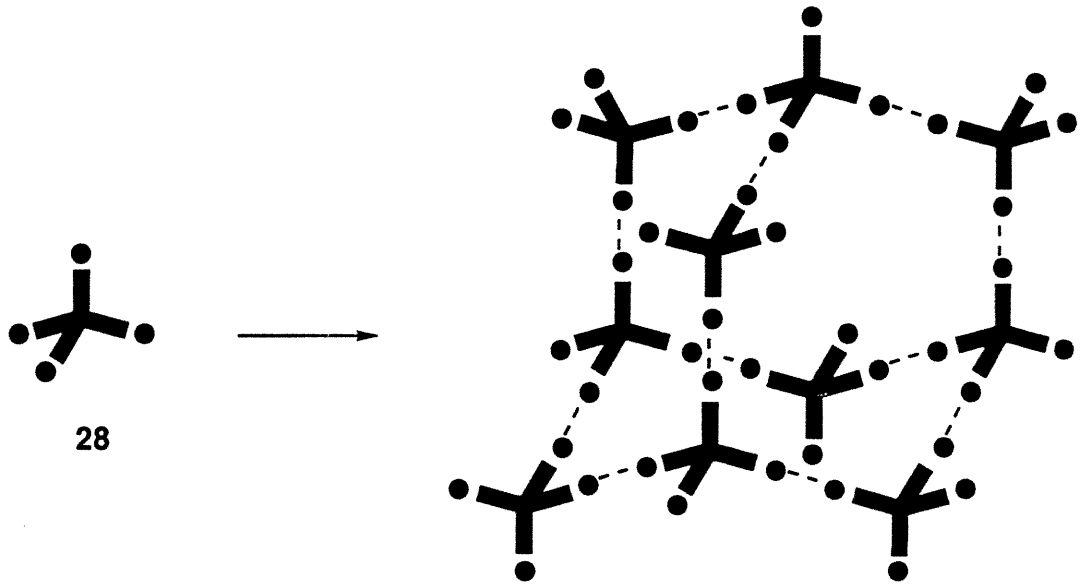

28 29

Scheme 1. Diamondoid network constructed from hypothetical tectons **28** by self-assembly.

In fact, it was known almost fifty years ago that crystals of ice and of potassium dihydrogen phosphate KH_2PO_4 can form distorted diamondoid networks held together by hydrogen bonds[15]. In addition, in 1988 Ermer and co-workers[13a] published an influential paper in which they first pointed out that diamondoid networks can be formed by the self-assembling of complex organic molecules with tetrahedrally directed sticky subunits. For example, 1,3,5,7-adamantanetetracarboxylic acid generates such a network via intermolecular hydrogen bonding under suitable conditions. They found that the empty spaces of the large hollow diamondoid lattices are filled by four interpenetrating equivalent lattices to avoid large cavities according to the close-packing principles. They indicated that these results might suggest a new way to construct novel solid-state host-guest inclusion

compounds and that the adamantanetetracarboxylic acid could be viewed as a sort of self-inclusion compound. However, the tetracarboxylic acid cannot enclathrate guest molecules without lowering the degree of interpenetration since the five diamondoid lattices are tightly interwoven. To achieve the target of lowering the degree of interpenetration and to make the formation of solid-state host-guest compounds possible, they considered several modifications: 1) steric modulation of the adamantane core structure by introducing two oxo or methylidene groups in the 2 and 6 positions of the tetraacid[13b, e]; 2) increased flexibility and strength of hydrogen bonds[13d]; 3) employment of more voluminous guest molecules[13e].

In this thesis, I will summarize our efforts to develop the strategy of molecular tectonics[10e, 13-14] and show how it is possible to design and synthesize tectons which give rise to aggregates with a variety of architectural and functional features.

CHAPTER 2

INITIAL DESIGN OF AN ORGANIC TECTON ABLE TO GENERATE DIAMONDOID NETWORKS

2.1 Design and synthesis of tecton I

Tecton **I** is designed to incorporate tetrahedrally oriented pyridones in a rigid framework like hypothetical compound **28** mentioned in the introduction section. In addition, tecton **I** is chosen to be easy to synthesize. Its retrosynthetic analysis is shown in

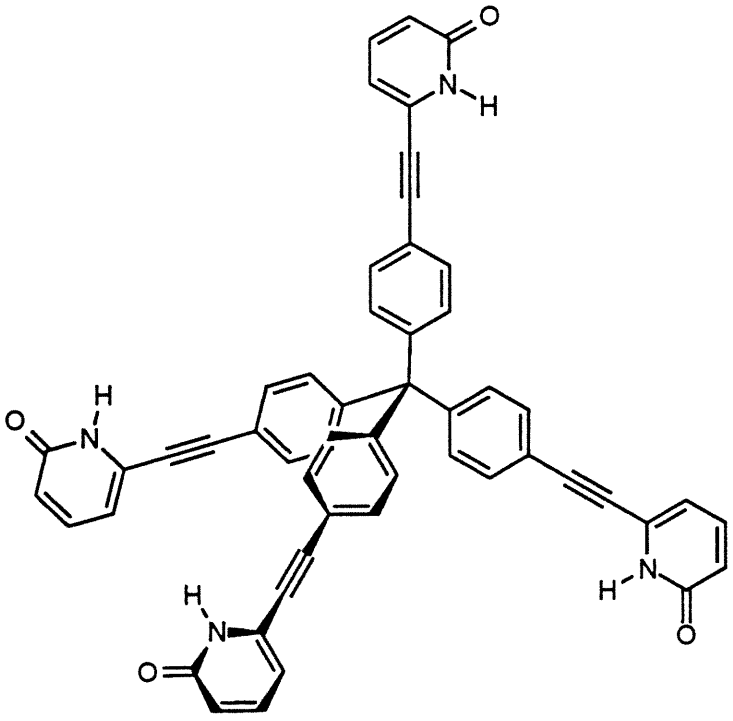

I

Scheme 2

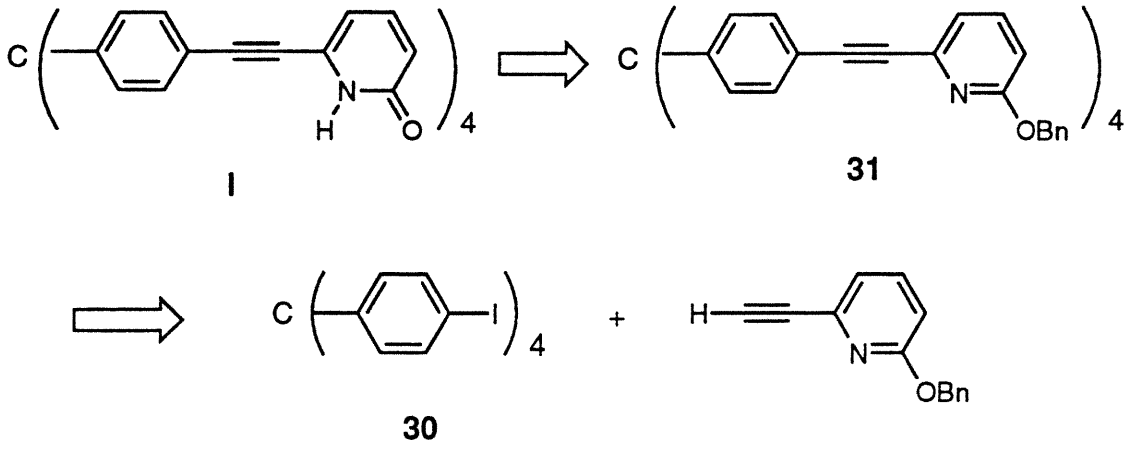

Scheme 3

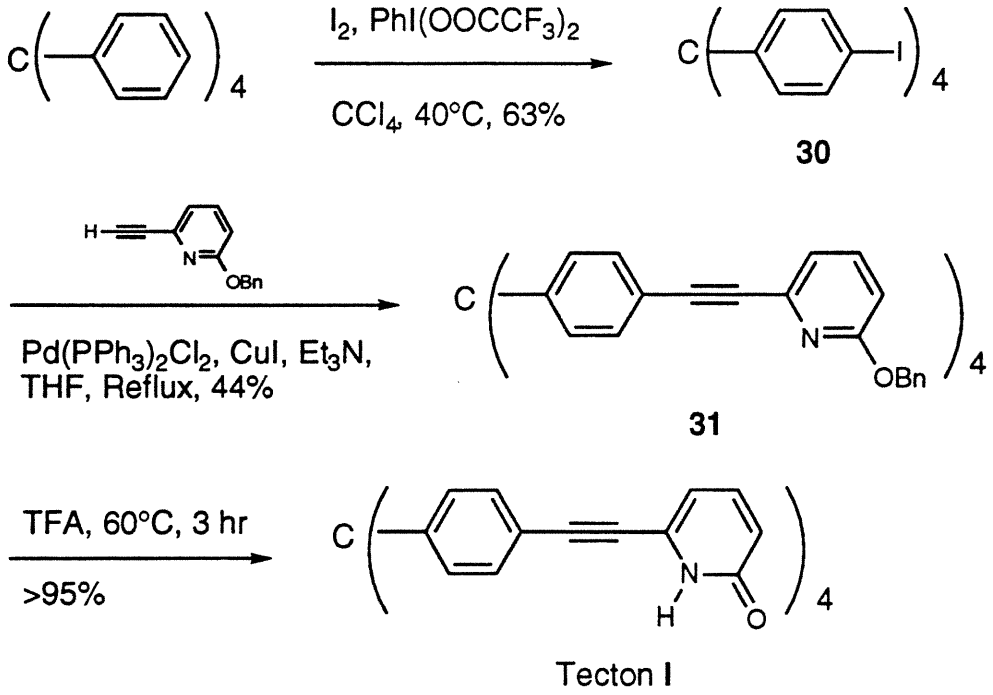

Scheme 2. Tecton **I** employs tetraphenylmethane as the tetrahedral core and connects four sticky pyridones by rigid triple bonds. Tecton **I** was synthesized from tetraphenylmethane[17] in three steps as shown in Scheme 3. Iodination[18] of tetraphenylmethane gave tetraiodide **30** in 63% yield, which was coupled[19] with 6-ethynyl-2-(phenylmethoxy)pyridine[10d] to give tetrapyridine **31** in 44% yield. Deprotection with trifluoroacetic acid (TFA) then provided tecton **I** in almost quantitative yield.[20]

2.2. Prediction of the crystal structure of tecton I

Although considerable effort has been made by several groups of scientists[2h, 21], the detailed prediction of crystal structures is currently extremely difficult or even impossible. Nevertheless, we began to speculate about different arrangements of tecton **I** in the crystal. One crucial consideration is whether intermolecular hydrogen bonding is strong enough to override the forces that favor close-packing. If the forces favoring close-packing are less important than hydrogen bonding, it means that highly directional interactions may be energetically more significant instead of van der Waals forces in determining the solid state structure of tecton **I**. For this case, the crystal structure of tecton **I** would be likely to consist of networks with various degrees of interpenetration. However, in all organic solids, van der Waals interactions are energetically significant. Although they are crucial for nonpolar molecules in terms of crystal structure-directing effects, they may not be unimportant even in crystals of molecules containing functional substituents and hydrogen bonding capability. As a matter of fact, it is quite difficult to predict whether the directional interactions will prevent efficient close-packing or whether van der Waals forces will distort directional interactions from some ideal geometry. In the light of all discussed above, it is likely that the most plausible crystal structure of tecton **I** will be the result of compromises of several types of weak and strong interactions.

Scheme 4

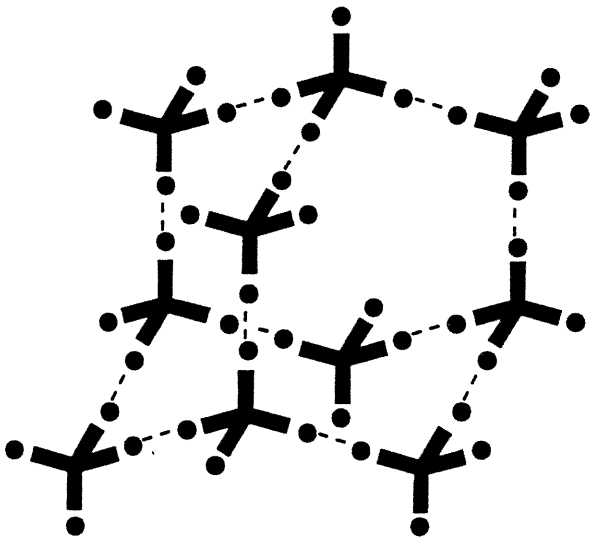

29

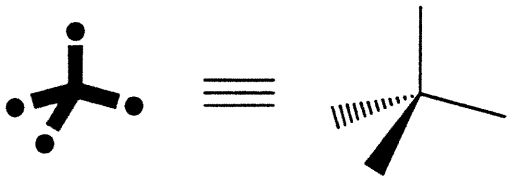

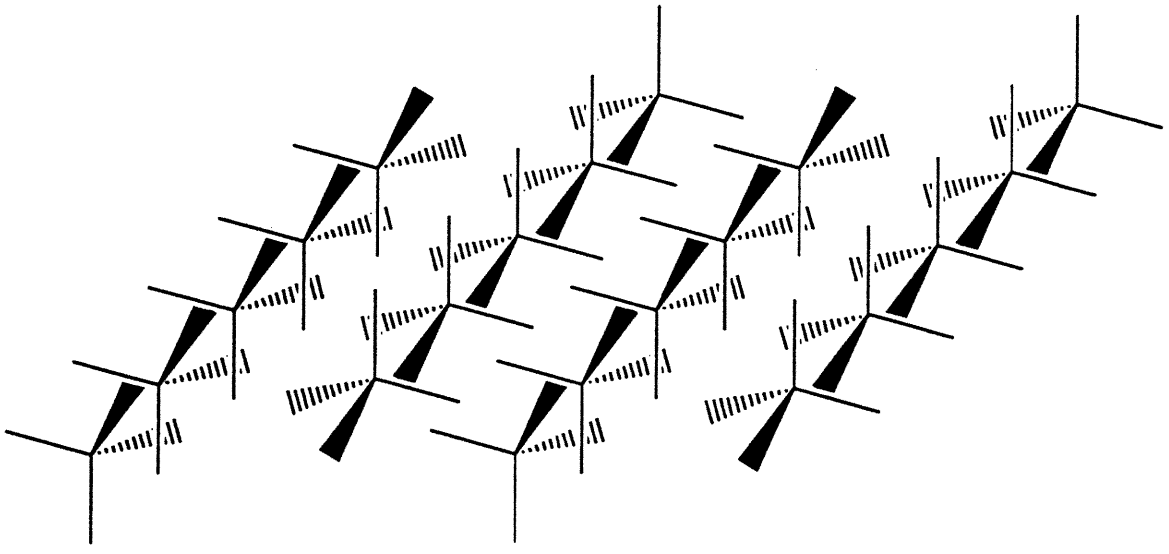

32

Nonetheless, tecton **I** should have a very strong tendency to form diamondoid networks held together by hydrogen bonding. The tetrahedrally oriented pyridone rings should be able to direct tecton **I** to self-assemble into aggregates with a diamondoid framework as shown in Scheme 4, as a consequence of its ability to participate in hydrogen bonding. On the other hand, if we hypothesize that van der Waals forces are significant in the crystal structure, the molecular geometry of tecton **I**, including such factors as its size, shape and surface contour, becomes the most important factor in determining its crystal packing. In this case, tecton **I** may pack in such a way that molecules sit on top of each other along an n-fold axis to form a column and then extend to the other two dimensions via centrosymmetric pairwise hydrogen bonding motif by using screw axes, glide planes and translation symmetry elements to generate the entire crystal. The possible packing mode **32** is shown schematically in Scheme 4. Comparing the diamondoid framework **29** with close-packed mode **32**, we find that the neighboring hydrogen-bonded tectons in diamondoid framework **29** have almost exactly the same packing relationship as those shown in **32**. This means that the compatibility of hydrogen bonding with van der Waals forces in the hypothetical crystal packing of tecton **I** should endow tecton **I** with a strong propensity to generate superdiamondoid lattices in its crystal structure.

The long distances of about 20 Å between the tetrahedral centers of neighboring hydrogen-bonded tectons, which will be called the 'intertectonic distance', lead to a huge empty internal space. As a result, this hypothetical network is not energetically favorable according to Kitaigorodsky's close-packing principles of organic solids[22]. It is well known that molecules which obey the close-packing principles strive towards a maximum coordination number and packing efficiency. Molecules incorporating high internal symmetry and polar substituents, such as hydroquinone and trimesic acid[23], usually construct very open cage-like structures. However, the low packing coefficients that would result in such structures are avoided by enclathration of the solvent or the interpenetration

of unconnected lattices. Ermer's study of adamantane-1,3,5,7-tetracarboxylic acid (**33**), its derivatives **34-37** and its analogue **38**[13] (shown in Figure 12) indicated that in order to

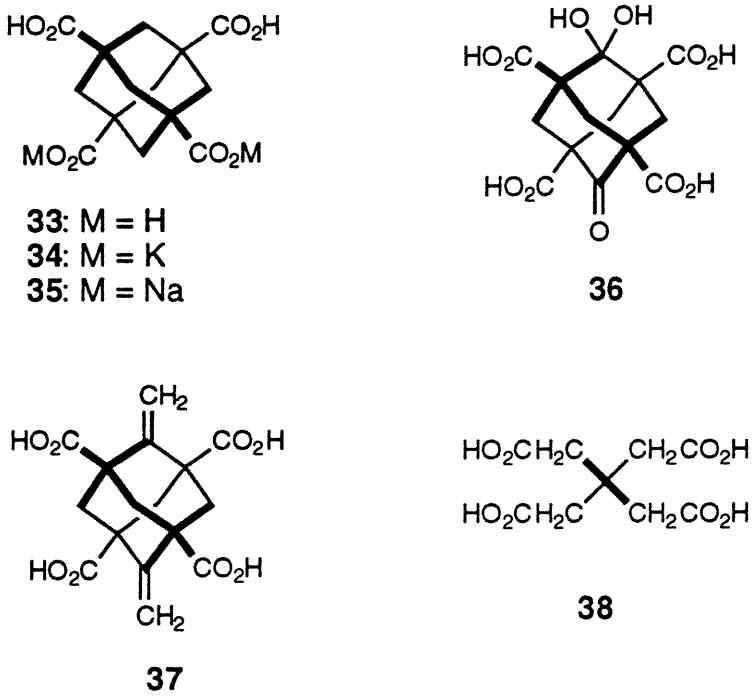

Figure 12. Ermer's tectons **33-38**

avoid this hollowness dilemma, the open space of diamondoid networks is filled in the crystal by symmetry-equivalent diamondoid lattices in various degrees of interpenetration, which results in a sort of self-inclusion compound, or in a lower degree of interpenetration with simultaneous enclathration of guest molecules, which results in solid-state host-guest inclusion compounds. Since the longest intertectonic distance in Ermer's tectons is about 10 Å, just half that of tecton **I**, we predicted that tecton **I** would reveal a new type of solid-state host-guest inclusion compound.

2.3. The crystal structure of tecton I revealed by X-ray crystallographic analysis.

After extensive experimentation, we found that tecton **I** could be crystallized from a mixed solvent system which consisted of carboxylic acids as the principal component, methanol as a diluent, and hexane as a precipitating agent. When acetic or propionic acid were used as solvents, the system consistently produced high yields of quite long needle-shaped crystals, whose composition was shown by ^{1}H NMR spectroscopy to be **I**•8 RCOOH (R = CH_3, CH_2CH_3). An X-ray crystallographic study of tecton **I**•8 CH_3CH_2COOH revealed that a diamondoid network induced by hydrogen bonding between pyridone rings is not formed under these conditions of crystallization. Instead, an alternative six-fold diamondoid network directed by π-stacking of pyridone rings is produced (Figure 13). However, when larger carboxylic acids, such as butyric acid, were employed, crystallization of tecton **I** from the system of butyric acid/MeOH/hexane reproducibly gave high yields (about 84%) of plates of approximate composition tecton **I**•2 $CH_3CH_2CH_2CO_2H$. The change of the shape and composition of the crystals implied that a different structure had been formed. An X-ray crystallographic study of this new structure confirmed that the sticky pyridone sites interact in the expected way to induce self-assembly of the diamondoid network shown in Figure 14. Because of the large intertectonic separation, the structure is built of seven mutually interpenetrating diamondoid lattices. These results confirm that 1) tecton **I** has a strong propensity to generate diamondoid lattices in the crystal, and 2) tecton **I** indeed provides novel types of solid host-guest inclusion compounds. We were eager to learn why the hydrogen bonded diamondoid network favored in butyric acid is thwarted when smaller carboxylic acids are employed as solvents. To understand this, we need to inspect the two crystal structures more closely and carefully.

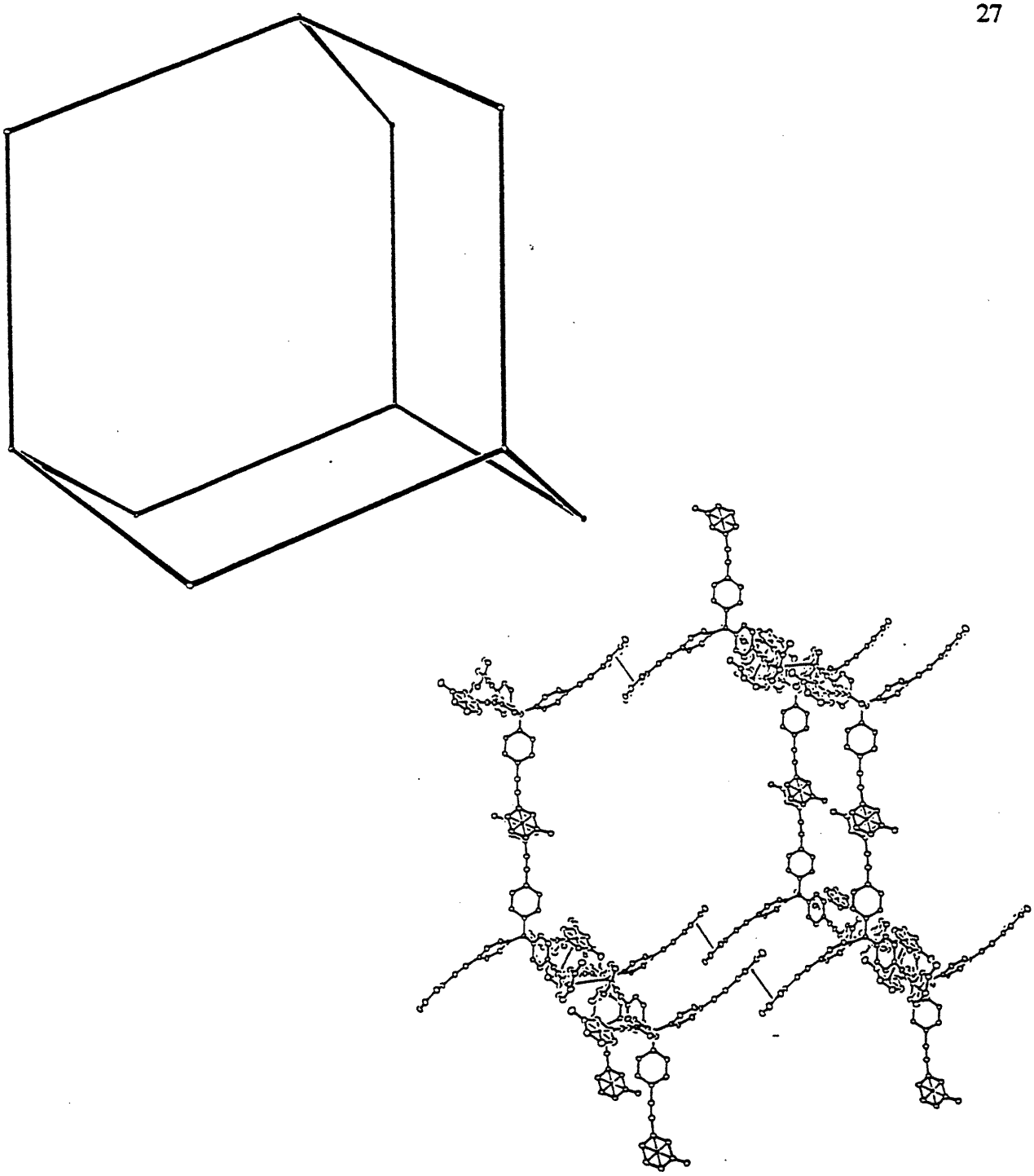

Figure 13. ORTEP drawing of part of the diamondoid network present in crystals of tecton I•8 $CH_3CH_2CO_2H$. The tetrahedral centers of the ten tectons shown in the drawing define a slightly distorted adamantane, shown on top. Non-hydrogen atoms are represented by ellipsoids corresponding to 50% probability. Propionic acid and all hydrogen atoms are omitted for clarity.

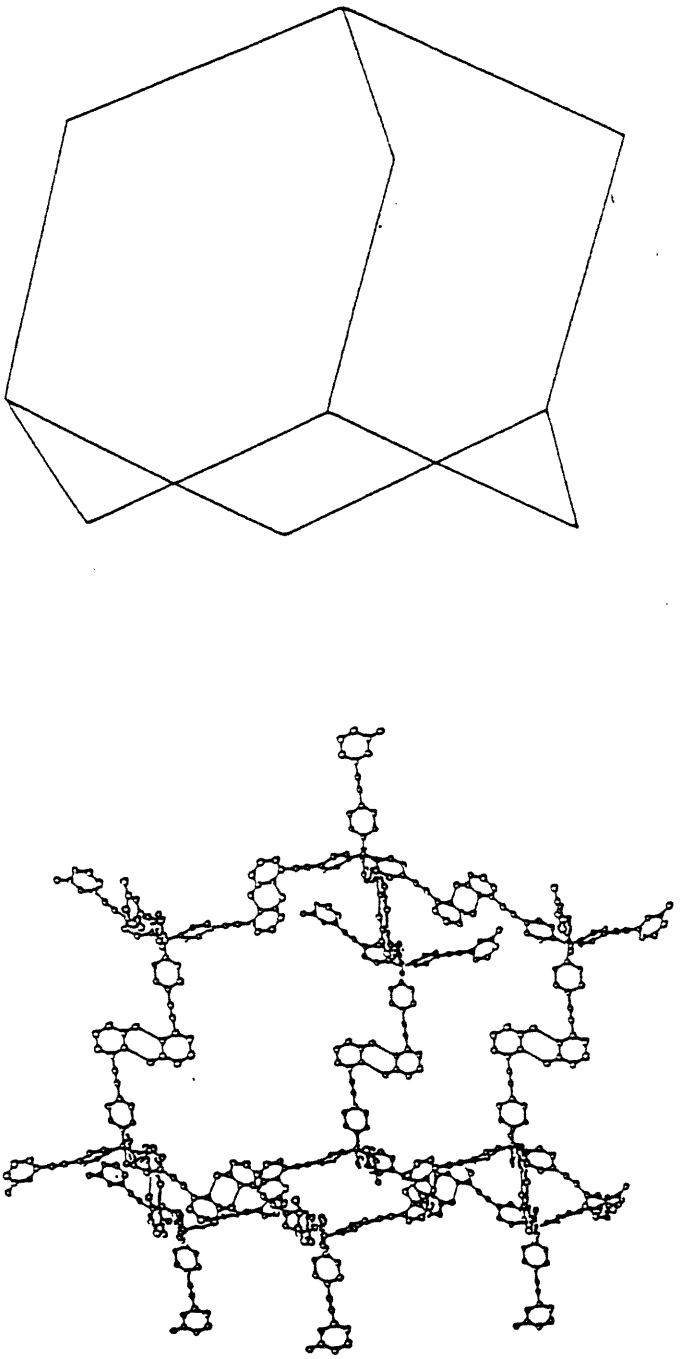

Figure 14. ORTEP drawing of part of the diamondoid network present in crystals of tecton I•2 $CH_3CH_2CH_2CO_2H$. The tetrahedral centers of the ten tectons shown in the drawing define a distorted adamantane, shown on top . Non-hydrogen atoms are represented by ellipsoids corresponding to 50% probability. Butyric acid and all hydrogen atoms are omitted for clarity.

2.4. The crystal structure of tecton I•8 CH_3CH_2COOH

In the crystal structure of tecton I•8 CH_3CH_2COOH, we find discrete adduct **39** (Figure 15) in which each of the four sticky pyridone sites associates with two molecules

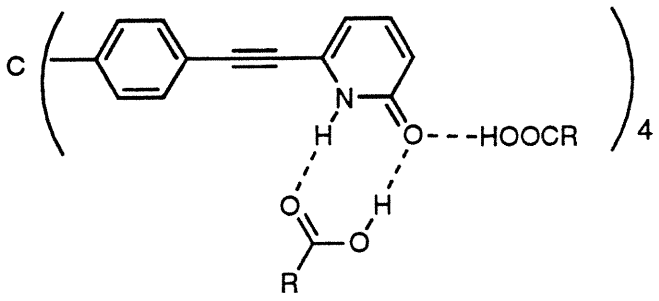

39 (R = CH_2CH_3)

of carboxylic acid (Figure 16). This was unexpected and a bit disappointing, since the strong tendency of pyridones and related heterocycles to self-associate had served as a reliable guiding principle in the successful design of simpler tectons[10f-g]. However, it still gave us a lot of information to help us understand the behavior of tecton **I** either in solution or in the solid state.

At first we did not realize that the discrete adduct **39** actually associates via π-stacking, leading to the self-assembly of aggregates with a superdiamondoid framework. As a pattern of molecular recognition, hydrogen bonding is a more directional and stronger intermolecular interaction than π–π interaction[24-25], although the latter has been known for over half a century and is widely investigated and used in chemistry, biology, and material science as an important and attractive class of intermolecular force. From Figure 17 we can see that all possibilities of forming intermolecular hydrogen bonds between the tectons in order to induce self-assembly of superdiamond aggregates are forbidden by the

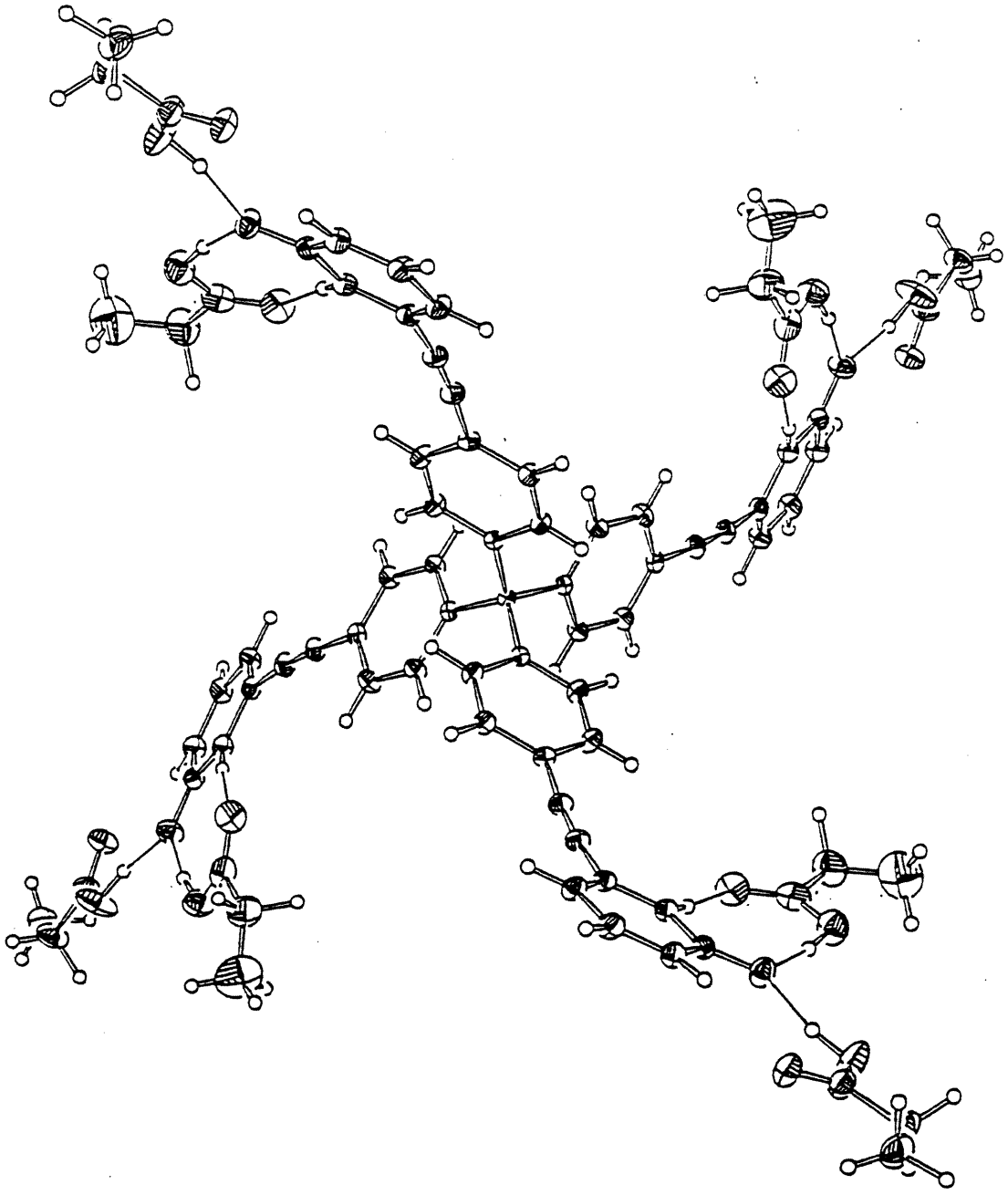

Figure 15. Complete adduct **39** viewed down the **c** axis. Non-hydrogen atoms are represented by ellipsoids corresponding to 50% probability. Hydrogen atoms are represented by spheres of arbitrary size.

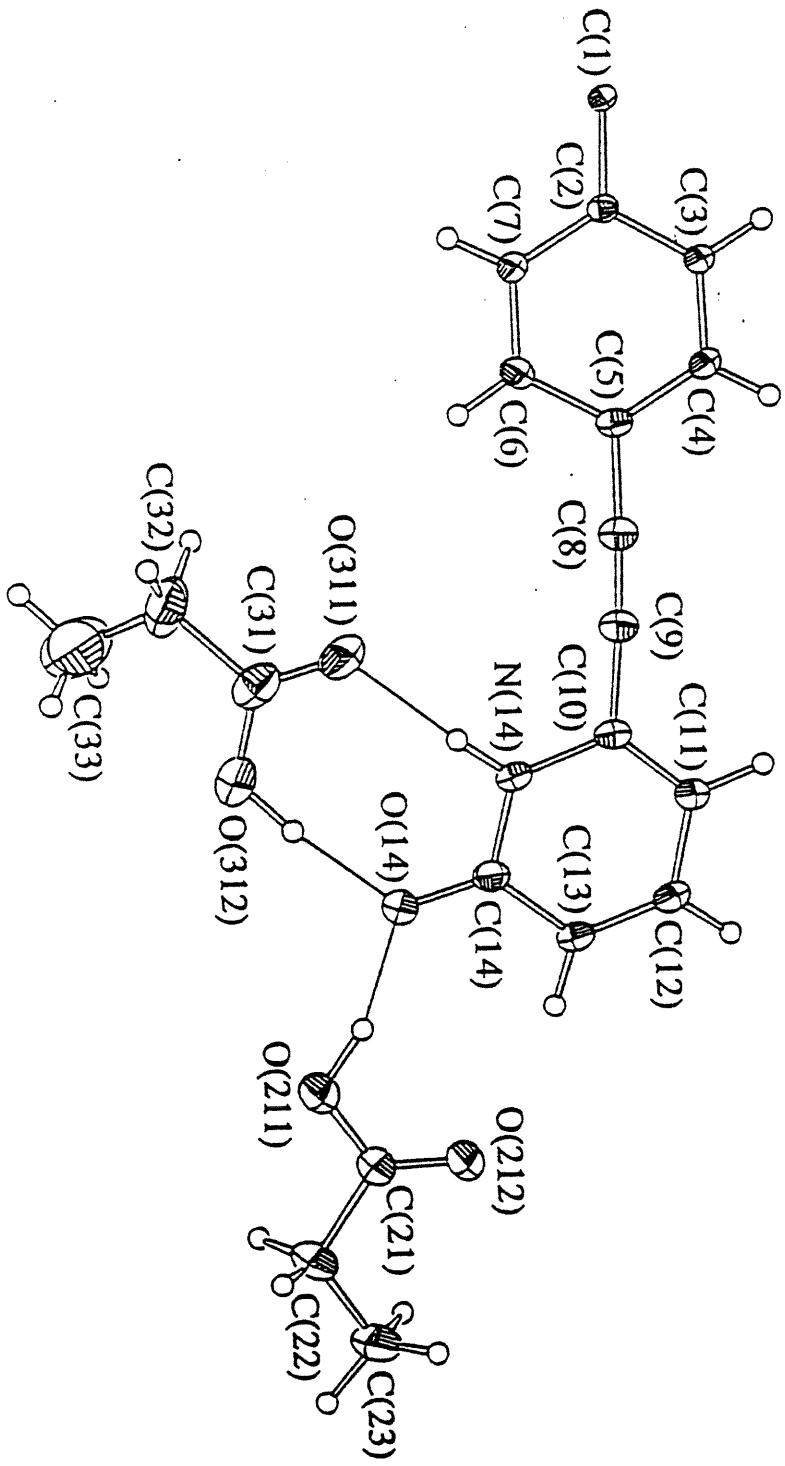

Figure 16. The asymmetric unit present in crystals of tecton I•8 $CH_3CH_2CO_2H$. Non-hydrogen atoms are represented by ellipsoids corresponding to 50% probability, and hydrogen atoms by spheres of arbitrary size.

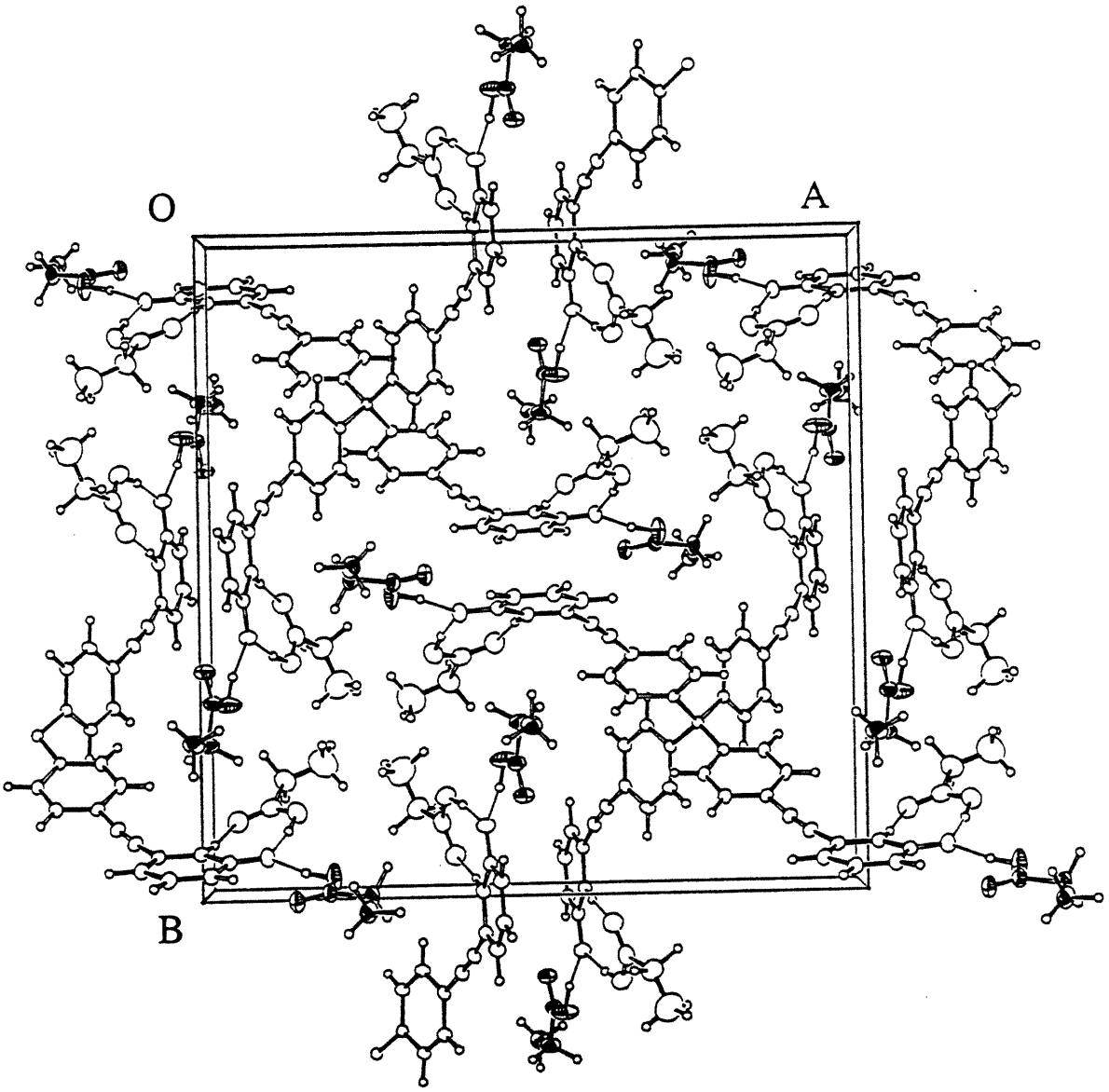

Figure 17. ORTEP view of the packing arrangement of tecton **I**•8 $CH_3CH_2CO_2H$ along the **c** axis. Non-hydrogen atoms are represented by ellipsoids corresponding to 50% probability, and hydrogen atoms by spheres of arbitrary size.

association of tecton **I** with propionic acids. It seems that adduct **39** packs along the crystallographic c axis to form a column and then these columns dovetail in the other two dimensions according to close-packing principles to give the final crystal structure. This yields a channel defined by four neighboring tectons, which is fully filled with molecules of propionic acid. Two pyridone rings from neighboring tectons interact by overlapping each other to form a stable π-stacking arrangement. Close inspection reveals that the crystal structure of tecton **I**•8 $CH_3CH_2CO_2H$ is constructed of diamondoid networks that are induced not by hydrogen bonding but by π-stacking of pyridone rings.

The geometry of π-π interaction adopted by tecton **I** may be summarized in the following way: (1) The π-systems of two pyridone rings from neighboring tectons **I** are antiparallel with opposed dipoles of the carbonyl group of pyridone and with an interplanar separation of 3.35 Å (Figures 18 and 19). (2) The center-to-center distance between the π-stacked pyridones is 3.73 Å (Figures 20 and 21). (3) One pyridone ring is center-to-center offset relative to the other by 1.64 Å along the orientation of the carbonyl group of pyridone (Figure 22). (4) The π-stacked pyridones are not rotated relative to one another.

A superadamantane framework cut out of one diamondoid lattice formed by the π-stacked tecton **I** is shown in a different way in Figures 23 . Because the edge of the framework, which is defined as the distance between the centers of two neighboring π-stacked tectons, is as long as 19.44 Å, huge open spaces are evidently created by the architecture and are filled by five other symmetry-equivalent diamondoid lattices so that the degree of interpenetration turns out to be six. The six interlaced diamondoid lattices are translationally equivalent. They interpenetrate each other along the c axis with the translation distance of the cell edge c=7.787 Å, as shown in Figure 24. Although the degree of interpenetration (6) is even higher than the highest degree observed by Ermer (5)[13a], large channels are still formed in the direction of translation of the interlocking diamondoid networks (Figures 25 and 26). Figures 25 and 26 show views along the c axis

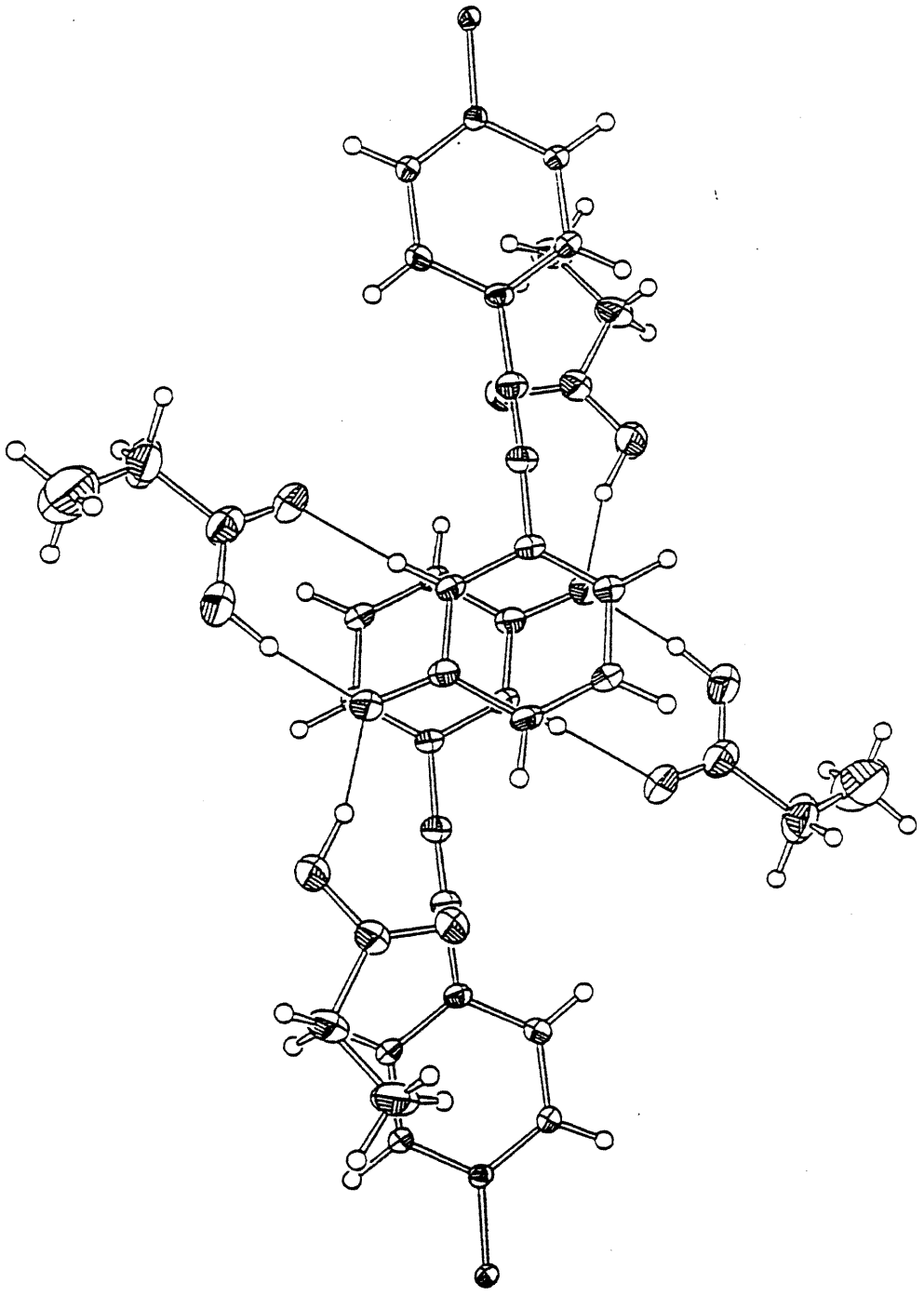

Figure 18. Top view of the intertectonic π-stacking observed in the crystal structure of tecton **I**•8 $CH_3CH_2CO_2H$. Only the asymmetric unit of two neighboring tectons **I**•8 $CH_3CH_2CO_2H$ is shown. Non-hydrogen atoms are represented by ellipsoids corresponding to 50% probability, and hydrogen atoms by spheres of arbitrary size.

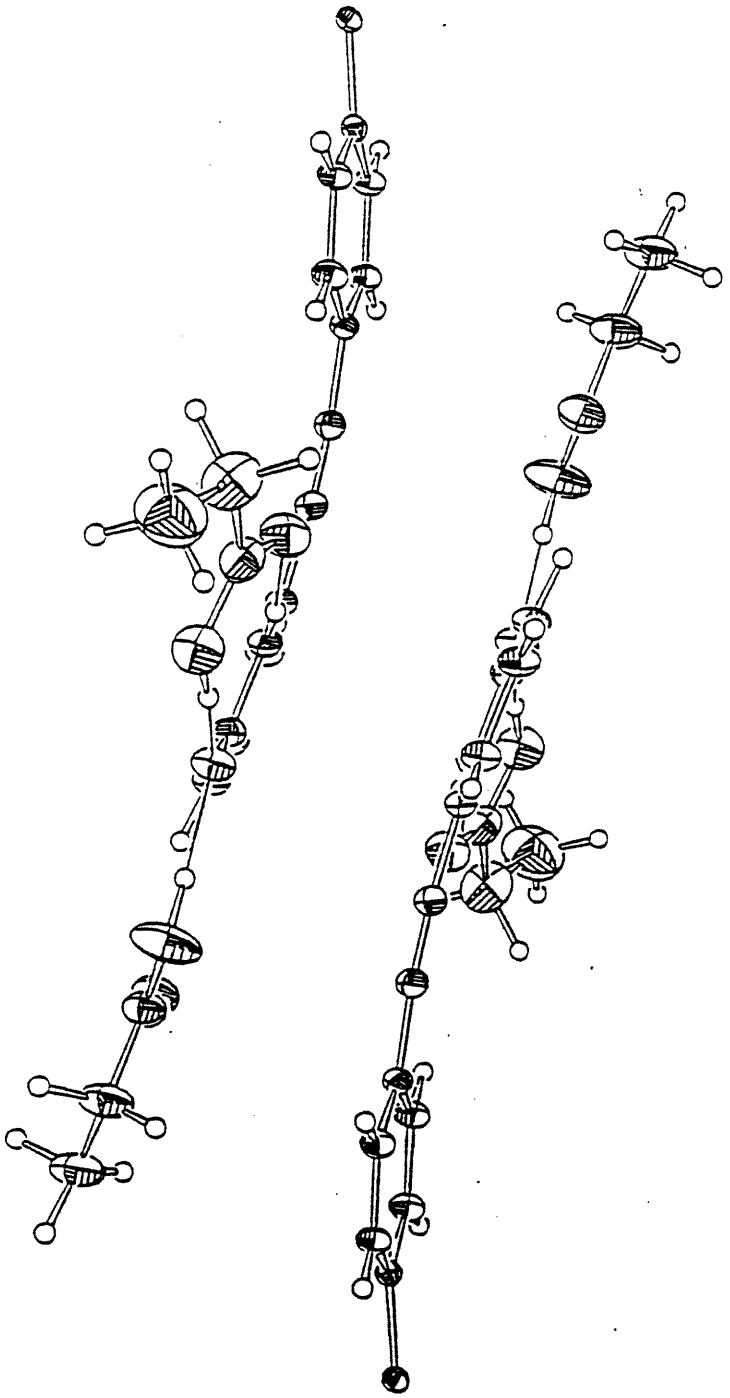

Figure 19. Side view of the intertectonic π-stacking observed in the crystal structure of tecton **I**•8 $CH_3CH_2CO_2H$. Only the asymmetric unit of two neighboring tectons **I**•8 $CH_3CH_2CO_2H$ is shown. Non-hydrogen atoms are represented by ellipsoids corresponding to 50% probability, and hydrogen atoms by spheres of arbitrary size.

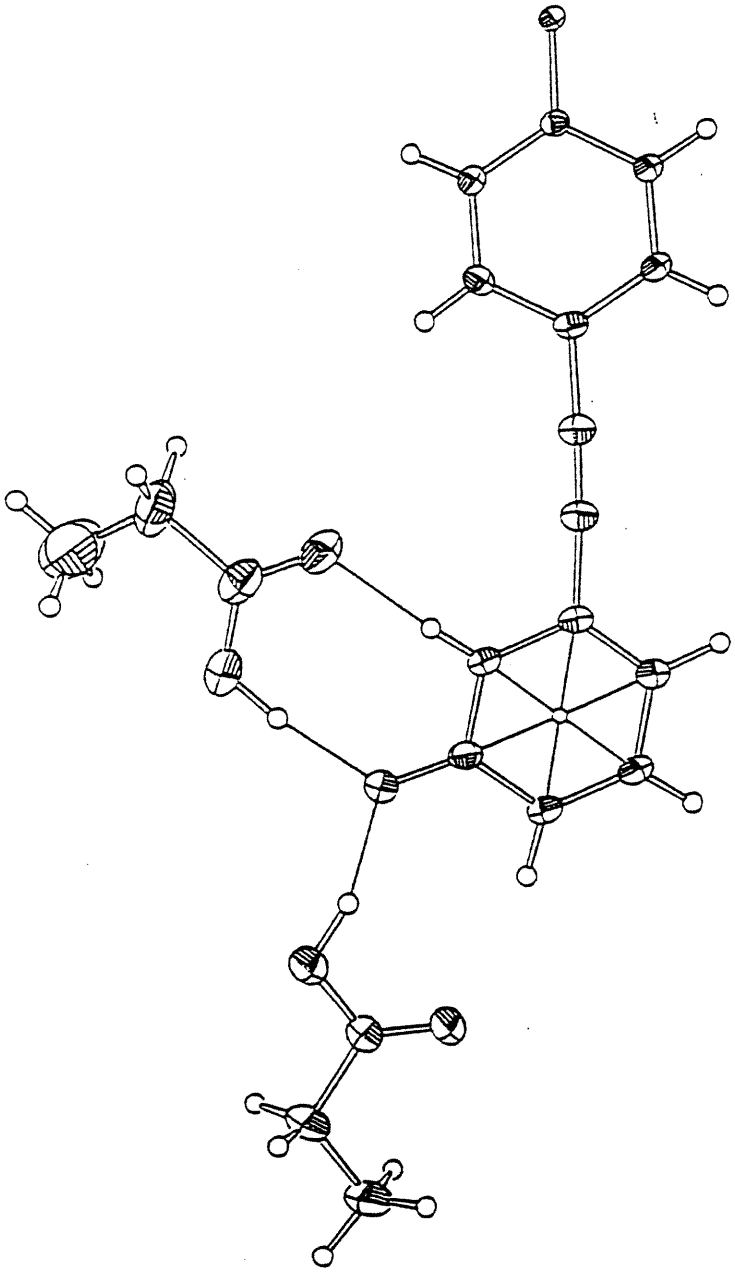

Figure 20. The asymmetric unit present in crystals of tecton I•8 $CH_3CH_2CO_2H$, showing the center of the pyridone ring defined in the crystal structure. Non-hydrogen atoms are represented by ellipsoids corresponding to 50% probability, and hydrogen atoms by spheres of arbitrary size.

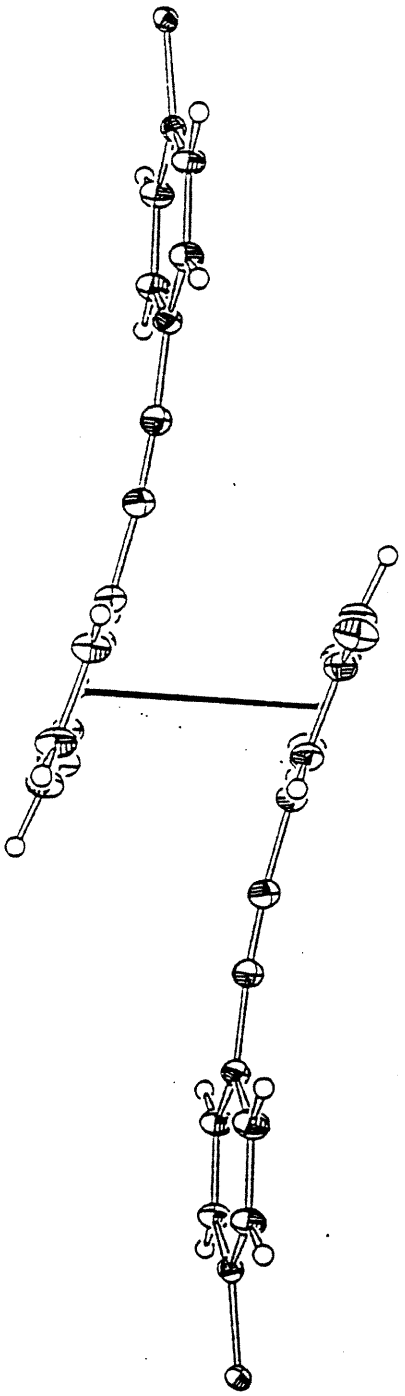

Figure 21. Side view of the intertectonic π-stacking observed in the crystal structure of tecton **I**•8 $CH_3CH_2CO_2H$, showing the centre-to-centre distance between π-stacked pyridone rings defined in the crystal structure. Propionic acid is omitted for clarity.

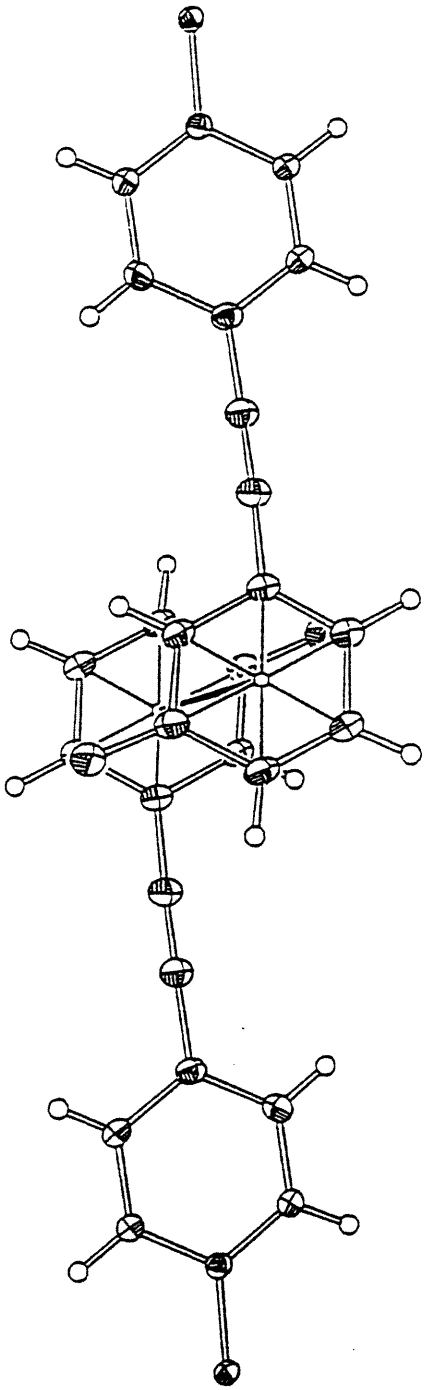

Figure 22. Top view of the intertectonic π-stacking observed in the crystal structure of tecton I•8 $CH_3CH_2CO_2H$, showing the centre-to-centre offset along the dipole orientation of the carbonyl group of pyridone. Propionic acid is omitted for clarity.

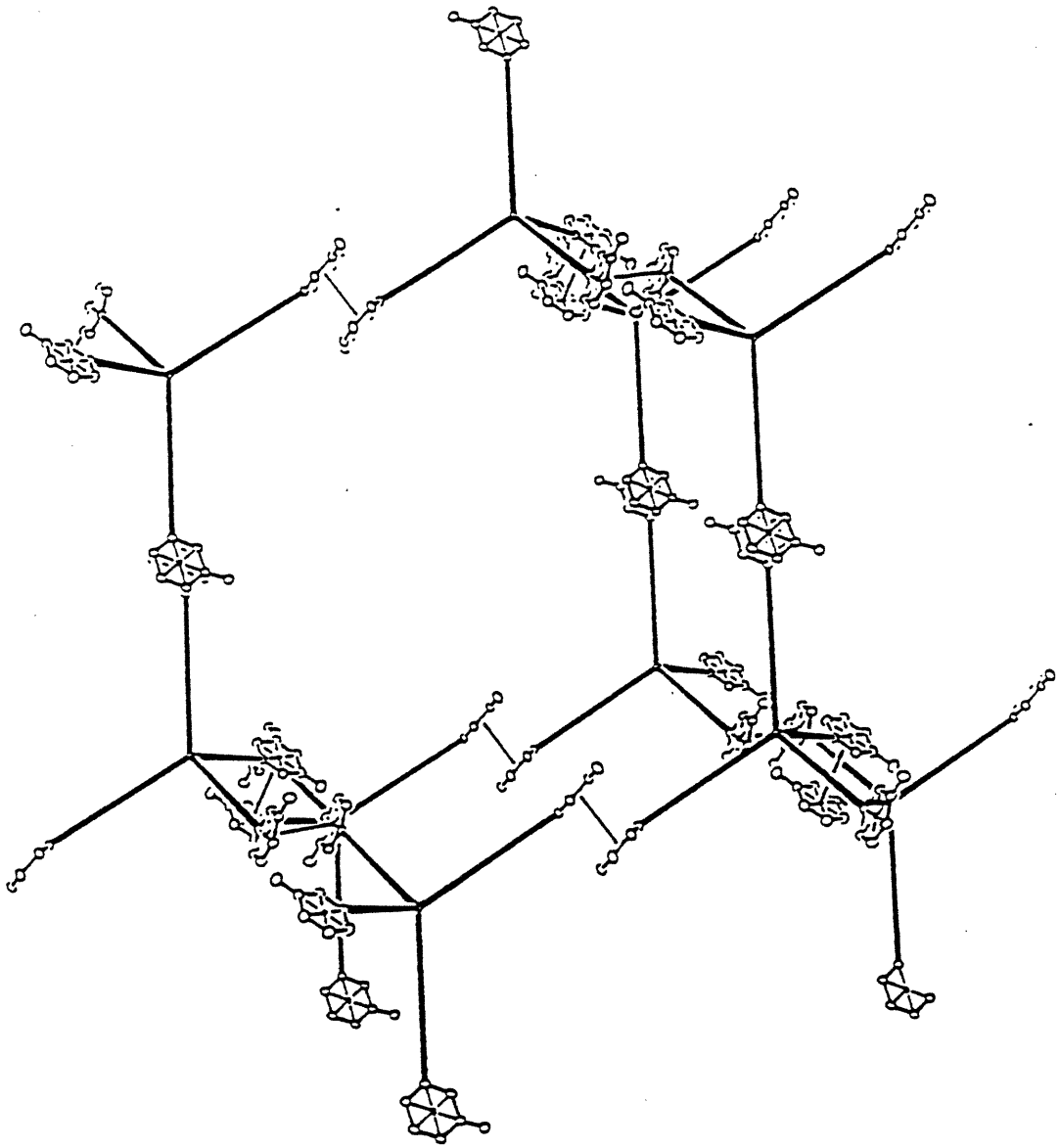

Figure 23. View of the superadamantane framework of tecton I•8 $CH_3CH_2CO_2H$ cut out of one diamondoid lattice induced by π-stacked tectons whose tetrahedral core structures are represented by solid sticks.

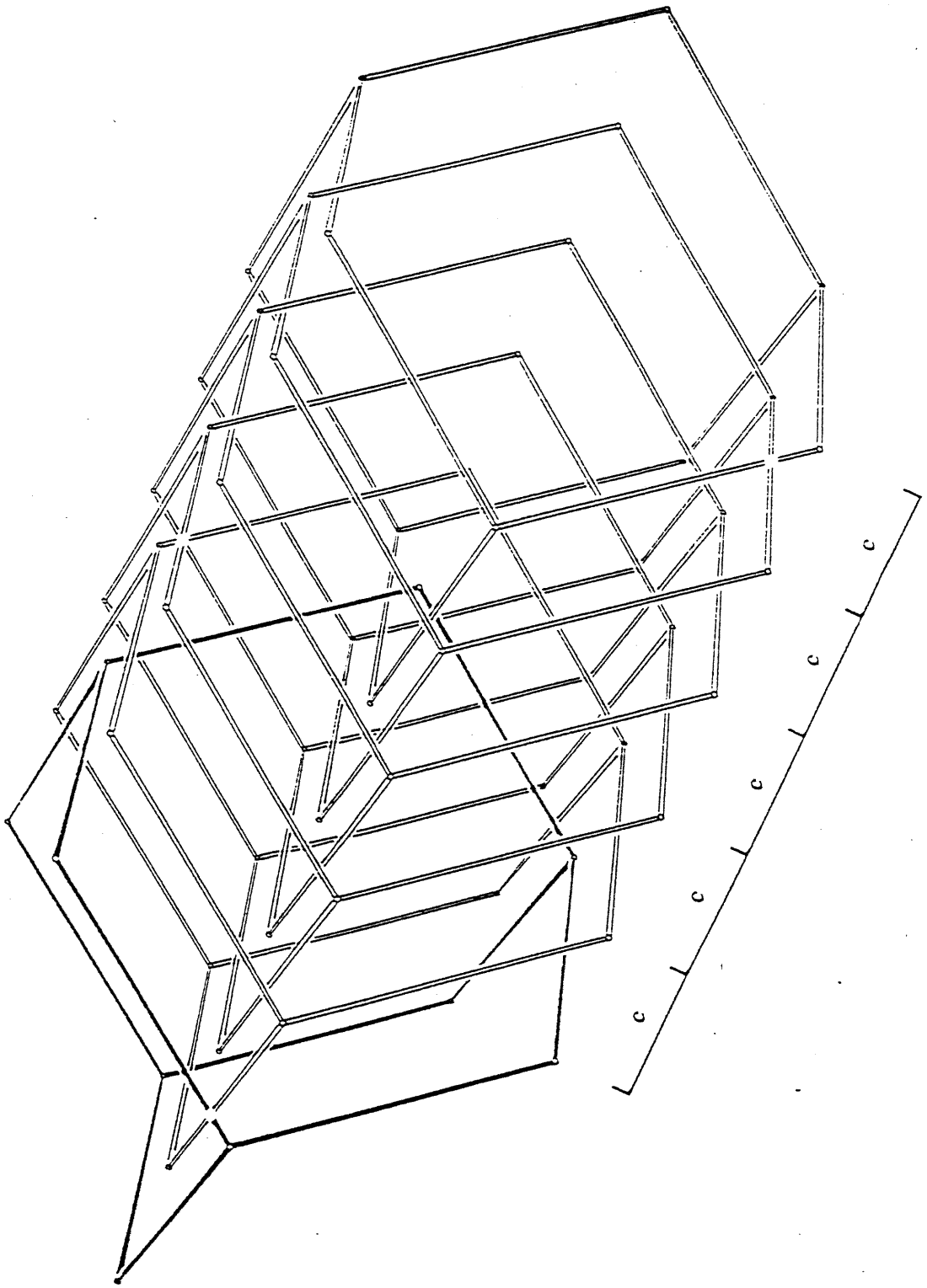

Figure 24. Schematic view of the six interpenetrating diamondoid networks present in tecton **I**•8 $CH_3CH_2CO_2H$, each represented by one superadamantane framework . They interpenetrate each other along the **c** axis translational-equivalently. Only the central carbon atoms of tecton **I** are shown. The interconnecting rods symbolize the π-stacked asymmetric units of two neighboring tectons as shown in Figure 22.

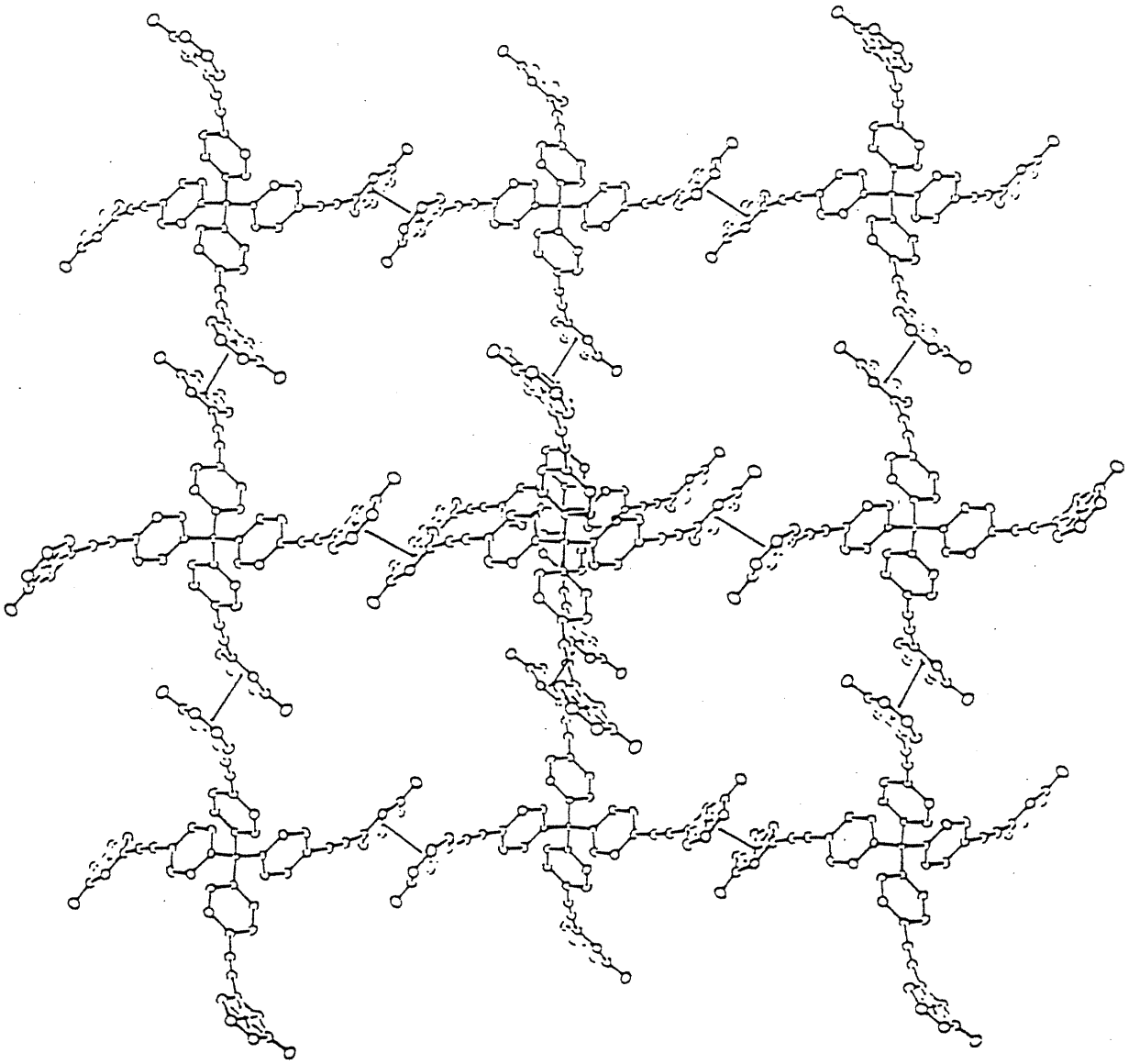

Figure 25. View of a π-stacked superadamantane unit of a diamondoid lattice of tecton **I**•8 $CH_3CH_2CO_2H$ down the **c** axis. Propionic acid is omitted for clarity.

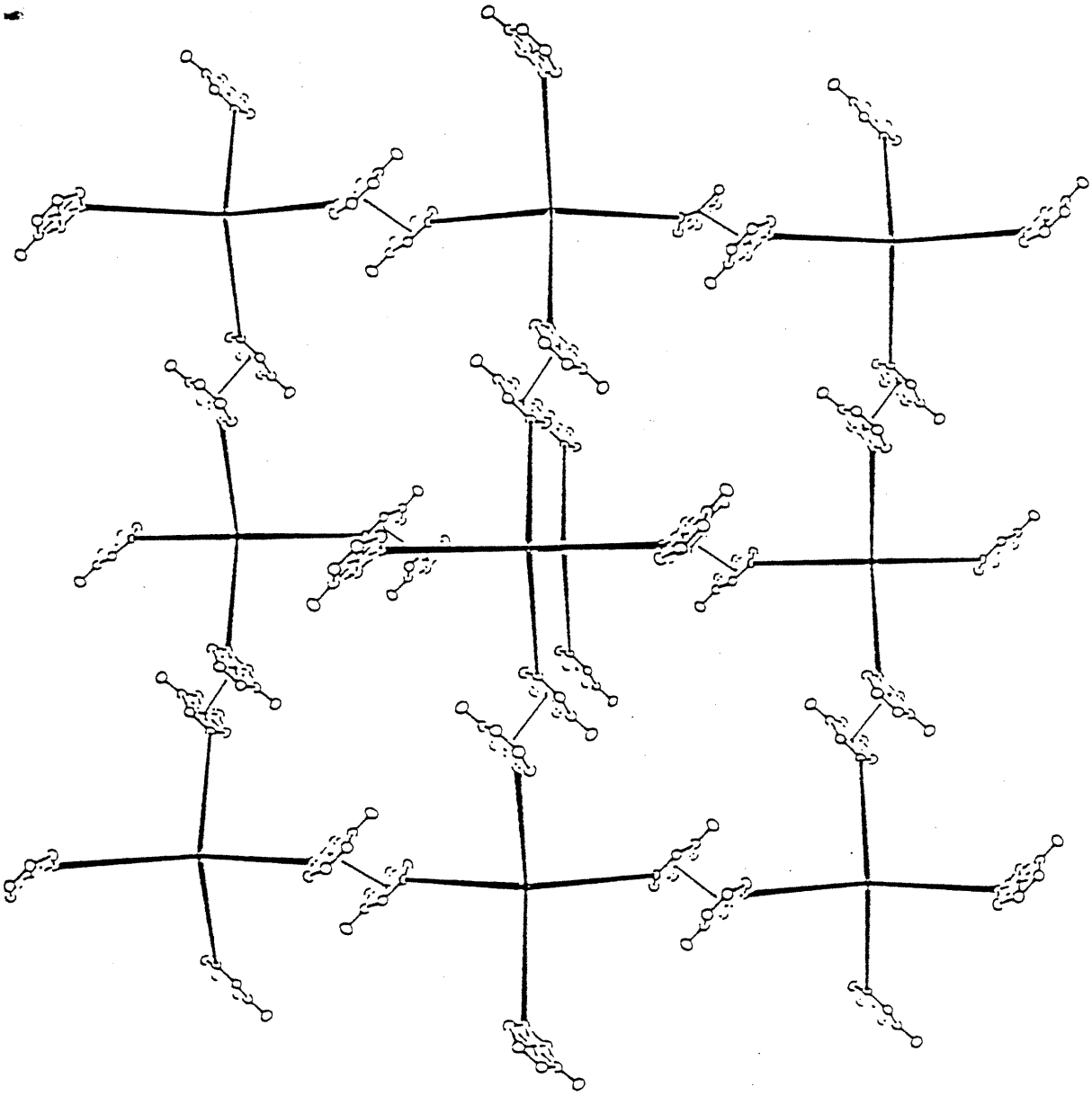

Figure 26. Schematic veiw of a π-stacked superadamantane unit of the diamondoid lattice of tecton **I**•8 $CH_3CH_2CO_2H$ down the **c** axis, in which the core structure of tecton **I** is represented by four tetrahedrally oriented solid sticks for clarity.

of one superadamantane framework cut out of a diamondoid lattice. In Figure 26, the detailed core structures of the tectons are simplified and represented by solid sticks. Four very spacious channels are well-defined by π-stacked tectons which are filled with molecules of propionic acid. In Figures 27 and 28, an individual four-sided channel present in the diamondoid lattices is shown in either cylinder-ball or space-filling stereoviews. In order to avoid a high degree of hollowness, a large number of molecules of acetic or propionic acid could be enclathrated in these channels. However, this would cause a highly unfavorable entropy of enclathration. In this situation, there seem to be two choices: (1) the diamondoid lattice collapses and a non-diamondoid structure is generated by adopting another packing mode; or (2) the unfavorable entropy of enclathration is overcome by formation of as many hydrogen bonds as possible.

In our case, tecton **I** was crystallized from a mixed solvent system mainly containing carboxylic acid. This makes things more complicated because the carboxylic acid is not only the solvent but a hydrogen-bond donor and acceptor also. There must be a competition involving hydrogen bonding and molecular recognition between various molecules in the system. One of the hydrogen-bonding rules suggested by Etter[3b] is that the best hydrogen-bond donor and the best hydrogen-bond acceptor will preferentially form hydrogen bonds to one another. Because the carbonyl oxygen in an amide is a stronger acceptor than the carbonyl oxygen in an acid, and because the OH group in an acid is a stronger donor than the NH group of an amide, hydrogen-bond preferences may be expected to help direct the co-assembly of tecton **I** and carboxylic acids to form the mixed aggregate presented in Figure 15. Similar doubly hydrogen-bonded systems have been found in N-acyl amino acids and other amide-acid crystals, and their influence on crystal packing patterns has been studied[2j]. It was indicated that doubly hydrogen-bonded amides are more stable than the singly hydrogen-bonded ones by average values of 2.1 to 3.2 kcal/mol , after the "hydrogen-bonding energies" of these motifs were calculated as they

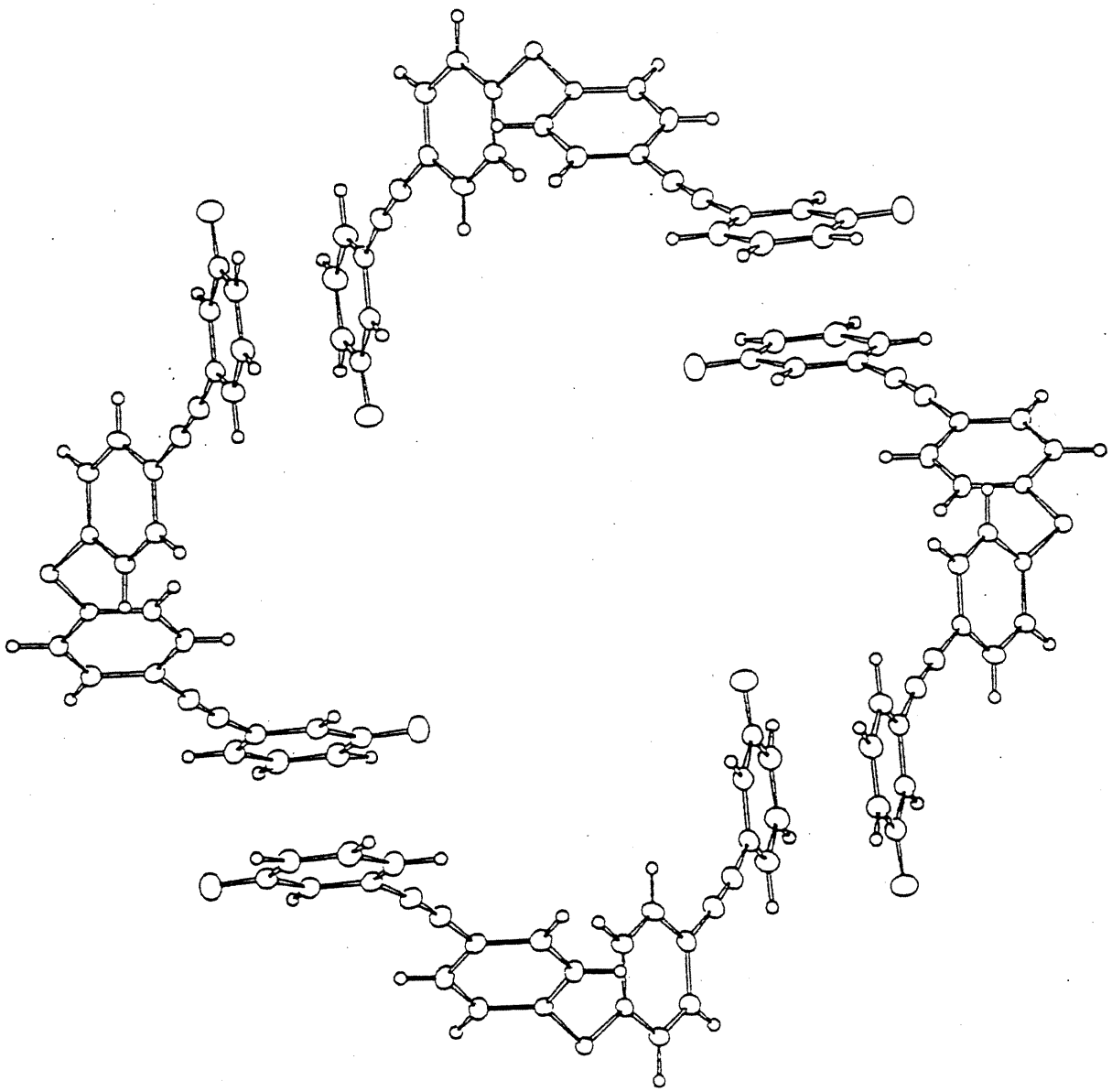

Figure 27. View down the **c** axis of an individual four-sided channel present in the diamondoid lattices of tecton **I**•8 $CH_3CH_2CO_2H$.

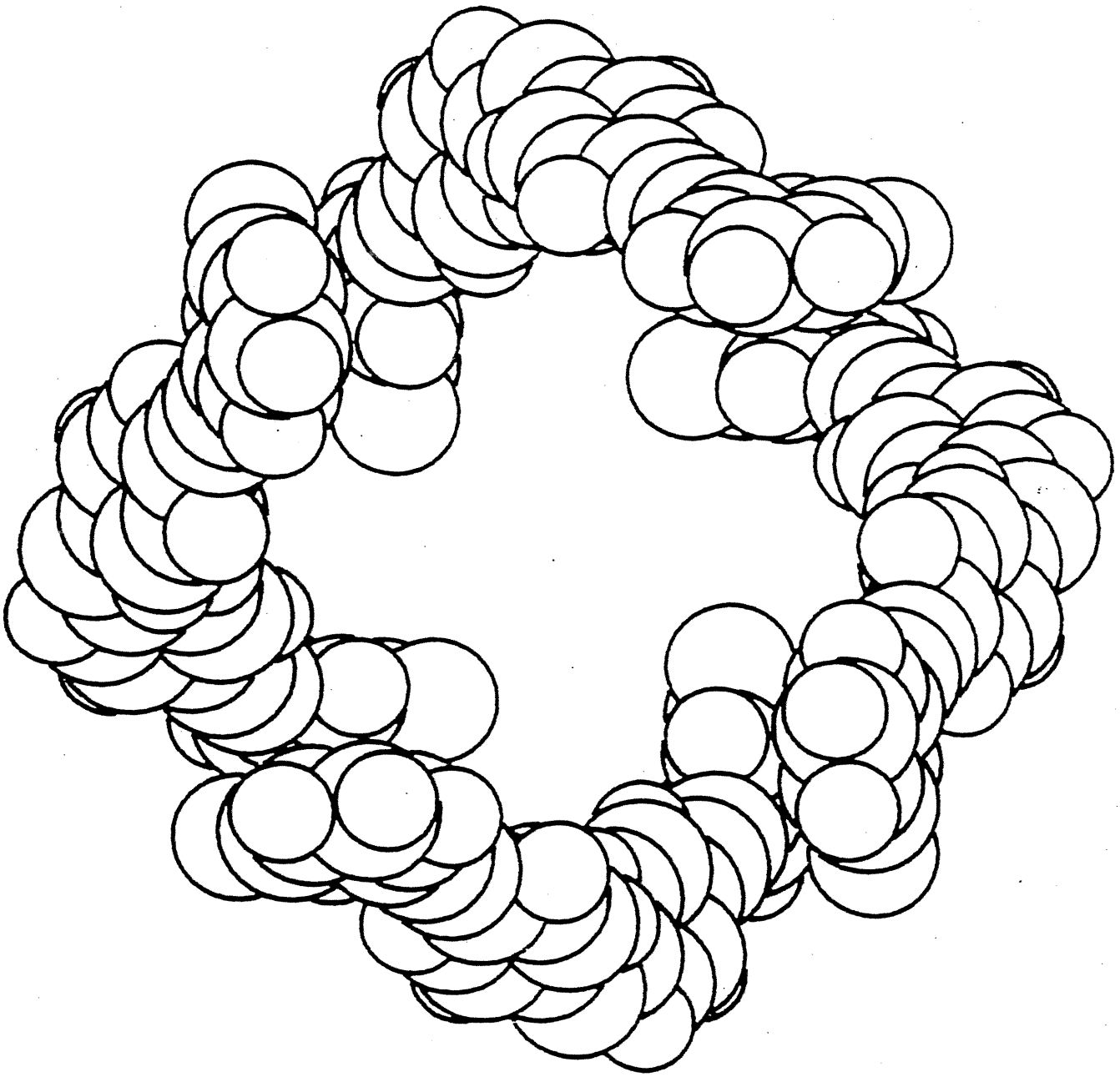

Figure 28. Space-filling view (down the **c** axis) of an individual four-sided channel present in the diamondoid lattices of tecton **I**•8 $CH_3CH_2CO_2H$.

appear in their crystal structures. Apparently, the energetically favored hydrogen-bonding patterns are adopted preferentially under this set of conditions in order to avoid the entropically unfavorable enclathration, and that is why the normal pairwise hydrogen-bonding pattern between pyridones is interrupted. From Figure 15 we can see that in adduct **39**, each pyridone ring is hydrogen-bonded with two molecules of propionic acid. The striking affinity of the carbonyl groups of pyridones for carboxylic acids may be a very useful characteristic in molecular recognition. We will see later how this important property of tecton **I** causes carboxylic acids to become enclathrated selectively in channels of diamondoid networks.

If the hydrogen bonds are strong enough to form diamondoid networks at the expense of the forces of close packing, the space defined by the networks will be forced to accommodate molecules of solvents or other guests. As mentioned above, since acetic acid is a relatively small molecule, a corresponding large number will be needed to fill the voids in an open diamondoid network. Therefore, the failure of tecton **I** to form the expected hydrogen-bonded networks in acetic and propionic acid might be partially attributed to an especially unfavorable entropy of enclathration. In order to avoid this problem, we decided to try to use larger acids, expecting to diminish the unfavorable entropy of enclathration by decreasing the number of enclathrated guest molecules.

One of the consequences of close-packing is that chemically distinct molecules with the same shape and volume should have identical crystal structures. Empty spaces between close-packed molecules are significant since they may be partially filled by larger substituent groups in crystal structures of closely related molecules. Therefore, this concept of structural flexibility is used widely in solid-state chemistry, topochemistry, and structural mimicry. This means that unoccupied space in a close-packed crystal structure may be used to slightly modify the shape or volume of the molecule within limits without a change in the crystal structure. In the light of this, it is not surprising that tecton **I**•8 $CH_3CH_2CO_2H$ and tecton **I**•8 CH_3CO_2H have the same crystal structure. However, we

wondered whether tecton **I**•8 $CH_3CH_2CH_2CO_2H$ would also result in the same type of crystal when butyric acid is employed as solvent. We assumed that if larger carboxylic acids were used as solvents, at some point the channel might become too crowded to be tolerated by the structural flexibility of the π-stacked crystal structure. If so, it may collapse and another packing mode involving hydrogen bonding may be forced to be generated by the driving force of adopting more energetically favorable molecular aggregation patterns. In fact, crystallization from butyric acid yielded crystals with a new stoichiometry, tecton **I**•2 $CH_3CH_2CH_2CO_2H$.

2.5. The crystal structure of tecton I•2 $CH_3CH_2CH_2CO_2H$

The best way to analyze the crystal structure of tecton **I**•2 $CH_3CH_2CH_2CO_2H$ may be by comparing it with the structure of tecton **I**•8 $CH_3CH_2CO_2H$. Ermer indicated that the diamondoid crystal packing of tetraacid **33** cannot be of perfect cubic symmetry, since the molecular symmetry is too low and threefold symmetry axes are not possible. The extent of deviation from ideal symmetry may be dependent upon the rigidness of the tetrahedral core structures of tectons and the orientation of functional groups attached to the core structure. However, in our case, when tecton **I** is crystallized from different carboxylic acids, structures belonging to crystal systems of different symmetry are obtained. This phenomenon indicates that tecton **I** may have different molecular symmetry in crystals obtained under different condition. The extent of deviation of the observed diamondoid lattice depends on the rigidness and symmetry of tectons. Alternatively, the tectonic molecular symmetry may be determined by the packing environment. From Figures 13 and 14 we can see that diamondoid lattices built up of hydrogen-bonded tectons

are more distorted than those formed from π-stacked tectons. In Table 1, the symmetry both of their crystal system and of individual tectons themselves are listed. It will be shown

Table 1. Symmetry of crystal system and individual tectons

	Tecton **I**•8 $CH_3CH_2CO_2H$	Tecton **I**•2 $CH_3CH_2CH_2CO_2H$
crystal system	tetragonal	monoclinic
space group	$P4_2/n$	C2/c
molecular symmetry	S_4	C_2

later how the crystal packing environment in turn affects the molecular symmetry of tecton **I**.

It is known that intramolecular non-bonded interactions between carbon and hydrogen atoms are responsible for the adoption of certain preferred conformations in crystals. They must be taken into account when predicting crystal structures of flexible molecules. Compared with Ermer's tectons, tecton **I** is more flexible. Its molecular symmetry is decided by not only the conformations of the pyridone rings with respect to the core structure but the conformations of phenyl rings of the core structure itself respect to one another as well. The pyridone rings are essentially planar, and their conformation with respect to the core structure may be characterized through the C(16)-C(15)-C(110)-N(114) torsion angle and the other three corresponding angles (shown in Figure 29). The conformations of the phenyl rings with respect to one another may be defined through the C(13)-C(12)-C(1)-C(22) torsion angle and related angles. Another very important conformation is that of the pyridone rings with respect to the frame of a diamondoid lattice and may be characterized through the N(114)-C(110)-C(1)-C(210) torsion angle shown in

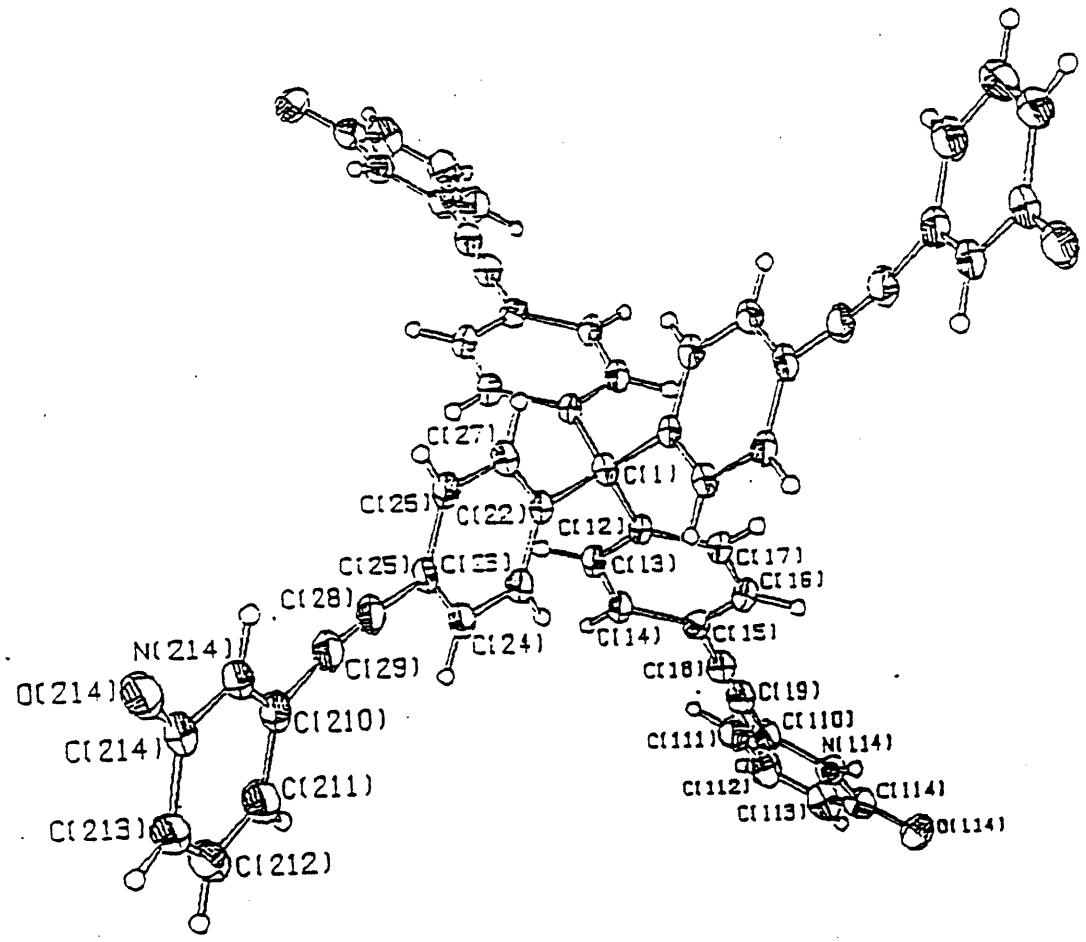

Figure 29. ORTEP view of tecton I•2 $CH_3CH_2CH_2CO_2H$ viewed down the **b** axis showing the numbering scheme. Non-hydrogen atoms are represented by ellipsoids corresponding to 50% probability. Hydrogen atoms are represented by spheres of arbitrary size.

Table 2. Conformations existing in the crystal structures of **I**•8 $CH_3CH_2CO_2H$ and **I**•2 $CH_3CH_2CH_2CO_2H$

Conformations	**I**•8 $CH_3CH_2CO_2H$	**I**•2 $CH_3CH_2CH_2CO_2H$
C(16)-C(15)-C(110)-N(114)	12.5 (3)°	4.6 (6)°, 27.4 (6)°
C(13)-C(12)-C(1)-C(22)	66.8 (3)°	68.3 (6)°, 65.6 (6)°
N(114)-C(110)-C(1)-C(210)	5.9 (3)°, 102.3 (3)°	24.0 (6)°, 83.6 (6)°

Ermer has described the deviation of diamondoid lattices as *elongation* or *compression.*[13a] From Figure 30 we can see that a diamondoid lattice can be defined by

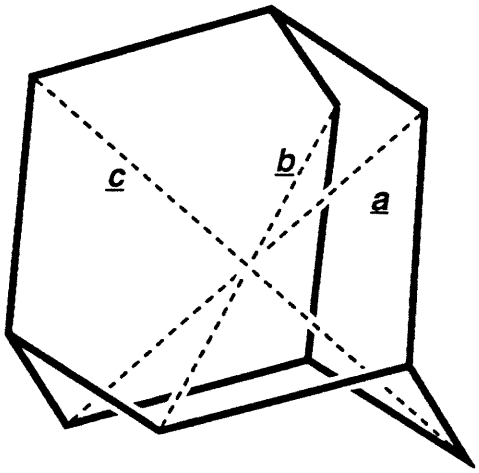

Figure 30. A diamondoid lattice showing its three dimensional indices.

three dimensional indices which are arbitrarily described as $\underline{a}$, $\underline{b}$ and $\underline{c}$. If they are the same in distance, a cubic crystal system will be generated. That is what is found in diamond itself. If one of them is either longer or shorter than the other two, a tetragonal crystal system will be obtained and a distorted diamondoid lattice is brought about. The deformation of the lattice is described as *elongation* when one index is longer than the other two, and as *compression* when it is shorter. In the case of tecton **I**•2$CH_3CH_2CH_2CO_2H$, a more highly distorted diamondoid lattice is formed since none of the three indices is equal to another and a monoclinic crystal system is favored. The relationship between the dimensional indices of diamondoid lattices and the observed crystal systems is shown in Table 3. A compression of diamondoid lattices occurs in

Table 3. Relationship between the dimensional indices of diamondoid lattices and crystal systems

Dimensional Indices	Crystal System	Examples
$\underline{a} = \underline{b} = \underline{c}$	Cubic	Diamond
$\underline{a} = \underline{b} \neq \underline{c}$	Tetragonal	Ermer's tectons **34-38** and **I**•8$CH_3CH_2CO_2H$
$\underline{a} \neq \underline{b} \neq \underline{c}$	Monoclinic	**I**•2$CH_3CH_2CH_2CO_2H$

the crystal structure of Ermer's tecton **33**, while an elongation is found in tecton **38**, **I**•8$CH_3CH_2CO_2H$ and **I**•2$CH_3CH_2CH_2CO_2H$. In Table 4, the dimensional indices of distorted diamondoid lattices of **I**•8$CH_3CH_2CO_2H$ and **I**•2$CH_3CH_2CH_2CO_2H$ are listed. In light of the unit cell dimensions and the degrees of interpenetration, the distorted diamondoid lattices of tecton **I**•8$CH_3CH_2CO_2H$ and tecton **I**•2 $CH_3CH_2CH_2CO_2H$ can be easily defined as shown in Figures 31 and 32. Both in the crystal structures of **I**•8$CH_3CH_2CO_2H$ and of **I**•2 $CH_3CH_2CH_2CO_2H$, the interpenetration of the symmetry-

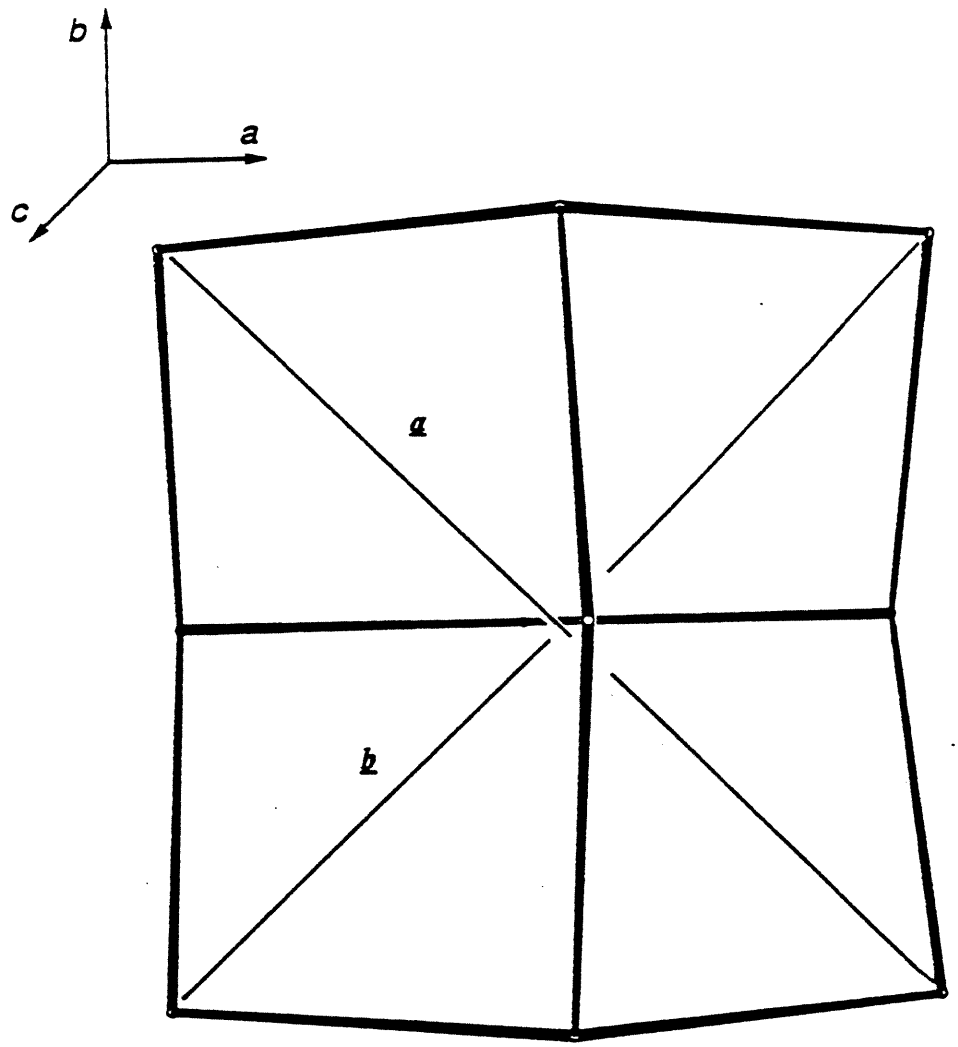

Figure 31. Projection (down the **c** axis) of an individual superadamantane cut out of a diamondoid lattice in tecton I•8 $CH_3CH_2CO_2H$. Only the central carbon atoms of tecton I are shown. The interconnecting rods symbolize the intertectonic hydrogen bonding. The labels ***a*** and ***b*** represent the dimensions of the distorted diamondoid lattice, and **a**, **b**, and **c** represent the crystallographic axes.

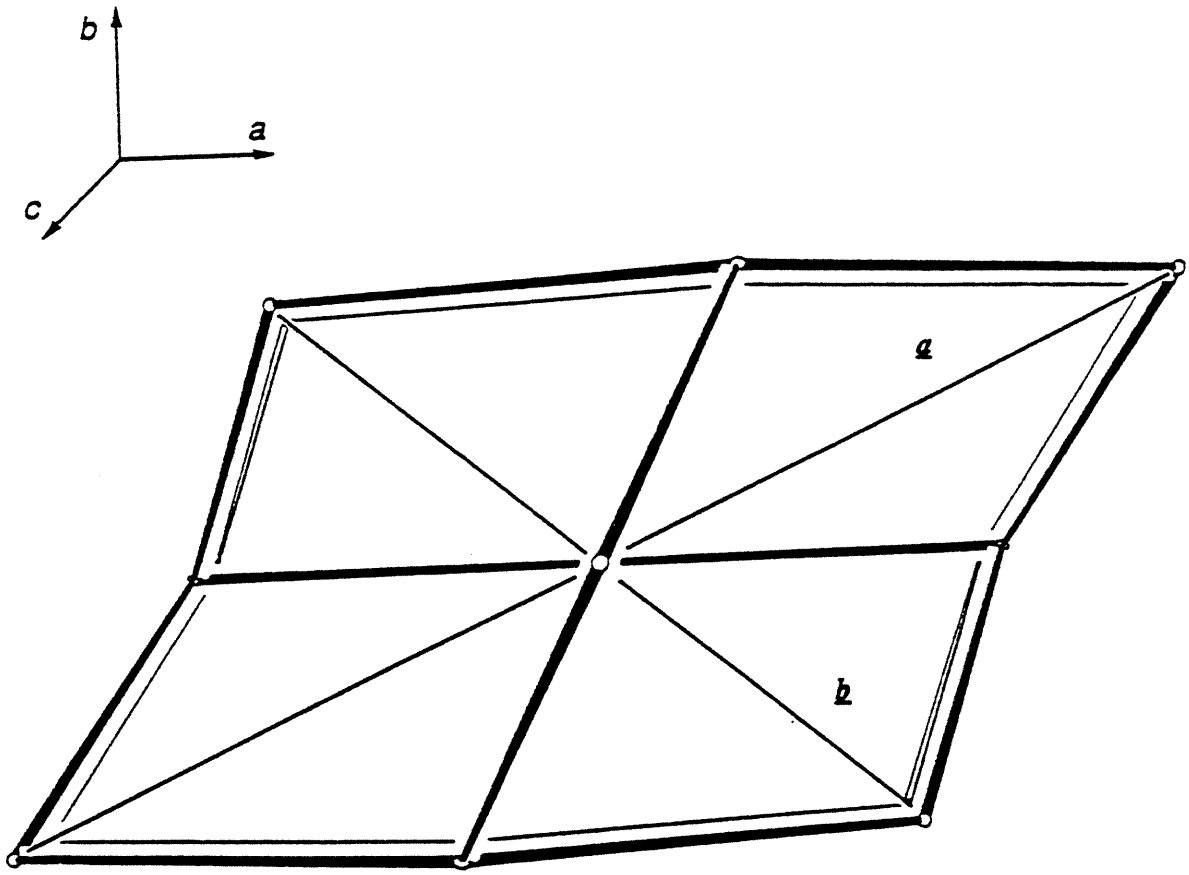

Figure 32. Projection (down the **b** axis) of an individual superadamantane cut out of a diamondoid lattice in tecton I•2 $CH_3CH_2CH_2CO_2H$. Only the central carbon atoms of tecton **I** are shown. The interconnecting rods symbolize the intertectonic hydrogen bonding. The labels *a* and *b* represent the dimensions of the distorted diamondoid lattice, and **a**, **b**, and **c** represent the crystallographic axes.

Table 4. Unit cell parameters of I•8$CH_3CH_2CO_2H$ and I•2$CH_3CH_2CH_2CO_2H$ and the dimensional indices of the distorted diamondoid lattices

Tecton	Unit cell dimensions (Å)	Dimensional indices of distorted lattice (Å)
I•8$CH_3CH_2CO_2H$	**a** = 21.977 (2)	$\underline{a}$ = 43.954
	b = 21.977 (2)	$\underline{b}$ = 43.954
	c = 7.7866 (9)	$\underline{c}$ = 46.720
I•2$CH_3CH_2CH_2CO_2H$	**a** = 31.249 (7)	$\underline{a}$ = 43.347
	b = 7.350 (4)	$\underline{b}$ = 33.843
	c = 23.145 (6)	$\underline{c}$ = 51.450

equivalent diamondoid lattices occurs along the longest index of the distorted diamondoid lattice. In the case of I•8 $CH_3CH_2CO_2H$, it is along the crystallographic **c** axis; in the case of I•2 $CH_3CH_2CH_2CO_2H$, it is along the crystallographic **b** axis. We do not think that this is merely a coincidence. To fully understand this observation, we tried to find further evidence supporting the idea that interpenetration always occurs along the direction of the longest index of a distorted diamondoid lattice, since it might be the most efficient way to avoid hollowness via close-packing. In the crystal structure of Ermer's tecton **33**, interpenetration occurs along the diagonal of a rectangle formed by two fused superadamantane frameworks as defined in Figure 33, since in this case a compressed tetragonal diamondoid lattice is generated so that there is no longest index. However, in the crystal structures of tectons **34**, **36**, and **38**, the elongated distorted diamondoid lattices all interpenetrate one another along the direction of longest index. Apparently, it must provide

the most efficient packing in order to avoid hollowness and meanwhile derive the most energetically favored enclathration of guest molecules. For example, in the crystal structure

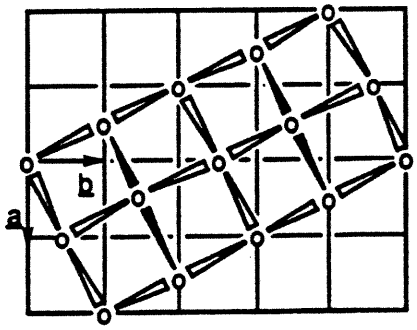

Figure 33. Schematic illustration of the translational equivalence of the five interpenetrating diamondoid lattices in the crystals of tecton **34**, i.e., of the relationship between the translational vector **b** and the diamondoid lattice geometry. The view shows a projection down the crystallographic **c** axis.[13a]

of tecton **I**•2 $CH_3CH_2CH_2CO_2H$, interpenetration along either ***a*** or ***b*** will result in larger channels which need to accommodate a large number of molecules of butyric acid to avoid hollowness, therefore bringing about an even more unfavorable entropy of enclathration.

In Figure 34, a distorted diamondoid lattice in the crystal structure of **I**•2 $CH_3CH_2CH_2CO_2H$ is presented, with only the central carbon atoms of tecton **I** shown as small spheres and the interconnecting black solid sticks symbolizing the intertectonic hydrogen bonding. The crystallographic axes and the dimensions of the diamondoid lattice are also shown. Figure 35 shows how a second distorted diamondoid lattice, presented with small spheres and white solid sticks, interlaces into the first one by shifting along the crystallographic **b** axis by a distance corresponding to the value of the cell edge (7.350 Å). Figure 36 shows that the seven interpenetrating diamondoid networks of tecton **I** are translationally equivalent, and they are merged into each other by translating them along the **b** axis by a distance of 7.350Å.

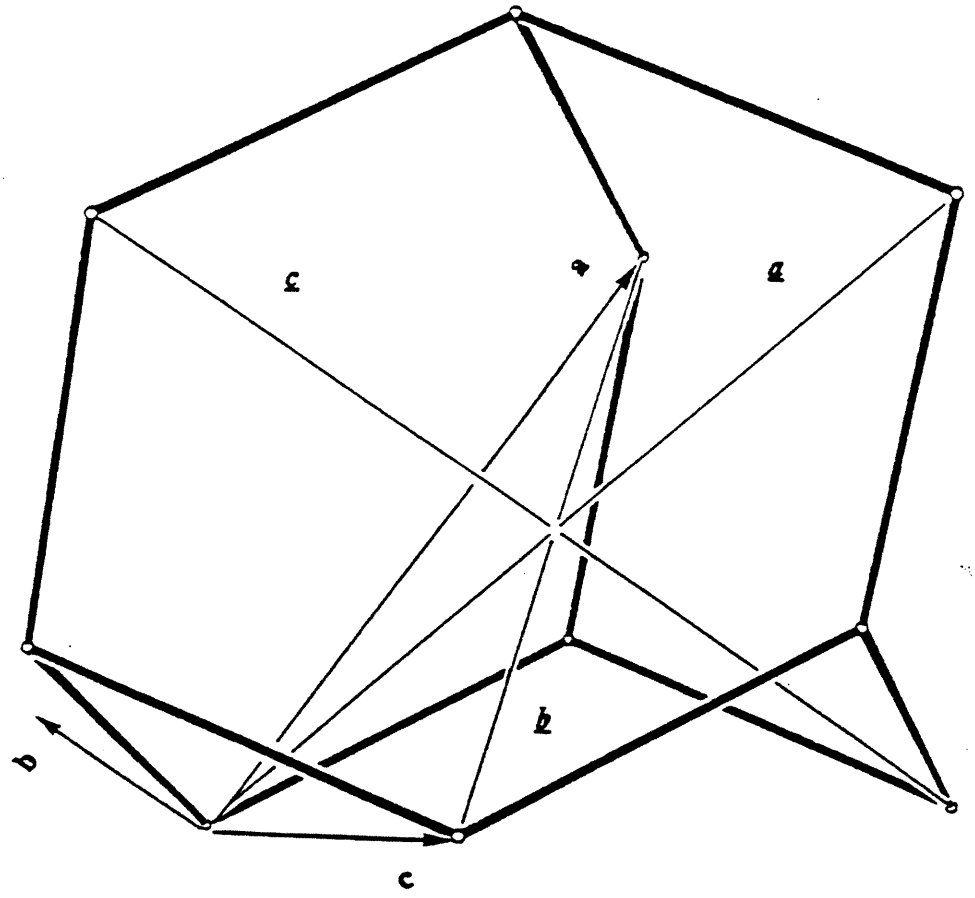

Figure 34. An individual superadamantane cut out of the diamondoid lattice formed by tecton I•2 $CH_3CH_2CH_2CO_2H$. Only the central carbon atoms of tecton I are shown. The interconnecting rods symbolize the intertectonic hydrogen bonding. The labels ***a*** , ***b*** and ***c*** represent the dimensions of the distorted diamondoid lattice, while **a**, **b** and **c** represent the crystallographic axes.

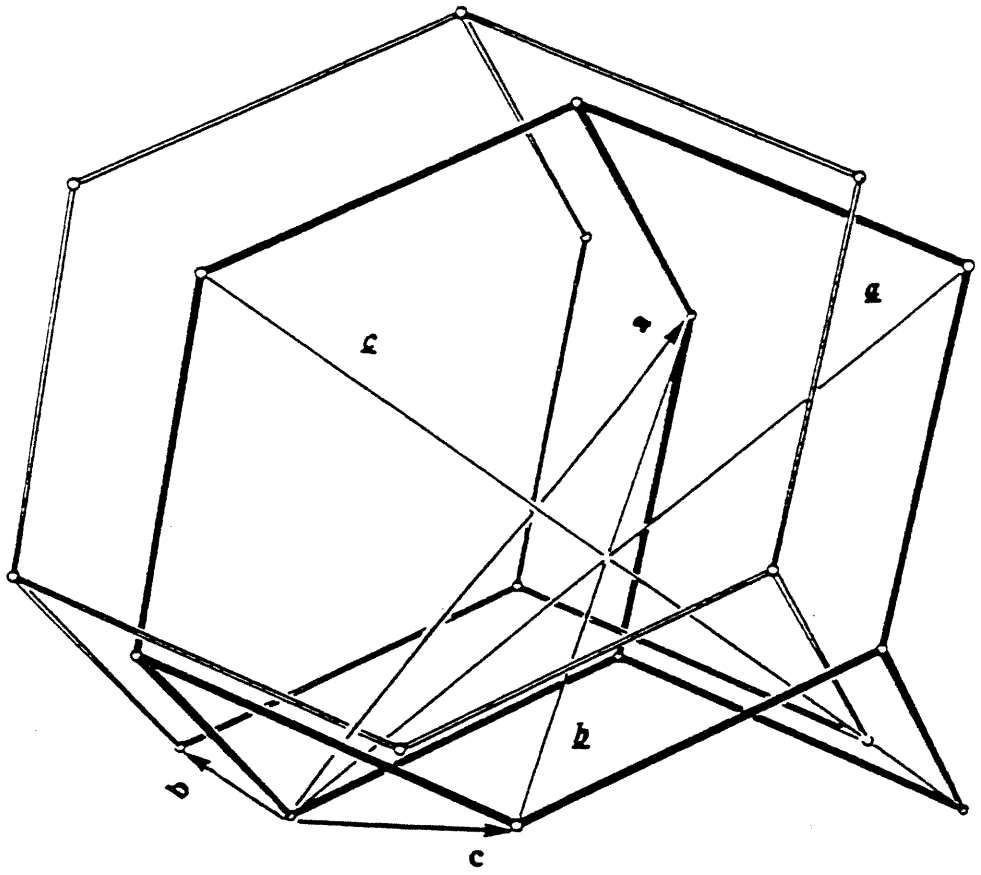

Figure 35. View of the crystal structure of tecton **I**•2 $CH_3CH_2CH_2CO_2H$ showing a second distorted diamondoid lattice (represented with small spheres and white solid sticks) interlaced into the first one (represented with small spheres and black solid sticks). The two networks are related by shifting along the crystallographic **b** axis by a distance corresponding to the value of the cell edge (7.350 Å). The label **c** represents the longest index of the distorted diamondoid lattice.

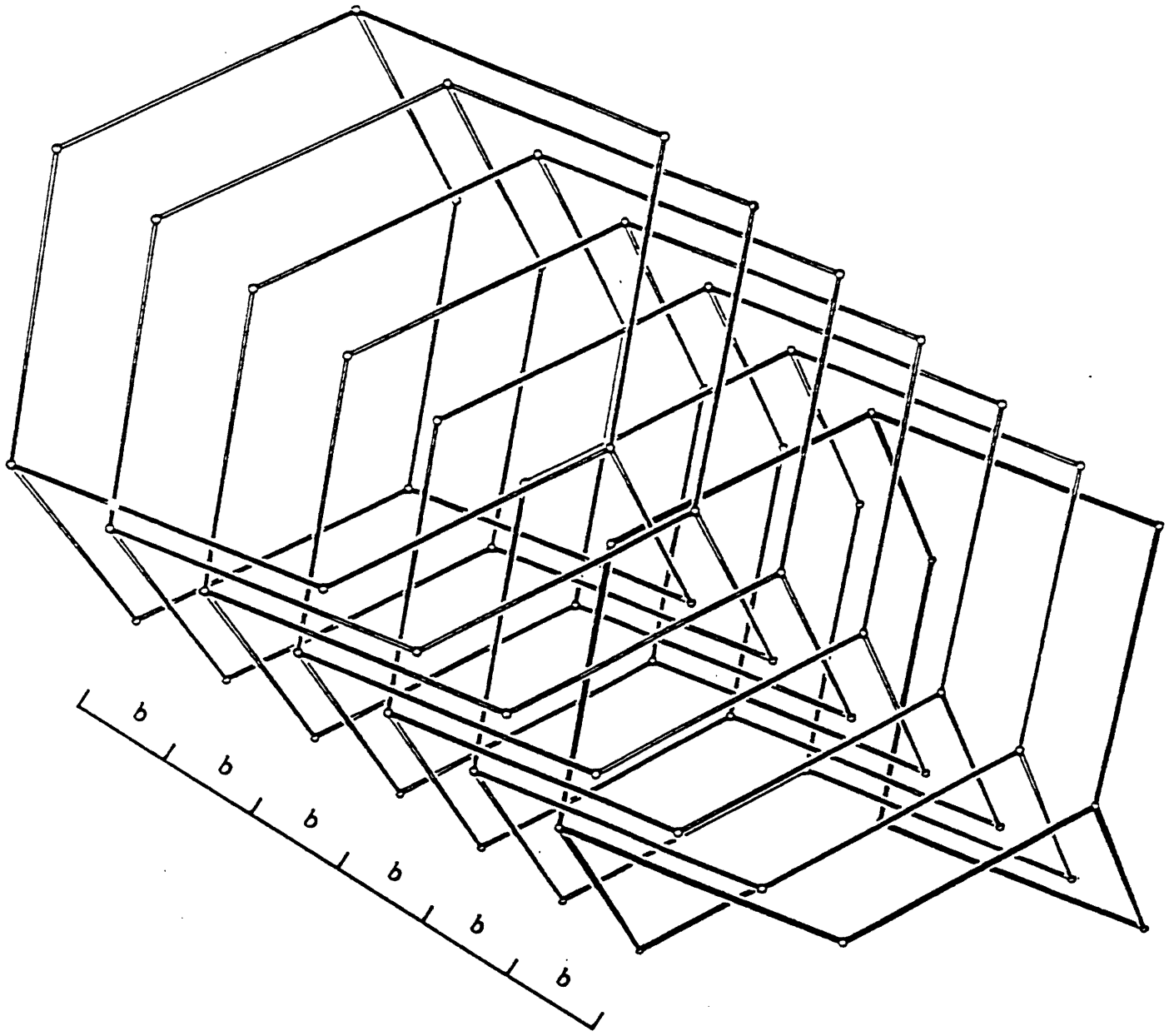

Figure 36. Seven interpenetrating diamondoid networks in the crystal of tecton I•2 $CH_3CH_2CH_2CO_2H$ are merged into each other by translating them along the **b** axis by a distance of 7.350 Å.

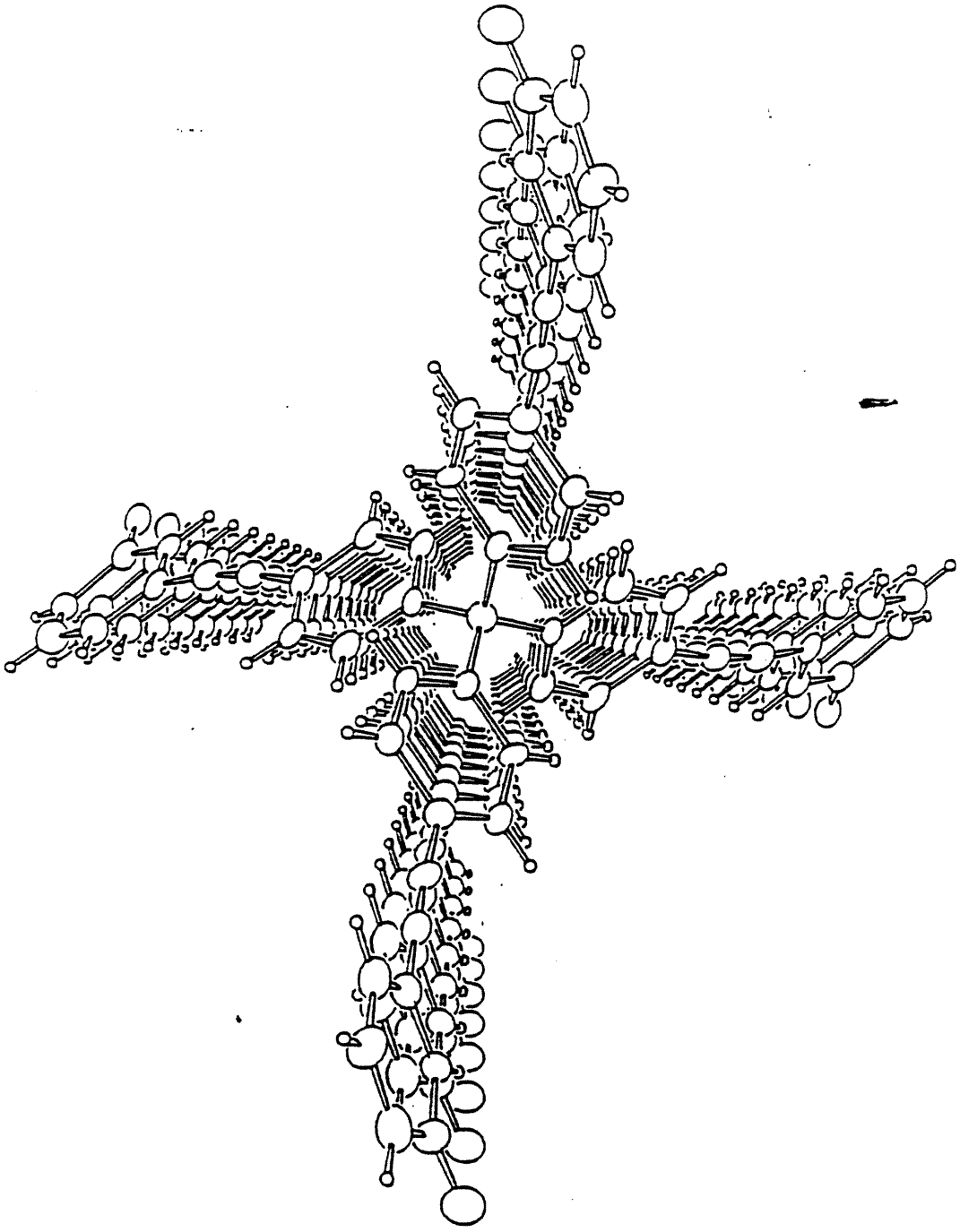

Figure 37. Top view of the stacking of tecton **I**•2 $CH_3CH_2CH_2CO_2H$ down the **b** axis. Non-hydrogen atoms are represented by ellipsoids corresponding to 50% probability. Hydrogen atoms are represented by spheres of arbitrary size.

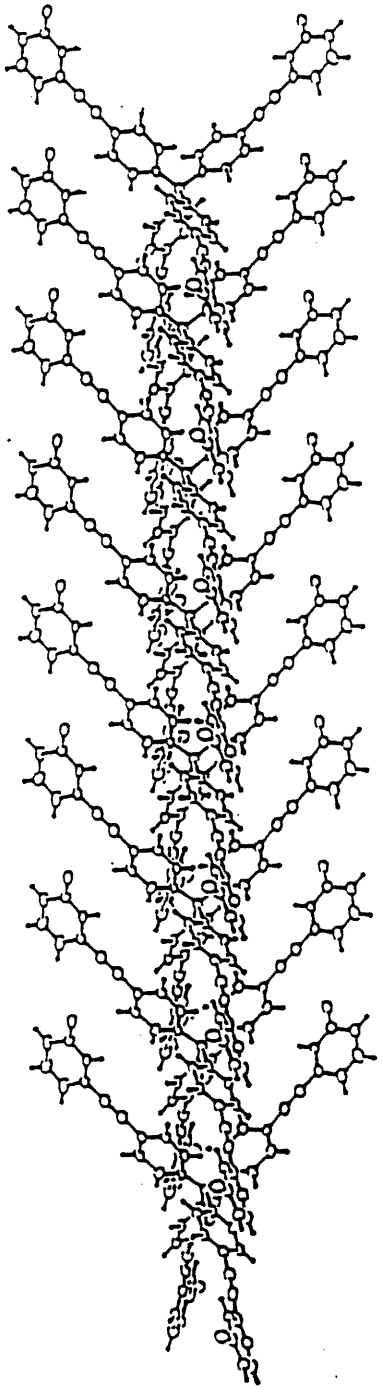

Figure 38. Side view of tectonic stacking in crystals of tecton I•2 $CH_3CH_2CH_2CO_2H$ along the **b** axis. Non-hydrogen atoms are represented by ellipsoids corresponding to 50% probability. Hydrogen atoms are represented by spheres of arbitrary size.

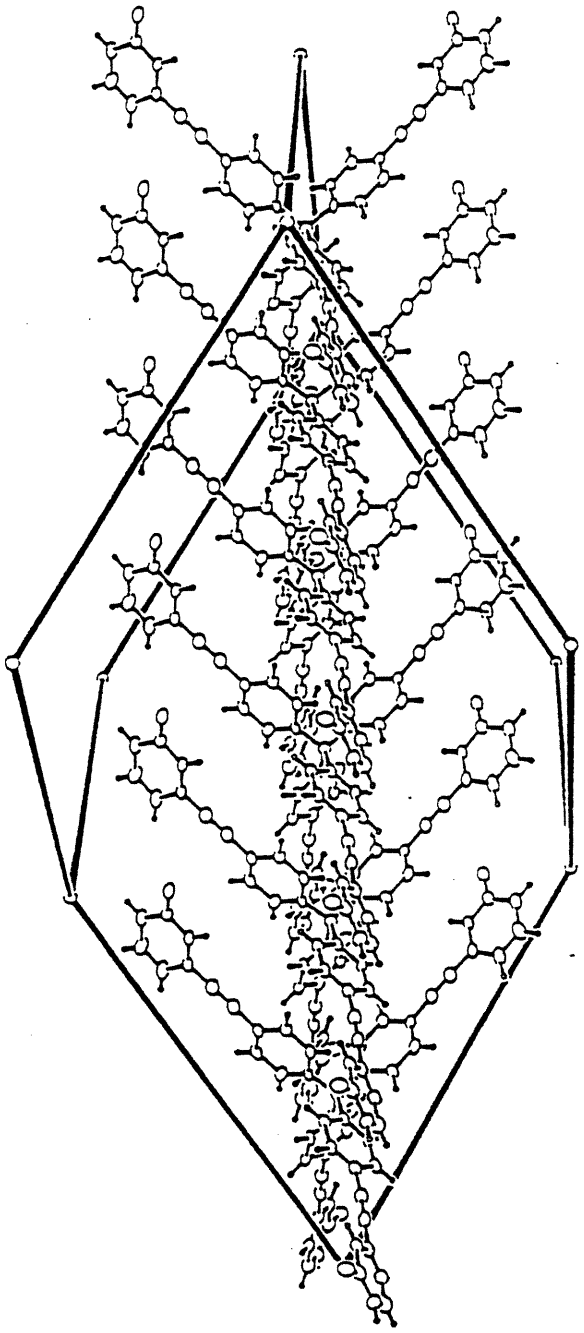

Figure 39. The relationship between an individual hydrogen-bonded diamondoid lattice and the stacking of molecules of tecton I. The diamondoid lattice is represented by small spheres and black solid sticks. Non-hydrogen atoms are represented by ellipsoids corresponding to 50% probability. Hydrogen atoms are represented by spheres of arbitrary size.

We have mentioned that the strong propensity of tecton **I** to generate diamondoid networks induced by hydrogen bonding might be brought about by the compatibility of hydrogen bonding and van der Waals forces in the crystal packing of tecton **I**. Figures 37, 38 and 39 show how tectonic molecules stack along the crystallographic **b** axis by sitting on top of each other and then self-assemble under the direction of intermolecular hydrogen bonding into supramolecular aggregates with diamondoid networks. In Figure 37, a top view of the stacking of tecton **I** along the **b** axis is shown. Figure 38 shows a side view of the stacking. Figure 39 shows the relationship between a hydrogen-bonded diamondoid lattice and the stacking of molecules of tecton **I**.

In Ermer's case, the cavity of a single hydrogen-bonded diamondoid lattice of tecton **33** is tightly filled by four other translationally equivalent lattices. They assumed that tecton **33** might not be able to enclathrate guest molecules without lowering the degree of interpenetration. However, in our case, the cavities of a single hydrogen-bonded superadamantane framework of tecton **I** correspond to a sphere roughly 40 Å in diameter instead of 12 Å as in Ermer's case. As a result, even though the degree of interpenetration is high (7-fold), there are still open channels formed along the **b** axis. Butyric acid is selectively enclathrated in these channels and is especially well-ordered in two parallel columns (Figure 40). In order to better understand the selective enclathration of molecules of butyric acid and their well-ordered arrangement in the channels, it is instructive to compare the crystal structure of **I**•2 $CH_3CH_2CH_2CO_2H$ with that of **I**•8 $CH_3CH_2CO_2H$. In Figure 41, a view of the unit cell down the **b** axis in the crystal of **I**•2 $CH_3CH_2CH_2CO_2H$ is shown. Comparison of it with the unit cell viewed down the **c** axis in the crystal of **I**•8 $CH_3CH_2CO_2H$ (shown in Figure 17) shows that the orientations of the acid molecules in the channels are nearly the same as those of the molecules of propionic acid (shaded), which are linked with pyridone rings of adduct **39** by single hydrogen bonds. Obviously, when the larger molecules of butyric acid are used as solvent,

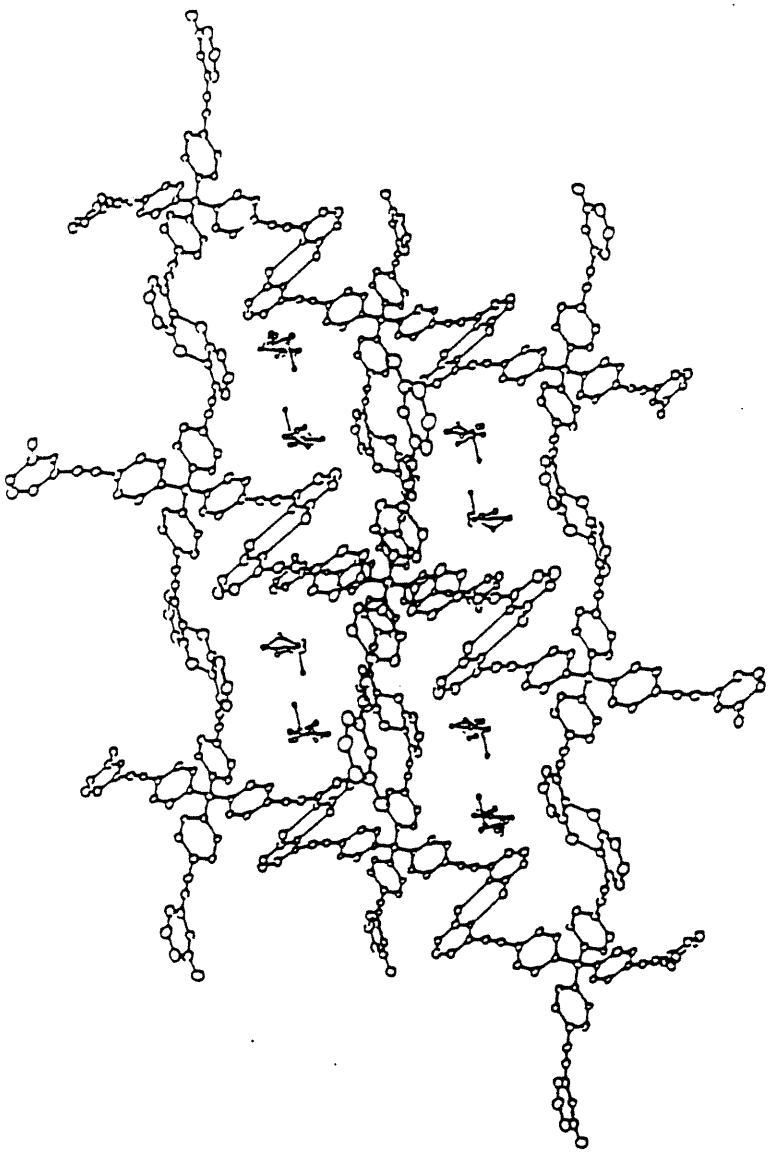

Figure 40. View along the **b** axis of crystals of tecton **I**•2 $CH_3CH_2CH_2CO_2H$ showing cross sections of the channels containing parallel columns of butyric acid.

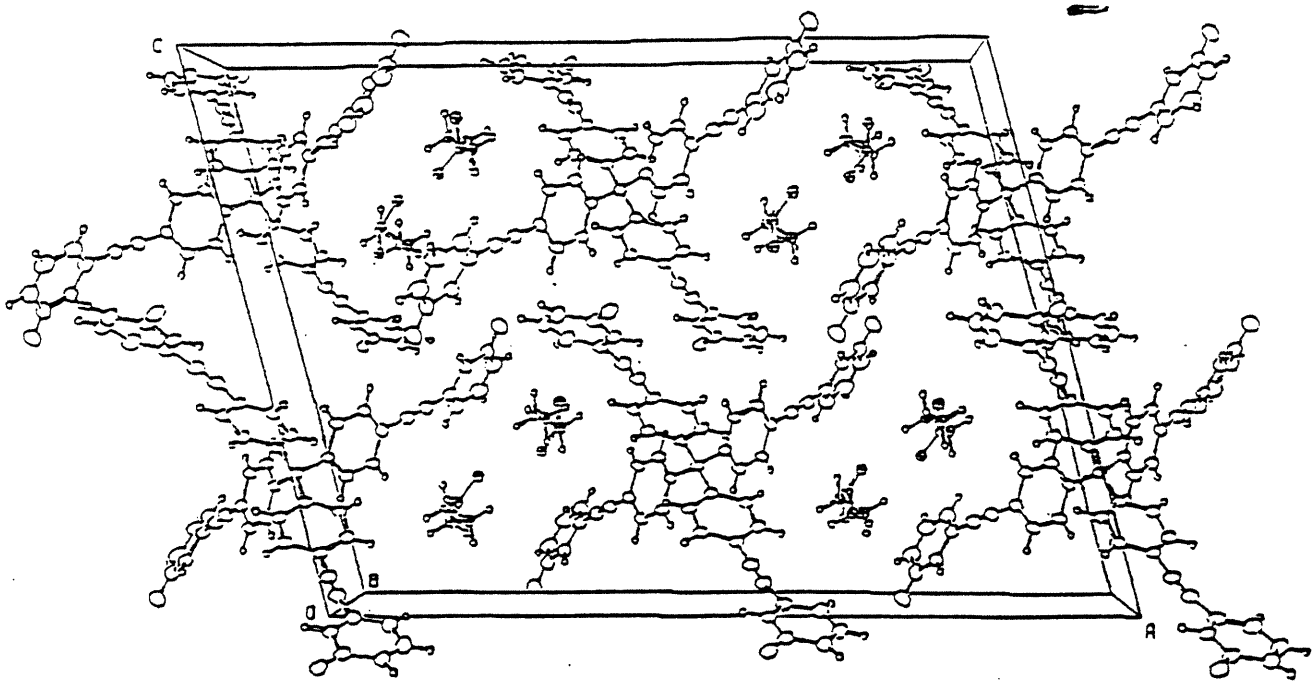

Figure 41. ORTEP view along the **b** axis of the packing arrangement of tecton I•2 $CH_3CH_2CH_2CO_2H$. Non-hydrogen atoms are represented by ellipsoids corresponding to 50% probability, and hydrogen atoms by spheres of arbitrary size. Arbitrary spheres are used for the butyric acid moiety.

channels become too crowded, so that the interaction of butyric acid with pyridone to form pairwise hydrogen bonds is no longer possible. Instead, direct pairwise hydrogen bonding between pyridone rings is favored and butyric acid becomes enclathrated in paired columns in channels as a result of the strong affinity of the carbonyl group of pyridone for carboxylic acids as we mentioned above. Another phenomenon revealed by comparison of these two crystal structures is that the diameter of the channels in crystals of tecton I•2 $CH_3CH_2CH_2CO_2H$ is smaller than that of the channels in crystals of I•8 $CH_3CH_2CO_2H$. This difference may be attributed to the driving force of energetically favorable crystal packing. In this packing environment, formation of hydrogen-bonded diamondoid networks and enclathration of butyric acid are energetically favorable. In order to avoid hollowness and unfavorable entropy of enclathration, tecton I tends to adjust its molecular symmetry and conformations to generate a more distorted diamondoid lattice, with an elongation factor of 1.52 instead of 1.06 in the crystal of I•8 $CH_3CH_2CO_2H$. As a consequence, a higher degree of interpenetration (favored by close packing) and a smaller size of channels (leading to the most energetically favored enclathration) are observed. In Figure 42, the cross sections of four adjacent channels defined by a distorted diamondoid network are shown. We note that every four-sided channel is constructed from two pairs of opposite walls which are built up of hydrogen-bonded pyridone rings. We have mentioned above that the conformations of the pyridone rings with respect to the frame of a diamondoid lattice may affect the size of the channels. From Figure 42 we can see that the smallest size of channels may be generated when all hydrogen-bonded pyridone rings adopt a conformation which makes them parallel to the plane of the cross section, and the largest size is generated when they are perpendicular to the plane of the cross section. To form channels with suitable size, tecton I regulates its conformations within certain crystal packing environments, and the results are shown in Table 2. In Figures 43 and 44 an

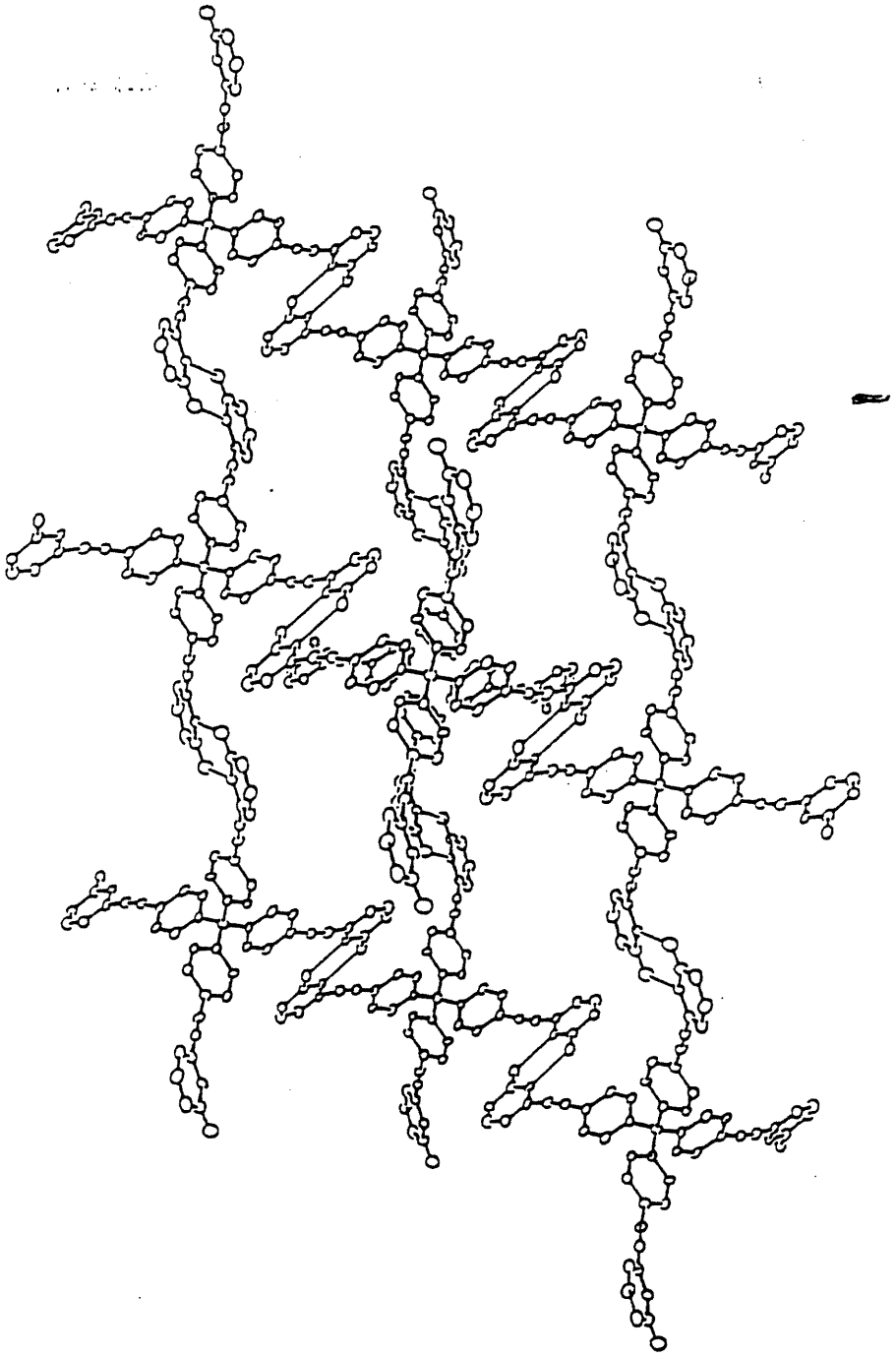

Figure 42. View along the **b** axis in crystals of tecton I•2 $CH_3CH_2CH_2CO_2H$ showing cross sections of the channels. Butyric acid is omitted for clarity.

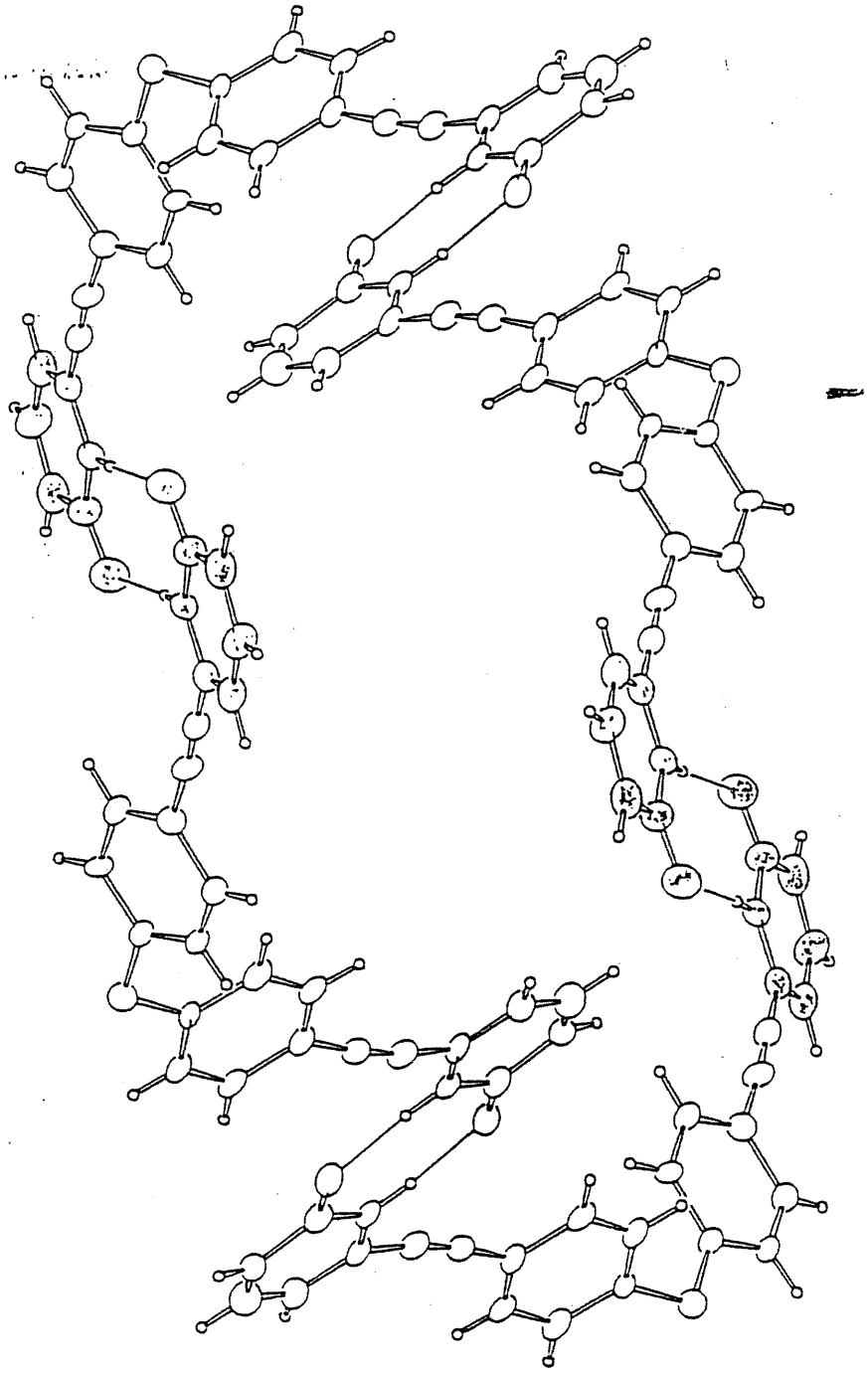

Figure 43. View (down the **b** axis) of an individual four-sided channel cut out from diamondoid lattices in crystals of tecton **I**•2 $CH_3CH_2CH_2CO_2H$.

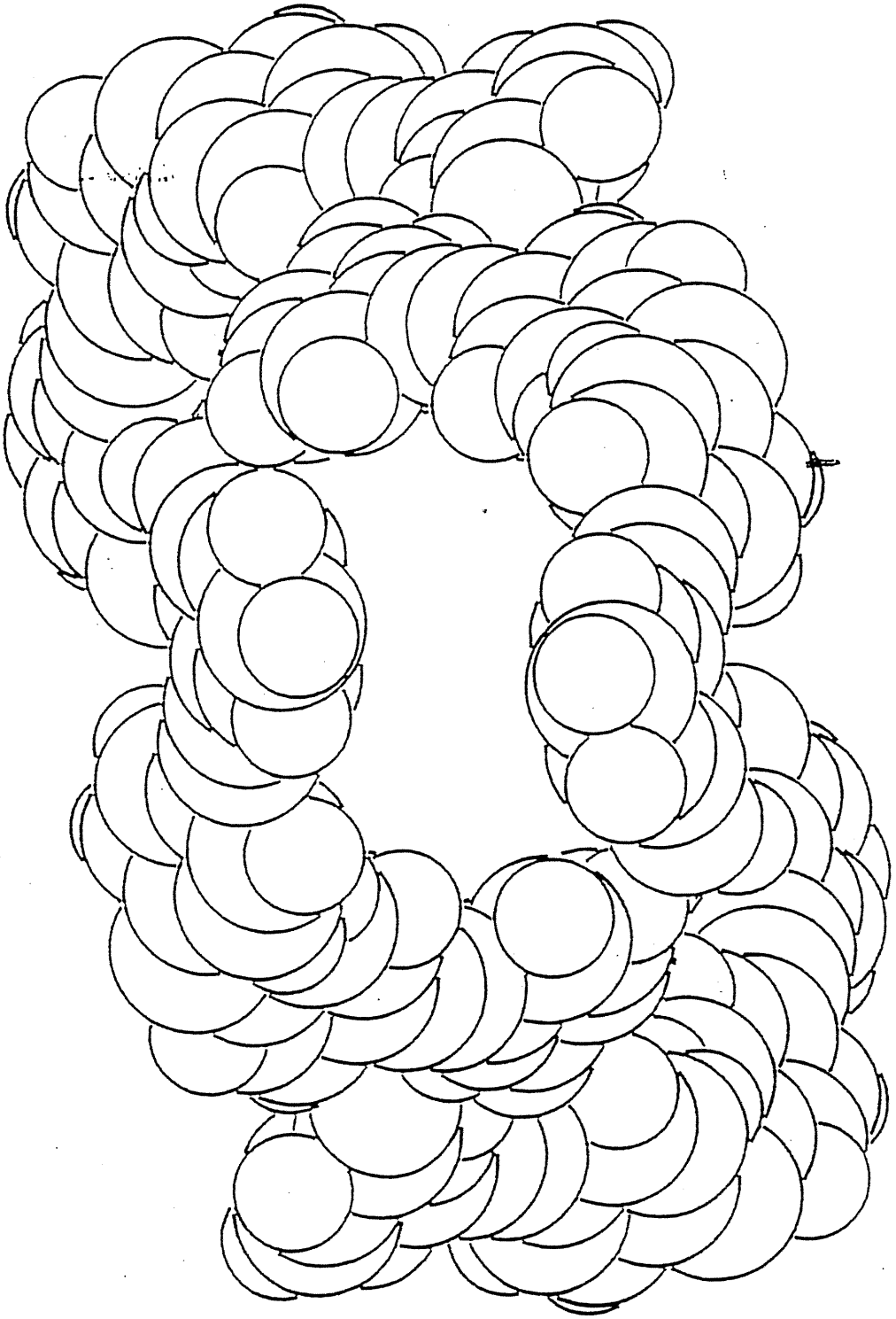

Figure 44. Space-filling view (down the **b** axis) of an individual four-sided channel cut out from diamondoid lattices with diameter 8.1 Å x 3.5 Å.

individual four-sided channel cut out of diamondoid networks is present either in cylinder-ball or space-filling stereoview. The distorted diamondoid networks define rectangular channels approximately 8.1 Å x 3.5 Å in diameter.

2.6. Crystallization of tecton I from other carboxylic acids

Thereafter, we tried to crystallize tecton I from carboxylic acids of different sizes (shown in Table 5). Crystallization of tecton I from mixtures containing larger carboxylic acids such as valeric and hexanoic acid in methanol/hexane provided plates of approximate compositions I•1$CH_3CH_2CH_2CH_2CO_2H$ and I•0.5 $CH_3CH_2CH_2CH_2CH_2CO_2H$, respectively, in yields of around 85%. Again, an X-ray crystallographic study of I•1$CH_3CH_2CH_2CH_2CO_2H$ indicated that since it has almost the same unit cell parameters

Table 5. The physical properties of carboxylic acids and the number n of acid molecules enclathrated per molecule of tecton I

carboxylic acid	propionic acid	butyric acid	isobutyric acid	valeric acid	isovaleric acid	hexanoic acid
n	8	1.5 ~ 2	2 ~ 2.5	1 ~1.5	3	0.5 ~ 0.9
d (g/cm^3)	0.993	0.964	0.950	0.939	0.937	0.927
Cosolvents	Hexane	MeOH & Hexane	Hexane	MeOH & Hexane	MeOH & Hexane	MeOH & Hexane

Table 6. X-ray determination of the structures of clathrates obtained by crystallizing tecton I from different carboxylic acids

Crystal Data	I•2 butyric acid	I•1 valeric acid	I•2 isobutyric acid
crystal system	Monoclinic	Monoclinic	Monoclinic
space group	*C2/c*	$P2_1/n$	*C2/c*
unit cell parameters			
a (Å)	31.249 (7)	31.137(8)	32.024 (12)
b (Å)	7.350 (4)	7.290(2)	7.448 (4)
c (Å)	23.145 (6)	23.006(5)	23.263 (10)
α (deg)	90	90	90
β (deg)	104.69 (2)	104.70 (2)	105.39 (3)
γ (deg)	90	90	90
vol ($Å^3$)	5142 (3)	5064 (4)	5350 (4)
Z	4	4	4
d_c (g/cm^3)	1.247	1.169	1.198
T_m (K)	180	215	235

as I•2$CH_3CH_2CH_2CO_2H$ (Table 6), it should have the same kind of crystal structure. This means that self-assembly occurs to give a closely similar diamondoid network with channels that selectively enclathrate valeric acid. The decrease in the number of enclathrated acids per molecule of tecton I may simply result from the increased size of the acid, which is energetically favorable because the entropy of enclathration becomes less negative.

The unoccupied space in a close-packed crystal structure may be utilized to permit slight modifications of the shape or volume of the component molecules within limits

without a change in the crystal structure. In light of this, we tried to crystallize tecton **I** from more highly branched carboxylic acids such as isobutyric and isovaleric acids, and crystals with similar morphology and approximate compositions confirmed by ^{1}H NMR as **I**•2$(CH_3)_2CHCO_2H$ and **I**•3$(CH_3)_2CHCH_2CO_2H$, respectively, were obtained. X-ray crystallographic analysis of the structure of **I**•2$(CH_3)_2CHCO_2H$ indicated that it has not

Table 7. Comparison of the crystal data for tecton **I**•0.3 $CH_3CH_2CO_2H$ •0.6 $CH_3CH_2CH_2CO_2H$ with the data for tecton **I**•8 $CH_3CH_2CO_2H$ and **I**•2 $CH_3CH_2CH_2CO_2H$

Crystal Data	**I**•8(propionic acid)	**I**•2(butyric acid)	**I**•0.3(propionic acid)• 0.6(butyric acid)
crystal system	Tetragonal	Monoclinic	Monoclinic
space group	*P4$_2$/n*	*C2/c*	*P2$_1$/n*
unit cell parameters			
a (Å)	21.977 (2)	31.249 (7)	31.507 (17)
b (Å)	21.977 (2)	7.350 (4)	7.381 (3)
c (Å)	7.7866 (9)	23.145 (6)	23.289 (11)
α (deg)	90	90	90
β (deg)	90	104.69 (2)	104.73 (4)
γ (deg)	90	90	90
vol (Å^3)	3760.7 (6)	5142 (3)	5238 (4)
Z	2	4	4
d_c (g/cm^3)	1.220	1.247	
T_m (K)	200	180	215

only almost the same unit cell parameters, but adopts the same crystal system and even the same space group. From Table 5 we can see that the number of enclathrated molecules of isobutyric or isovaleric acid may be somewhat larger than that observed for butyric acid. This may result from more nearly perfect close-packing at the expense of entropy of enclathration.

To prove that tecton **I** has a strong tendency and ability to self-assemble via hydrogen bonding into supramolecular aggregates with diamondoid networks, we tried to crystallize tecton **I** from a mixture of butyric acid and propionic acid in the molar ratio 1:1. X-ray crystallographic study of the resulting crystals of stoichiometry **I**•0.3 $CH_3CH_2CO_2H$ •0.6 $CH_3CH_2CH_2CO_2H$ (Table 7) indicated that a diamondoid network induced by hydrogen bonding instead of π-stacking is generated preferentially when both propionic and butyric acid are present in the solvent system. This evidence further proves that hydrogen bonding is a much more powerful tool for directing tectons to self-assemble into supramolecular aggregates in a predicted way.

CHAPTER 3

TECTONS WITH AMPLIFIED INTERTECTONIC ADHESION

We were not surprised to find that when crystals of tecton **I**•2$CH_3CH_2CH_2CO_2H$ were removed from the mother liquor and kept in air at room temperature, they no longer diffracted and were no longer single crystals. We assumed that it resulted from loss of butyric acid. An organic crystal is a perfect alignment of molecules, and any missing part must cause disorder. It has been indicated that molecular crystals which obey the close-packing principle tend towards a maximum packing efficiency. Packing coefficients for the vast majority of organic crystals are between 0.65 and 0.77. In our case, the quite open channels defined by the diamondoid networks are filled with molecules of butyric acid or other guests to avoid low packing co-efficients and the framework of channels is constructed by hydrogen bonding. Even though this framework may be durable enough to withstand a minor loss of enclathrated guests, it cannot resist forces favoring close packing when channels begin to be more empty. Therefore the ordered diamondoid lattices are destroyed under this circumstance. It is challenging to strengthen the framework of channels to override the forces that favor close packing.

Since the stickiness of tectons can be amplified by using rigid spacers to connect self-complementary asymmetric di- or tripyridones to a tetrahedral core of tetraphenylmethane, we designed tectons **II-V** as shown in Figure 45.

3.1. Design and synthesis of tectons II-III.

To synthesize tectons **II** and **III**, the key synthon is 3,6-dibromo-2-(phenylmethoxy)pyridine, which we can see from the retrosynthetic analysis shown in

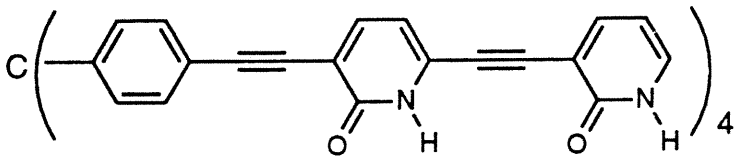

II

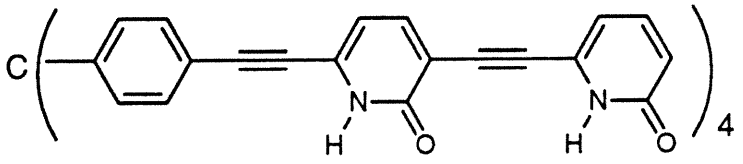

III

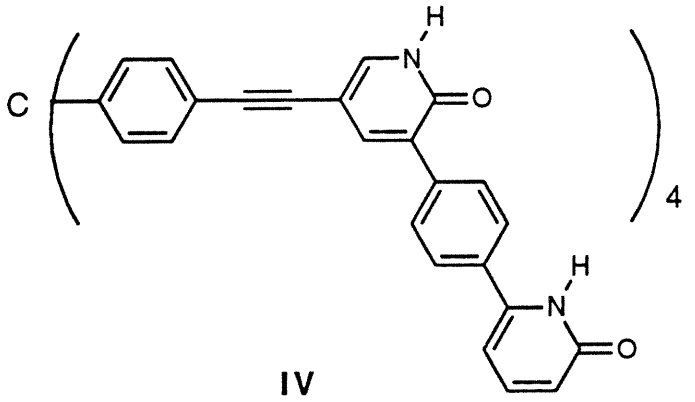

IV

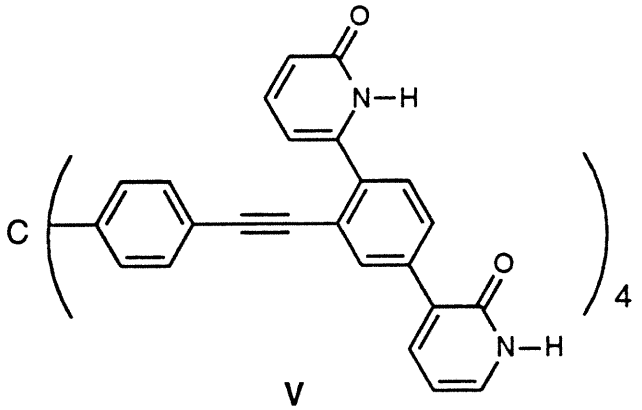

V

Figure 45. Tectons **II-V** designed to interact with amplified stickiness.

Scheme 5

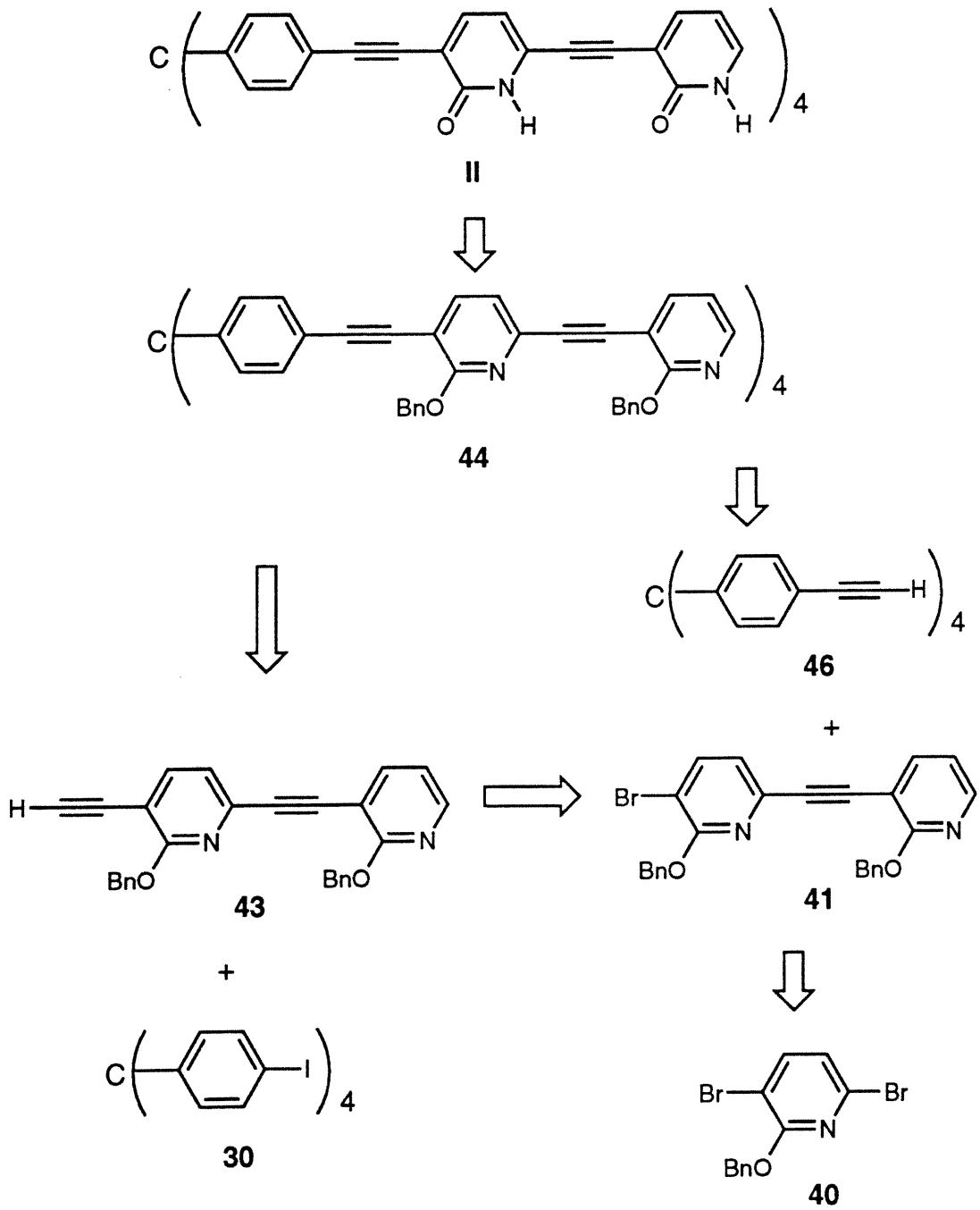

Scheme 6

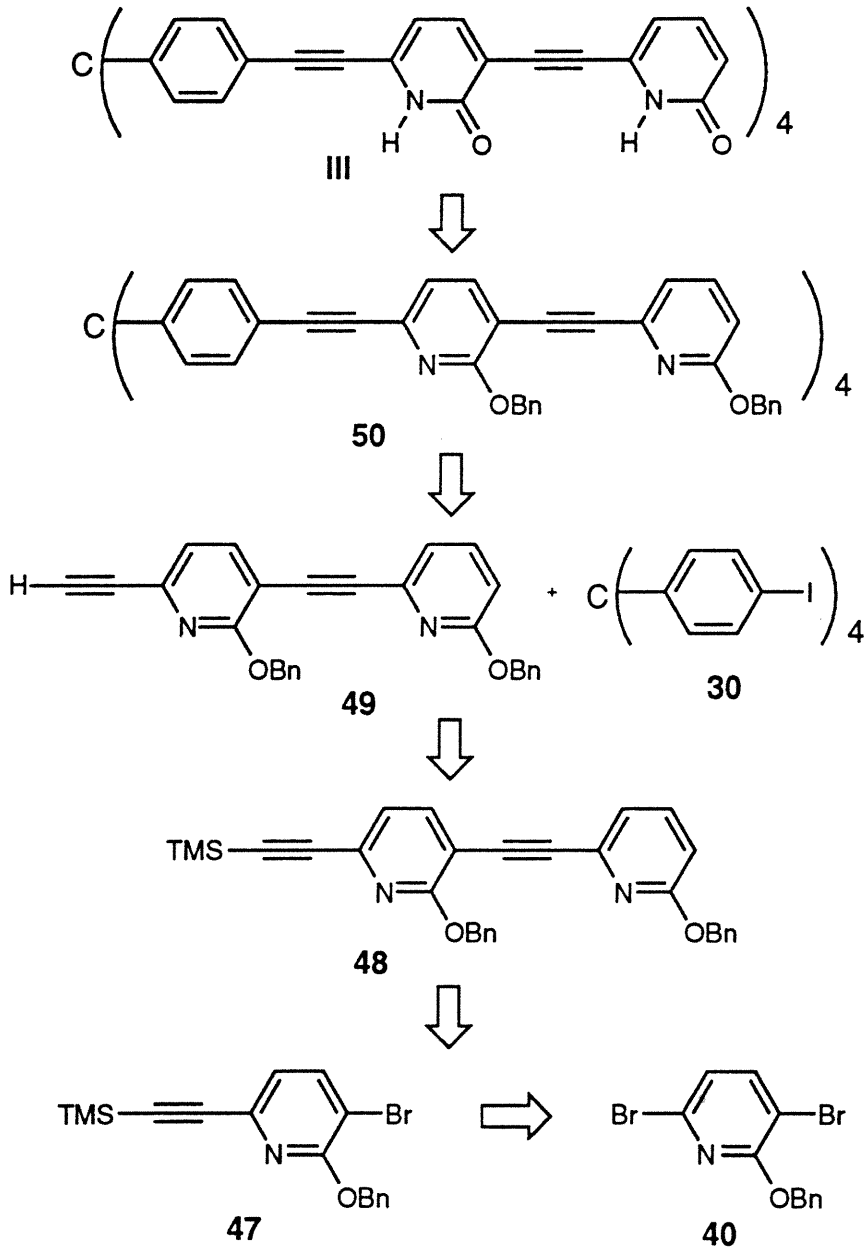

Scheme 7

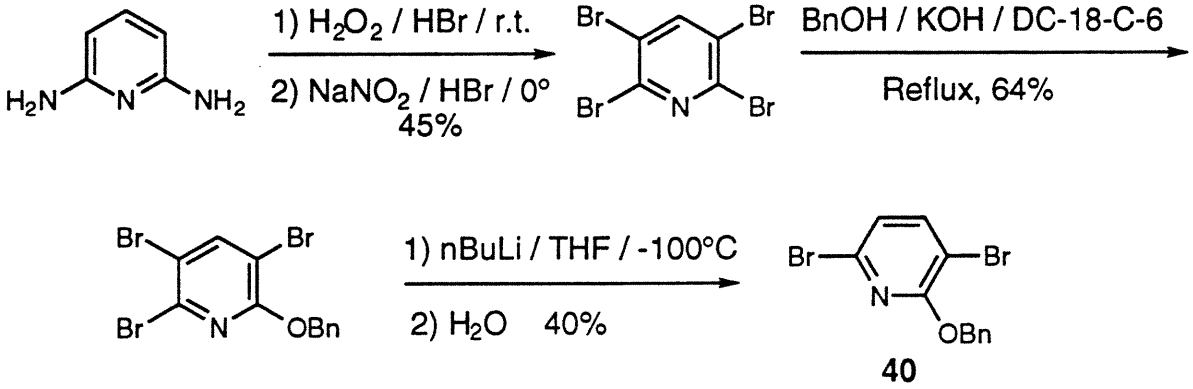

Scheme 8

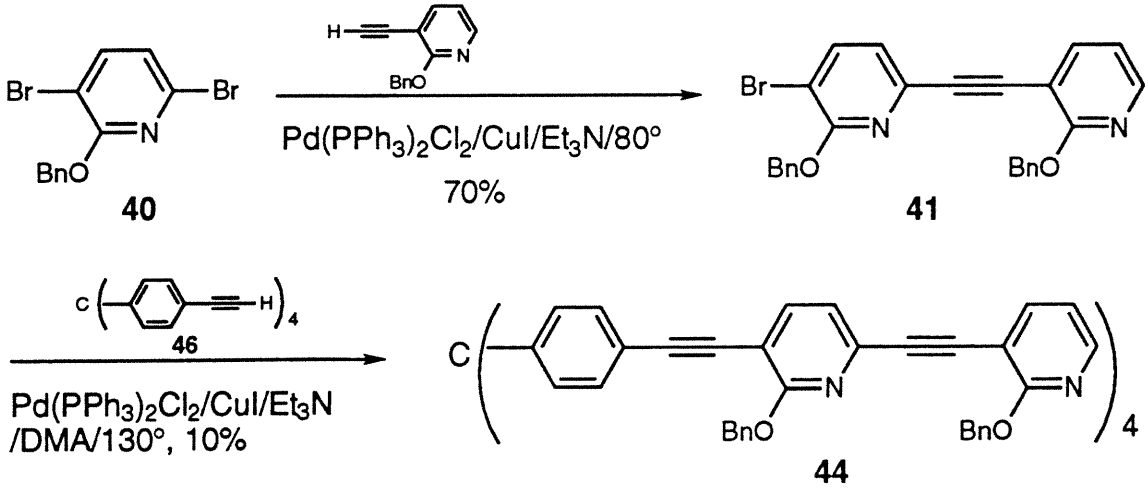

Schemes 5 and 6. Although the method of synthesis of dibromopyridine **40** has been well developed in our lab[26] as shown in Scheme 7, it is still a technically tricky and time-consuming job, and that is one of the reasons for trying to design dipyridines which can avoid the use of 3,6-dibromo-2-(phenylmethoxy)pyridine as the key synthon.

At first we tried to synthesize tetrakis(dipyridine) **44** from 3,6-dibromo-2-(phenylmethoxy)pyridine (**40**) in two steps as shown in Scheme 8. Cross coupling of

Scheme 9

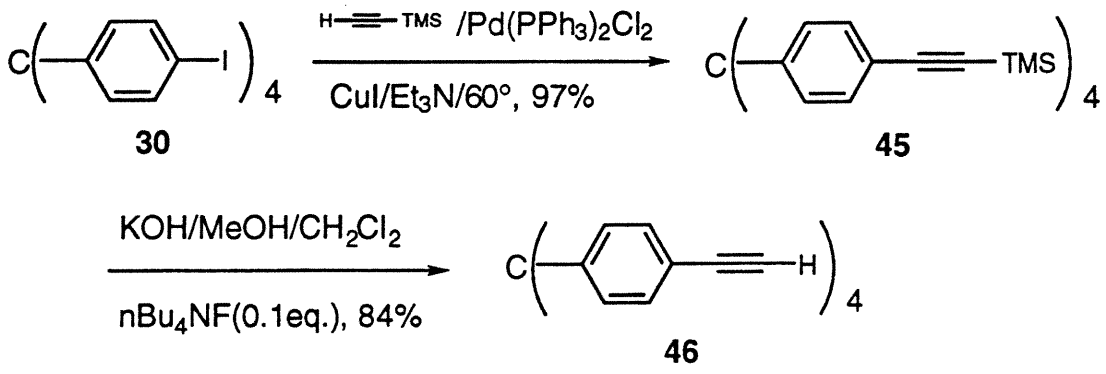

30 **45** **46**

Scheme 10

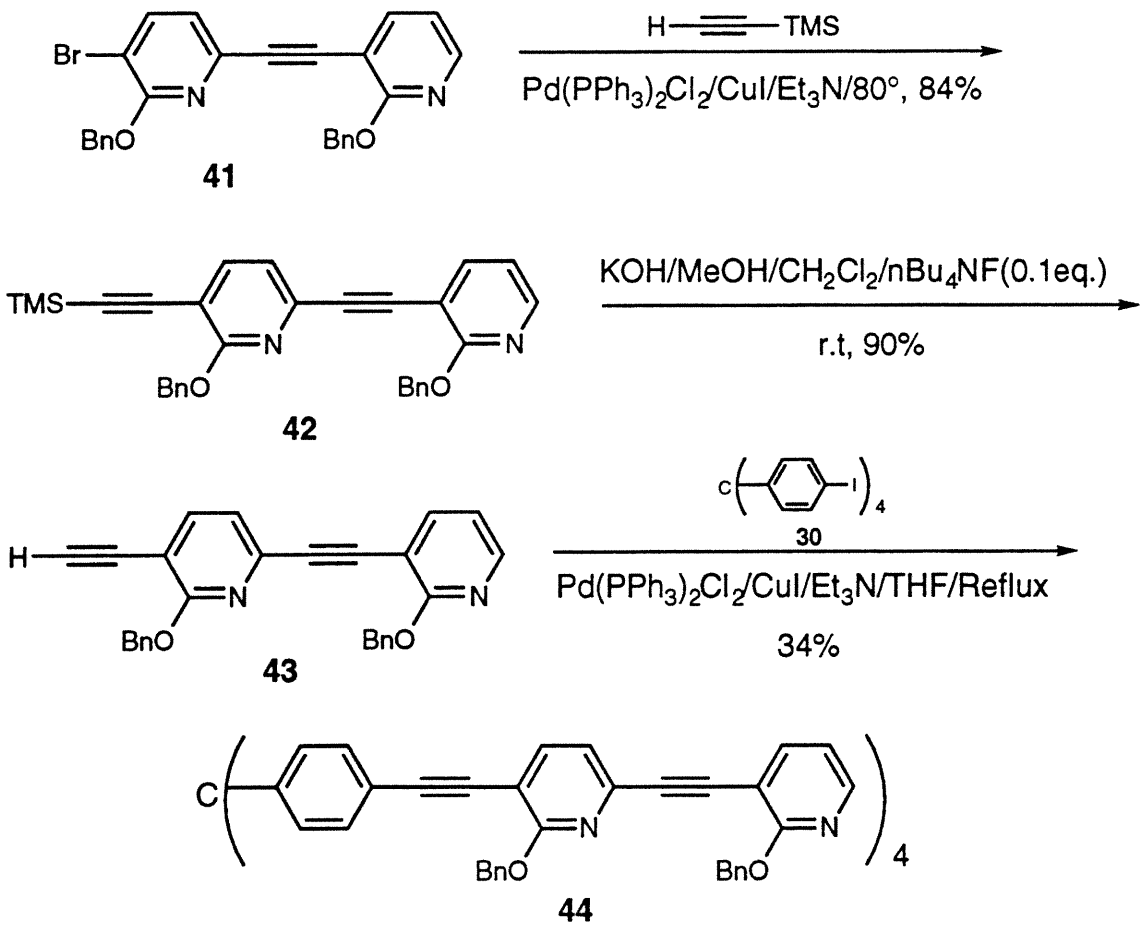

41 **42** **43** **44**

dibromopyridine **40** and 3-ethynyl-2-(phenylmethoxy)pyridine[10g] provided dipyridine **41** in 70% yield. It was coupled with tetrakis(4-ethynylphenyl)methane (**46**) which was made as shown in Scheme 9 to give tetrakis(dipyridine) **44** in a yield of 10% even at temperatures as high as 130°C overnight. We attribute the low yield of this coupling reaction to a competitive homocoupling reaction of tetrakis(4-ethynylphenyl)methane (**46**) which not only caused a sharp decline in the yield but also provided a complex mixture of products that made purification especially formidable. Therefore, we chose another way to synthesize tecton **II** from dipyridine **41** in three steps as shown in Scheme 10. Unfortunately, we found that cyclization happened when deprotection of

Scheme 11

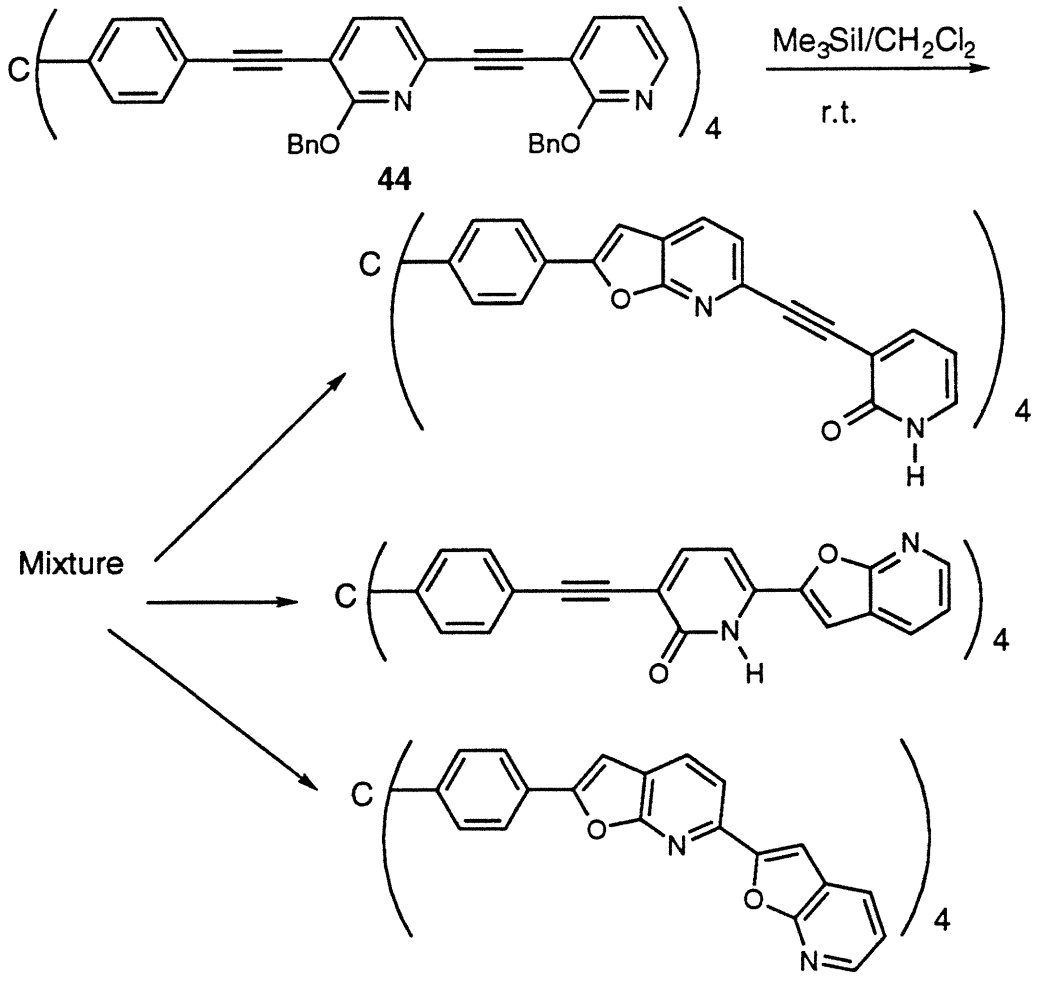

tetrakis(dipyridine) **44** was carried out at room temperature with iodotrimethylsilane (shown in Scheme 11) and gave a complicated product. In tetrakis(dipyridine) **44**, the triple bond connected to the phenyl ring appears to be much more reactive toward cyclization than the one between the two pyridine rings. For this reason, we turned to tecton **III** and hoped that careful deprotection of tetrakis(dipyridine) **50** would provide tecton **III** (Figure 45).

Tetrakis(dipyridine) **50** was synthesized from dibromopyridine **40** in four steps as presented in Scheme 12. The cross-coupling reaction of dibromopyridine **40** and

Scheme 12

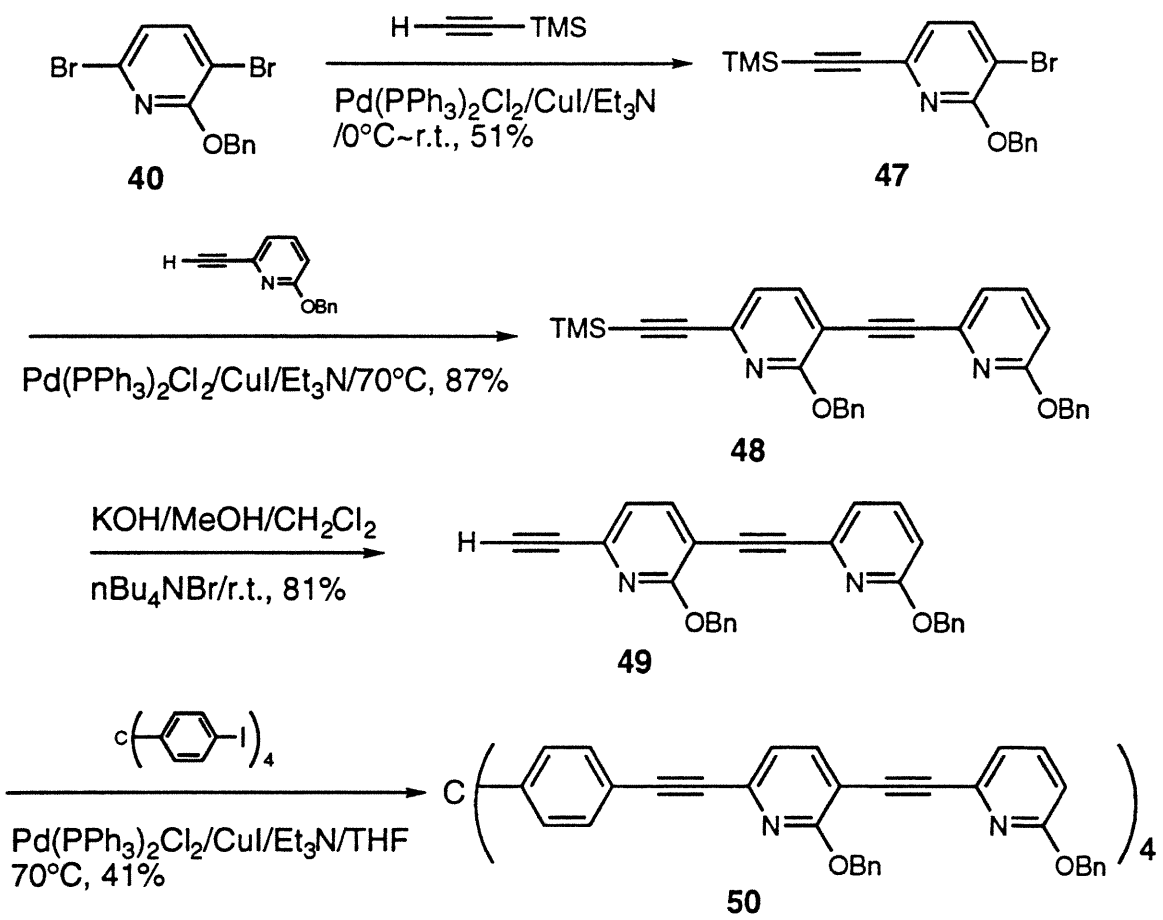

trimethylsilylacetylene was carried out at low temperature to raise the yield (51%) of cross-coupling at the 6-position to give compound **47**. It was then coupled with 6-ethynyl-2-(phenylmethoxy)pyridine to afford dipyridyltrimethylsilane **48**, which gave an 81% yield of dipyridylacetylene **49** after desilylation. Finally tetrakis(dipyridine) **50** was obtained by the cross-coupling reaction of compound **49** and tetraiodide **30** in 41% yield. Although we attempted to deprotect tetrakis(dipyridine) **50** by using TMSI in dilute solution at room temperature and lower temperature, cyclization occurred under the former conditions and starting material was recovered in the latter case.

3.2. Design and synthesis of tectons IV-V.

Several reasons then led us to design tectons **IV** and **V**. First, we wanted to avoid the tedious synthesis of dibromopyridine **40**. Second, because of the sensitivity of the triple bond to cyclization under varied conditions, it is a better strategy to avoid using triple bonds in the frame structure. Third, since solubility of tectons normally decrease when their stickiness is raised, we sought to improve solubility by using irregularly shaped tectons that do not pack easily in a crystal lattice. Last, as mentioned in Chapter 2, we considered that adjustability of the conformation of hydrogen-bonded pyridone rings is important to control the size and shape of channels defined by diamondoid networks. Items ***a*** and ***b*** shown in Scheme 13 present schematically a part of hydrogen-bonded tectons **IV** and **V**. In comparison to tecton **I** (item ***e*** shown in Scheme 13), much longer intertectonic distances might be defined in the aggregates of tectons **IV** and **V** if intermolecular hydrogen-bonding would occur in the expected way. As consequences, more open and durable channels (schematically shown in Schemes 14 and 15 as items ***c*** and ***d***) might be generated in the diamondoid networks constructed from tectons **IV** and **V**. From Schemes 14-16 we can see that the shapes of the channels ***c*** and ***d*** are rather similar to that of channel ***t*** (Scheme 16) which is constructed from tecton **I**. Therefore we roughly deduced

that tectons **IV** and **V** should be able to generate diamondoid networks induced by self-assembly under direction of intermolecular hydrogen-bonding.

Scheme 13

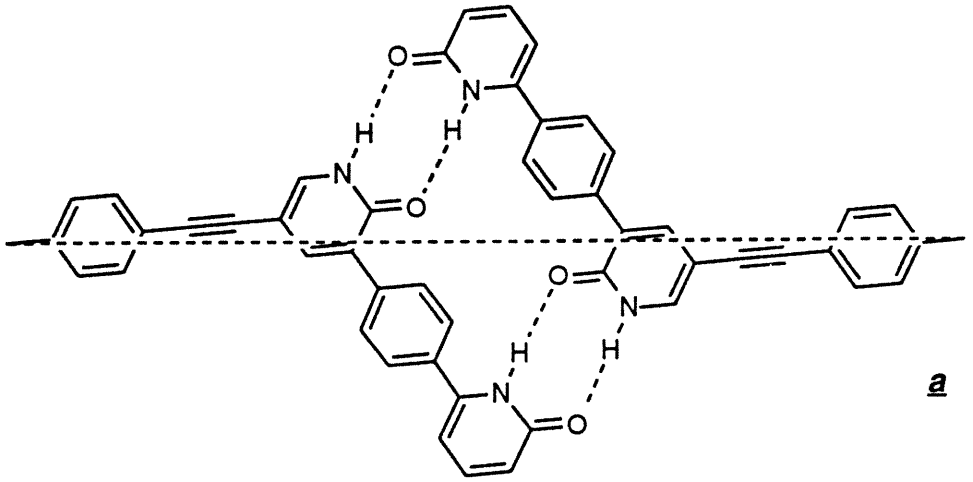

a

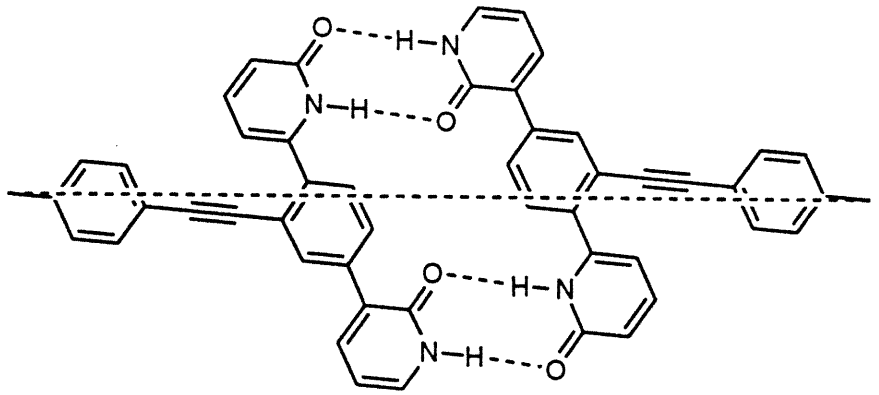

b

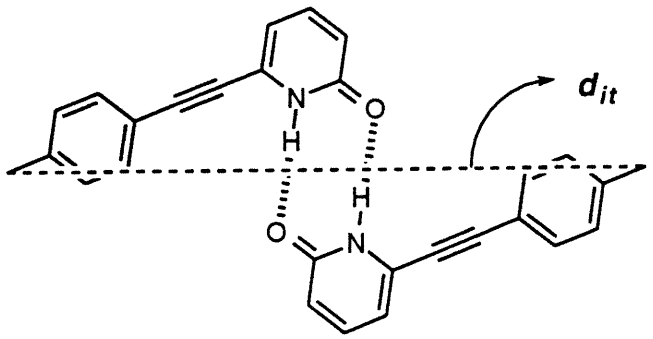

e

Scheme 14

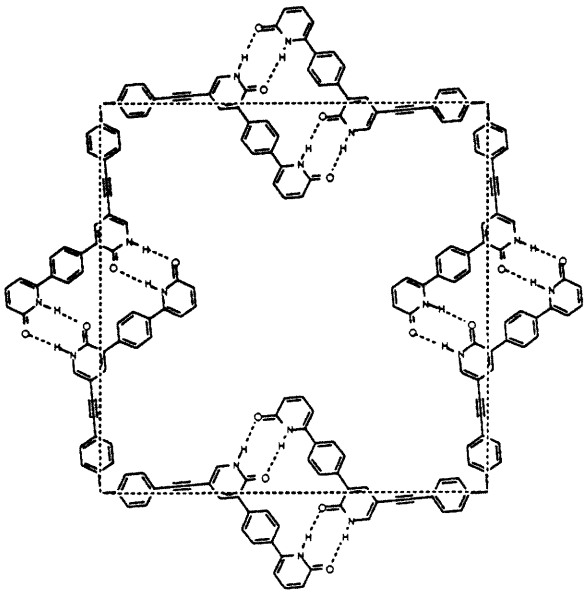

c

Scheme 15

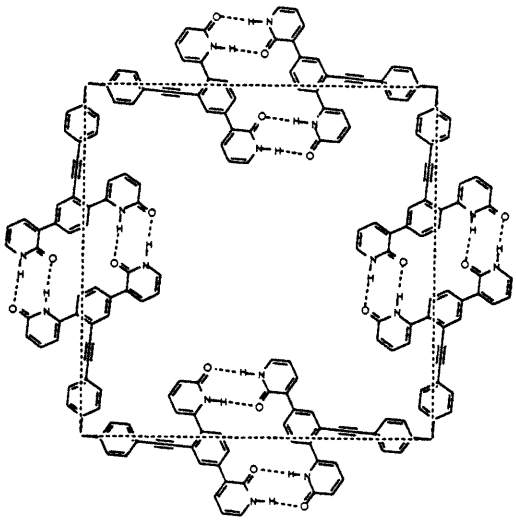

d

Scheme 16

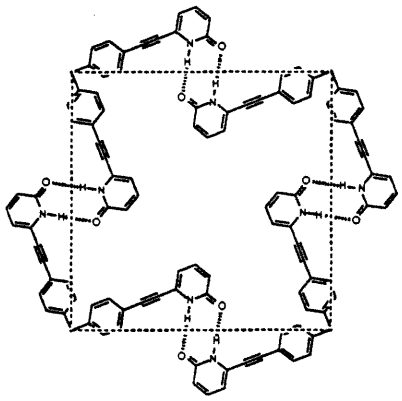

t

Scheme 17

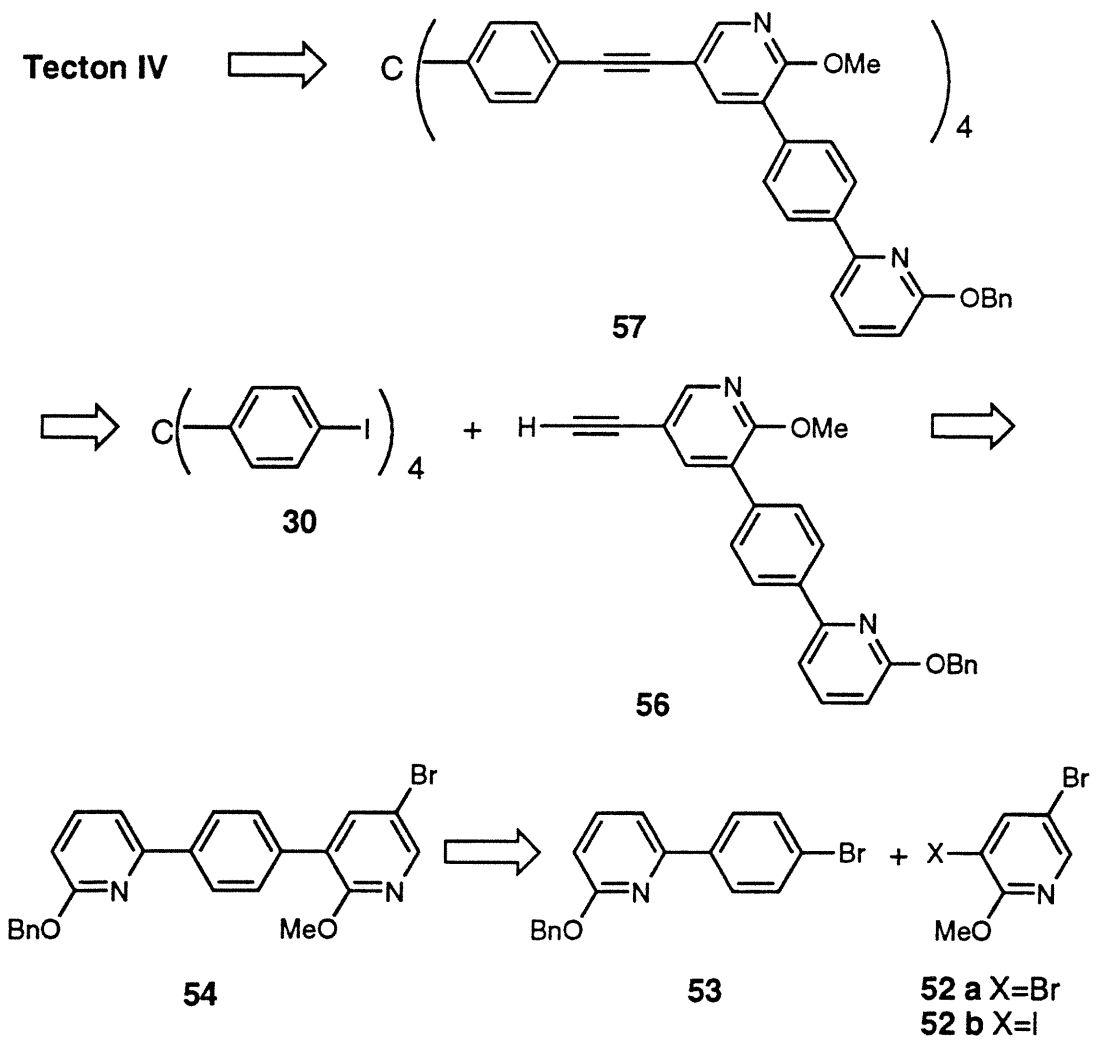

For all the reasons discussed above, we designed tecton **IV** and in light of the retrosynthetic analysis shown in Scheme 17, started its synthesis by the preparation of key synthon **52**, 3,5-dihalo-2-methoxypyridine[27-30]. 3,5-Dibromo-2-methoxypyridine (**52a**)[27] could be obtained in moderate yield by a one-step reaction (shown in Scheme 18). Under cross-coupling reaction conditions, the bromo group in the 3-position proved to be more reactive than that in the 5-position. As shown in Scheme 19, it was further coupled with bromide **53** to provide dipyridine bromide **54** in 47% yield. To confirm that we had in fact obtained the right product, we synthesized 5-bromo-3-iodo-2-methoxypyridine (**52b**)[28-30] in four steps (shown in Scheme 18). The iodo group is more reactive than the bromo group, and the coupling reaction of compounds **52b** and **53** gave dipyridine **54** in

Scheme 18

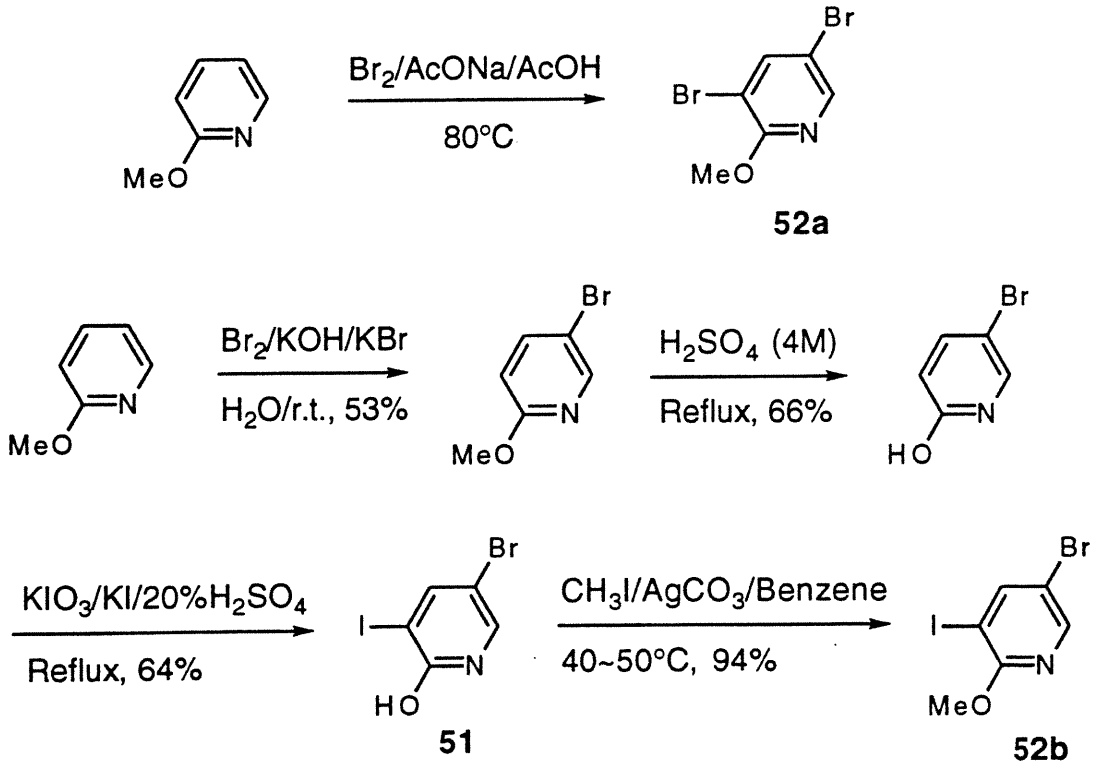

Scheme 19

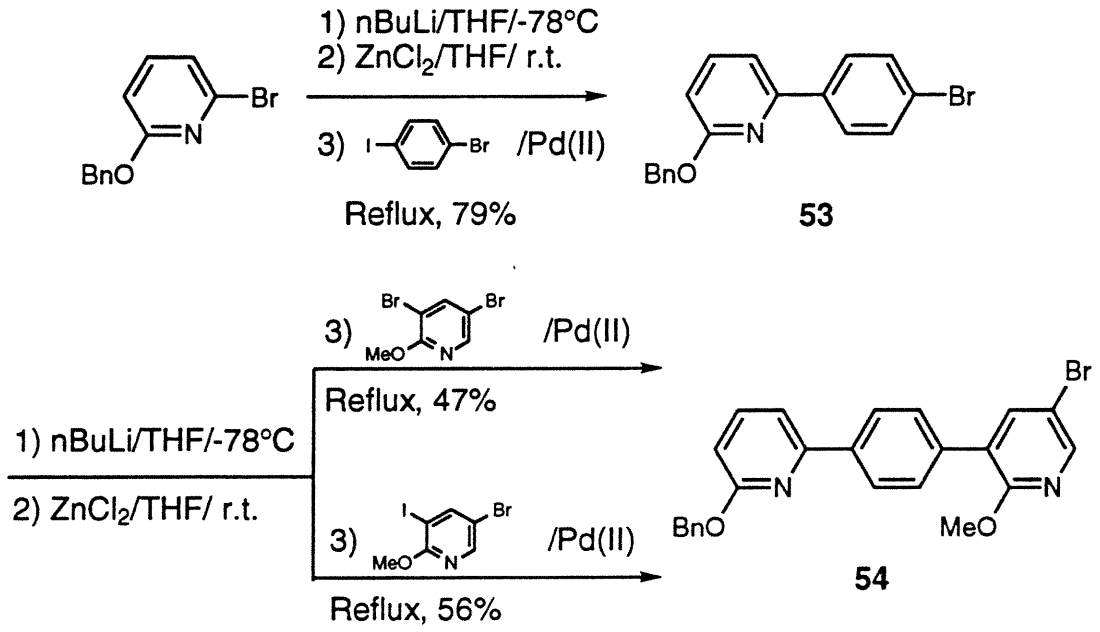

56% yield. Both ^{1}H and ^{13}C NMR spectra of dipyridine **54** made from compound **52b** are the same as those of dipyridine **54** derived from compound **52a**. Therefore, we gave priority to the preparation of tetrakis(dipyridine) **57** by the first method in four steps (shown in Scheme 20) in an acceptably high overall yield of 62%.

Simultaneously, we attempted to synthesize tetrakis(dipyridine) **64** (shown in Scheme 21) in different ways. From the retrosynthetic analysis as shown in Schemes 22 and 23, the strategy of making compound **64** should be based on a properly multisubstituted phenyl ring which is able to couple with 3- and 6-bromo-2-(phenylmethoxy)pyridine sequentially to finally provide dipyridylacetylene **63**. We chose aniline as starting material because the amino group not only has a strong effect on the orientation of halogenation of the aromatic ring but also can be converted to a halogen

group eventually. Kajigaeshi and co-workers[31] have reported a facile synthetic method for halogenating aromatic amines using quaternary ammonium polyhalides as halogenation

Scheme 20

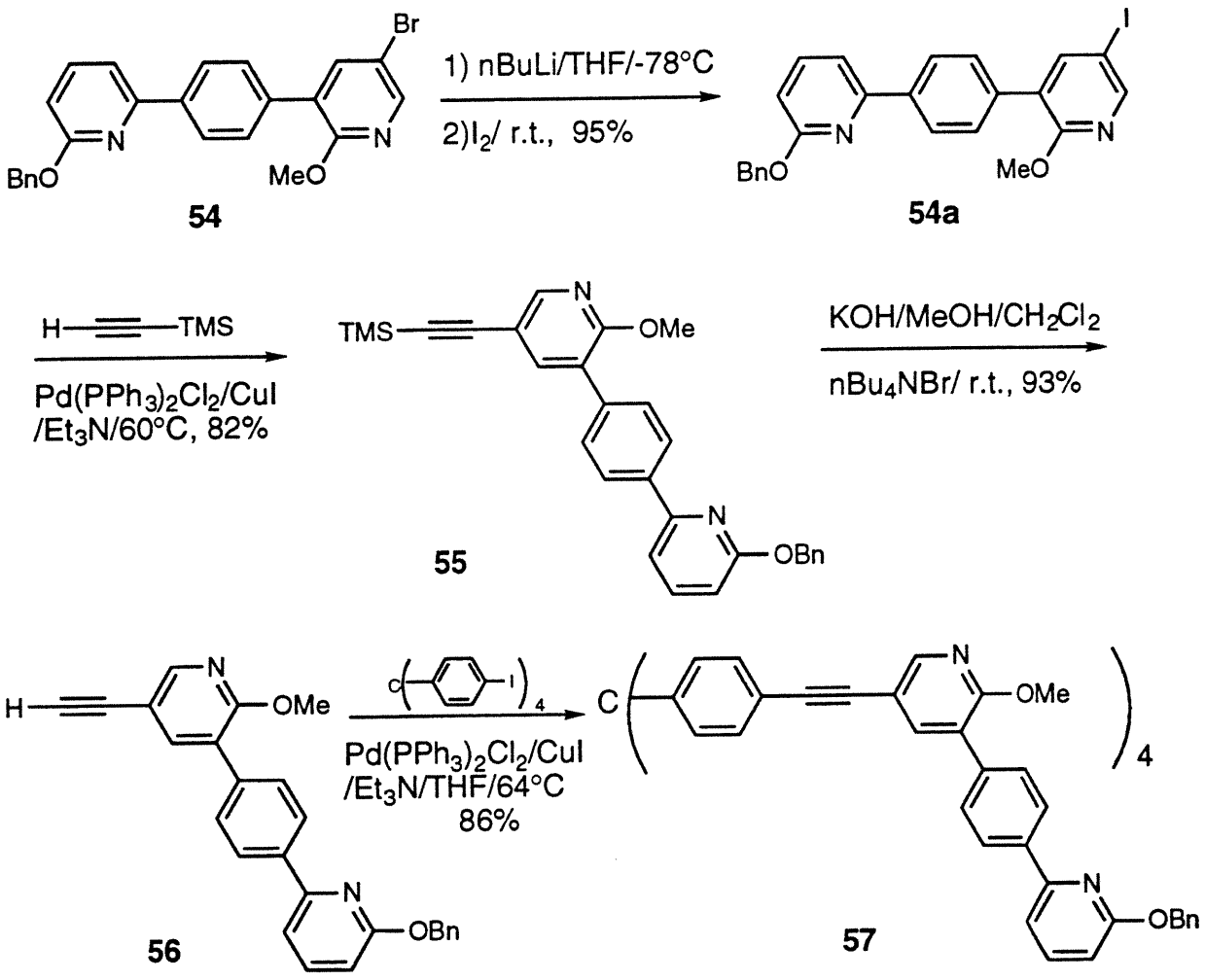

Scheme 21

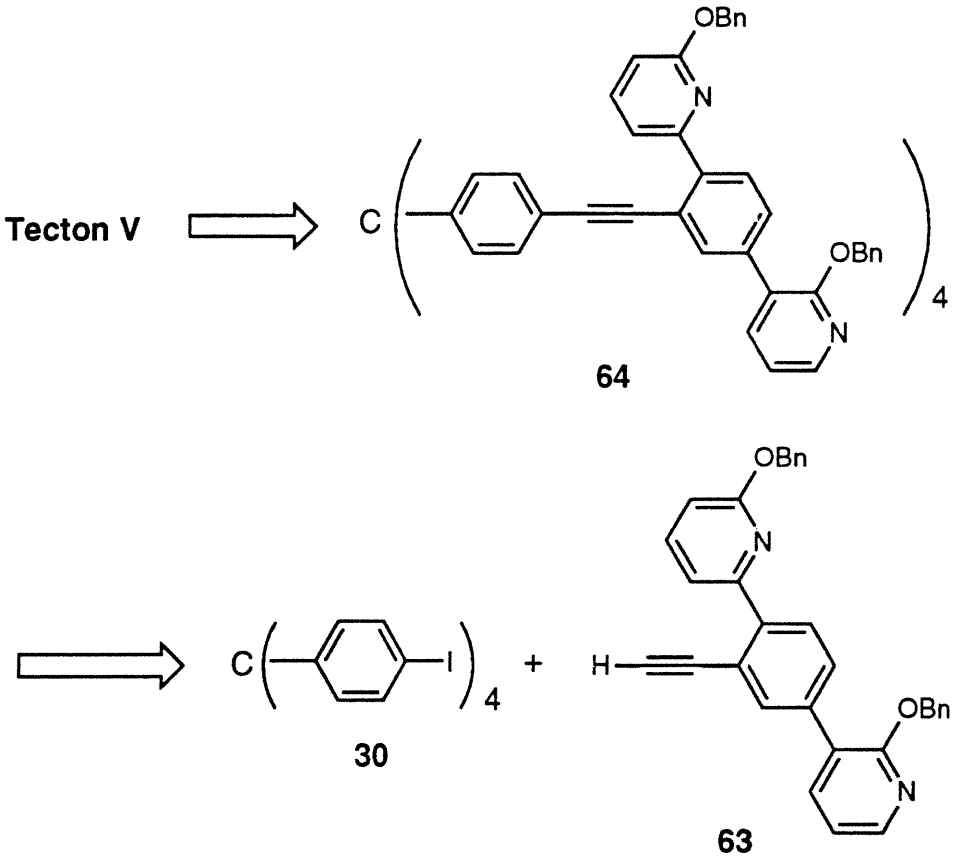

Scheme 22

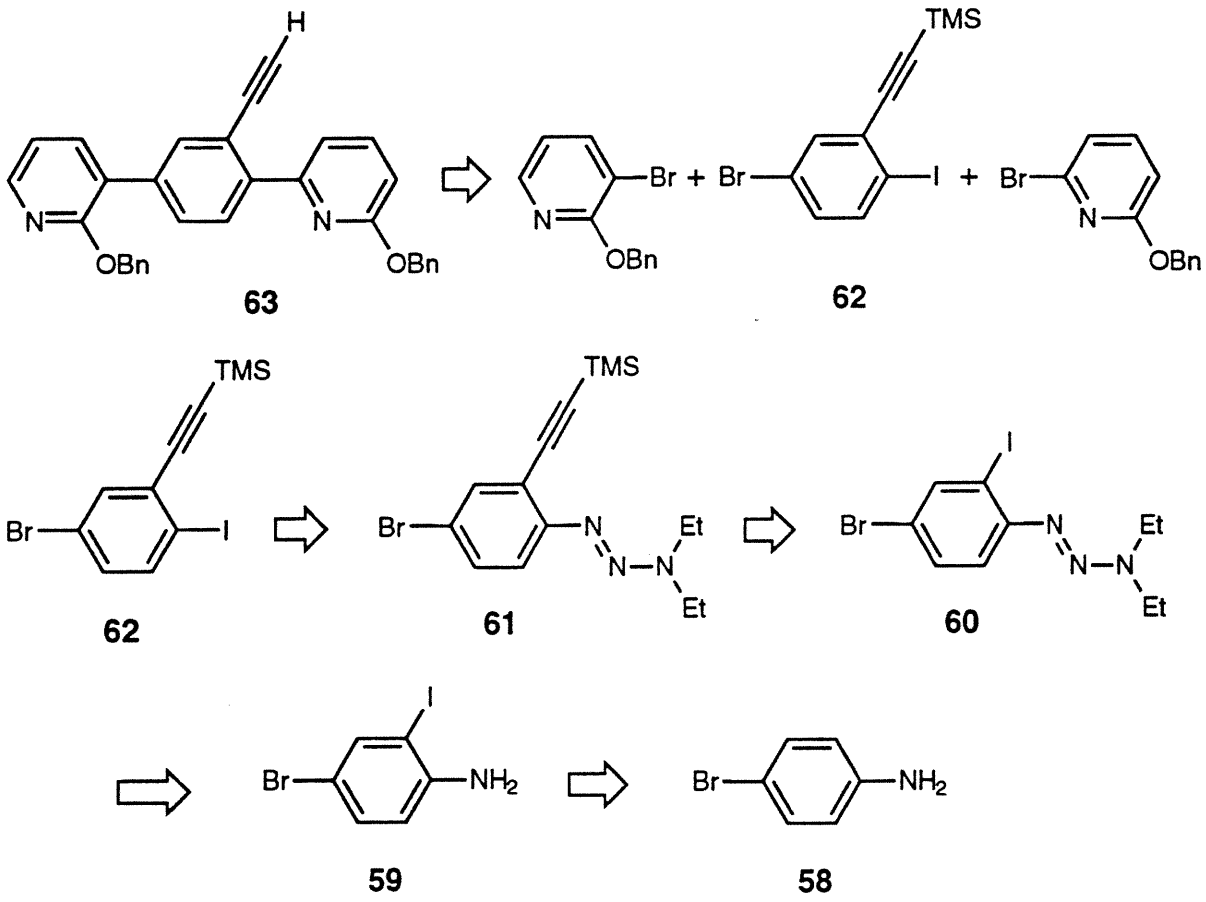

reagents. Barrio and co-workers[32] have developed a convenient synthesis of aryl halides from aryl amines via treatment of 1-aryl-3,3-dialkyltriazenes with trimethylsilyl halides. Recently, Moore and co-workers[33] discovered another convenient and mild procedure for preparing aryl iodides from triazenes in excellent yield under neutral conditions. With these procedures in mind, we started our strategy (shown in Scheme 24) by treatment of aniline with tetrabutylammonium tribromide ($TBABr_3$)[34] and benzyltrimethylammonium

dichloroiodate ($BTMAICl_2$)[31b] sequentially to obtain 4-bromo-2-iodoaniline (**59**) in fair yield. Compound **59** was then converted into 1-(4-bromo-2-iodophenyl)-3,3-diethyltriazene (**60**) by sequential treatment with $NaNO_2$ / HCl and K_2CO_3 / Et_2NH at 0°

Scheme 23

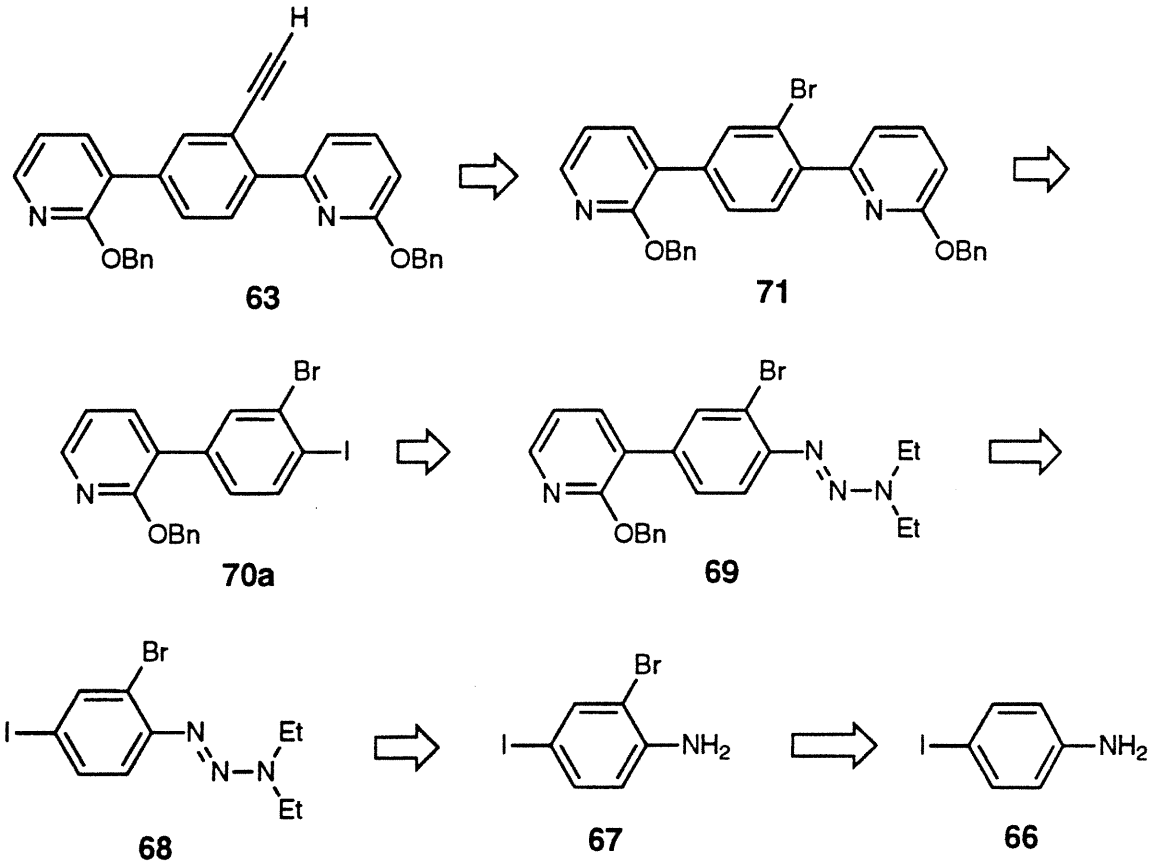

in 96% yield[32b]. Unfortunately, cross-coupling of compound **60** with trimethylsilylacetylene gave an almost 1:1 mixture of aryl triazenes **61** and **65** in a yield of 81%. Apparently, there is no chemoselectivity in the cross-coupling reaction despite the normal difference in reactivity between bromide and iodide. This may result from steric

hindrance of the triazenyl group. In addition, we were unable to separate compounds **61** and **65** from one another by flash chromatography on silica gel.

We then tried the alternative synthesis shown in Scheme 25. Unfortunately, the bromination of 4-iodoaniline gave a mixture of 2-bromo-4-iodoaniline and 2,4-dibromoaniline, and they could not be separated from each other by flash chromatography

Scheme 24

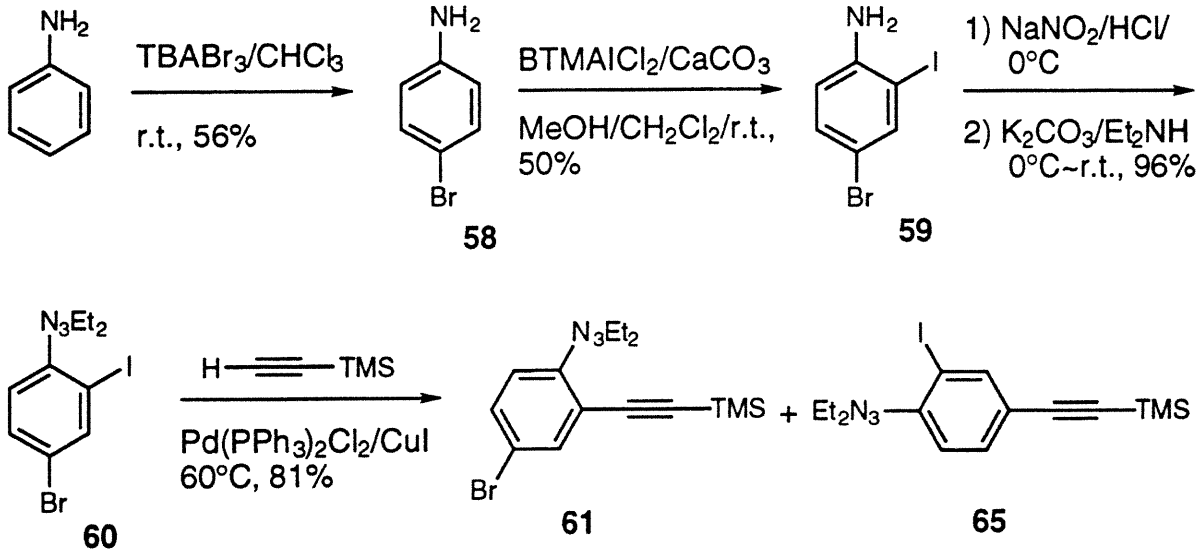

on silica gel. In light of the poor selectivity of triazene **60** in coupling reactions catalyzed by Pd(II), we elected to carry out cross-coupling of the mixture of triazenes **68** with a pyridylzinc chloride in the expectation of obtaining para-coupled product **69** in a yield of more than 50%. Therefore we did not try further purification of dihalides **67a** and **67b**, and we instead converted crude compound **67** directly to a mixture of triazenes **68**, which was then coupled with a pyridylzinc chloride to provide triazene **69** in 57% yield. Unfortunately, iodide **70a** was not afforded by applying Moore's method[33] of conversion of triazenes to aryl iodides even when the reaction was carried out during longer periods

and at higher temperatures. On the other hand, Barrio's method[32] caused simultaneous deprotection of benzyloxy group so that the conversion of triazene **69** in this way gave a mixture of pyridine **70a** and pyridone **70b**. Although compound **70b** was finally isolated from the mixture in poor yield, reprotection of the pyridone ring is needed in order to continue the synthesis. Because of the multiple difficulties encountered, we abandoned the synthesis.

Scheme 25

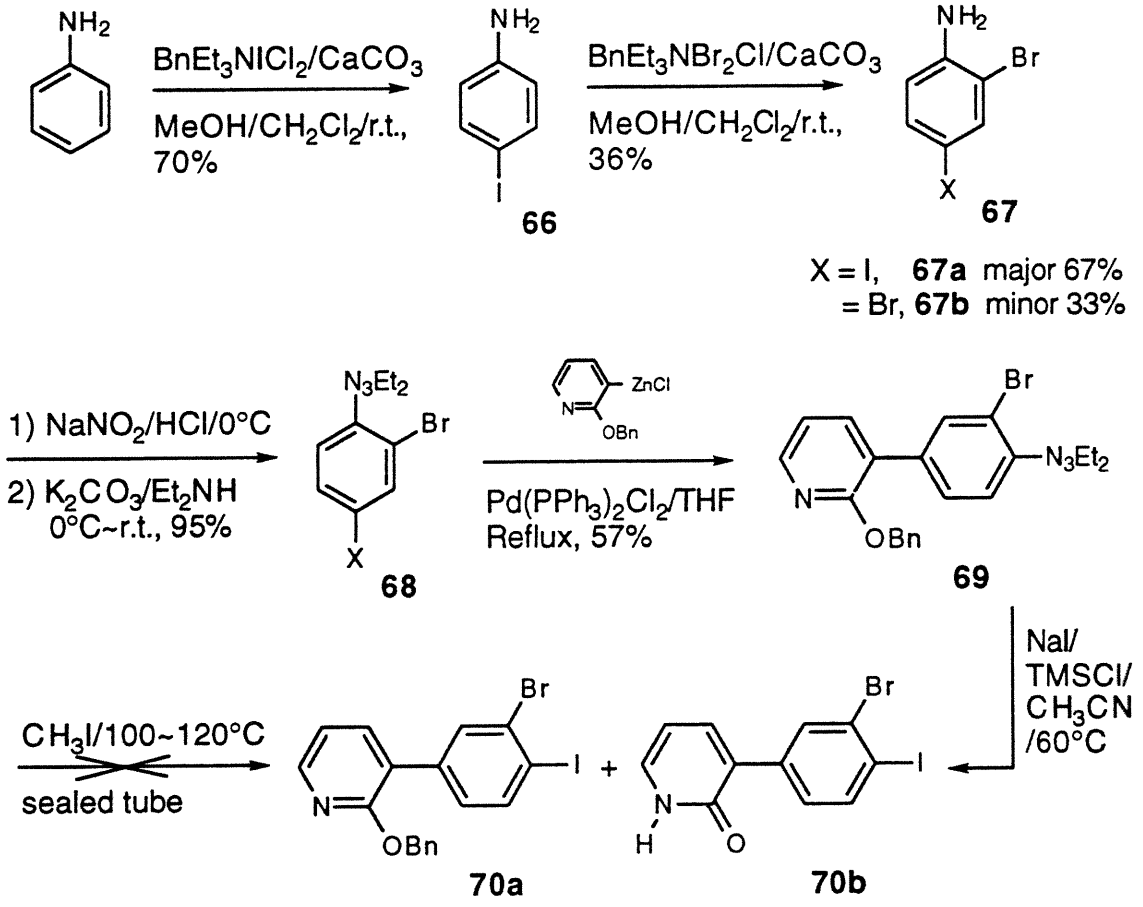

The work described above shows that to obtain tectons with amplified intertectonic adhesion, both clever design and ingenious synthetic strategies are required. Cyclization

happened during deprotection of tetrakis(dipyridine) **44** (Scheme 5) and **50** (Scheme 6) may be difficult to avoid, but we are optimistic that tectons **IV** and **V** (Scheme 45) can be synthesized, and we believe that they have been designed cleverly and thoughtfully. In fact, we have obtained tetrakis(dipyridine) **57** by a quite simple and reliable synthetic strategy in an acceptable yield. What remains is to find a more efficient method for deprotecting this compound to obtain tecton IV, which will require additional effort and time. In the case of tecton **V**, we could not even obtain tetrakis(dipyridine) **64** (Scheme 21) by the synthetic strategy that we chose to implement. To succeed, we will need to overcome problems caused by poor regioselectivity in cross-coupling reactions, and we will need to find more suitable masking groups that can subsequently be converted into aryl halides for cross-coupling. We expect these problems to be solved by further work.

CHAPTER 4

FUNCTIONALIZED TECTONS

In Chapter 2 we have shown that tecton **I** is capable of generating an open network built of seven interpenetrating diamondoid lattices by self-assembly. The ability of channels defined by diamondoid networks to enclathrate carboxylic acids selectively in the presence of other solvents such as methanol and hexane encouraged us to investigate if it is possible to create functionalized tectons that might be able to generate networks with channels or cavities with more specific chemical or physical properties. To create tectons like these, one of the most important things which should not be ignored is that the stickiness of the tectons should not be weakened. Therefore while we tried to introduce more functional features in tecton **I**, we considered carefully the effect of these functional features on the stickiness of the tecton. One interesting possibility is to introduce an amino group into tecton **I**. Inuzuka and co-workers[35] have investigated the lactam-lactim tautomerization of monoamino-substituted 2-pyridinols in THF. They found that the lactam form is more stable than the lactim form in monoamino-2-pyridinol. In addition, among the four amino-2-pyridones, 6-amino-2-pyridone has the largest dimer formation energy and 3-amino-2-pyridone the smallest (shown in Table 8). It is noteworthy that in addition to 6-amino-2-

pyridone, the calculated dimer formation energy of 4-amino-2-pyridone is larger than that of 2-pyridone as well. Beak and co-workers[36] have discussed the effect of 3- and 6-substituents on the self-association of 2-pyridones. They discovered that substituents which can interfere with intermolecular hydrogen bonding will reduce the self-association

Table 8. The hydrogen bond energies (ΔH_D), corrected hydrogen bond energies (ΔH_{Dc}), and equilibrium distances (R_e) of monoamino-substituted 2-pyridone dimers, as calculated by the CNDO/2 method.[35]

Dimer	Sym.	R_e(H•••O) (Å)	$-\Delta H_D$(kJmol^{-1})	$-\Delta H_{Dc}$(kJmol^{-1})
3-Amino-2-pyridone	C_{2h}	1.48	84.9	38.6
4-Amino-2-pyridone	C_{2h}	1.45	101	45.7
5-Amino-2-pyridone	C_{2h}	1.47	91.3	41.4
6-Amino-2-pyridone	C_{2h}	1.46	109	49.1
2-Pyridone	C_{2h}	1.46	95.7	43.4

Table 9. Association of hydroxypyridine-pyridones measured by vapor pressure osmometry.[36]

Substrate	Concentration, M	Solvent	% associated dimer
71a	5×10^{-2}	methylene chloride	86±5
72	5×10^{-2}	methylene chloride	68±9
73	5×10^{-2}	methylene chloride	35±7

of the pyridinol-pyridone systems (see Table 9 and Figure 46). Comparison of the association of 3-substituted pyridone **72** with 4-substituted pyridone **71a** shows that the

former is less associated because of steric repulsion in 3-position. Moreover, the effect of the 3-carboalkoxy substituent in the association of pyridone **73** relative to that of compound **71a** and **72** apparently results in a further decrease in association partially due to the formation of an intramolecular hydrogen bond as shown in structure **74**. In tecton **I**,

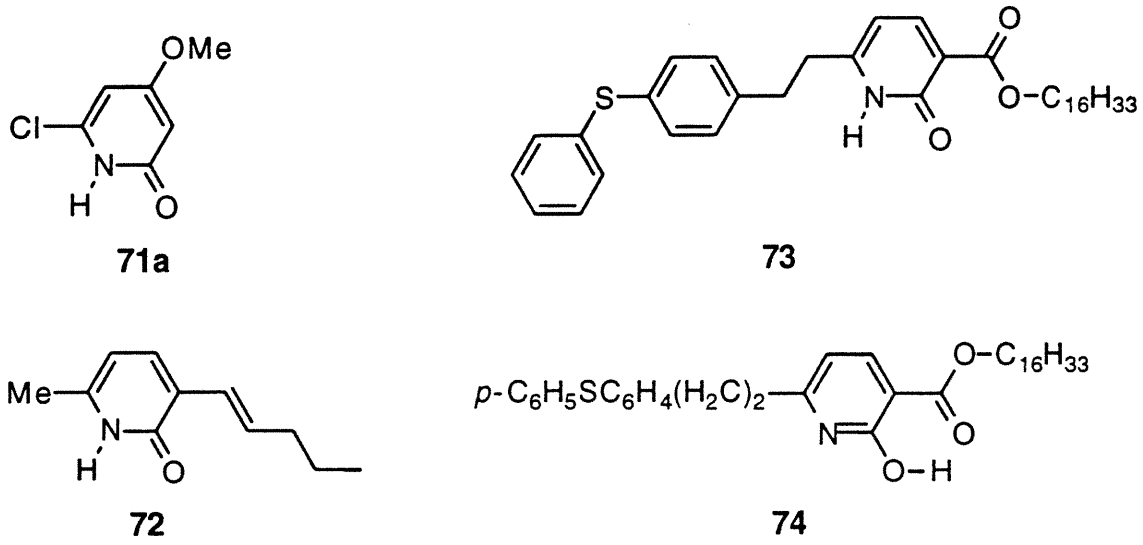

Figure 46. Structures of substrates cited in Table 9.[36]

the 6-position of the pyridone rings is connected to the tetrahedral core structure. This leaves the 4-position available for introducing an amino group, which should not have any negative effects on association. Therefore we designed new tecton **VI** as shown in Scheme 26. In order to investigate the effect of the substituent's position and electronic properties on the stickiness of the tecton, we also decided to study tecton **VII** (shown in Scheme 26), in which two bromo groups are introduced in the 3- and 5-positions.

To synthesize tecton **VI**, we first made 4-amino-6-bromo-2-(phenylmethoxy)pyridine[37a-b] (**75a**) from 2,6-dibromopyridine in four steps as presented in Scheme 27. After desilylation of the coupling product **76a** of bromopyridine **75a** and trimethylsilylacetylene, pyridylacetylene **77a** was coupled with tetraiodide **30** to provide tetrapyridine **78a** in 80% yield. Unfortunately, when we tried to deprotect tetrapyridine

78a with TFA at different temperatures for different lengths of time, pure tecton **VI** was never afforded. Other methods failed as well, possibly because 4-aminopyridines are moderate bases with a pKa around 9.7, and the triple bond is quite sensitive to electrophilic

Scheme 26

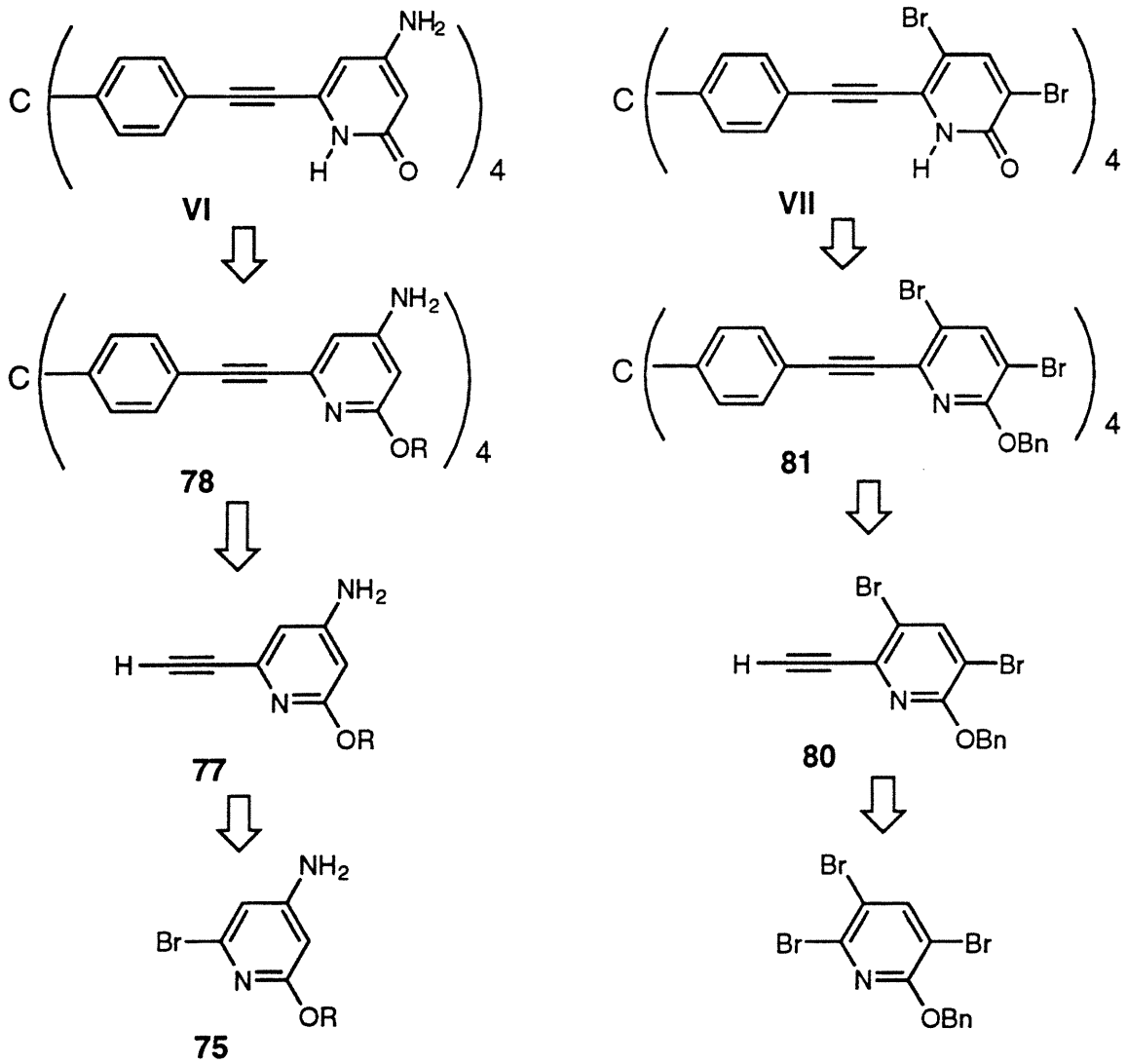

Scheme 27

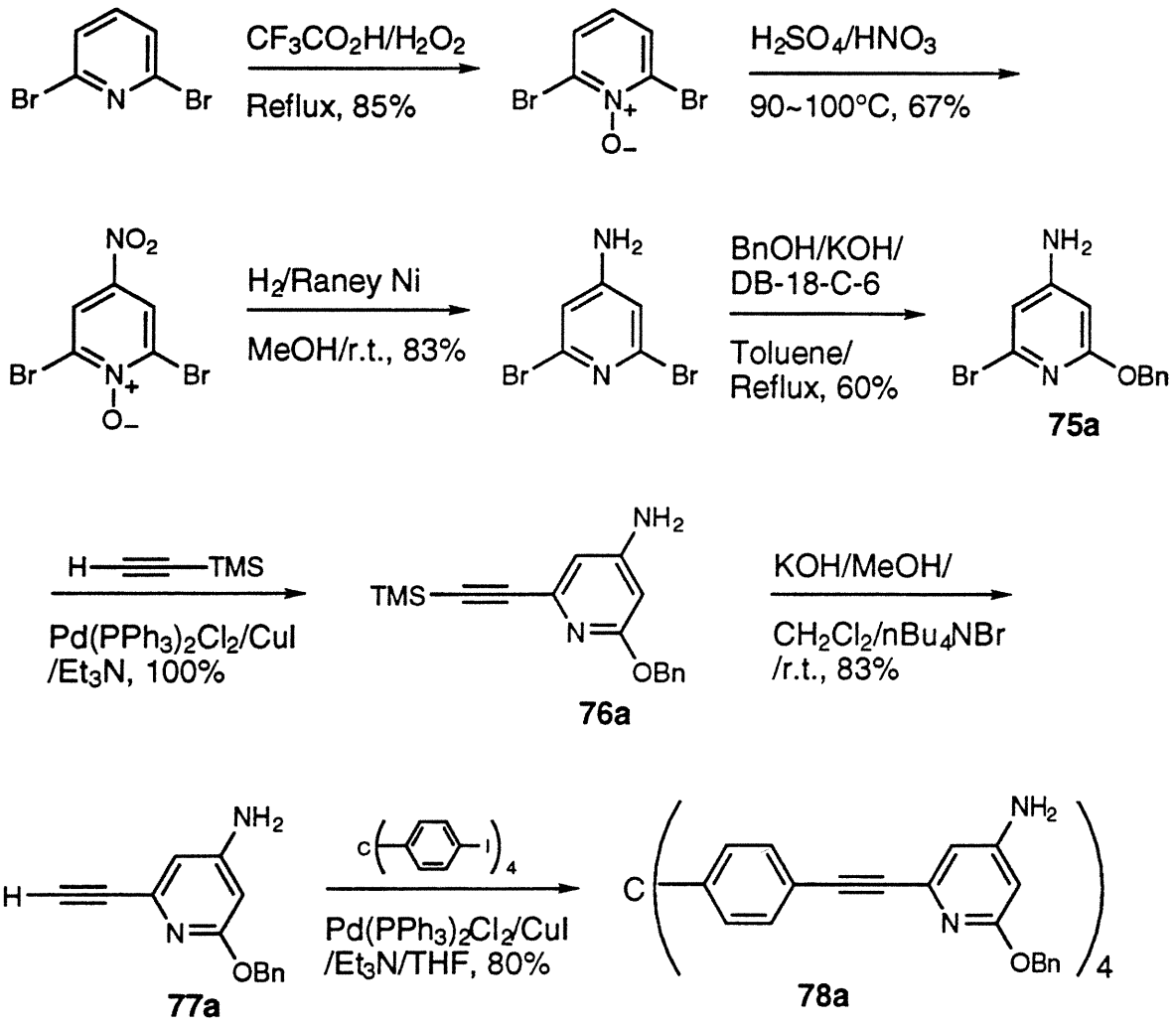
CF3CO2H/H2O2
Reflux, 85%
H2SO4/HNO3
90~100°C, 67%
H2/Raney Ni
MeOH/r.t., 83%
BnOH/KOH/
DB-18-C-6
Toluene/
Reflux, 60%
75a
H—≡—TMS
Pd(PPh3)2Cl2/CuI
/Et3N, 100%
76a
KOH/MeOH/
CH2Cl2/nBu4NBr
/r.t., 83%
77a
Pd(PPh3)2Cl2/CuI
/Et3N/THF, 80%
78a

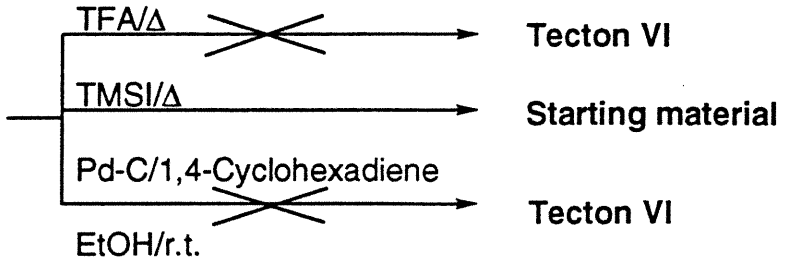
TFA/Δ
Tecton VI
TMSI/Δ
Starting material
Pd-C/1,4-Cyclohexadiene
EtOH/r.t.
Tecton VI

Scheme 28

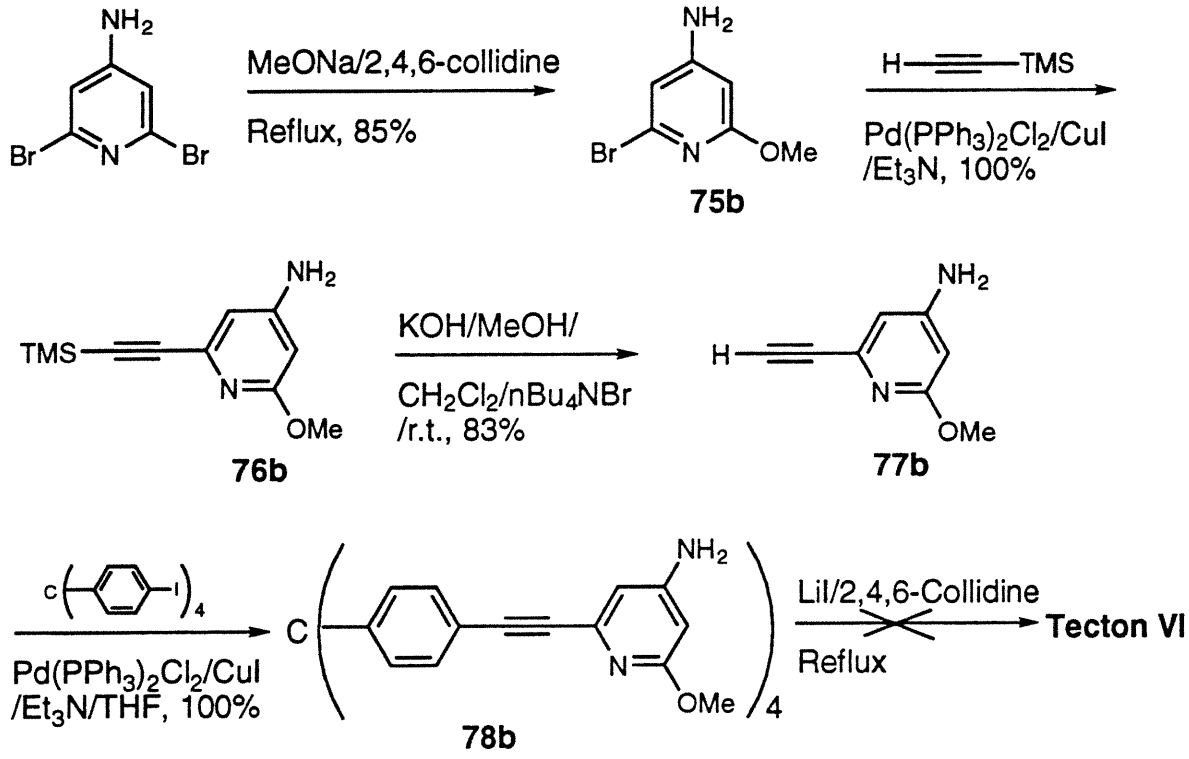

addition. As a consequence, we decided to protect the masked pyridones as a methoxypyridine instead, and we attempted to synthesize tetrakis(aminopyridine) **78b** (shown in Scheme 28). Unfortunately, attempts to deprotect tetrakis(aminopyridine) **78b** using LiI in 2,4,6-collidine[37c] with heating for 2 days failed to give pure tecton **VI**, and we were only able to obtain a small amount of what appeared to be a mixture of products deprotected to different extents.

The method devised by Richard for making 3,6-dibromo-2-(phenylmethoxy)-pyridine (**40**) leads to 3,5,6-tribromo-2-(phenylmethoxy)pyridine as an intermediate product (shown in Scheme 7).[26] Dibromopyridyl acetylene **80** could be provided in two steps, by coupling 3,5,6-tribromo-2-(phenylmethoxy)pyridine with trimethylsilylacetylene

to give compound **79** in 44% yield, which was then desilylated in 41% overall yield. The product was further coupled with tetraiodide **30** to give tetrakis(dibromopyridine) **81** in

Scheme 29

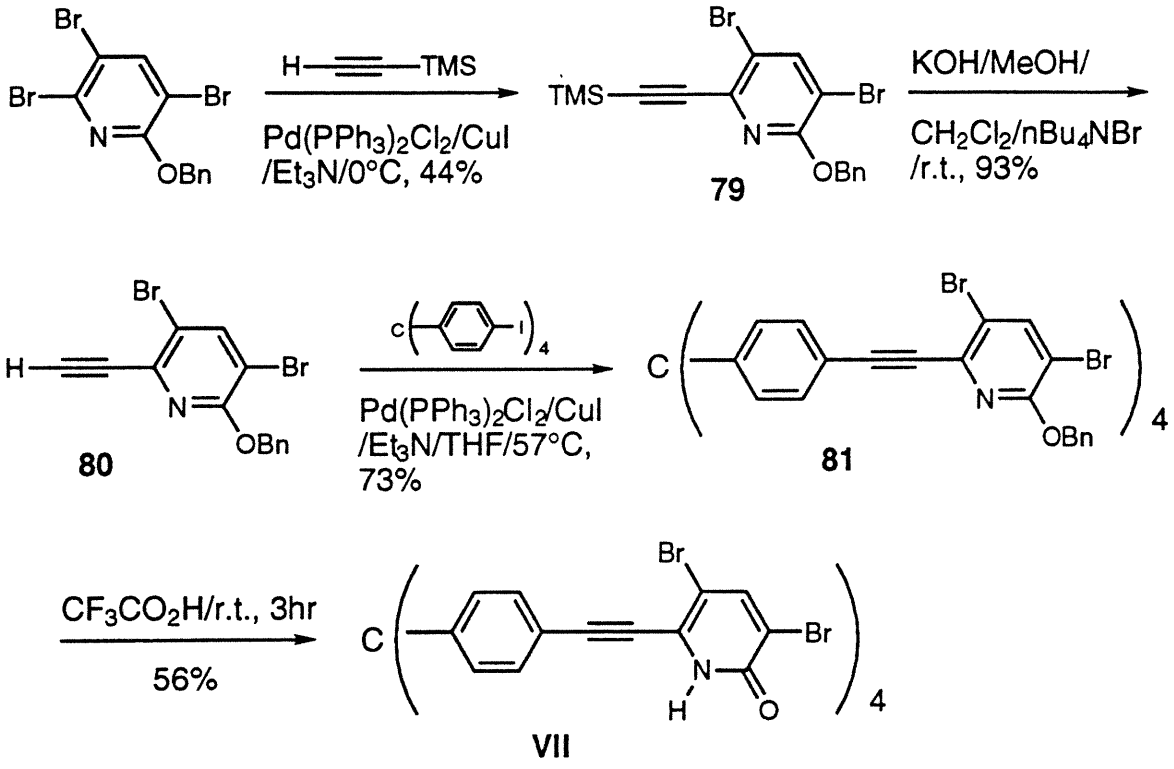

73% yield. Deprotection of compound **81** with TFA at room temperature in 3 hours gave tecton **VII** in 56% yield (shown in Scheme 29). We tried to crystallize tecton **VII** from carboxylic acids but did not get crystals.

This work shows that the introduction of the amino groups introduced into tecton **I** makes the deprotection of either tetrapyridine **78a** or **b** much more difficult. This is unfortunate, because it is important to design and synthesize organic solid materials with

more specific chemical and physical properties. In addition, even though we could not crystallize tecton **VII** to provide crystals suitable for X-ray structure determination, the bromo groups present in tetrapyridine **81** might be useful for further introducing some other functional groups into tecton **I** in order to produce tectons with unusual properties.

CHAPTER 5

TECTONS WITH MODIFIED ARCHITECTURAL FEATURES

It has been shown that the intertectonic distance in diamondoid networks derived from tecton **I** is around 19-20 Å, and that the network defines open channels with diameters of 8.1 Å x 3.5 Å as shown in Figure **44**. It is noteworthy that even though the degree of interpenetration is as high as seven, almost nanosized and well-defined channels are still formed. When tecton **I** was crystallized from different carboxylic acids, the individual tectonic subunits proved to have different symmetries. Those crystallized from propionic acid were shown to have S_4 symmetry in the crystal, while those crystallized from butyric acid have C_2 symmetry. This phenomenon implies that the detailed geometry adopted by the tecton has an important effect on its organization in the solid state. Following the crystallographic laws of close packing, the tectons pack themselves along axes of either 4- or 2-fold symmetry with intermolecular distances 7.79 Å and 7.35 Å, respectively. Apparently, these distances are determined by the conformation of the tecton and by the pattern of hydrogen bonding they finally adopt under the direction of the principles of close packing. These observations encouraged us to modify the architectural features to find out more about the relationship between the size and shape of the tecton, the strength of intertectonic interaction, and the nature of the resulting networks. Meanwhile, the stickiness of tectons is a factor that cannot be neglected when new tectons with modified geometries are designed.

5.1. Isomers of tecton I which are able to define longer intertectonic distances and therefore may generate diamondoid networks with more open channels.

There are three isomers of tecton **I** as shown in Scheme 30 and Scheme 31. Although the tetrahedral architectural feature is maintained in these isomeric tectons, the geometry of hydrogen bonding with respect to the core structure has changed. We can describe it by introducing parameters ϕ and θ. We define the parameter ϕ as the angle of orientation of the dipole of the enamine group with respect to the tetrahedral framework of tectons, while parameter θ represents the angle of orientation of the carbonyl group with respect to the tetrahedral framework of tectons (shown in Scheme 30 and 31). Parameter d_{it} represents the intertectonic distance (shown in Scheme 32). From Scheme 32 we can see that the different intertectonic distances are derived by intermolecular hydrogen bonding which has different geometries. While ϕ values vary from 60 to 180°, the intertectonic distances increase from tecton **I** to tecton **X**. Tectons **VIII** and **IX** have the same ϕ values, 120°, but different θ values, 120° and 0°, as shown in items ***f*** and ***g***. Therefore, different intertectonic distances result as shown in items ***f*** and ***g***. From Scheme 32 we can suggest that item ***h*** defines the longest intertectonic distance. This means that if tectons **VIII-X** could self-associate to generate infinite diamondoid networks, channels defined by the networks of tecton **X** might be the most open ones. In Scheme 33, schematic representations of the channels which might be derived by the diamondoid networks of tectons **VIII-X** are shown. Item ***i*** represents the channels derived from tecton **VIII**, item ***j*** from tecton **IX** and item ***k*** from tecton **X**. It seems that channel ***k*** is the most open one, and the conformation of hydrogen-bonded pyridone rings with respect to the frame of diamondoid lattices, which has been defined in Chapter 2, seems to have almost no effect on the diameters of channel ***k***. Therefore, we decided to try to make tectons **VIII-IX**.

Scheme 30

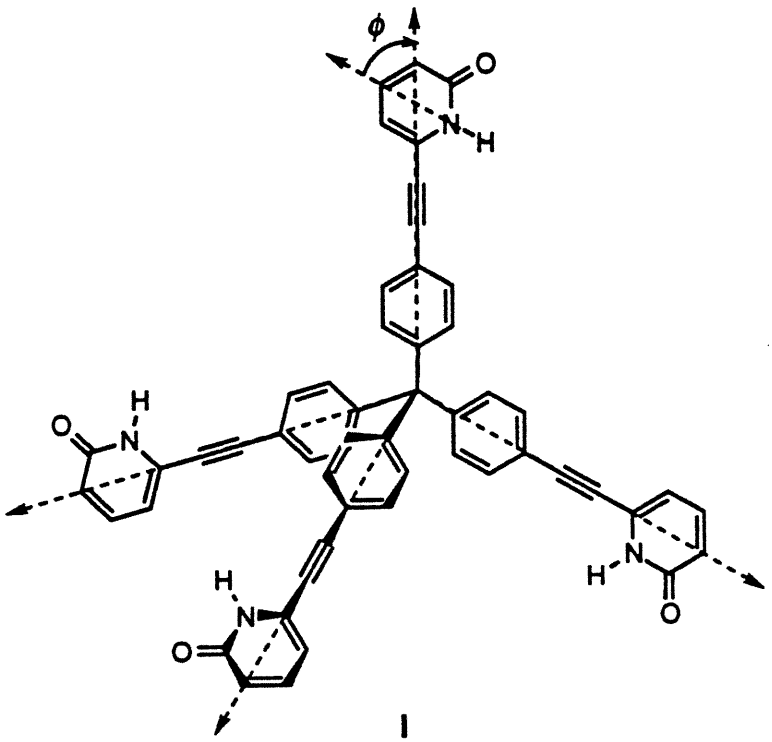

I

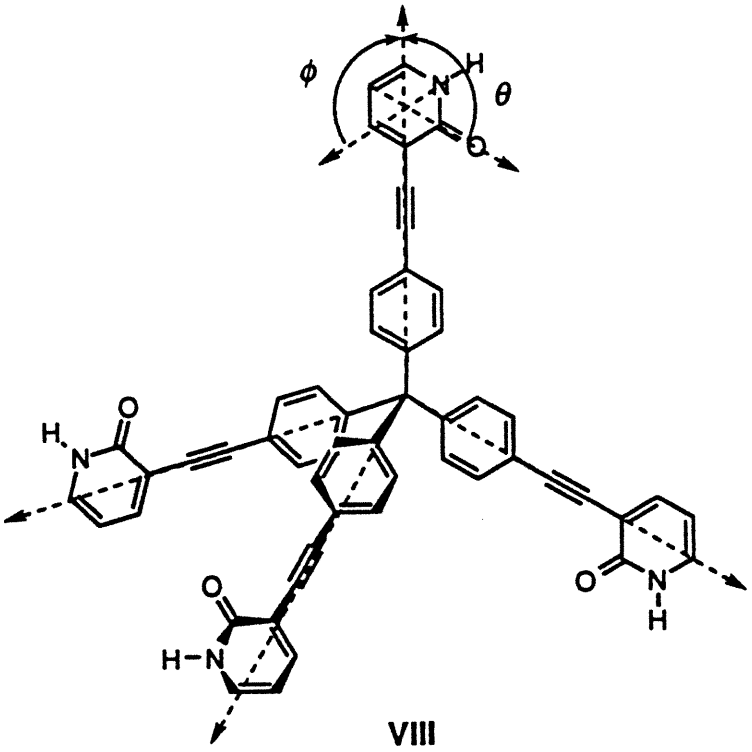

VIII

Scheme 31

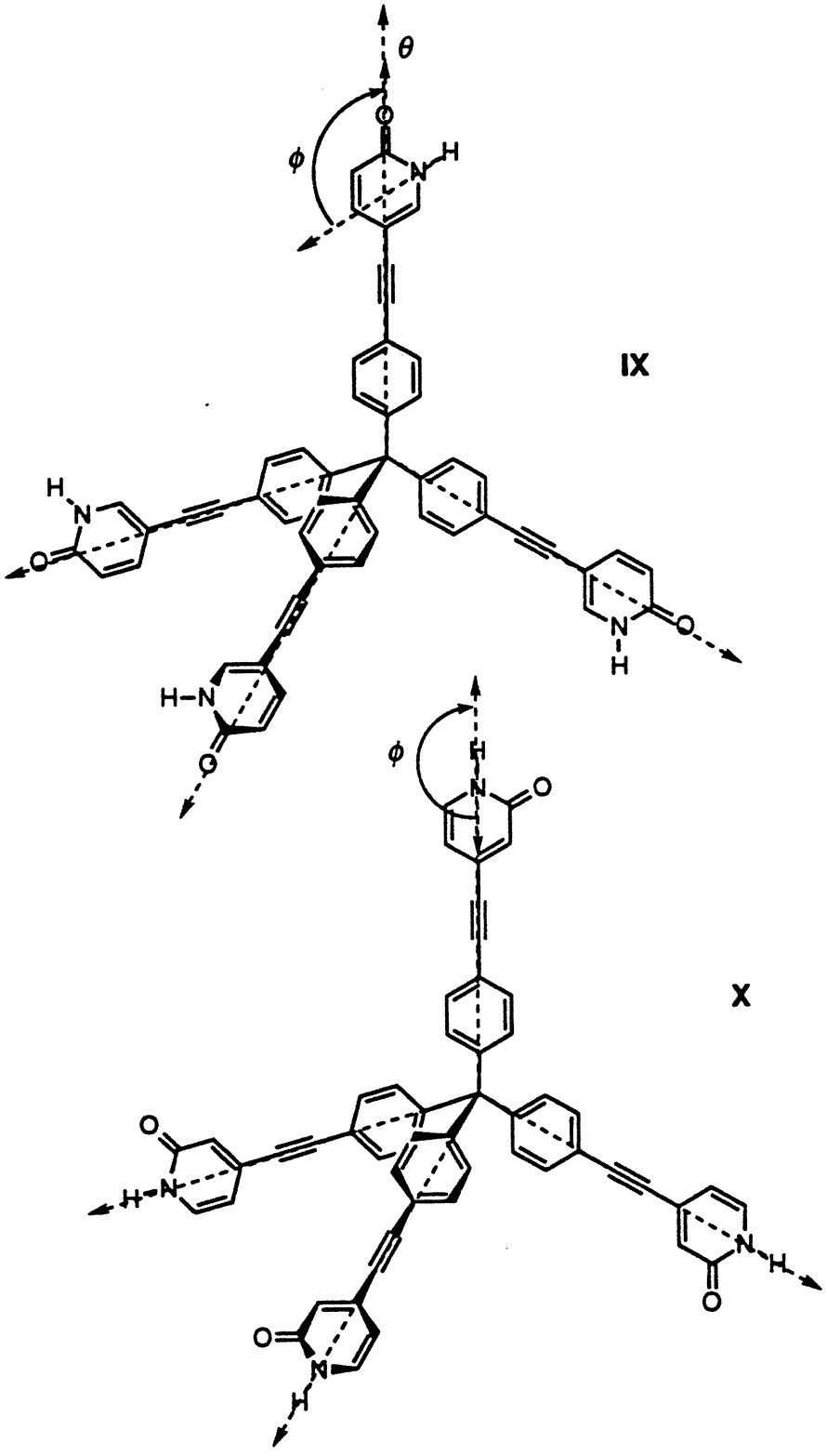

Scheme 32

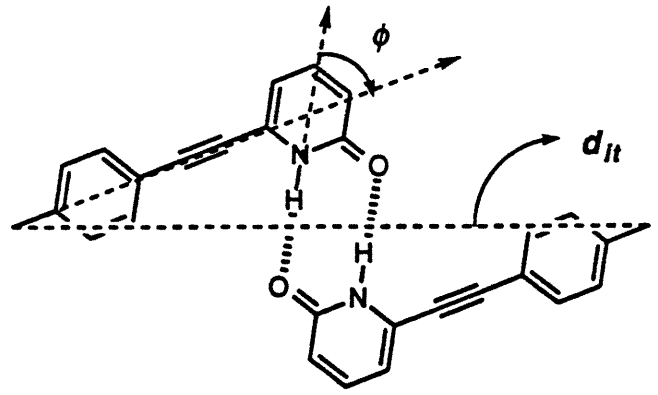

$\phi_e = 60°$

e

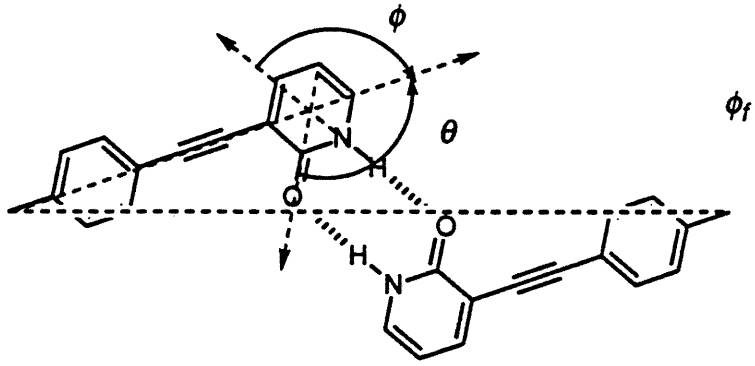

$\phi_f = 120°$, $\theta_f = 120°$

f

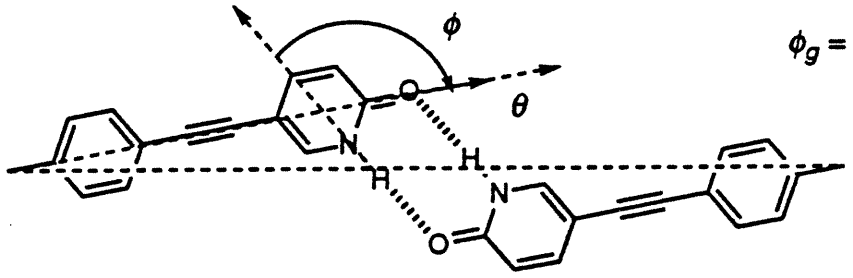

$\phi_g = 120°$, $\theta_g = 0°$

g

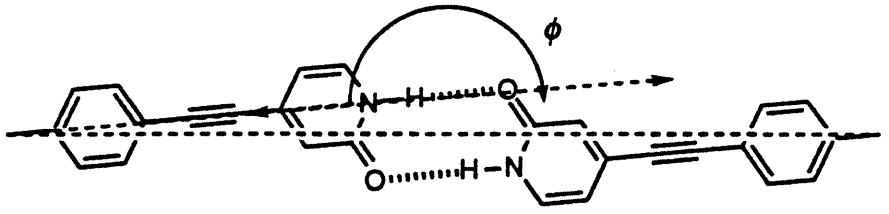

$\phi_h = 180°$

h

Scheme 33

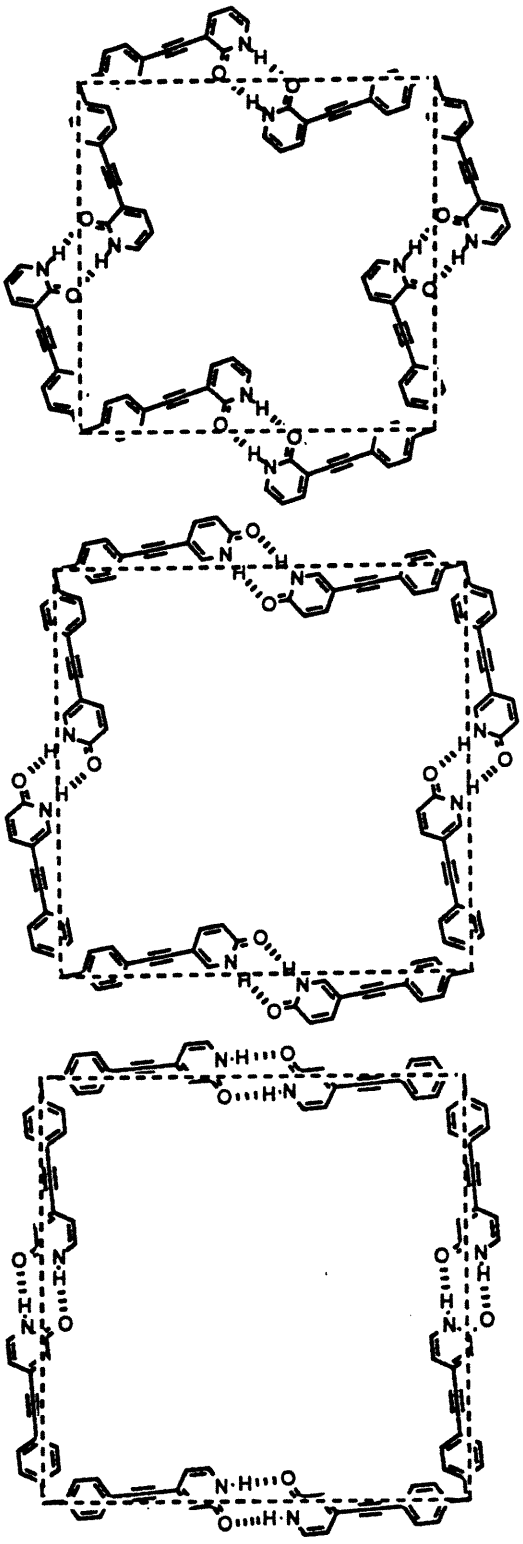

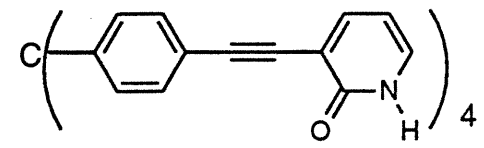

VIII

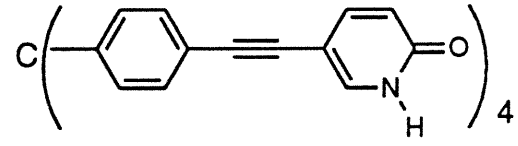

IX

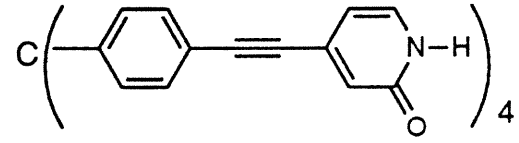

X

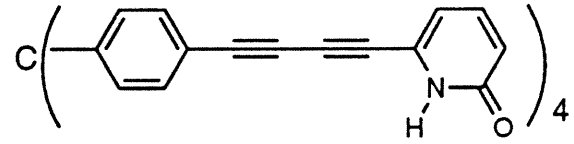

XI

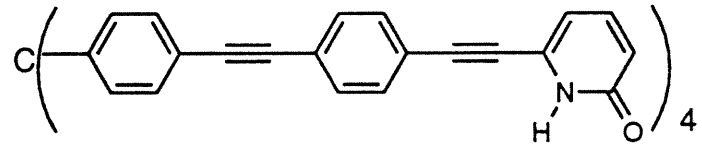

XII

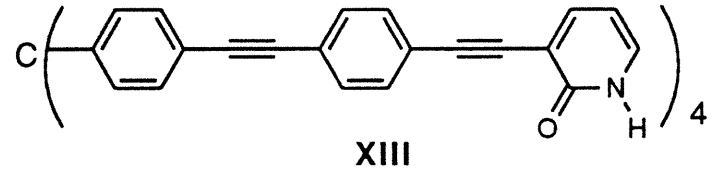

XIII

Figure 47. Tectons designed and synthesized with modified architectural features

(continued on page 109)

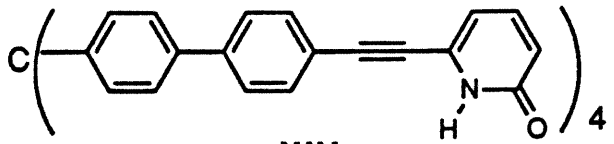

XIV

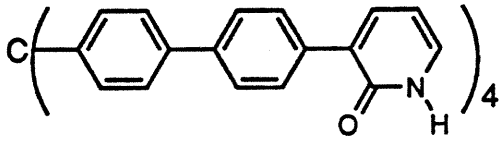

XV

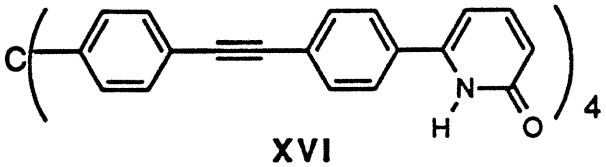

XVI

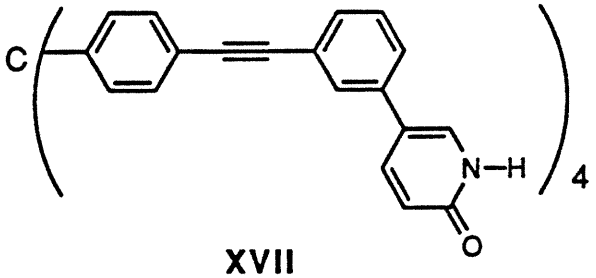

XVII

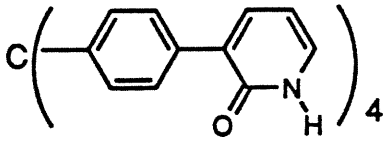

XVIII

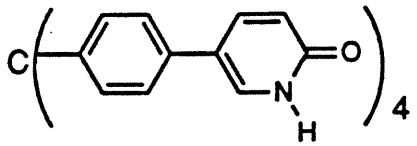

XIX

Figure 47. Tectons designed and synthesized with modified architectural features.

Since even a methyl group in the 6-position is effective in reducing association in the 2-pyridone system, we expected that tecton **VIII** (one of the isomers of tecton **I** shown in Figure 47) would be able to self-associate more strongly than tecton **I** to form a diamondoid network with somewhat larger channels resulting from the longer intertectonic distance (shown in Scheme 32). Tecton **VIII** was made by deprotection of tetrapyridine **82** with TMSI in quantitative yield. Compound **82** was synthesized by coupling tetraiodide **30**

Scheme 34

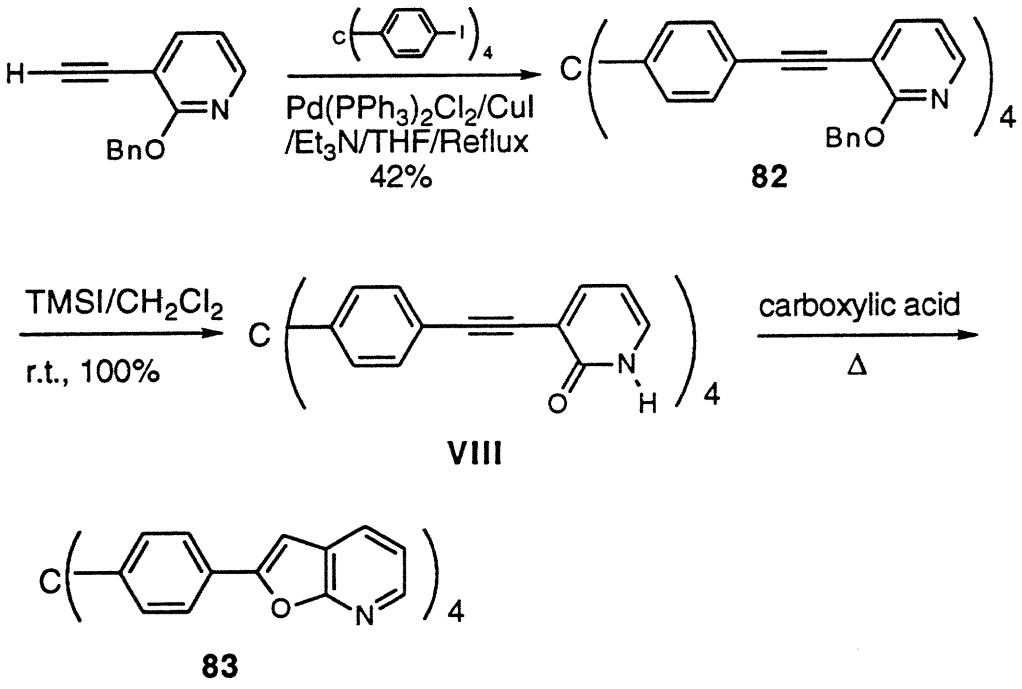

with 3-ethynyl-2-(phenylmethoxy)pyridine in 42% yield (shown in Scheme 34). We then tried to crystallize tecton **VIII** from carboxylic acids, and first found that it is less soluble in either small (such as acetic and propionic) or large (such as butyric and isobutyric) carboxylic acids than is tecton **I**. Then we found that cyclization occurred to give

compound **83** (shown in Scheme 34) when tecton **VIII** was dissolved in carboxylic acids at higher temperatures during longer periods of time. The poor solubility of tecton **VIII** in simple carboxylic acids may reflect enhanced stickiness. Therefore we chose more acidic carboxylic acids such as 2-chloropropionic acid as solvents, and we found that tecton **VIII** could be dissolved in it by being heated briefly at 80°C. However, the crystallization from 2-chloropropionic acid was not very promising, since it again induced the formation of cyclized product **83**. In an attempt to avoid the cyclization, we turned to basic solvents such as dibutylamine, aniline, and acetonitrile. After extensive experiments, we succeeded in crystallizing tecton **VIII** from a solvent system of DMF/diisopropylamine. X-ray diffraction revealed that crystals of tecton **VIII** from DMF/diisopropylamine were seriously disordered, so that detailed crystallographic analysis could not be carried out.

Tecton **IX** has pyridone rings substituted in the 5-position. This reduces steric hindrance to hydrogen bonding, and it is evident that the hydrogen bond formed between molecules of tecton **IX** must be favorable. In addition, as shown in Scheme 33, we can

Scheme 35

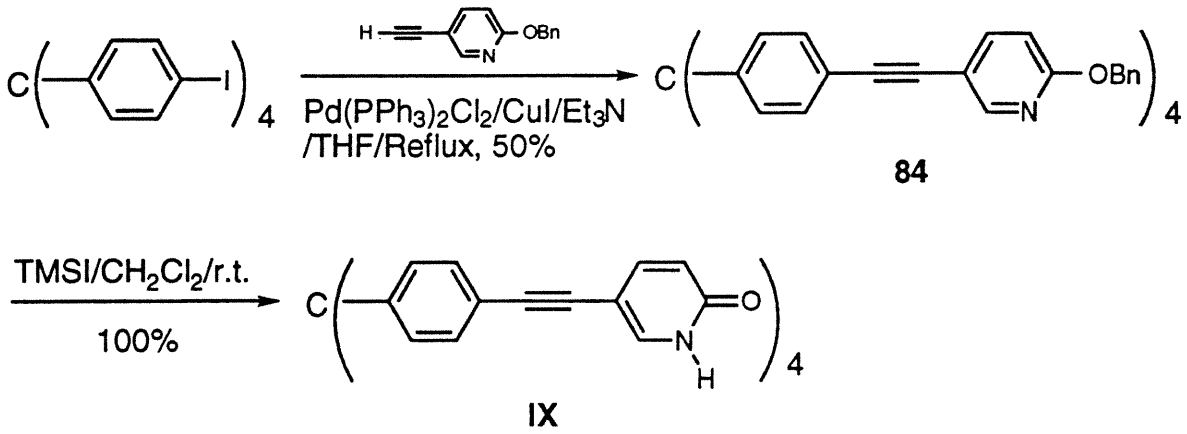

imagine that if tecton **IX** is capable of self-assembling to generate a diamondoid network, the size of the channels formed in the networks should be larger than those in networks derived from tecton **I** and **VIII**, since the intertectonic distance is larger. This suggests that

in order to favor formation of a diamondoid network from tecton **IX**, larger guest molecules must be employed to avoid low packing coefficients; however, it is also possible that the enhanced stickiness of tecton **IX** may help override the forces that favor close packing. Tecton **IX** was synthesized in two steps in 50% overall yield as presented in Scheme 35. It is noteworthy that decomposition was found to occur when tetrapyridine **84** was deprotected in TFA under heating. Tecton **IX** proved to have poor solubility in simple carboxylic acids and even in 2-chloropropionic acid. Crystallization of tecton **IX** from propionic, butyric, isovaleric, and 2-chloropropionic acid gave no crystals suitable for X-ray analysis but only microcrystalline precipitates.

5.2. Design and synthesis of larger tectons which may be able to generate diamondoid networks with more open channels because of lengthened intertectonic distances.

Comparison of the three tectons **I**, **VIII**, and **IX** described above demonstrates that while 2-pyridone rings as sticky sites can be connected to a tetrahedral core structure in different positions, these changes are likely to have a complex effect on the geometries of the resulting networks. Therefore, to be simplified, comparable and logical, we decided to choose the connection pattern adopted by tecton **I** as representative, and to make further changes of geometry based closely on this model in order to explore the relationship of the size, and shape of tectons with respect to the strength of intertectonic interaction. For this reason, we designed larger tectons **XI**, **XII**, and **XIV-XVI** (shown in Figure 47).

The 1,3-butadiyne structural feature in tecton **XI** is not easy to construct, and we worked hard to find an effective access. Negishi and co-workers[38] indicated that Pd-catalyzed cross-coupling of a haloalkyne with an alkynylmetal containing Li, Mg, Zn, Al, and Sn typically leads to the formation of nearly statistical 1:2:1 mixtures of homo- and cross-coupled products with the combined yields generally around 100%. In Scheme 36 several routes to synthesize tecton **XI** are shown by retrosynthetic analysis.

Scheme 36

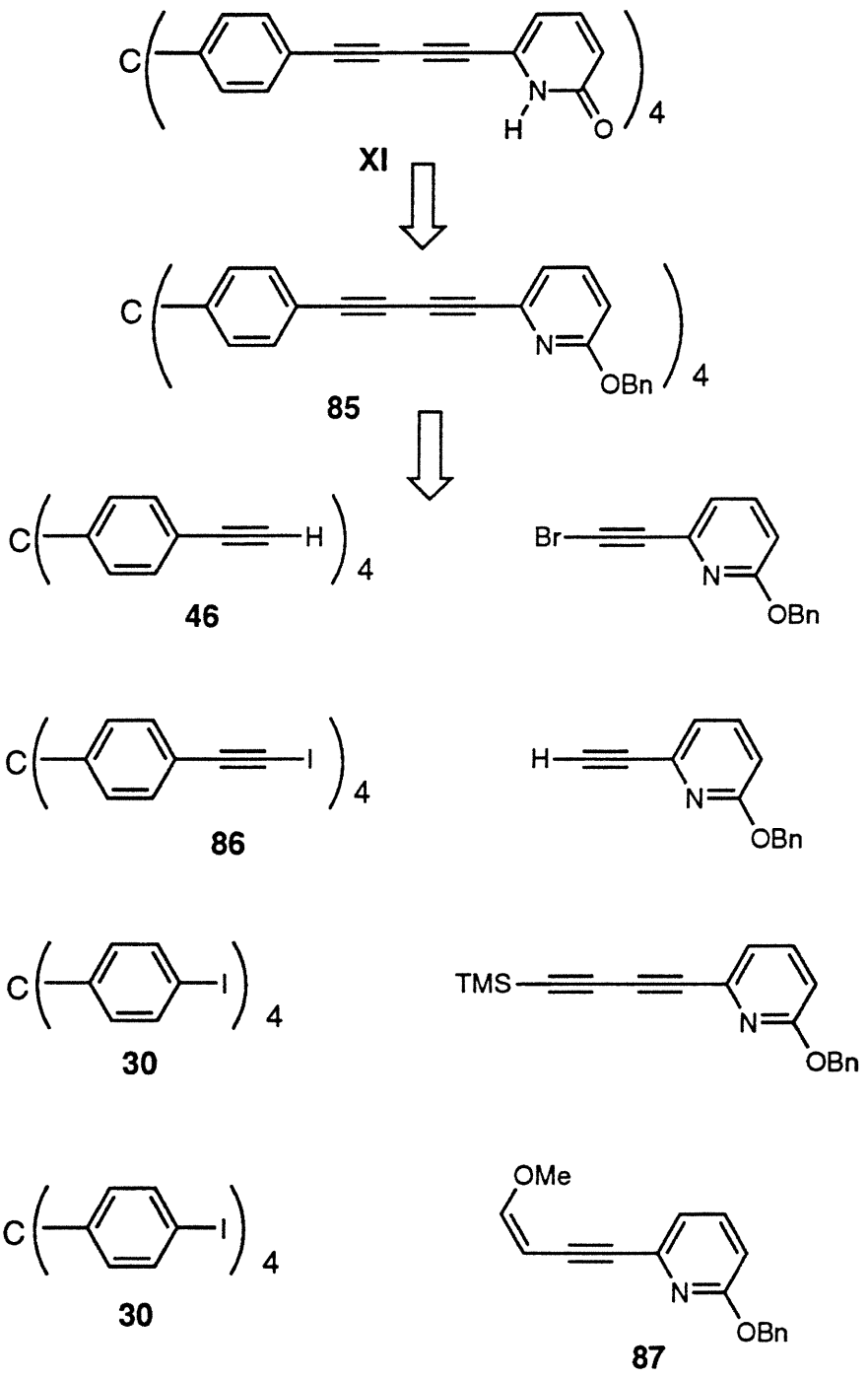

When we tried to synthesize tecton **XI** by cross-coupling of tetraacetylene **46** (synthesized as shown in Scheme 9) and 2-(bromoethynyl)-6-(phenylmethoxy)pyridine[10d] (shown in Scheme 37), homo-coupling products were favored and the cross-coupled product was not obtained. Holmes and co-workers[39] reported that the cleavage of

Scheme 37

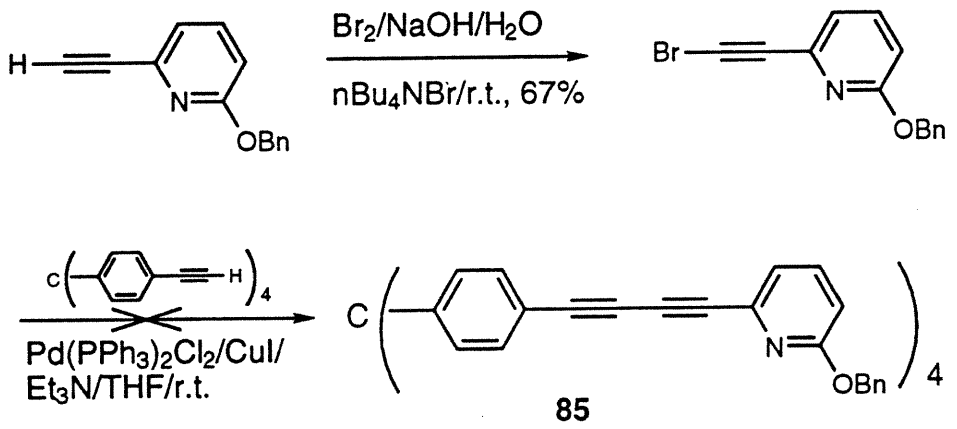

85

bis(trimethylsilyl)butadiyne with methyl lithium-lithium bromide complex in ether at room temperature gives a quantitative yield of lithium trimethylsilylbutadiyne. In light of this method, we used butyllithium as the reagent of metallation to metallate bis(trimethylsilyl)butadiyne in THF at -78°C and then converted the resulting lithium acetylide to (trimethylsilyl)butadiynylzinc chloride. This reagent was then coupled with 6-bromo-2-(phenylmethoxy)pyridine via Pd-catalysis to provide 2-(phenylmethoxy)-6-[4-(trimethylsilyl)-1,3-butadiynyl]pyridine[10d] in 60% yield. The product was further coupled with tetraiodide **30** as shown in Scheme 38 to provide tetrapyridine **85**, unfortunately in very poor yield.

Wityak and co-workers[40] reported that the Pd/Cu-catalyzed cross coupling reaction of alkynes and iodoalkynes gives hetero-coupled products in moderate to high yield.

However, even when freshly made iodoacetylene **86** was used to couple with pyridylacetylene under the conditions suggested by Wityak's method, tetrapyridine **85** was

Scheme 38

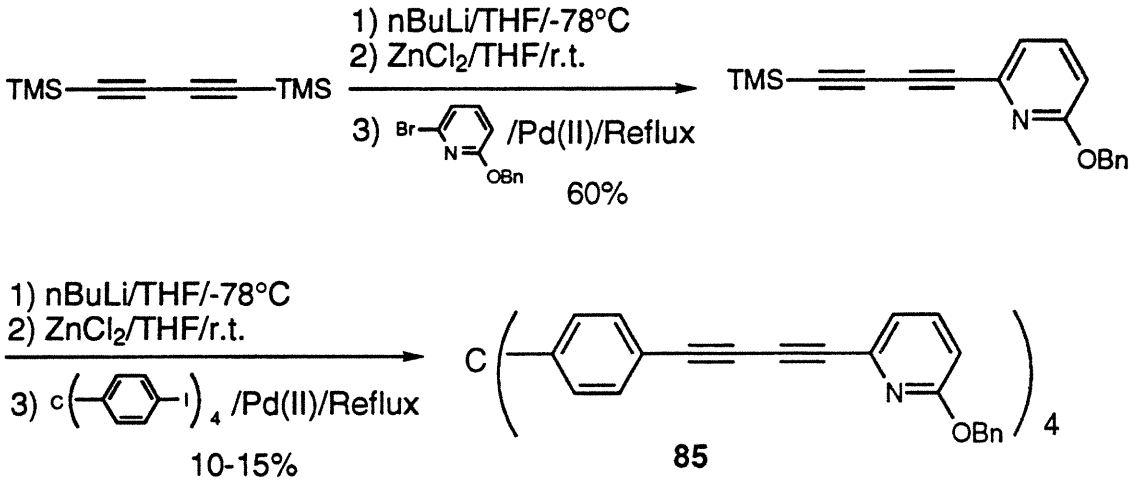

Scheme 39

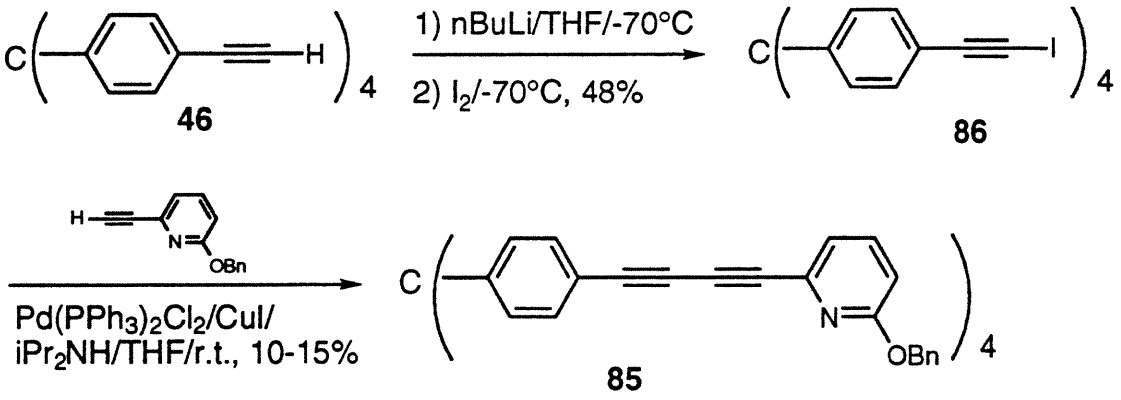

still obtained in poor yield (shown in Scheme 39).

Zweifel and co-workers[41] have investigated the use of (Z)-1-methoxy-1-buten-3-yne, which is commercially available at low cost, as a precursor to prepare 1-trialkylsilyl-4-alkyl-1,3-butadiyne in high yield. An attractive advantage of this method is that the methoxyenyne can be converted into a substituted 1,3-diyne in successive steps so as to

avoid the isolation and purification of butadiyne as an intermediate product. Therefore, we prepared compound **87** via Pd/Cu-catalyzed coupling reaction of (Z)-1-methoxy-1-buten-3-yne and 6-bromo-2-(phenylmethoxy)pyridine in 89% yield and converted compound **87** into tetrapyridine **85** in 45% yield by successive treatment with 2 equivalents of LDA in

Scheme 40

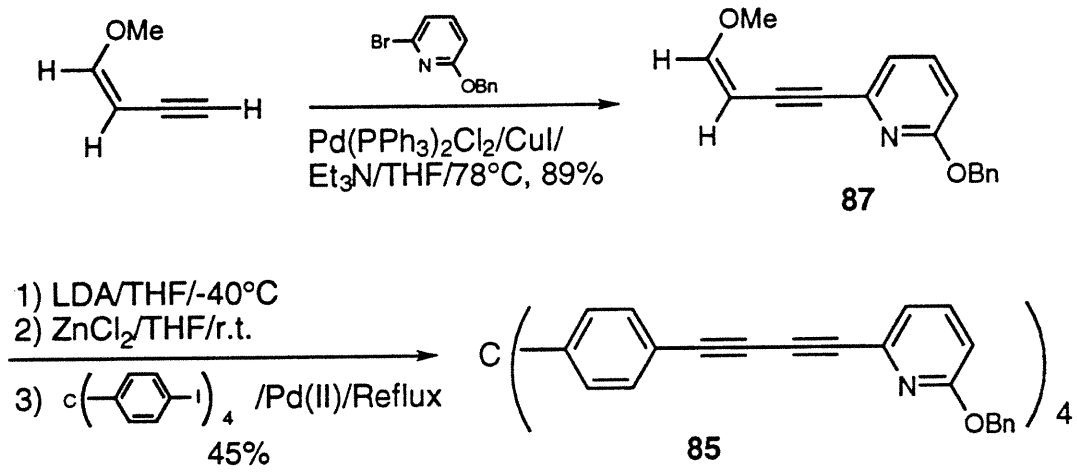

THF at -40°C followed by zinc chloride in room temperature and then by a mixture of tetraiodide **30** and Pd(II) catalyst in THF under reflux (shown in Scheme 40). Deprotection of tetrapyridine **85** in TFA under heating gave tecton **XI** in 80% yield.

We tried to crystallize tecton **XI** from acetic, propionic, and 2-chloropropionic acid with hexane, THF, and toluene as co-solvents, but none of these systems gave crystals. Apparently, tecton **XI** is less soluble in carboxylic acids than is tecton **I**. We then tried to crystallize tecton **XI** from other solvent systems with DMF as principle solvent and hexane, toluene, and alkylamines as co-solvents. However, we still did not obtain any crystal suitable for X-ray crystallographic analysis.

While we struggled to find a more promising access to prepare tecton **XI**, we simultaneously designed and synthesized tecton **XII** (shown in Scheme 41 and 42), which

incorporates a 1,4-diethynylphenylene spacer. The size of tecton **XI** is evidently much larger than that of tecton **I**. It was prepared successfully in five steps in reasonable yield.

Scheme 41

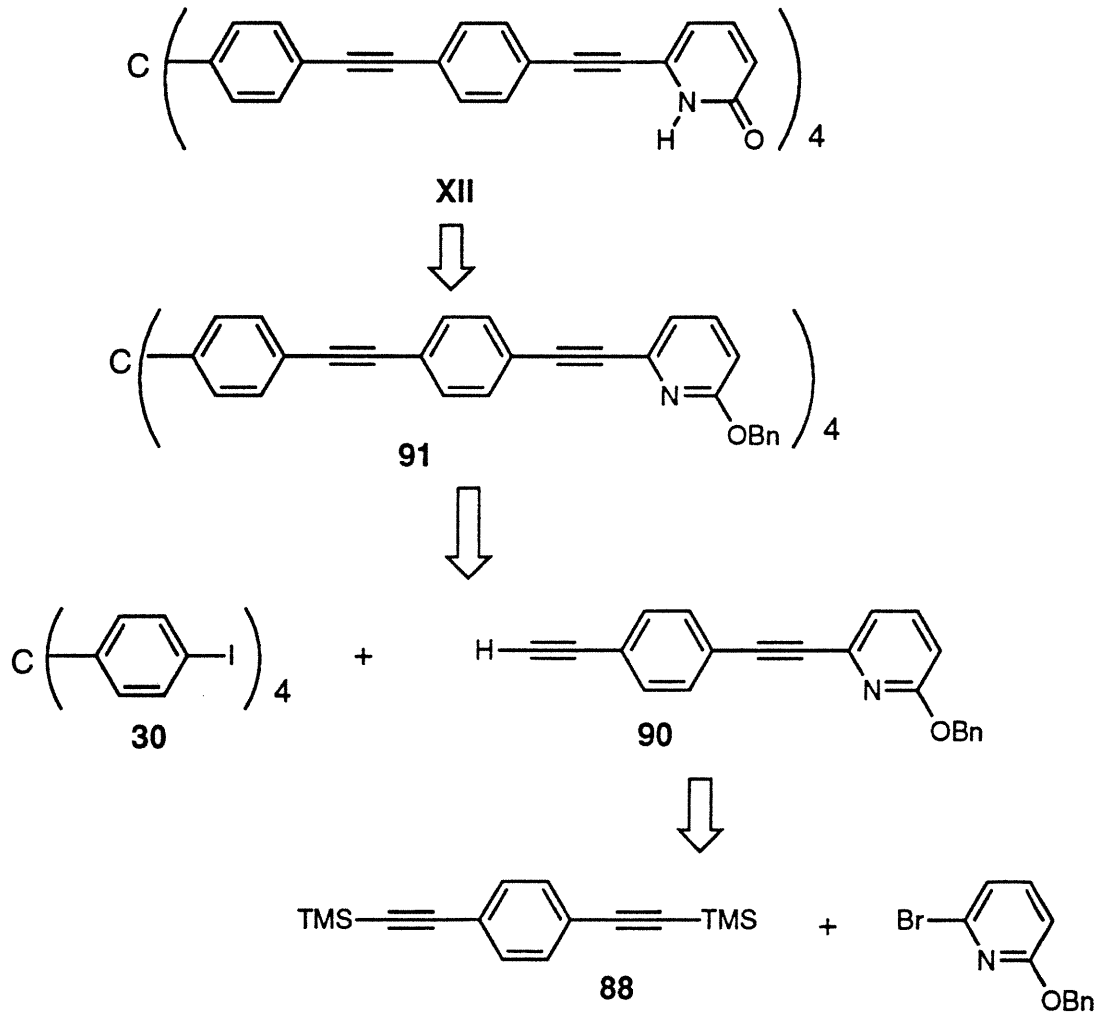

The Pd/Cu-catalyzed cross-coupling reaction of 1,4-diiodobenzene, which is commercially available and not expensive, and trimethylsilylacetylene provided 1,4-bis(trimethylsilyl-ethynyl)benzene (**88**) in almost quantitative yield. Treatment of compound **88** with one equivalent of butyllithium produced the corresponding lithium acetylide, which was converted to the alkynylzinc chloride by treatment with one equivalent of $ZnCl_2$. It was

heteroarylated by coupling with 6-bromo-2-(phenylmethoxy)pyridine in the presence of Pd(0) as catalyst to give compound **89** in 60% yield. After being desilylated and coupled

Scheme 42

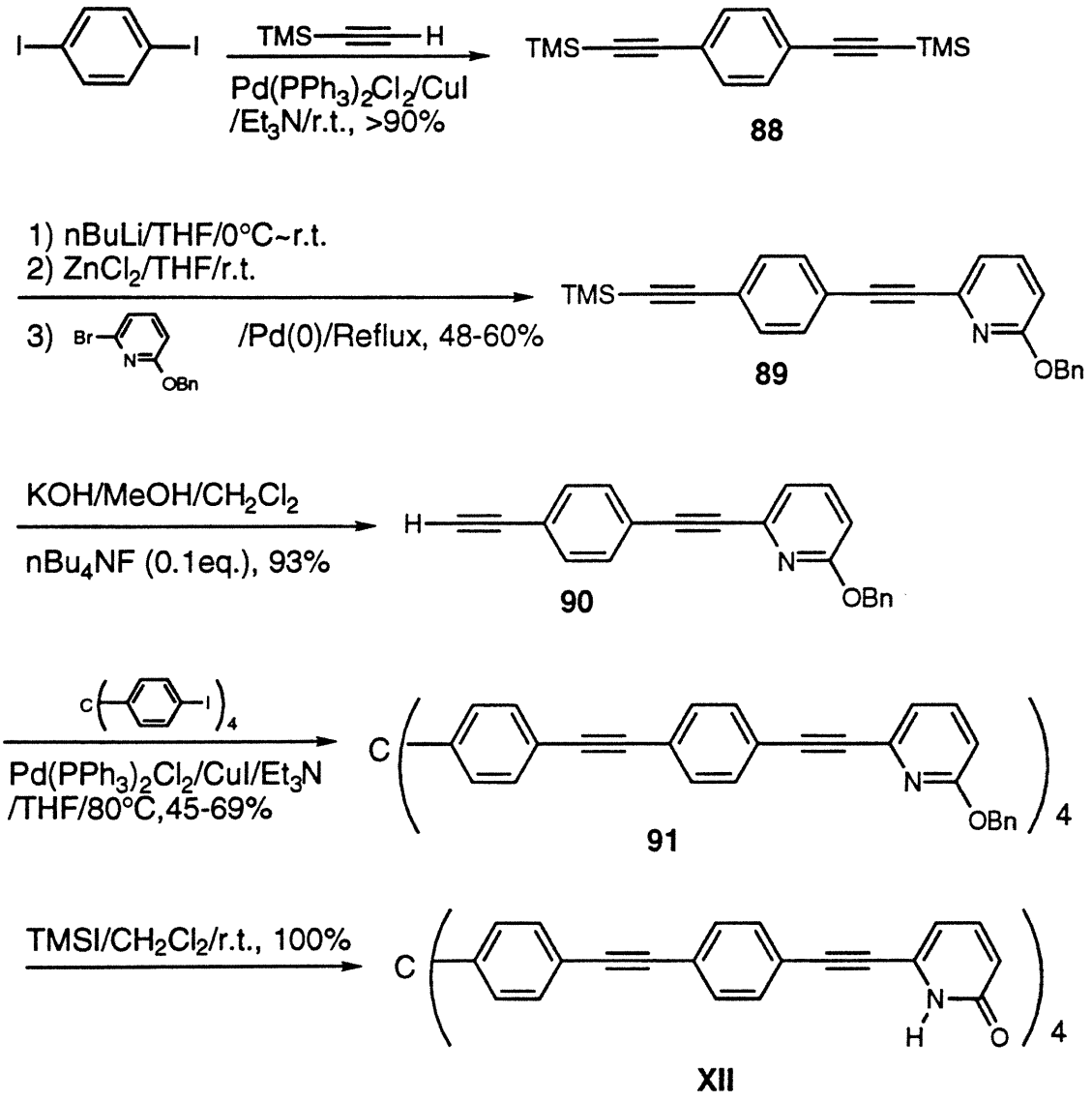

with tetraiodide **30** in the routine way, it yielded tetrapyridine **91** in 69% yield. Treatment of **91** with TMSI gave tecton **XII** in quantitative yield.

We found that the solubility of tecton **XII** in acetic acid is quite poor. We placed a saturated solution of tecton **XII** in acetic acid in a vial open to air at room temperature. Four days later we found that needle-shaped crystals had separated from solution and their composition was shown by ^1H NMR spectroscopy to be **XII**•$8CH_3CO_2H$. Unfortunately, we were unable to obtain crystals big enough for X-ray structure determination. When we tried to crystallize tecton **XII** from other carboxylic acids (as shown in Table 10), we found that its solubility increased but it precipitated as a powder.

Table 10. Results of crystallization of cecton **XII** from carboxylic acids

Solvent System	Product / component
acetic acid	crystals / **XI**•$8CH_3CO_2H$
butyric acid / MeOH / hexane	powder
valeric acid / MeOH / hexane	powder
isovaleric acid / MeOH / hexane	powder and very fine crystals
diphenylacetic / isovaleric acid / MeOH / hexane	powder
benzylcinnamic / isovaleric acid / MeOH / hexane	powder

Since we did not obtain suitable crystals of tectons **XI** and **XII**, we tried to make other tectons with similar sizes. Unfortunately, attempts to make tectons **XIV** and **XV** (Schemes 43 and 44) by using Pd-catalyzed cross-coupling of tetraiodide **30** with either organozinc reagents or boronic acids were unsuccessful.

We therefore designed tecton **XVI** (shown in Scheme 45) to minimize cross-coupling between aromatic halides. As shown in Scheme 46, tecton **XVI** was synthesized in four steps by employing compound **53** as precursor. Bromide **53** was converted to iodide **96** by metallation with butyllithium, followed by treatment with solid iodine.

Scheme 43

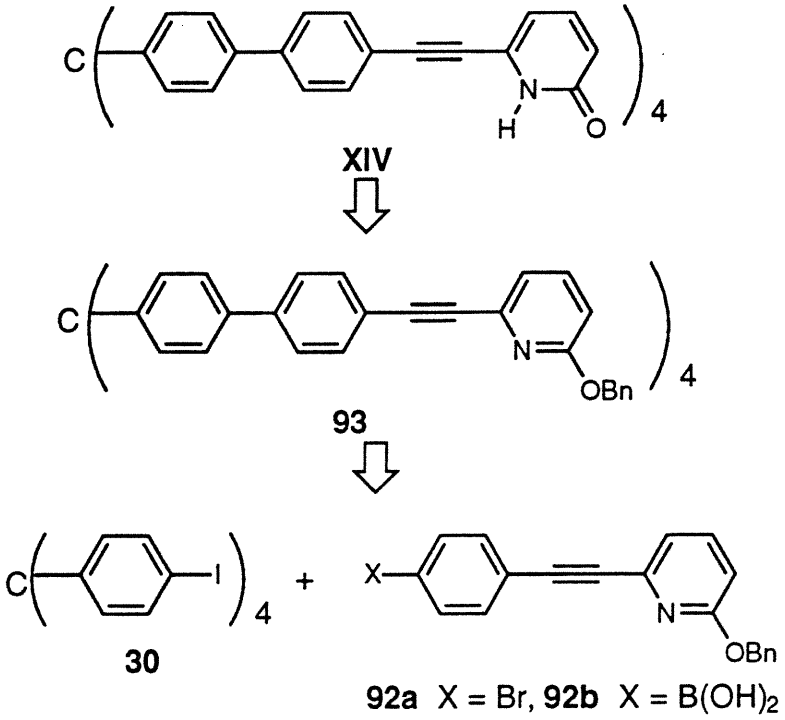

Scheme 44

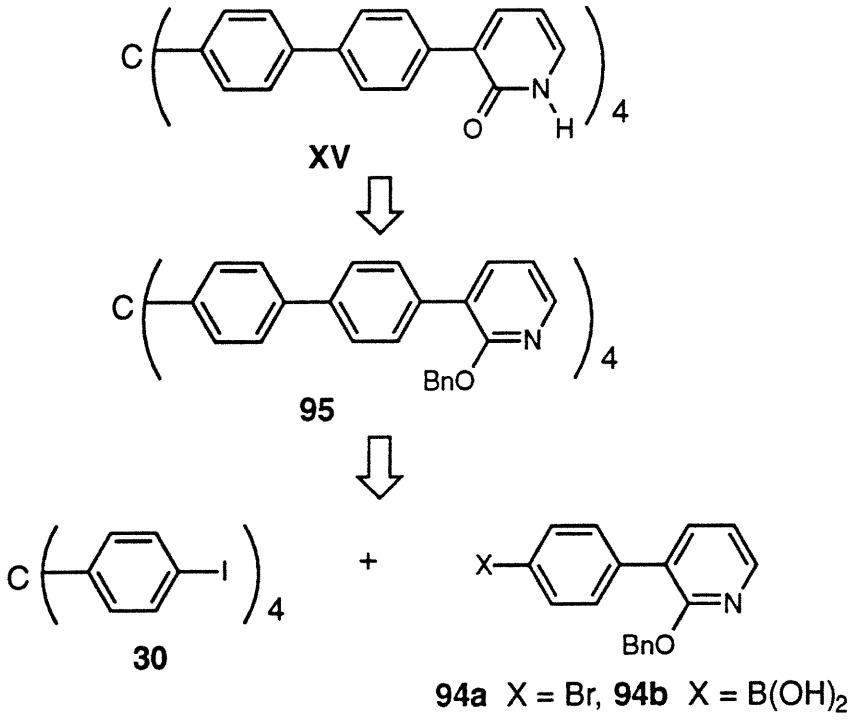

Scheme 45

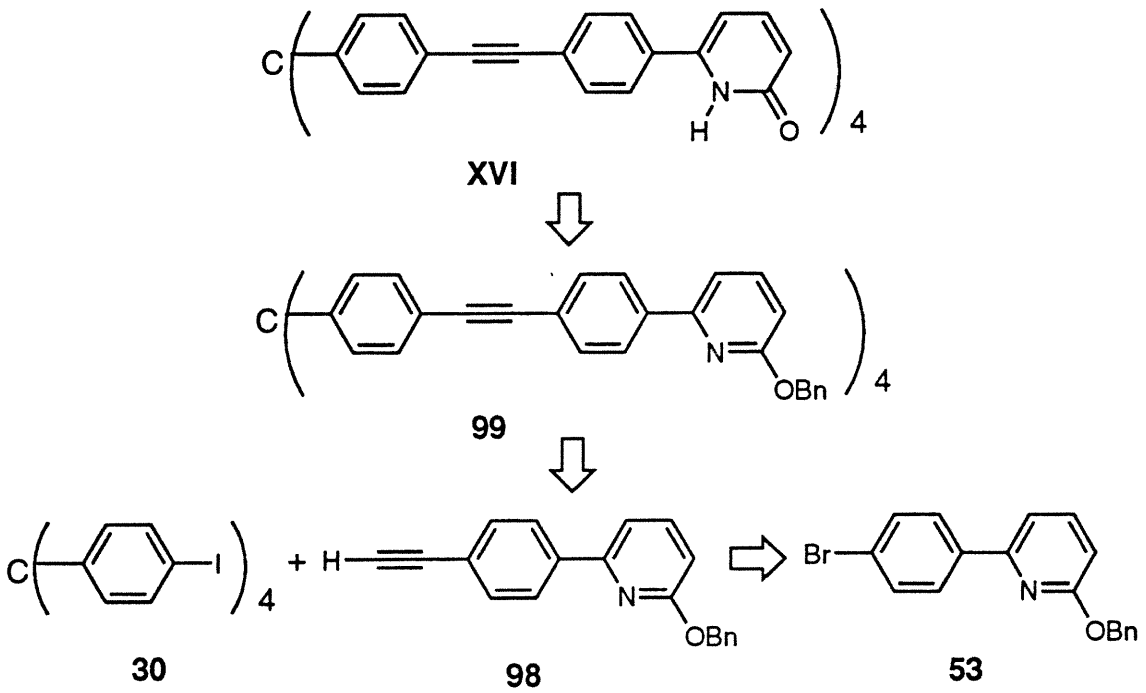

Alkynylation of compound **96** by Pd/Cu-catalyzed cross-coupling with trimethylsilylacetylene, followed by desilylation of the resulting cross-coupled product **97**, gave alkynylated product **98** in 71% overall yield. It was then further coupled with tetraiodide **30** under the same reaction conditions to provide tetrapyridine **99** in 41% yield. Deprotection of **99** in dry dichloromethane with TMSI gave tecton **XVI** in quantitative yield.

The failure of various larger tectons to provide crystals suitable for X-ray diffraction made us pay more attention to the shape of the tecton rather than only the size of the tecton. We have mentioned before that larger tectons must define longer intertectonic

Scheme 46

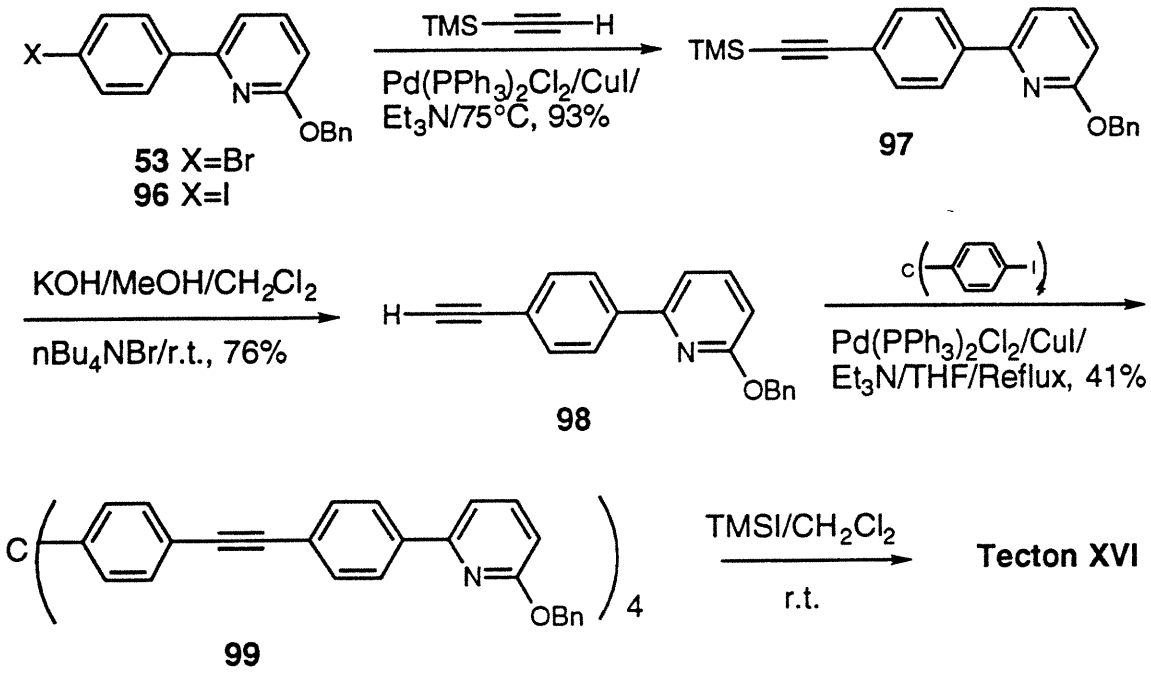

distances (represented as d_{it}) and this would bring about more serious non-close-packing or higher degrees of interpenetration if crystal structures similar to those of tecton **I** were formed. As shown in Scheme 47, the intertectonic distance increases strikingly from item *e* to item *i*. We can estimate these distances on the basis of the crystal structure of tecton **I** in order to evaluate the hollowness of these larger tectonic assemblies. As presented in Table 11, if we presume that these larger tectons would generate the same kind of distorted diamondoid lattices as those generated by tecton **I**, then the intertectonic distances would be raised from 19.7 Å in the case of tecton **I** (item *e* in Scheme 47) to 33.0 Å in the case of tecton **XII** (item *i* in Scheme 47), and the degree of interpenetration might increase to as high as 12. To the best of our knowledge, no publications have ever discussed in detail whether interpenetration may cause strain in crystal structures so as to result in a limit of the

Scheme 47

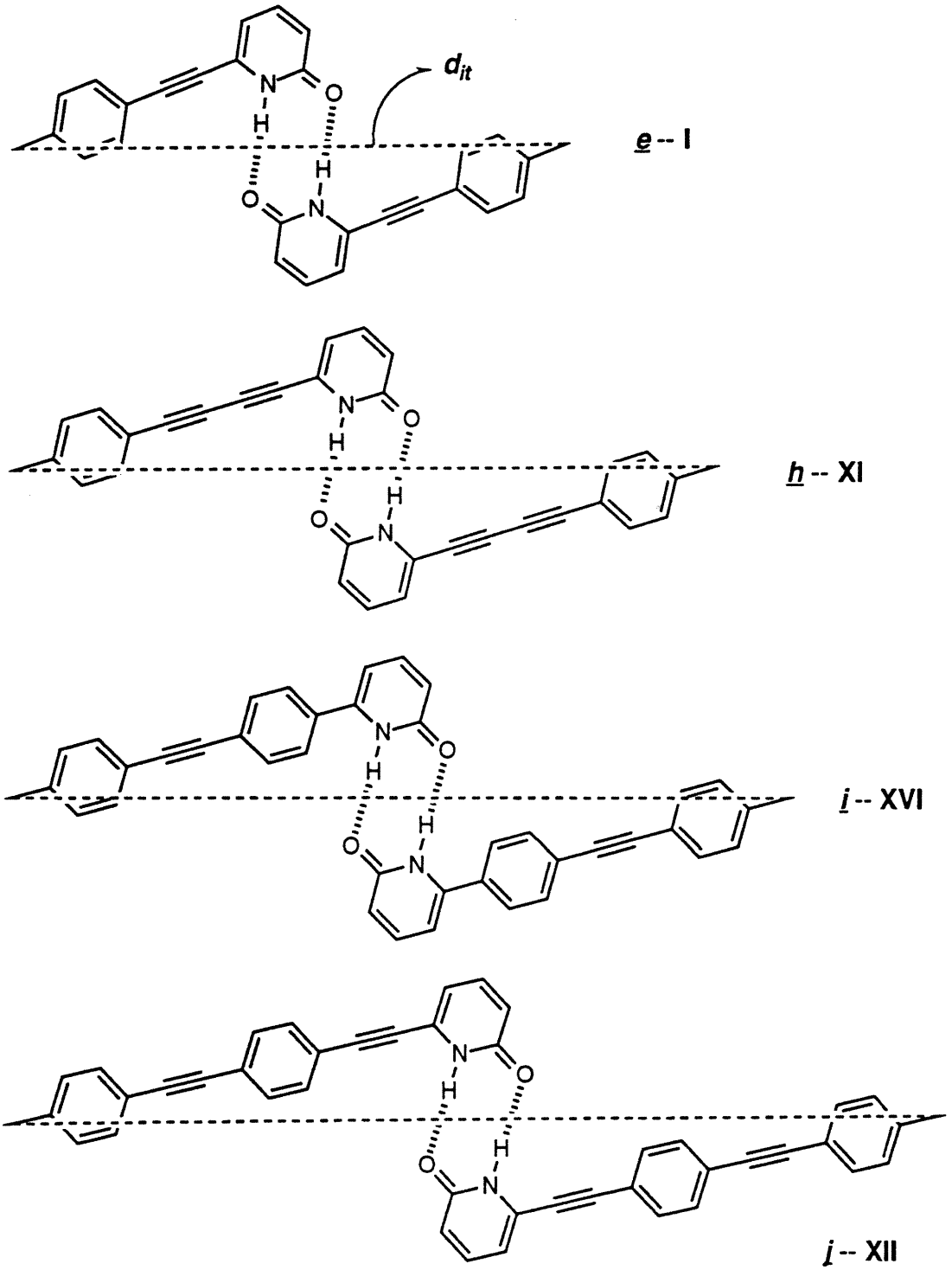

Table 11. The degree of interpenetration and some geometric parameters for various diamondoid lattices estimated on the basis of the crystal structure of tecton **I**

Tecton	d_{it} (Å) (calculated)	ς (Å)	Degree of inter-penetration	Diameter of channels (Å)
I	19.7	51.5	7	8.1 x 3.5
XI	24.9	65.1	9	10.3 x 4.4
XVI	27.5	71.9	10	11.3 x 4.9
XII	33.0	86.3	12	13.6 x 5.9

degree of interpenetration. However, Ermer[13d] indicated that either compression or elongation of hydrogen-bonded diamondoid lattices might lead to strain to some extent as a result of pairwise hydrogen bonding between the carboxyl groups. In self-inclusion compound **33**[13a], for example, the comparatively long hydrogen bonds (2.763 Å rather than the normal value approximately 2.6 Å) indicate that the diamondoid packing of the tetraacid molecules cannot be accomplished without generating some nonbonded strain between the interpenetrating lattices. In the case of tecton **I**, the molecules adopt pairwise hydrogen bonding with a 169° bond angle rather than the normal angle of 180° in order to generate elongated diamondoid networks with suitably sized channels that avoid unfavorable enclathration. Although the strain discussed here is tolerated in the case of tecton **I** by generating energetically stable close-packed crystals, we can expect that it may be a factor that renders crystallization of larger tectons much more difficult when the degree of interpenetration is considerably enhanced.

5.3. Tectons with geometries resistant to close packing

5.3.1 Design and synthesis of tecton XVII

We wondered whether it might be possible to design a tecton which would result in increased porosity in the solid state by varying its shape, but without changing its strength of intermolecular interaction or its general size. As a result, tecton **XVII** was designed and its retrosynthetic analysis showed that it would be easy to prepare (Scheme 48). The key synthon, 1-bromo-3-iodobenzene, was synthesized as shown in Scheme 49 in 3 steps with an overall yield of 80%. Angular tetrapyridine **103** was provided in 32% overall yield in

Scheme 48

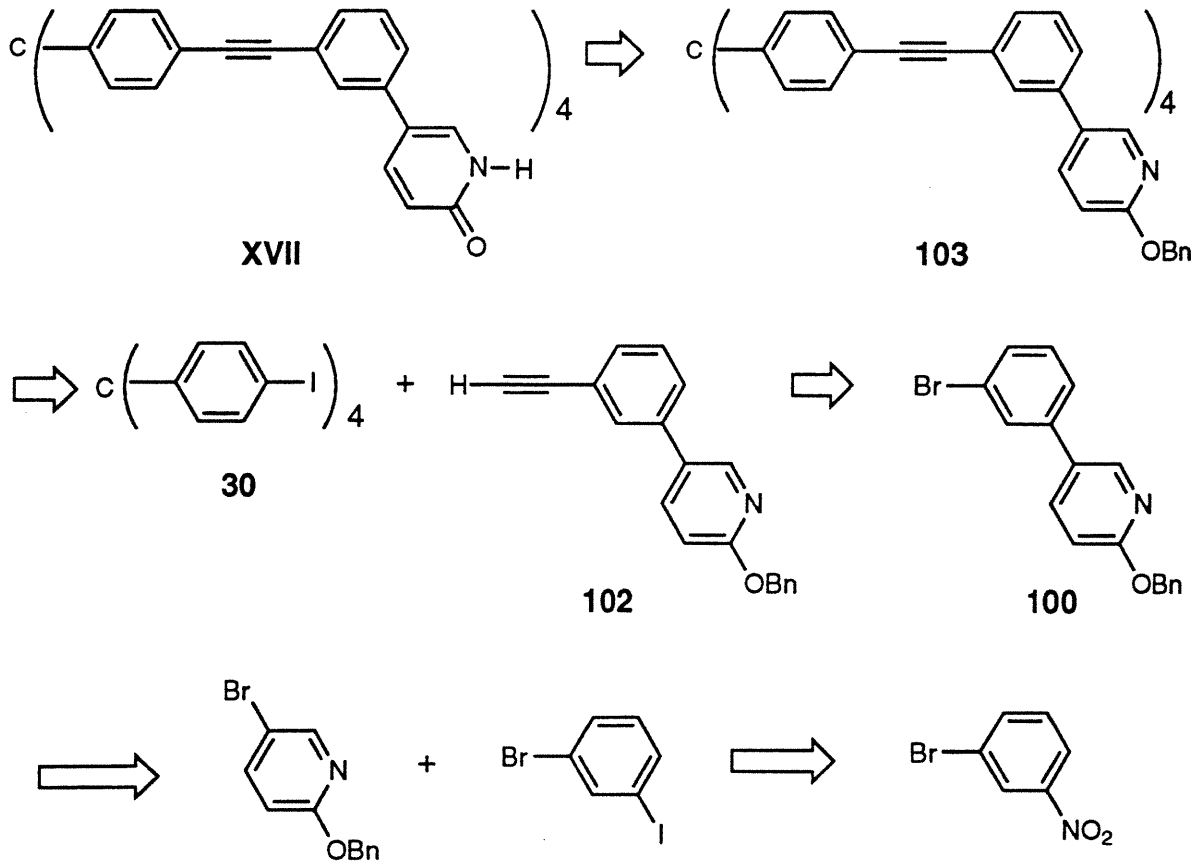

Scheme 49

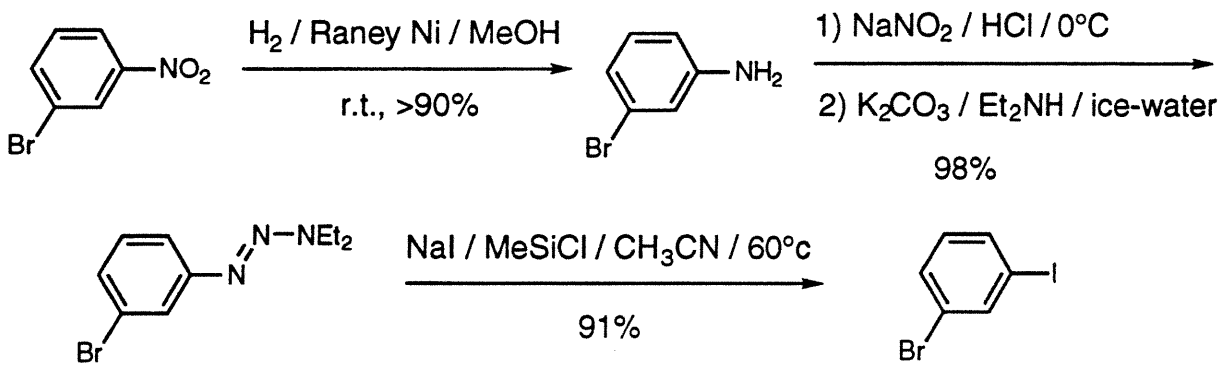

five steps as shown in Scheme 50. Deprotection of it with TMSI in dry dichloromethane at room temperature gave tecton **XVII** in quantitative yield.

We tried to crystallize it from carboxylic acids, such as propionic, butyric, valeric, and hexanoic acid, but the solubility of tecton **XVII** in these acids is too poor to permit effective crystallization. After extensive experiments, tecton **XVII** was finally crystallized from a mixed solvent system of DMF/MeOH.

5.3.2 Crystal structure of tecton XVII.

The numerous failures to determine the structure of the larger tectons that we designed and synthesized made the successful crystallization of tecton **XVII** more exciting, intriguing, and important. The information provided by its X-ray crystallographic analysis promised to be very valuable for us in better understanding the behavior of tectons in the solid state.

Tecton **XVII** is a more conformationally flexible molecule. As shown in Table 12, conformations of pyridone rings with respect to the core structure in tecton **I** may be

Scheme 50

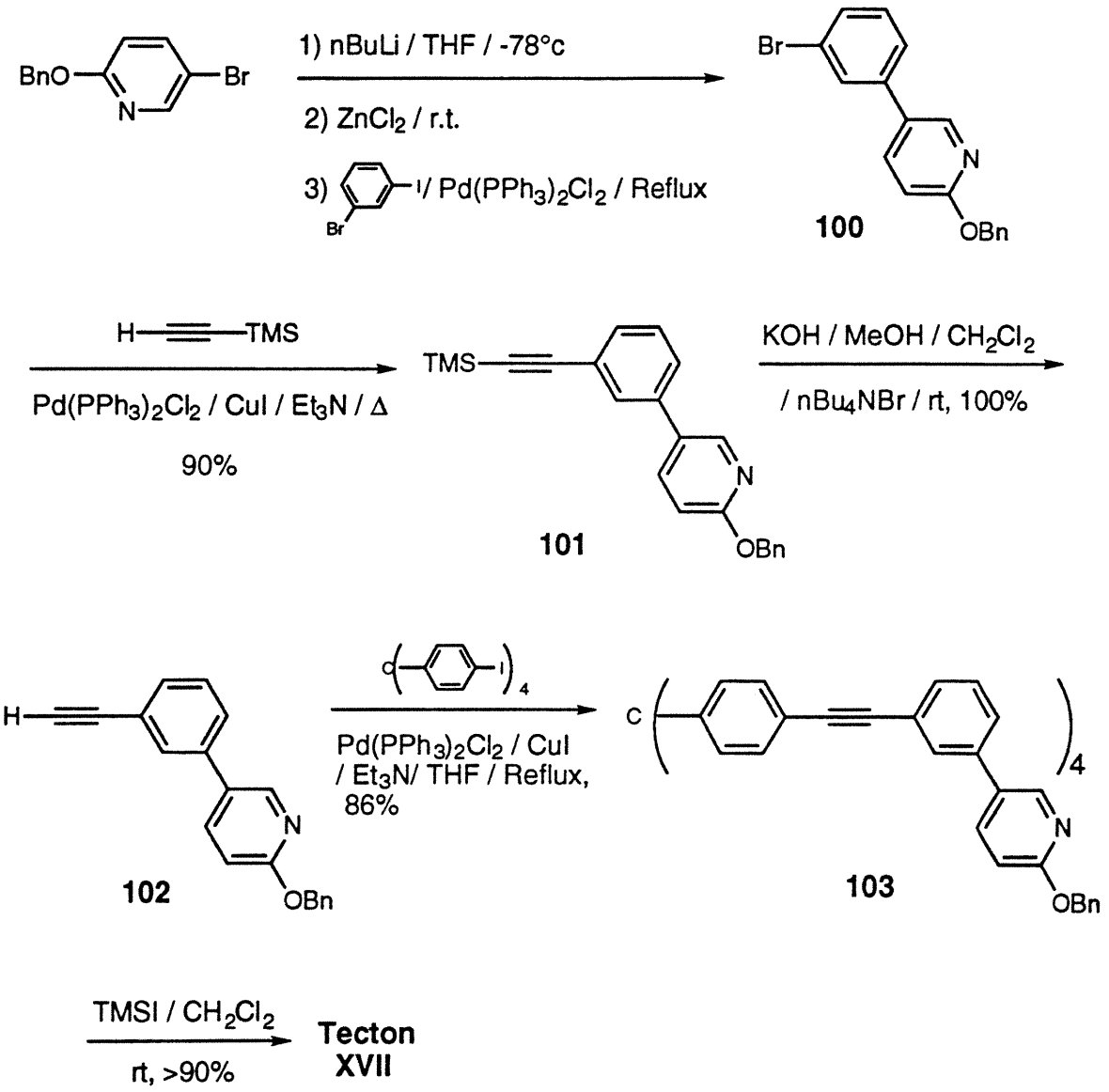

determined by the torsion angle *t*C4-C5-C10-N14. In tecton **XVI**, these conformations may be represented either with torsion angle *t*C4-C5-C16-N20 or *t*C12-C13-C16-N20, since the geometry of hydrogen bonding with respect to the tetrahedral core structure does not depend upon these conformations. However, in tecton **XVII** the conformation of the pyridone rings with respect to the core structure may be determined by the two torsion

Table 12. Conformational flexibility of tectonic molecules

Asymmetric unit of tectons	Conformations of the pyridone rings
I 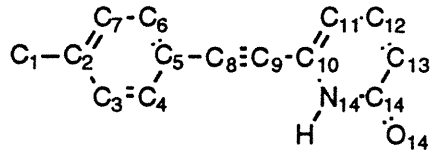	$t_{C4\text{-}C5\text{-}C10\text{-}N14}$
XVI 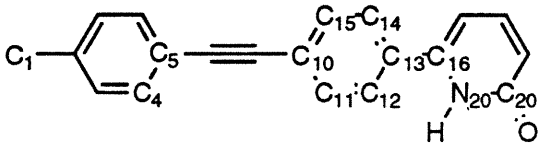	$t_{C4\text{-}C5\text{-}C16\text{-}N20}$ or $t_{C12\text{-}C13\text{-}C16\text{-}N20}$
XVII 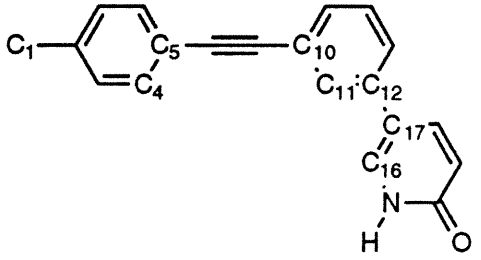	$t_{C4\text{-}C5\text{-}C10\text{-}C11}$ & $t_{C11\text{-}C12\text{-}C17\text{-}C16}$

angles *t*C4-C5-C10-C11 and *t*C11-C12-C17-C16. If it is supposed that the torsion angle *t* C4-C5-C10-C11 is constant, then as the torsion angle *t* C11-C12-C17-C16 changes from 0 to 180°, various geometries of hydrogen bonding with respect to the tetrahedral core structure and various intertectonic distances may be derived. In Scheme 51, item ***m*** shows the geometry of hydrogen bonding and the intertectonic distance derived for a torsion angle *t* C11-C12-C17-C16 of 0°; and item ***n*** presents those derived for a torsion angle *t* C11-C12-C17-C16 of 180°. Obviously, this flexibility makes tecton **XVII** capable of approaching one of several energetically stable polymorphs in the solid state.

X-ray crystallographic study has revealed that the crystal structure of tecton **XVII** consists of non-diamondoid and non-interpenetrating supramolecular aggregates induced

Scheme 51

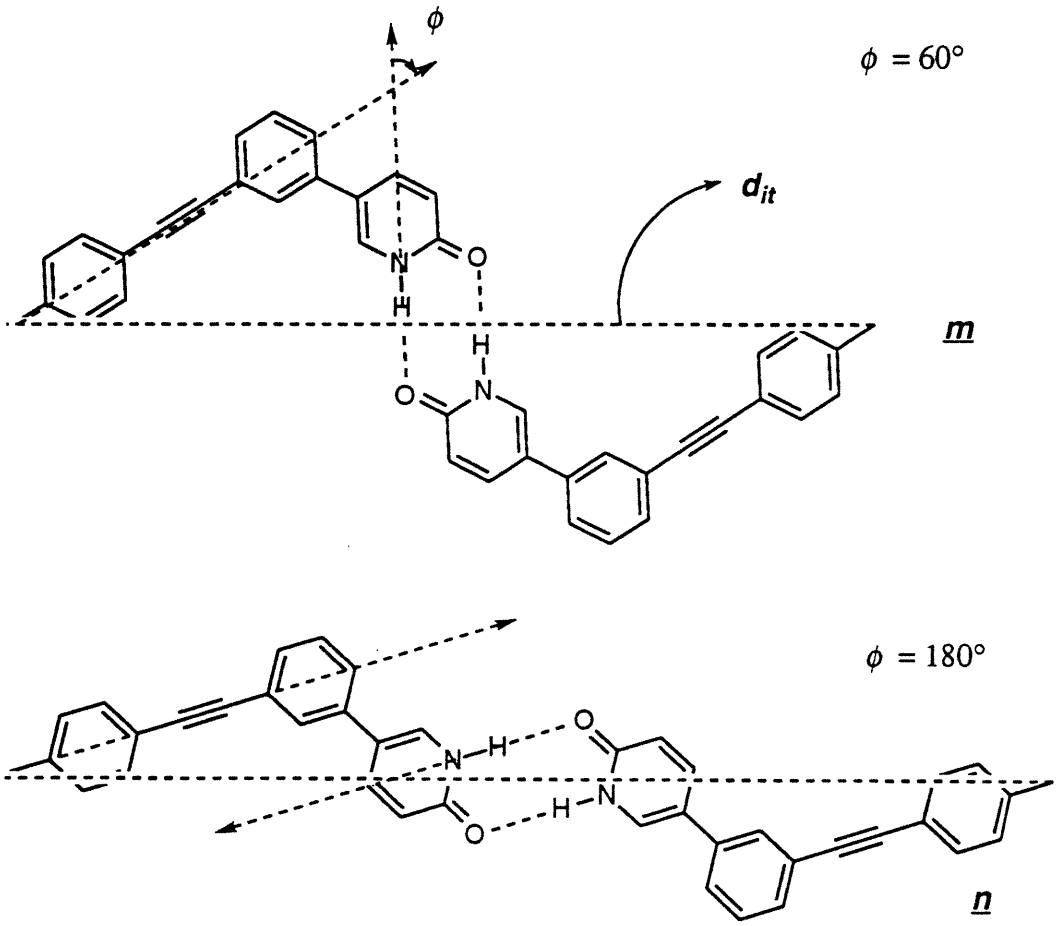

by single rather than pairwise hydrogen bonding between pyridone rings. Simultaneously, nanosized channels, 14 Å x 4 Å in diameter, are defined by the self-assembled aggregates. In the channels, molecules of DMF are enclathrated selectively.

To make a comparison, the unit cell parameters of tectons **I** and **XVII** are listed in Table 13, and in Figure 48, ORTEP views along the **b** axis of the packing arrangement in crystals of tectons **XVII** and **I** are shown. They are obviously isomorphous and it is

(a)

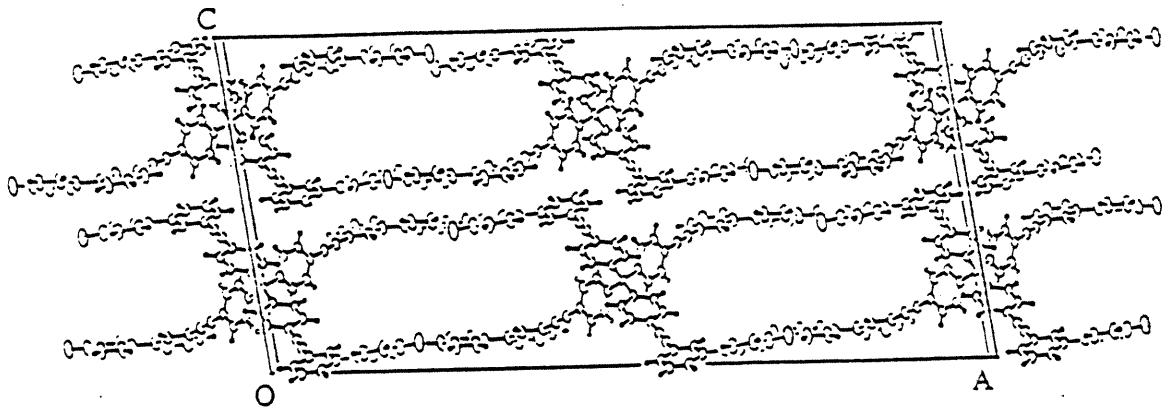

(b)

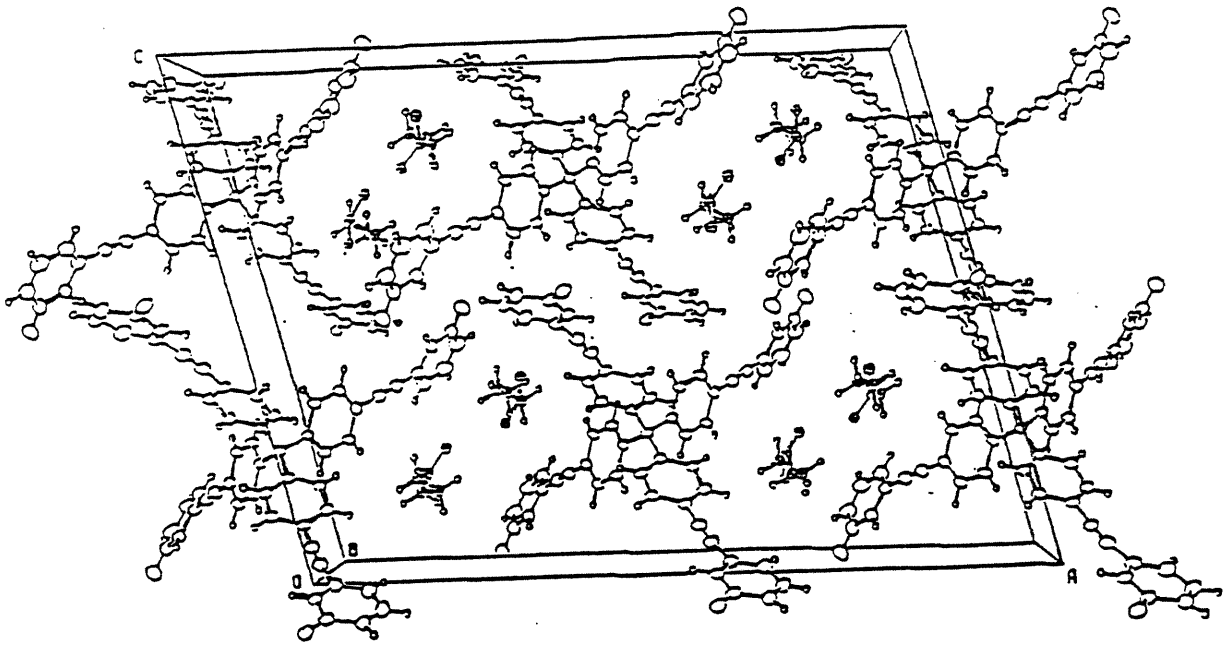

Figure 48. ORTEP views along the **b** axis of the packing arrangements in crystals of tectons **XVII** (a) and **I**•2 $CH_3CH_2CH_2CO_2H$ (b). Non-hydrogen atoms are represented by ellipsoids corresponding to 50% probability, and hydrogen atoms by spheres of arbitrary size. Arbitrary spheres are used for the butyric acid moiety.

Table 13. Comparison of the crystal data for tecton **XVII**•4DMF with the data for tecton **I**•2$CH_3CH_2CH_2CO_2H$

Crystal Data	**I**•2$CH_3CH_2CH_2CO_2H$	**XVII**•4DMF
crystal system	Monoclinic	Monoclinic
space group	*C2/c*	*C2/c*
unit cell parameters		
a (Å)	31.249 (7)	46.338 (16)
b (Å)	7.350 (4)	7.344 (2)
c (Å)	23.145 (6)	22.072 (8)
α (deg)	90	90
β (deg)	104.69 (2)	98.72 (3)
γ (deg)	90	90
vol ($Å^3$)	5142 (3)	7424 (4)
Z	4	4
d_c (g/cm^3)	1.247	1.240
T_m (K)	180	215

noteworthy that translation along the **b** axis in the crystal structure of tecton **XVII** occurs almost in the same way as what is observed in tecton **I**. In both cases, translation along the **b** axis is around 7.3 Å. Kitaigorodsky[22a] investigated the crystal structures of several tetraaryl compounds composed of molecules $X(C_6H_5)_4$, where X is a tetravalent element. In Table 14, their crystal data are shown for comparison. It was found that the structures of these compounds form an isomorphous series. After studying the conformations for the series by taking tetraphenylmethane as a representative, Kitaigorodsky indicated that although the translation along the c axis is comparatively small in all the structures, there is

no contact between molecules related by translation along the **c** axis, since the conformations that may result in a contact are forbidden. Therefore, we may characterize

Table 14. Crystal data for various tetraaryl compounds[22a]

Compound	Crystal system	Cell parameters	Space group	Molecular symmetry in crystal	$d_{X\text{-}C}$ (Å)
$C(C_6H_5)_4$	tetr.	a = 10.86 Å; c = 7.26 Å; Z=2	$P\bar{4}2_1c$	$\bar{4}$	1.50
$Si(C_6H_5)_4$	tetr.	a = 11.30 Å; c = 7.08 Å; Z=2	$P\bar{4}2_1c$	$\bar{4}$	1.94
$Ge(C_6H_5)_4$	tetr.	a = 11.60 Å; c = 6.85 Å; Z=2	$P\bar{4}2_1c$	$\bar{4}$	1.98
$Sn(C_6H_5)_4$	tetr.	a = 11.85 Å; c = 6.65 Å; Z=2	$P\bar{4}2_1c$	$\bar{4}$	2.17
$Pb(C_6H_5)_4$	tetr.	a = 12.03 Å; c = 6.55 Å; Z=2	$P\bar{4}2_1c$	$\bar{4}$	2.23

the parameter **c** as a typical crystal structural feature of close-packing of this series of tetraaryl compounds. Owing to the fact that hydrogen bonding is not involved in the crystal packing of these tetraaryl compounds, comparison of their structures with those of tectons **I** and **XVII** may lead to the conclusion that van der Waals forces are dominating in the crystal packing of both tectons **I** and **XVII**. Therefore, there is no significant breakdown of the close packing principle in these hydrogen-bonded crystals, since the characteristic structural feature of close packing, which is the distance of the translation or in other words the shortest distance between two non-hydrogen-bonded tectons, does not change, although the translation is along the **b** axis in our cases whereas it is along the **c** axis in the tetraaryl compounds.

From Scheme 51 we can see that much longer intertectonic distances than that of tecton **I** are defined either in item ***m*** or item ***n***. If diamondoid networks were formed in either way, much higher degrees of interpenetration would be inevitable to prevent the

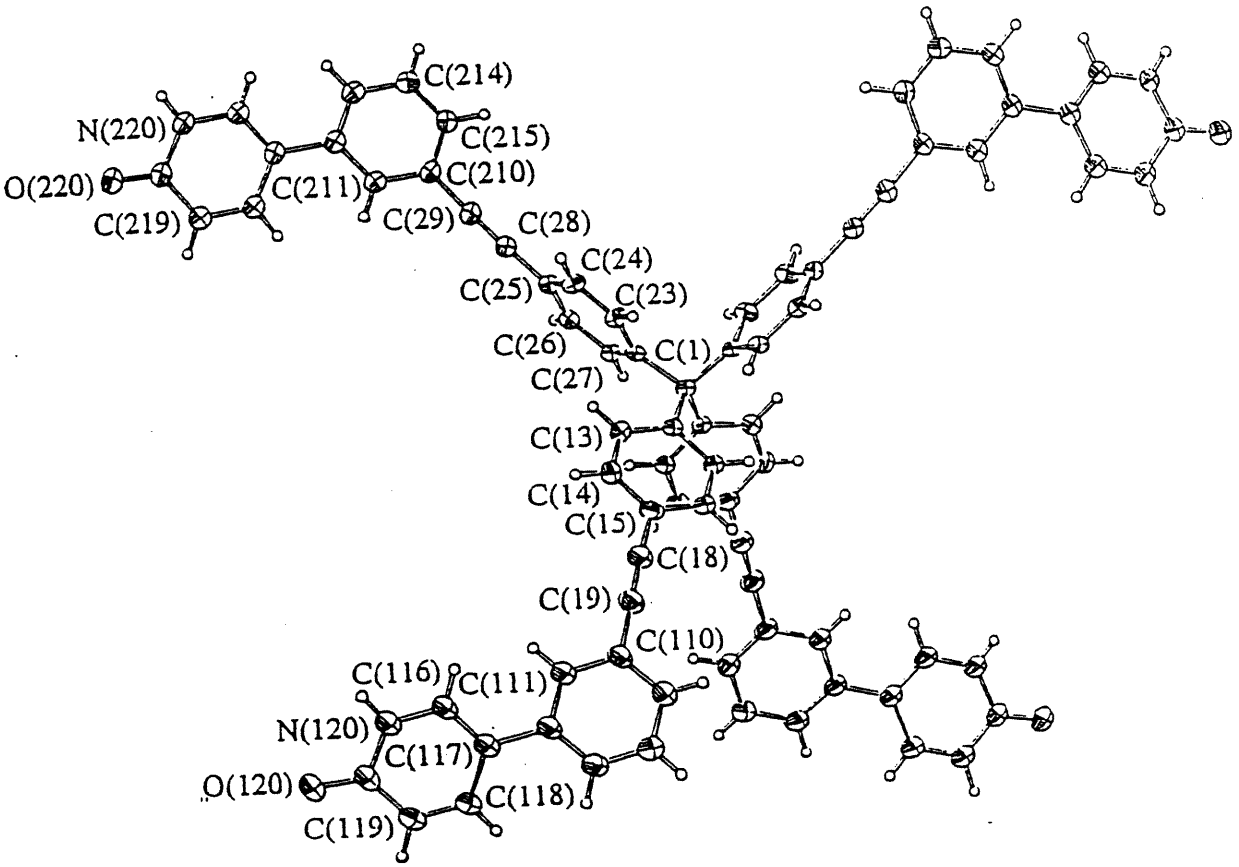

Figure 49. ORTEP view of tecton **XVII** along the **b** axis with the numbering scheme adopted. Non-hydrogen atoms are represented by ellipsoids corresponding to 40% probability. Hydrogen atoms are represented by spheres of arbitrary size.

substantial hollowness characteristic of a diamondoid lattice with an edge as long as about 25 to 35 Å. In Figure 49, an ORTEP view of tecton **XVII** down the **b** axis is shown. Two of four asymmetric units of the tectonic molecule adopt the conformation shown in item ***m***, and the other two adopt that shown in item ***n***. The torsion angles for the two sets of asymmetric units are shown in Table 15. The combination of these two conformations in

Table 15. Torsion angles for the two sets of asymmetric units in a molecule of tecton **XVII**

Torsion angle	***m*** set of asymmetric units	***n*** set of asymmetric units
^{t}C4-C5-C10-C11	8.3 (3)°	90.9 (3)°
^{t}C11-C12-C17-C16	39.1 (3)°	149.7 (3)°

tecton **XVII** causes severe deviation of the orientation of the sticky sites from tetrahedral geometry. As a consequence, diamondoid networks induced by pairwise intertectonic hydrogen bonding are disfavored, and the high degree of interpenetration and strain which might result from it are avoided. Figure 50 shows how the tectonic molecules stack along the **b** axis by sitting on top of each other to form a column. The column approaches other columns of tectons under direction of intertectonic hydrogen bonding to generate layer networks with quite open channels. This two-dimensional layer network packs in the third dimension by using a glide plane via van der Waals forces to generate the entire crystal. In Figures 51 and 52, it is shown how the tectonic molecules self-assemble via single hydrogen bonds into a supramolecular aggregate. Apparently, compared with tecton **I**, van der Waals forces are more significant in the crystal packing of tecton **XVII**, since in order to achieve a better van der Waals packing, the normal and energetically favorable pairwise hydrogen bonding is sacrificed. Instead, the rare single hydrogen-bonding motif is

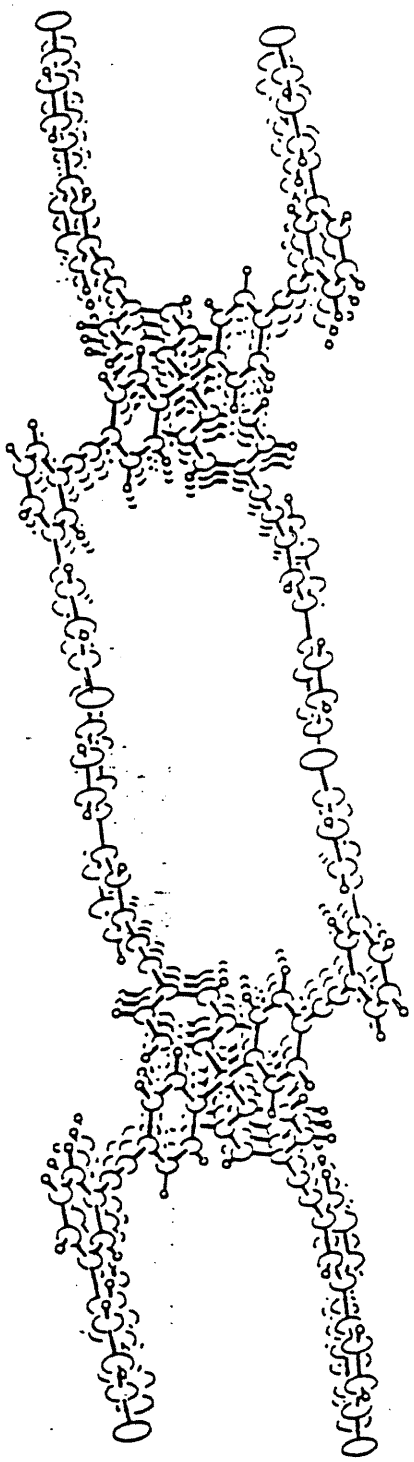

Figure 50. Top view of the stacking of tecton **XVII** down the b axis. Non-hydrogen atoms are represented by ellipsoids corresponding to 50% probability. Hydrogen atoms are represented by spheres of arbitrary size.

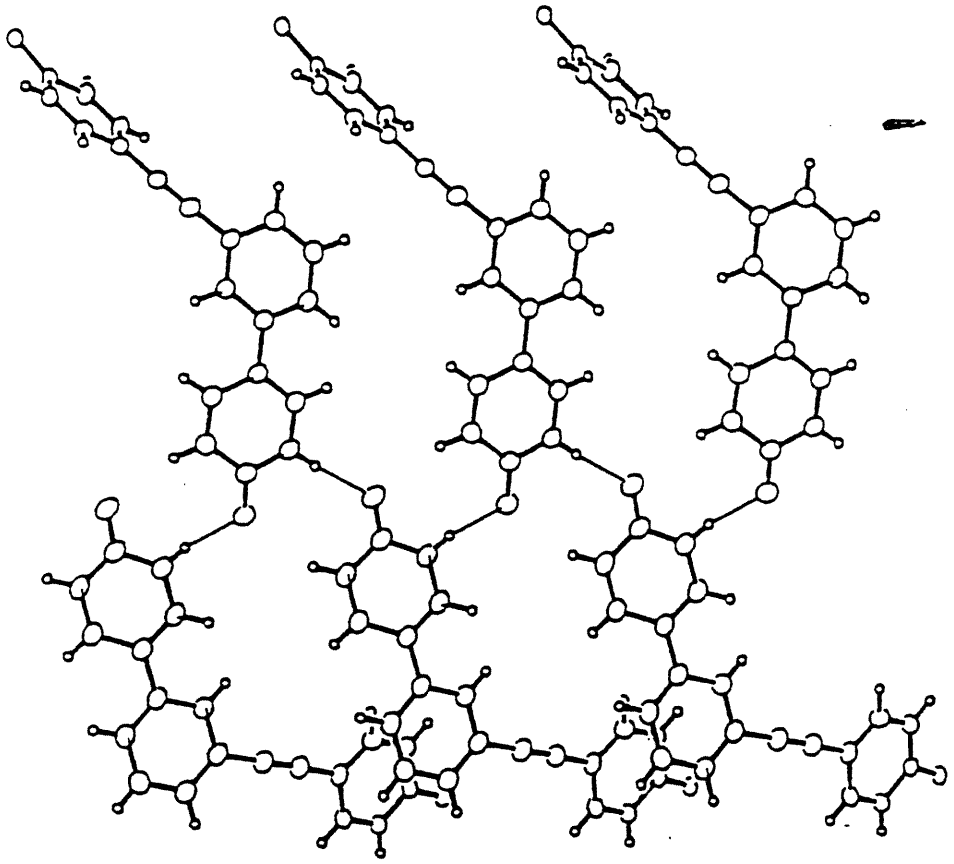

Figure 51. Top view of the single intertectonic hydrogen bonding observed in the crystal structure of tecton **XVII**. Only the asymmetric unit of neighboring tectons **XVII** is shown. Non-hydrogen atoms are represented by ellipsoids corresponding to 50% probability, and hydrogen atoms are represented by spheres of arbitrary size.

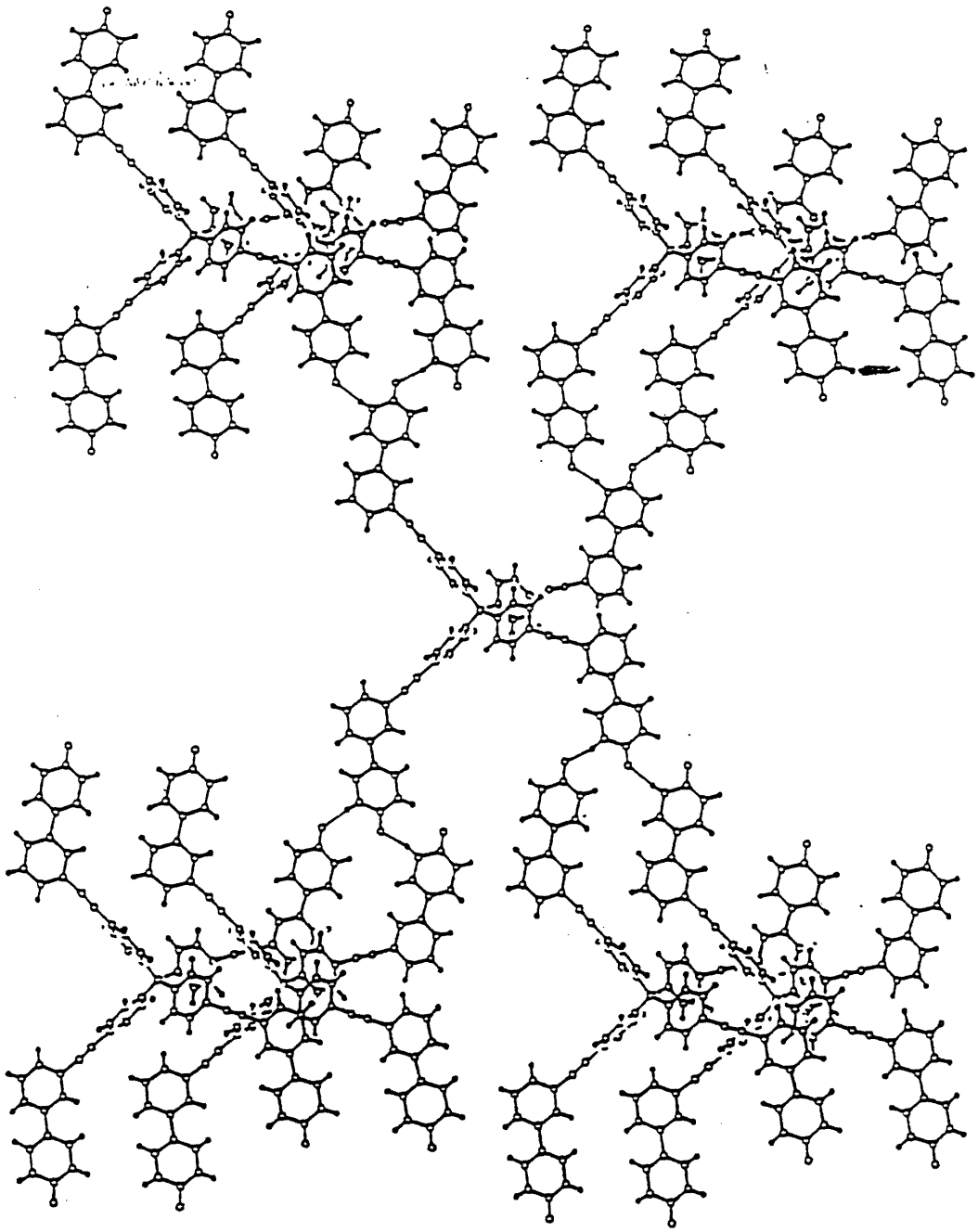

Figure 52. Side view of hydrogen-bonded tectons **XVII** stacking along the **b** axis by sitting on top of each other. Non-hydrogen atoms are represented by ellipsoids corresponding to 50% probability, and hydrogen atoms by spheres of arbitrary size.

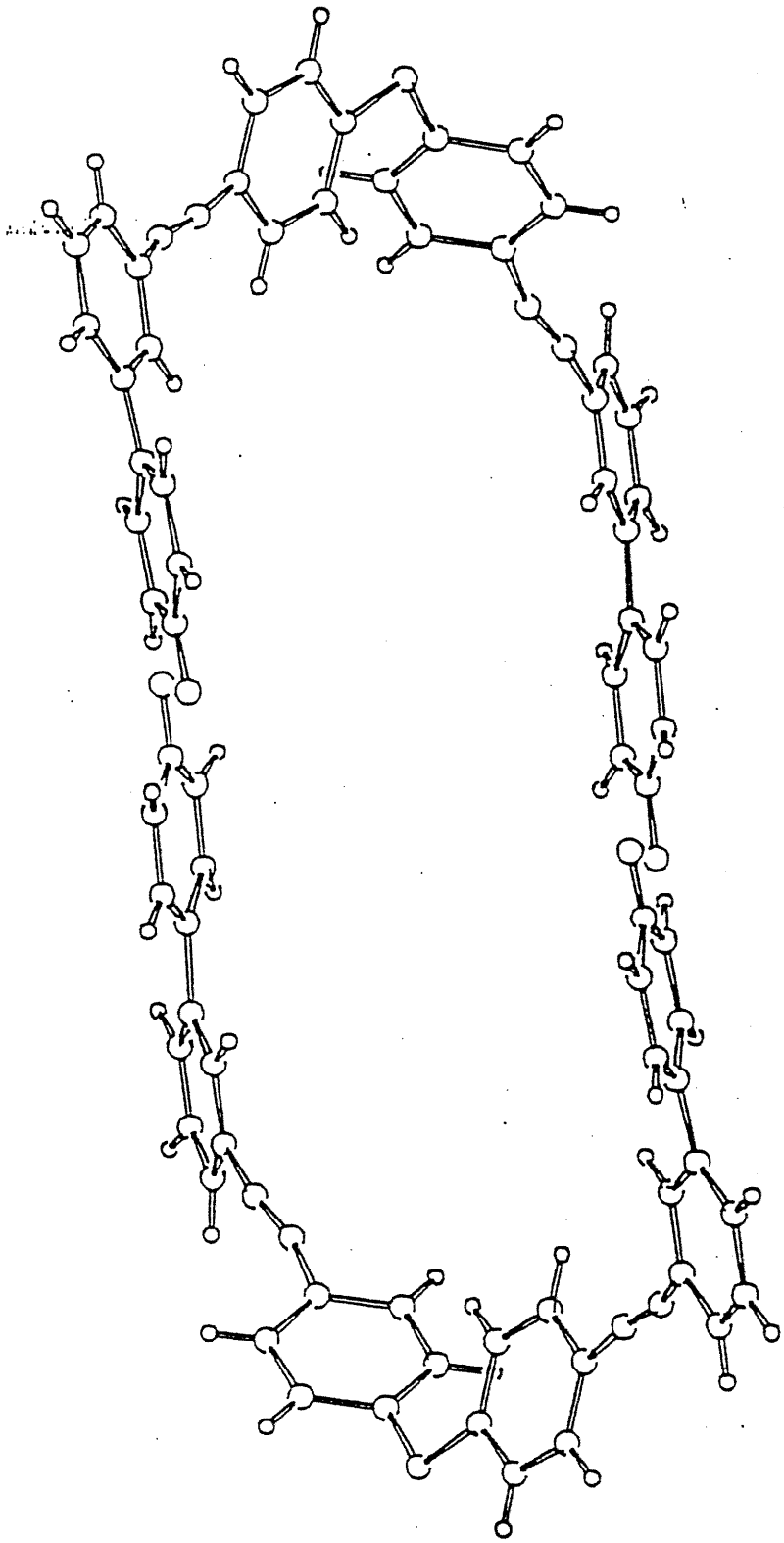

Figure 53. View (down the **b** axis) of an individual four-sided channel cut out of the layer networks in crystals of tecton **XVII**.

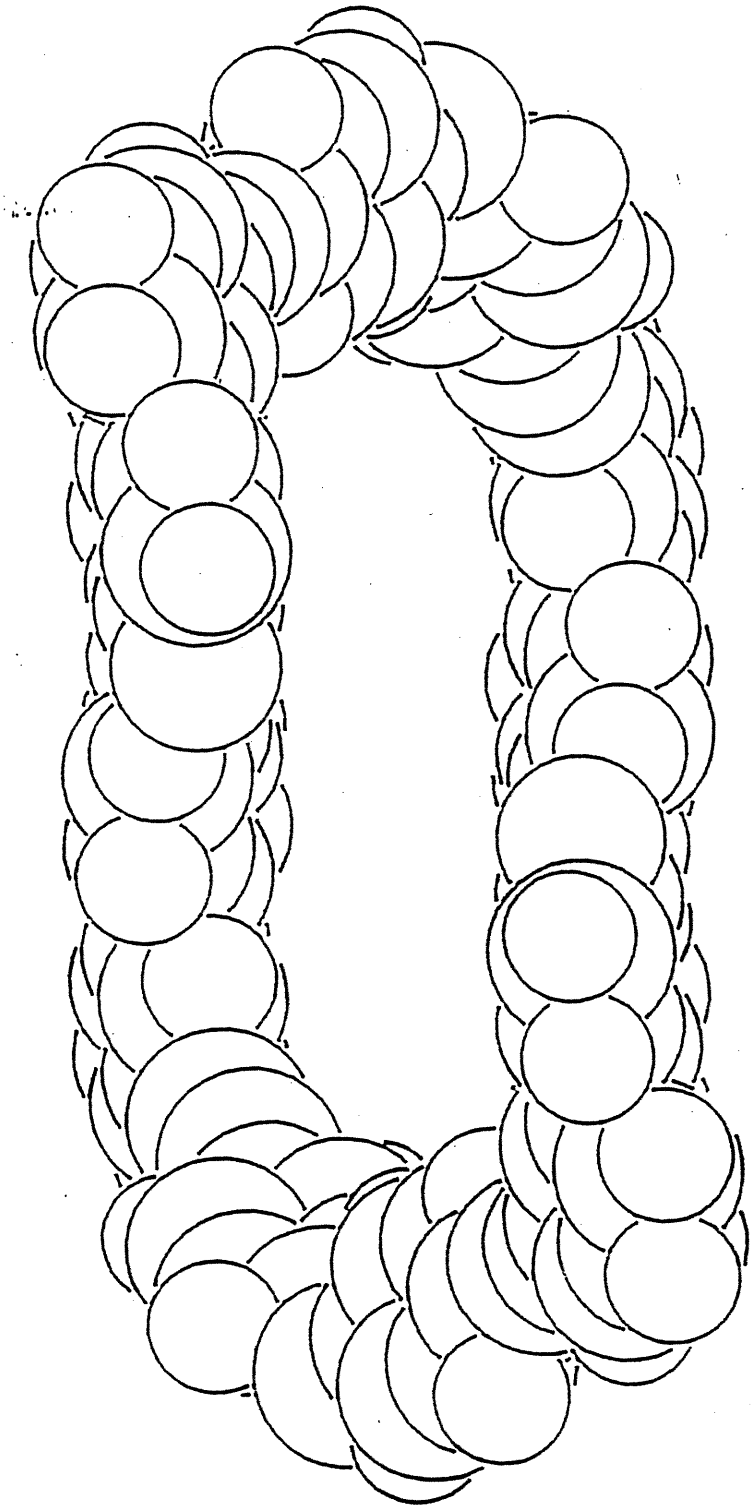

Figure 54. Space-filling view (down the **b** axis) of an individual four-sided channel cut out of the layer networks with diameter 14 Å x 4 Å.

employed. In Figures 53 and 54, an individual channel cut out of the layer networks is presented in both cylinder-ball and space-filling stereoviews.

5.4. Design and synthesis of smaller tectons which may be able to construct contracted diamondoid networks because of shorter intertectonic distances.

In an influential paper, Aakeröy and Seddon[42] provided a thoughtful discussion of the role that hydrogen bonds play in crystal engineering. They suggested that it is very important to understand the energetic contribution of hydrogen bonding to the lattice energy of a crystalline material, since the underlying assumptions about its usefulness in crystal engineering will be invalidated unless the hydrogen bond makes a significant energetic contribution. They indicated that direct measurements of lattice energies are not feasible and that accurate lattice energy calculations require much time and effort because they are based upon extensive empirical parameterizations. Nevertheless, a simple but reliable procedure for the calculation of the intermolecular potential energy in organic crystals is so highly desirable, both from a theoretical and from a practical point of view, since many properties of these crystals can be obtained from such calculations, and eventually the crystal structure might become predictable from molecular structure alone. A great computational simplification has been achieved in the so-called atom-atom potential method[22], by which the total lattice energy is a sum of two-body interactions only. Each of these is in turn a sum of terms which are supposed to represent the various interactions between atoms of different molecules in crystals. As the value of an empirical scheme increases with the number of properties it is able to predict and decreases with the number of parameters it must use, considerable effort has been made to devise a simple and efficient way to calibrate the packing energy of organic crystals, either without or with hydrogen bonding.

Gavezzotti and co-workers[43] have been particularly active in this area. It is important to emphasize that the lattice energy or the packing energy is a function of molecular size and shape[34d]. Therefore, the packing energy may not be easy to calculate precisely, but the energetic contribution of hydrogen bonding with a certain motif to the lattice energy should not vary widely with changes in the size and shape of an analogous series of compounds. However, an increase in the size of molecules with a certain pattern of hydrogen bonding will bring about a decrease in the fractional energetic contribution that hydrogen bonding makes to the lattice energy. For instance, the results of the work implemented by Michopoulos and Adam[44], which investigates atom-atom potentials and the crystal structure simulation of long straight-chain carboxylic acids, have proved that the Coulombic contribution, which is associated mainly with the intermolecular hydrogen bonding, remains approximately constant across the series of acids, while the lattice energy increases in line with the molecular length (as shown in Table 16).

Table 16. Energy contributions for straight-chain carboxylic acids (eV unit cell^{-1})[44]

Energy	C_2	C_3	C_4	C_5	C_{12}	C_{18}
U (Coul)	-1.71	-1.86	-1.78	-1.92	-1.51	-1.78
U (L-J)	-0.80	-1.33	-1.44	-1.92	-4.05	-7.00
U (Latt)	-2.50	-3.91	-3.26	-3.84	-5.56	-7.72
Coul. Contribution	68%	58%	55%	50%	27%	23%
Exptl *U* (Latt)	-2.83	-3.07	-3.33	-3.54	-6.33	-8.00

$U = \sum_{ij} U_{ij}(r_{ij})$, where i and j run over all atoms in the interacting molecules.

$U_{ij}(r_{ij}) = A_{ij}r_{ij}^{-9} - B_{ij}r_{ij}^{-6} + q_{ij}q r_{ij}^{-1}$, U_{ij}, the individual potential, is the sum of a 9-6 Lennard-Jones function plus a explicit Coulomb term.

We have mentioned in Chapter 3 that in order to obtain solid organic materials with high porosity, or in other words, supramolecular aggregates with nanosized cavities, the forces favoring close packing should be overridden by intermolecular hydrogen bonding. In the crystal packing of tectons **I** and **XVII**, van der Waals forces are evidently dominant rather than intermolecular hydrogen bonding. Because we wondered how important the energetic contribution of hydrogen bonding to the lattice energy should be, in order to make hydrogen bonding override forces favoring close-packing, we turned our attention to the design and synthesis of smaller tectons. It may be expected that the relative energetic contribution of hydrogen bonding should be more important in the lattice energies of smaller tectons than in that of tecton **I**.

The retrosynthetic analysis of tectons **XVIII** and **XIX** is shown in Scheme 52.

Scheme 52

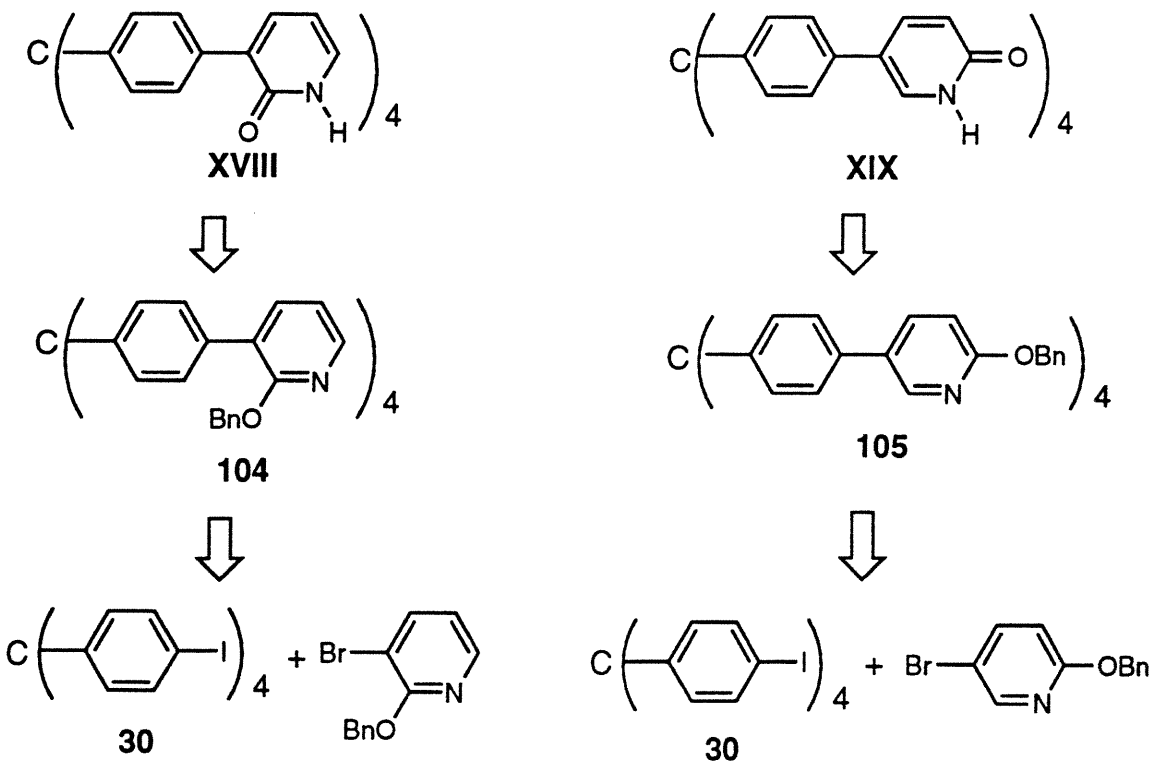

They are obviously easy to make. From Scheme 53 we can see that tecton **XIX** might not be able to generate a shorter intertectonic distance by formation of intermolecular hydrogen bonds, even though the spacing group of ethynylphenyl between pyridone and center carbon atom in tecton **I** has been replaced with a single phenyl group. Instead, an intertectonic distance which might be even slightly longer than that of tecton **I** will be

Scheme 53

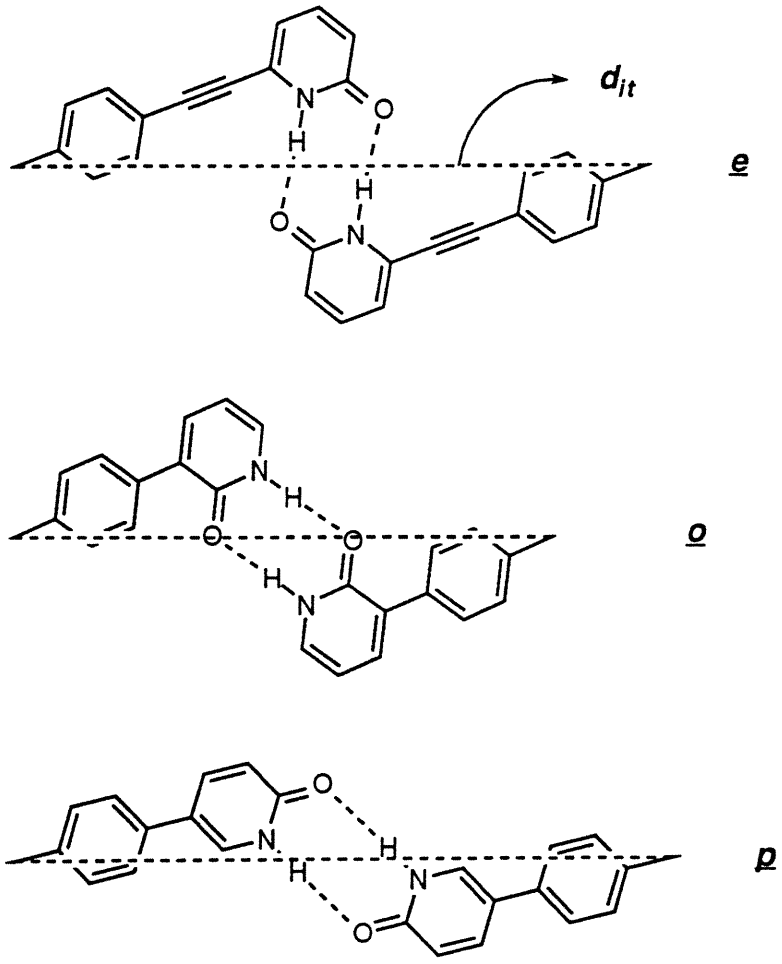

Scheme 54

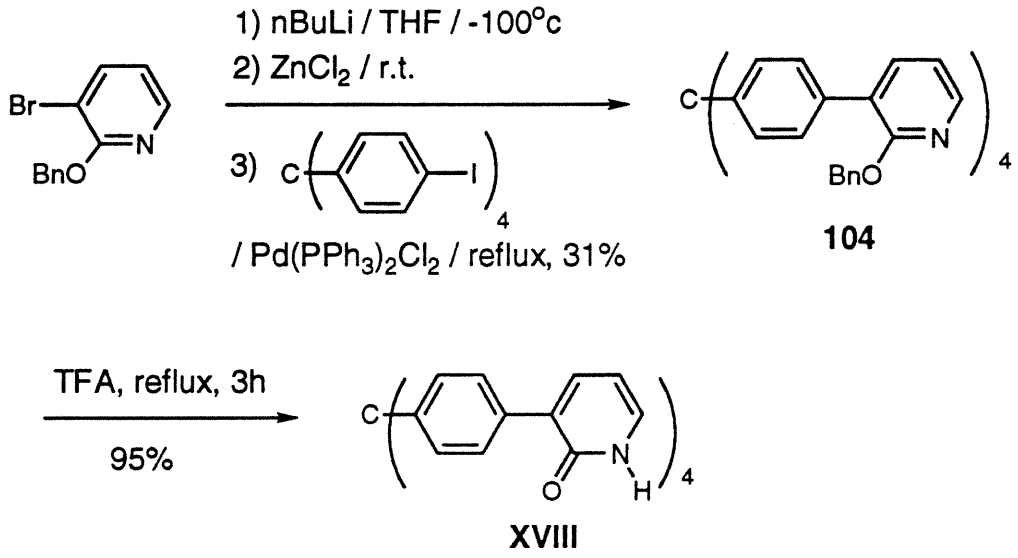

Scheme 55

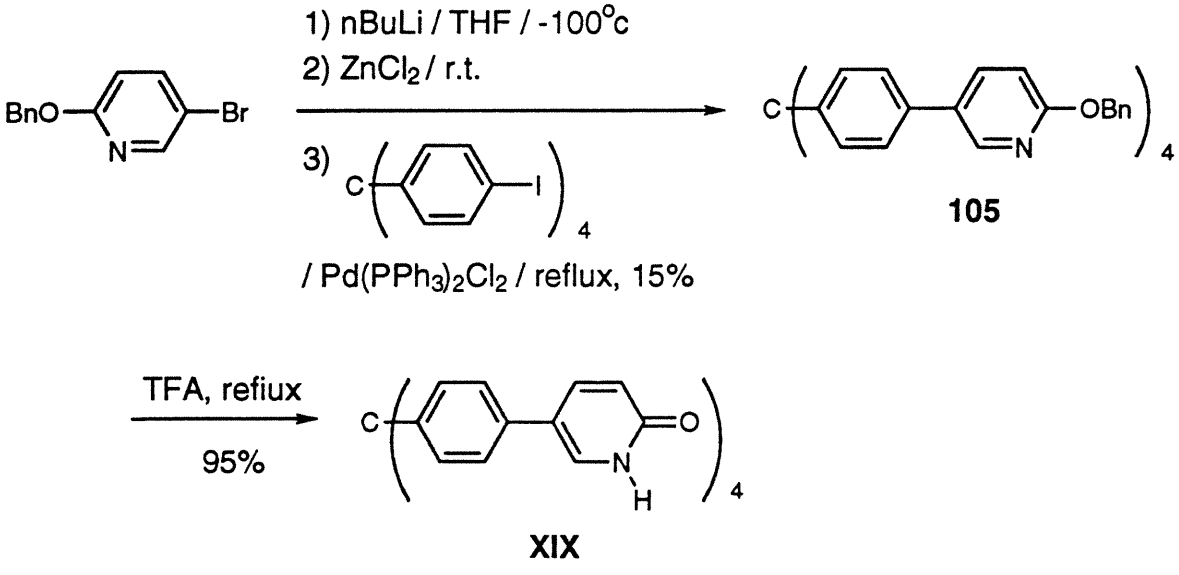

defined. In addition, the yield of tetrapyridine **105**, which was synthesized by cross-coupling of compound **30** with 5-bromo-2-(phenylmethoxy)pyridine (Scheme 55), is quite low (15%). As a result, tecton **XIX**, provided by deprotection of compound **105** in TFA in 95% yield (Scheme 55), became less attractive to us for the purpose of investigating smaller tectons. Moreover, we found that the solubility of tecton **XIX** is very poor in either carboxylic acids or DMF and DMSO. Even though we tried to crystallize tecton **XIX** from carboxylic acids in several ways, we did not obtain single crystals which were suitable for X-ray crystal structure study. The crystals we obtained were long, fine needles.

Thereafter we turned our attention to the synthesis and crystallization of tecton **XVIII**, which seems more promising than tecton **XIX** owing to its shorter intertectonic distance (shown in Scheme 53). It was synthesized by a cross-coupling reaction between compound **30** and 3-bromo-2-(phenylmethoxy)pyridine followed by treatment of tetrapyridine **104** with TFA under reflux to cleave the protecting group in an overall yield of 30% (Scheme 54). Like tecton **XIX**, tecton **XVIII** has poor solubility in carboxylic acids, and the crystals which we obtained were very fine, long needles even under conditions chosen to make the rate of crystallization as slow as possible. After extensive experiments, crystals suitable for X-ray crystallographic analysis were finally afforded via crystallization of tecton **XVIII** from a solvent system of DMF/Et_2NH.

5.5 Crystal structure of tecton XVIII.

X-ray crystallographic study of the crystal structure of tecton **XVIII** revealed that normal diamondoid networks induced by intermolecular hydrogen bonding with a degree of interpenetration of 5 are formed. The crystal data for tecton **XVIII** are listed in Table 17. Comparison of the crystal structure of tecton **XVIII** with that of tecton **I** and tetraphenylmethane reveals the following striking differences between tecton **XVIII** and

Table 17. Crystal data of tecton **XVIII**•4 DMF compared with those of tecton **I**•2 $C_3H_7CO_2H$ and tetraphenylmethane

Compound	Crystal system	Cell parameters	Space group	Molecular symmetry in crystal	d_{it} (Å)
$C(C_6H_5)_4$	tetr.	a = 10.86 Å; c = 7.26 Å; Z=2	$P\bar{4}2_1c$	$\bar{4}$	--
I•2 $C_3H_7CO_2H$	monoc.	a = 31.25 Å; b = 7.35 Å; c = 23.15 Å; β = 104.69°; Z=4	C2/c	$\bar{4}$	19.69
XVIII•4 DMF	tetr.	a = 11.52 Å; c = 40.42 Å; Z=4	$I\bar{4}1/a$	$\bar{4}$	16.37

Table 18. The calculated densities of tectons

Tecton	FW_{tecton}	V (Å^3)	Z	d_C (g/cm^3)
I	788.89	5142	4	1.019
XVII	1093.25	7424	4	0.978
XVIII	692.81	5367	4	0.857

$d_C = 1.660ZFW_tV^{-1}$

the latter compounds. Firstly, the characteristic structural feature, defined as the shortest distance between two non-hydrogen-bonded tectons, is 11.52 Å rather than normally 7.3

Å. In addition, the intertectonic distance in crystals of tecton **XVIII** (16.37 Å) is only 3 Å shorter than that of tecton **I** (19.69 Å), but the degree of interpenetration decreases steeply from 7 to 5. In order to compare the hollowness of **XVIII** with **I** and **XVII**, their calculated densities are listed in Table 18. To be comparable, the effect of enclathrated molecules on the density was not taken into account. Evidently, tecton **XVIII** is more hollow than the other two. Furthermore, another noteworthy difference is that the number of enclathrated molecules is raised from 2 molecules of butyric acid per molecule of tecton **I** to 4 molecules of DMF per molecule of tecton **XVIII**. It means that the diamondoid networks constructed from tecton **XVIII** are energetically more durable and stable, since more unfavorable enclathration occurs and is tolerated in the crystal packing of tecton **XVIII**. In addition, from Table 18 we can conclude that the superaggregates of tecton **XVIII** are hollower than those of tecton **XVII**, since the number of enclathrated DMF molecules is 4 either for tecton **XIII** or tecton **XVII**. This fact indicates that the diamondoid structure constructed from tecton **XVIII** is more tolerant to hollowness. All these phenomena imply that the energetic contribution of intermolecular hydrogen bonding to the lattice energy of the crystal structure must be more important, and consequently, intermolecular hydrogen bonding might play a leading role in the crystal packing of tecton **XVIII** instead of van der Waals forces. Closer examination of the crystal structure of tecton **XVIII** is summarized below.

5.5.1 Comparison of characteristic structural features of different tectonic aggregates.

As mentioned above, the shortest distance between the central carbon atoms of non-hydrogen-bonded tectons in their crystal structure is a characteristic structural feature of their crystal packing. If we take the crystal packing of tetraphenylmethane as a standard close packing model, in which there is no intermolecular hydrogen bonding involved, we

may conclude that in the packing of tecton **I**•8 $C_2H_5CO_2H$, **I**•2 $C_3H_7CO_2H$ and **XVII**•4 DMF, forces favoring close-packing are dominant, since their characteristic structural features are similar to that of tetraphenylmethane as shown in Table 19. However, in the

Table 19. The characteristic structural feature of tectons

Tecton	The characteristic structural feature (Å)
I•8 $C_2H_5CO_2H$	7.787
I•2 $C_3H_7CO_2H$	7.350
XVII•4 DMF	7.344
XVIII•4 DMF	11.52
Tetraphenylmethane	7.26

crystal packing of tecton **XVIII**, its characteristic structural feature (11.52Å) is much longer than what has been found in the series of tetraaryl compounds (around 7.3 Å). It may be conjectured that in networks derived from tecton **XVIII**, since the size of the molecule is smaller, the energetic contribution of hydrogen bonding to the lattice energy is more important and therefore hydrogen bonding becomes a dominant factor in the crystal packing. In Figure 55, ORTEP views along the **b** axis of the packing arrangement in the unit cells of tectons **XVIII** and **I** are shown for comparison. In Chapter 2, the observed crystal structures of tecton **I** suggest that crystallization may occur by the formation of aggregates in which the tectonic subunits pack along an n-fold axis, using the symmetry operator of translation, to form a column. Under the direction of intermolecular hydrogen bonding, using other symmetry operators, the entire crystal structure is then generated. In contrast to tecton **I**, it is possible that in the crystal packing of tecton **XVIII**, the aggregates

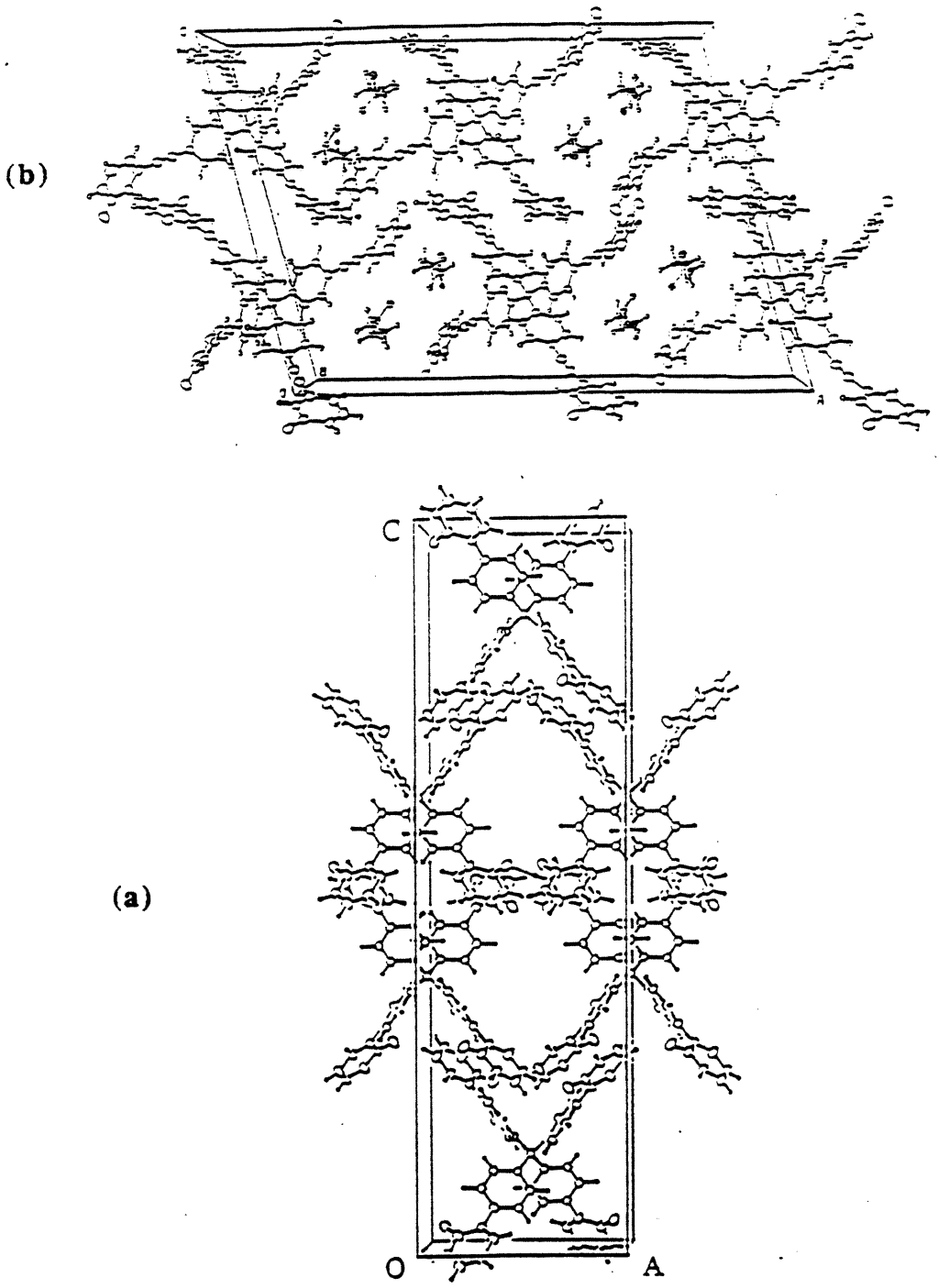

Figure 55. ORTEP views along the **b** axis of the packing arrangement in the unit cell of (a) tecton **XVIII**•4 DMF (disordered molecules of DMF are omitted for clarity) and (b) **I**•2 $CH_3CH_2CH_2CO_2H$. Non-hydrogen atoms are represented by ellipsoids corresponding to 50% probability, and hydrogen atoms by spheres of arbitrary size.

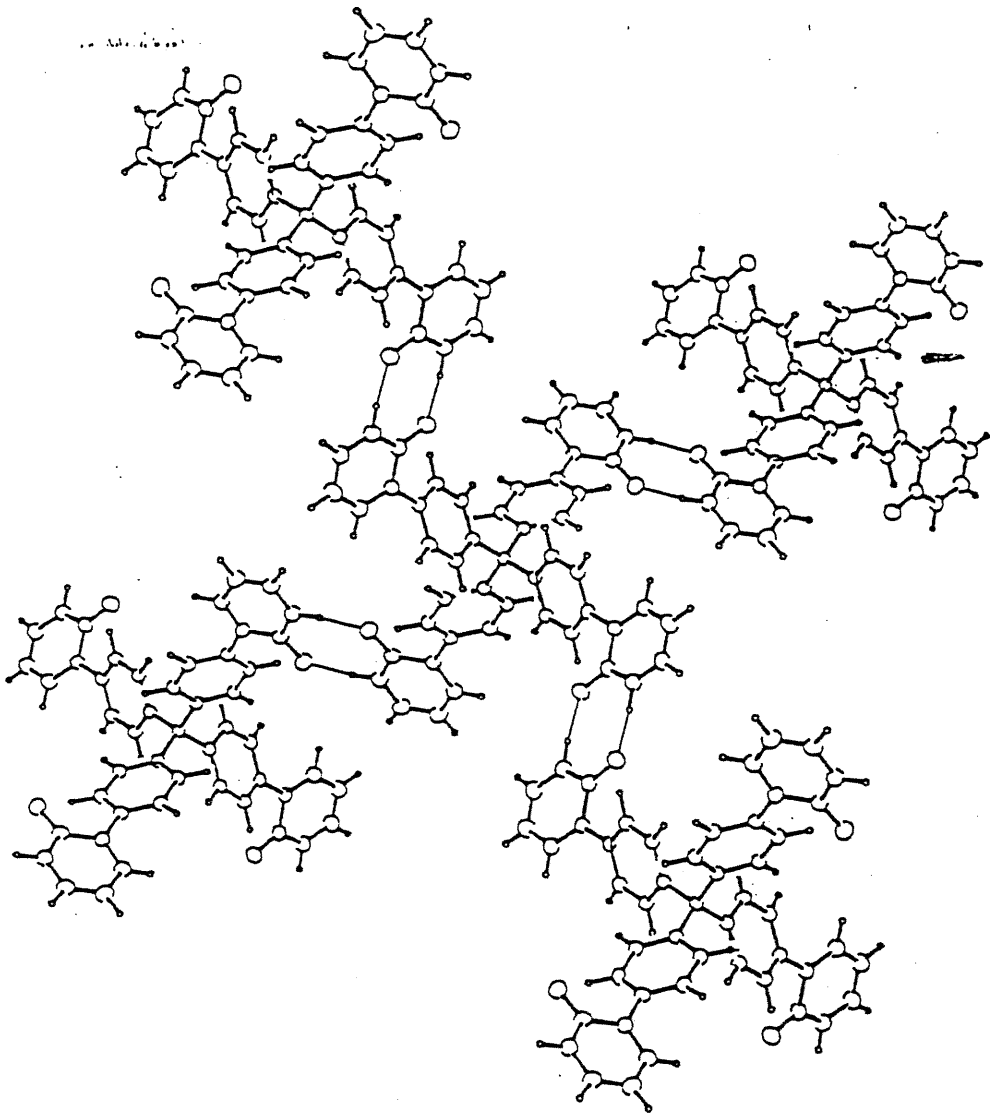

Figure 56. View of a tetrahedral molecular aggregate constructed from five hydrogen-bonded molecules of tecton **XVIII** down the **c** axis. Non-hydrogen atoms are represented by ellipsoids corresponding to 50% probability, and hydrogen atoms by spheres of arbitrary size.

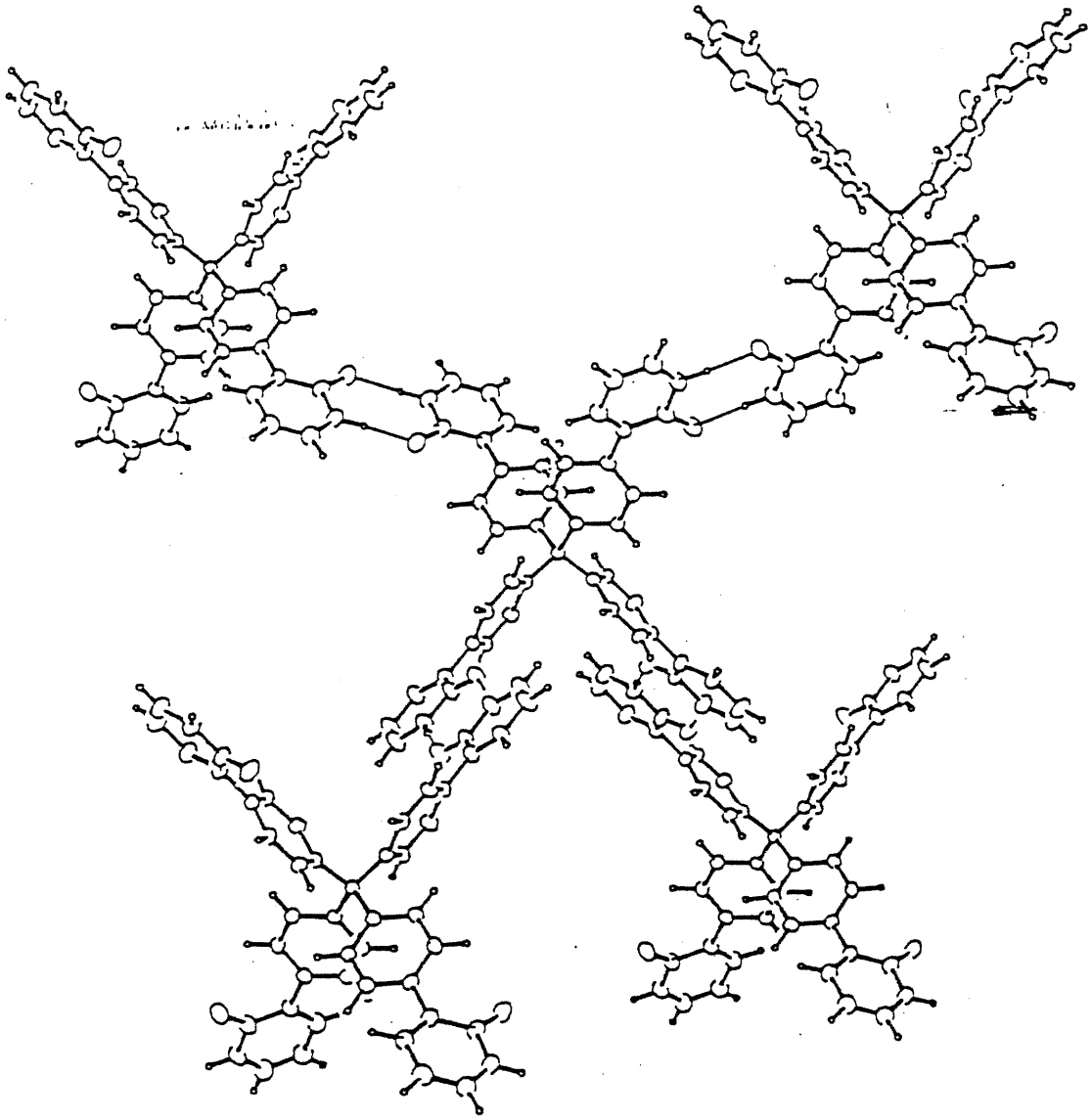

Figure 57. View of a tetrahedral molecular aggregate constructed from five hydrogen-bonded molecules of tecton **XVIII** down the **a** or **b** axis. Non-hydrogen atoms are represented by ellipsoids corresponding to 50% probability, and hydrogen atoms by spheres of arbitrary size.

are formed in such a way that each tecton primarily hydrogen-bonds with other four tectons to generate a tetrahedral molecular aggregate (shown in Figures 56 and 57), and then the entire crystal is constructed by applying a pure translation on the aggregate along the **a** and **b** axes, while a glide plane is applied on the aggregate along the **c** axis. In Figure 56, a view of the aggregate down the **c** axis (parallel to the 4-fold screw axis) is presented. In Figure 57, a view of the aggregate down the **a** or **b** axis (parallel to the 2-fold screw axis) is shown. Consequently in the crystal packing of tecton **XVIII**, intermolecular hydrogen bonding is more dominant than van der Waals forces and that is why the characteristic structural feature of tecton **XVIII** has been lengthened.

5.5.2 The low degree of interpenetration of 5.

The X-ray crystallographic study revealed that the intertectonic distance in crystals of tecton **XVIII** is 16.37 Å, and the molecular symmetry of tecton **XVIII** is S_4. Tecton **XVIII** is a somewhat more rigid molecule than either tectons **I** or **XVII**. Accordingly, we can conjecture that either elongation or compression of diamondoid networks constructed from tecton **XVIII** via intermolecular hydrogen bonding will cause serious strain and therefore might be disfavored. It has been indicated that the quite high degree of interpenetration of tecton **I** is partially brought about by the severe elongated diamondoid lattice of tecton **I**. Therefore the elongation of a diamondoid lattice might be forbidden as a result of the higher symmetry and rigidness of tecton **XVIII**, and this might be one of the reasons for its low degree of interpenetration. In Figures 58 and 59, a slightly distorted diamondoid lattice induced by intermolecular hydrogen bonding in the crystals of tecton **XVIII** is shown in different ways. In Chapter 2, we induced dimensional indices $\underline{a}$, $\underline{b}$, and $\underline{c}$ for a diamondoid lattice to describe its deviation. In Table 20 the dimensional indices

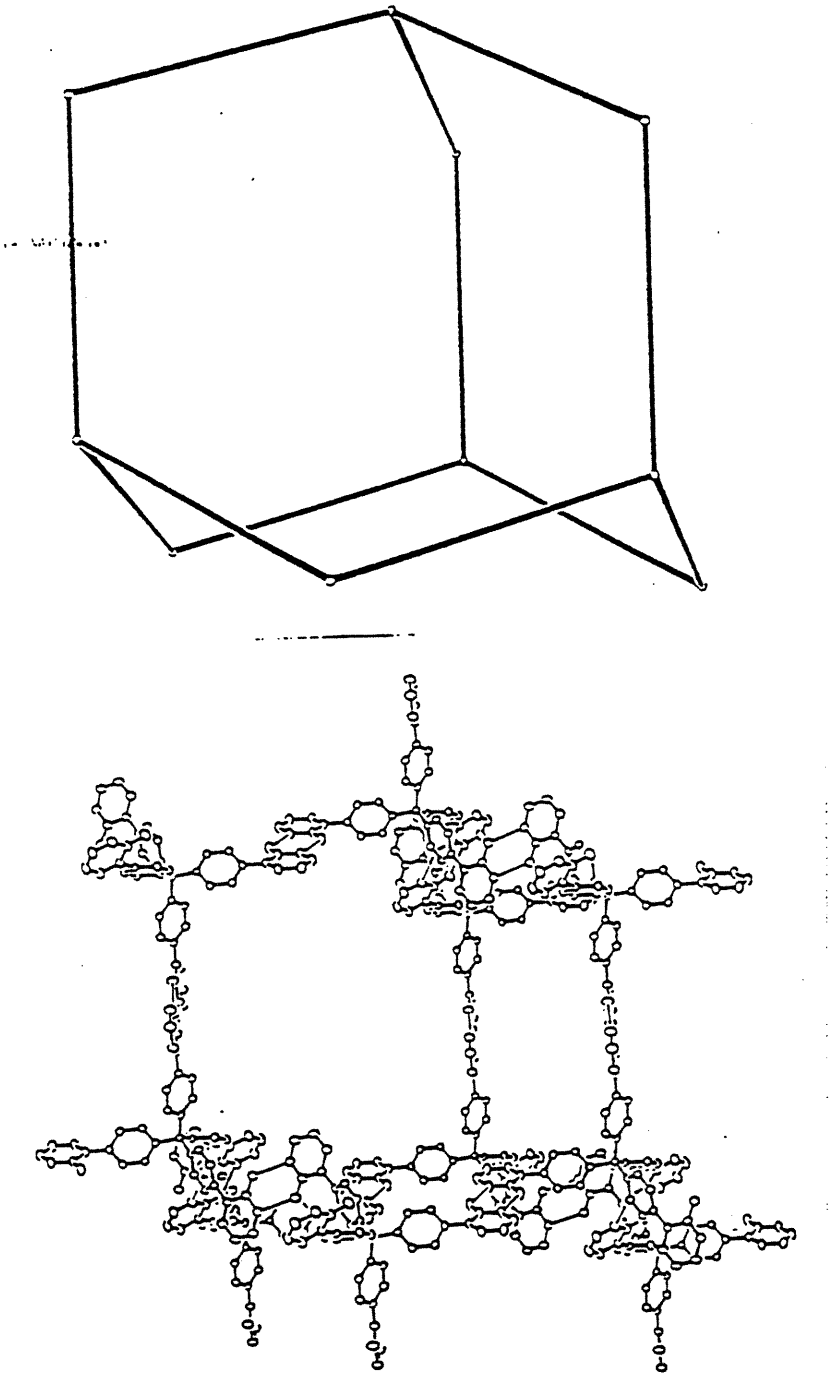

Figure 58. ORTEP drawing of part of the diamondoid network present in crystals of tecton XVIII•4 DMF. The tetrahedral centers of the ten tectons shown in the drawing define a slightly distorted adamantane, shown on top. Non-hydrogen atoms are represented by ellipsoids corresponding to 50% probability. Disordered molecules of DMF are omitted for clarity.

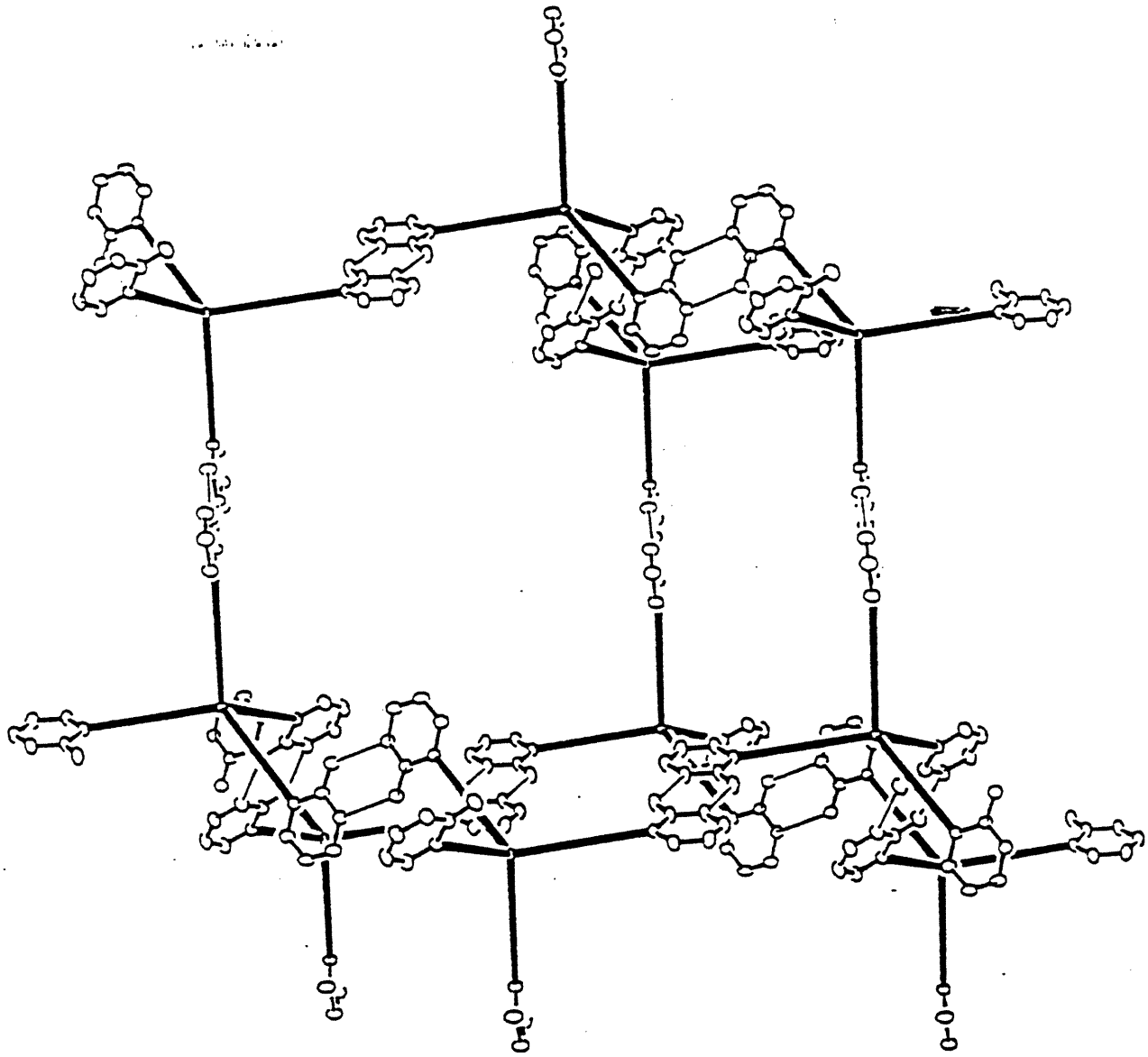

Figure 59. View of the superadamantane framework of tecton **XVIII**•4 DMF cut out of one diamondoid lattice induced by hydrogen-bonded tectons whose tetrahedral core structures are represented by solid sticks.

Table 20. The dimensional indices of diamondoid lattices generated by tectons **I** and **XVIII** and extent of elongation

Tecton	*a* (Å)	*b* (Å)	*c* (Å)	
I•8$CH_3CH_2CO_2H$	43.954	43.954	46.720	1.06
I•2$CH_3CH_2CH_2CO_2H$	43.347	33.843	51.450	1.19, 1.52
XVIII•4DMF	36.439	36.439	40.421	1.11

of diamondoid lattices constructed from tectons **I** and **XVIII** are listed. Obviously, the diamondoid lattice generated by tecton **XVIII** is slightly elongated. Another factor contributing to the low degree of interpenetration is that the shortest distance between two non-hydrogen-bonded tectons, the characteristic structural feature of tecton **XVIII**, is lengthened to 11.52 Å (compared with 7.3 Å) as a result of more important energetic contribution of hydrogen bonding to the lattice energy.

It may be pertinent to mention here how Ermer and co-workers[13b,e] lowered the degree of interpenetration in the packing of their tectons from 5 to 2. Their strategies may be described as follows. First, they modulated the architecture of the adamantane core by introducing two oxo or methylidene groups as in **36** and **37**, expecting that these groups might introduce steric effects that would reduce fivefold interpenetration. Secondly, they tried to replace enclathrated guests with other more voluminous molecules, hoping that the replacement might enforce a lower degree of interpenetration or even a single-fold diamondoid host architecture. However, they failed to implement the second strategy. This is not surprising because interpenetration is a phenomenon that is derived from close packing and that results from an interplay of several kinds of weak or strong intermolecular interactions during the crystal packing. If a single diamondoid lattice could be constructed from tecton **37** via intermolecular hydrogen bonding, it would need to be energetically

stable and durable in order to tolerate the unfavorable entropy of enclathration of guest molecules. The variation in the size, shape and volume of guest molecules might be helpful but it must have a quite limited effect, since it is not the determining factor in the crystal packing.

5.5.3 Interpenetration in the crystals of tecton XVIII.

In comparison to tecton **I**, the crystal structure of tecton **XVIII** is much more complicated. Its structure is quite similar to the crystal structure of one of Ermer's tectons, tecton **33**[13a]. The interpenetration of the five diamondoid lattices induced by hydrogen-bonded tecton **XVIII** occurs along both the crystallographic **a** and **b** axes. These five interpenetrating diamondoid lattices are translationally equivalent. They are interlaced by translating them along the **a** or **b** axis by a distance of 11.52 Å. The interpenetrating pattern of the five diamondoid lattices in the crystal structure of tecton **XVIII** is not as simple as that of the seven lattices in the crystal structure of tecton **I**. In the latter case (as shown in Figure 36), the six lattices represented with small spheres and white solid sticks simply merge into the lattice represented with black solid sticks one by one along the **b** axis by a distance of 7.350 Å. However, in the present crystal structure, the interweaving pattern is more intricate. In Figure 60, an individual diamondoid lattice cut out of the networks formed by tecton **XVIII** is shown in the view down the **a** or **b** axis (a) and the view down the **c** axis (c). Figures 61 and 62 show how the five diamondoid lattices interpenetrate one another along the **a** or **b** axis from different views. From Figure 61 we can see that the three diamondoid lattices presented with black solid sticks interlace each other along the **a** axis by a distance of 2 x 11.52 Å, and the two lattices presented with white solid sticks interlace in the same way. The further interpenetration of the white interlacing lattices into the black ones leads to the interpenetrating pattern of the five lattices in the crystal structure of tecton **XVIII**. They are translationally equivalent and interpenetrate one another by translating themselves along the a or b axis by a distance of 11.52 Å. From Figure 62 we

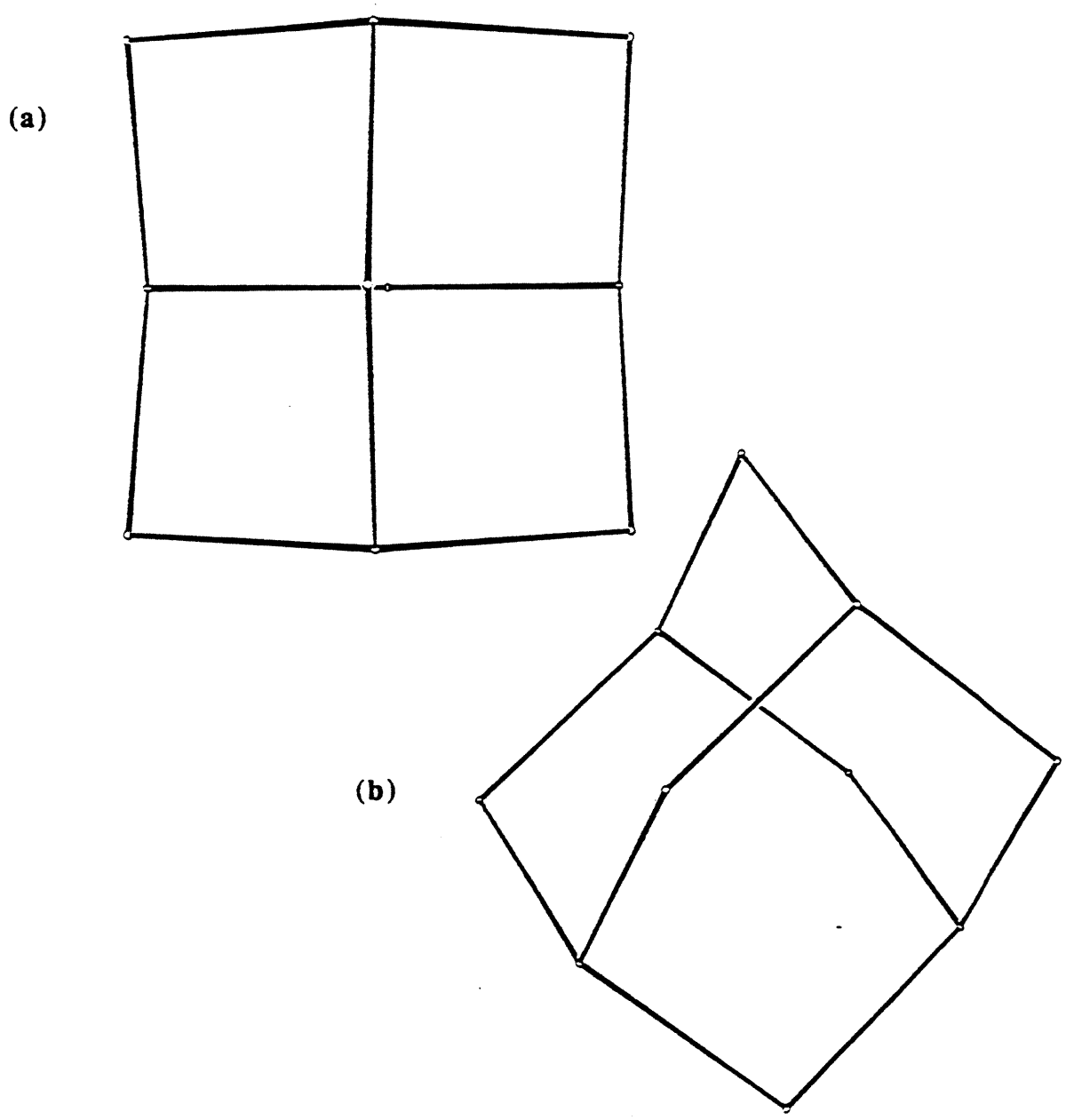

Figure 60. View down the **a** or **b** axis of an individual diamondoid lattice cut out of the networks formed by tecton **XVIII** (a), and its view down the **c** axis (b). Only the central carbon atoms of tecton **XVIII** are shown. The interconnecting rods symbolize the intertectonic hydrogen bonding.

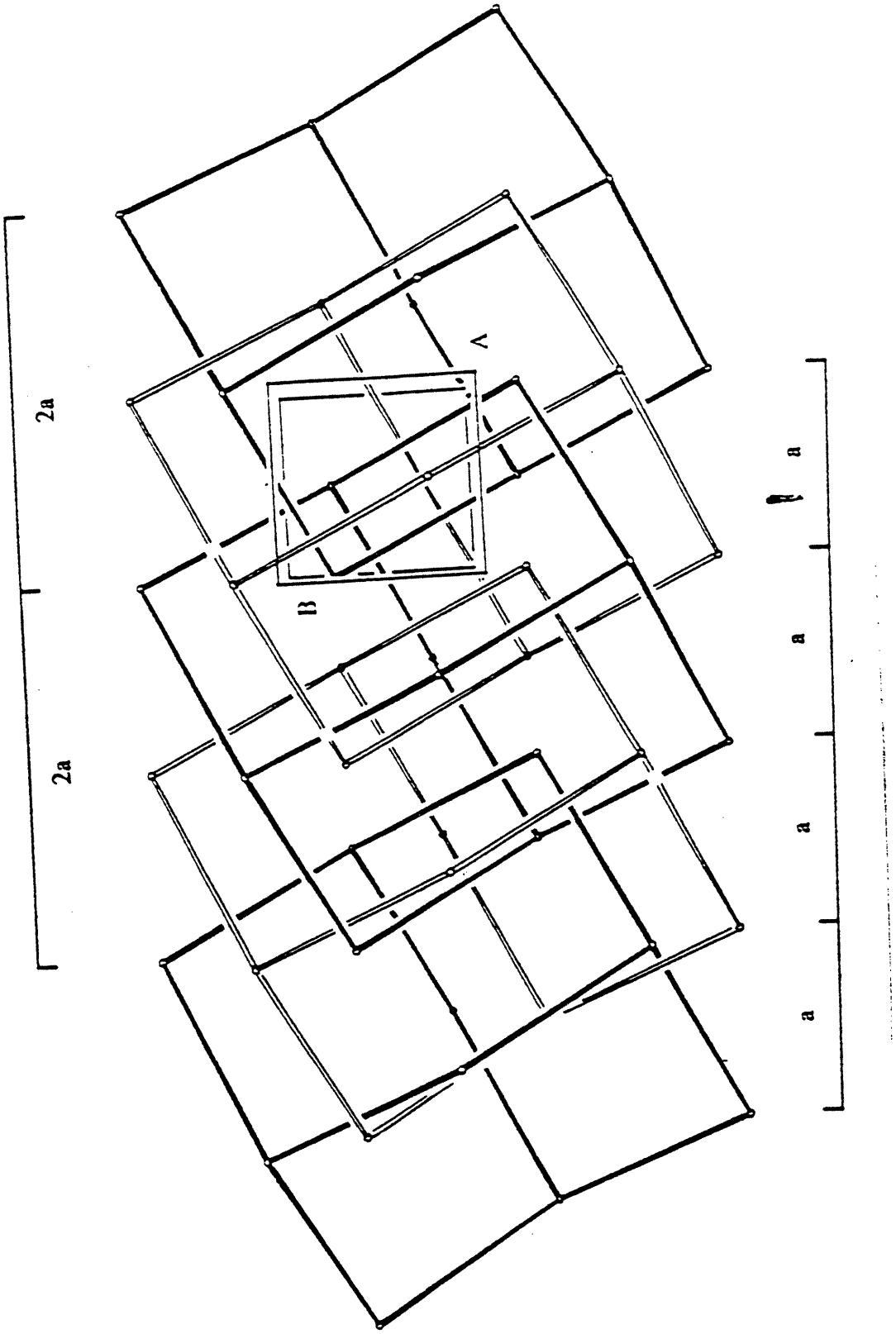

Figure 61. Five interpenetrating diamondoid lattices in the crystal of tecton XVIII•4DMF are interwoven by translating them along the **a** or **b** axis by a distance of 11.52 Å viewed along the **c** axis.

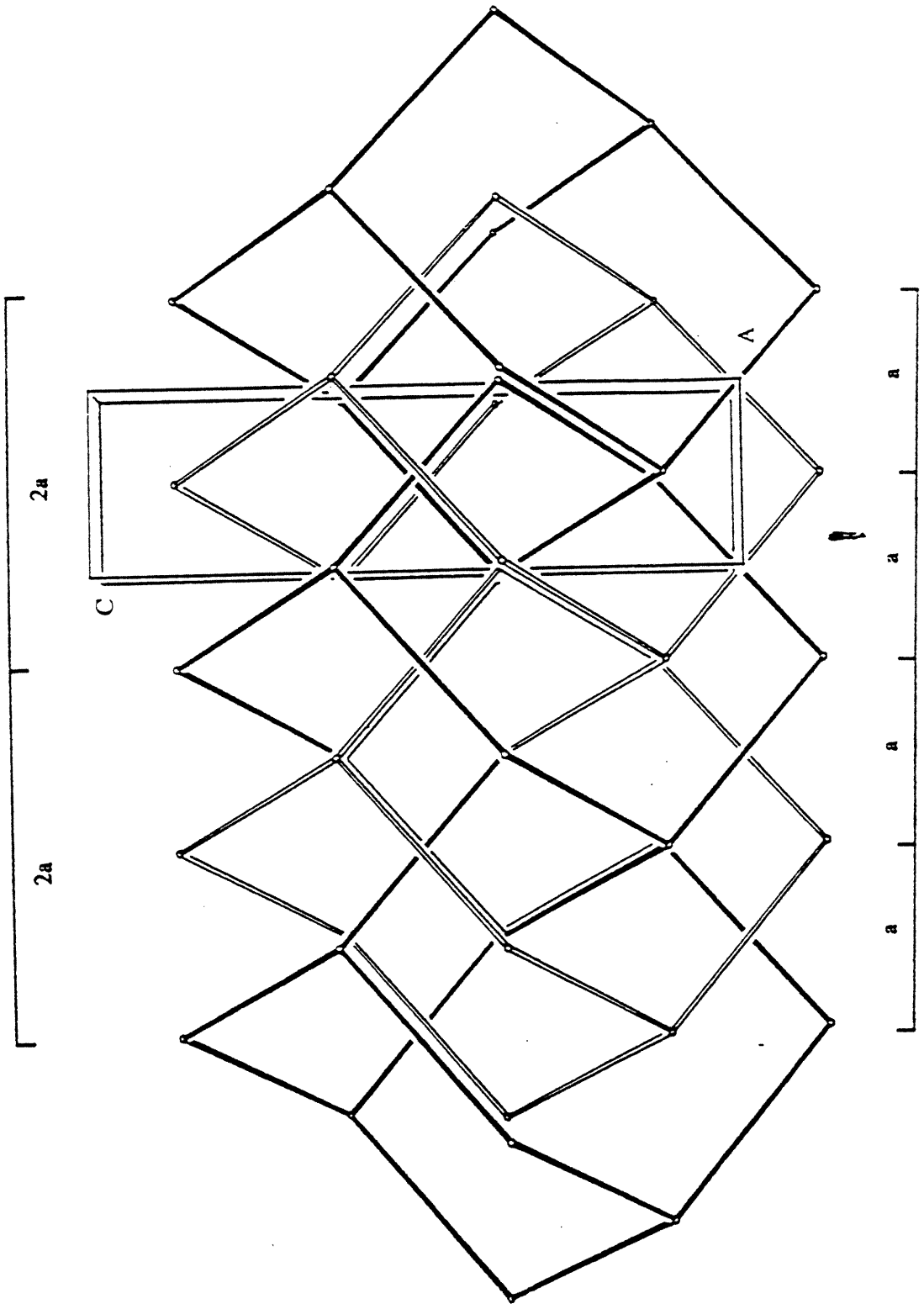

Figure 62. Five interpenetrating diamondoid lattices in the crystal of tecton XVIII•4DMF are interwoven by translating them along the a axis by a distance of 11.52 Å viewed along the b axis.

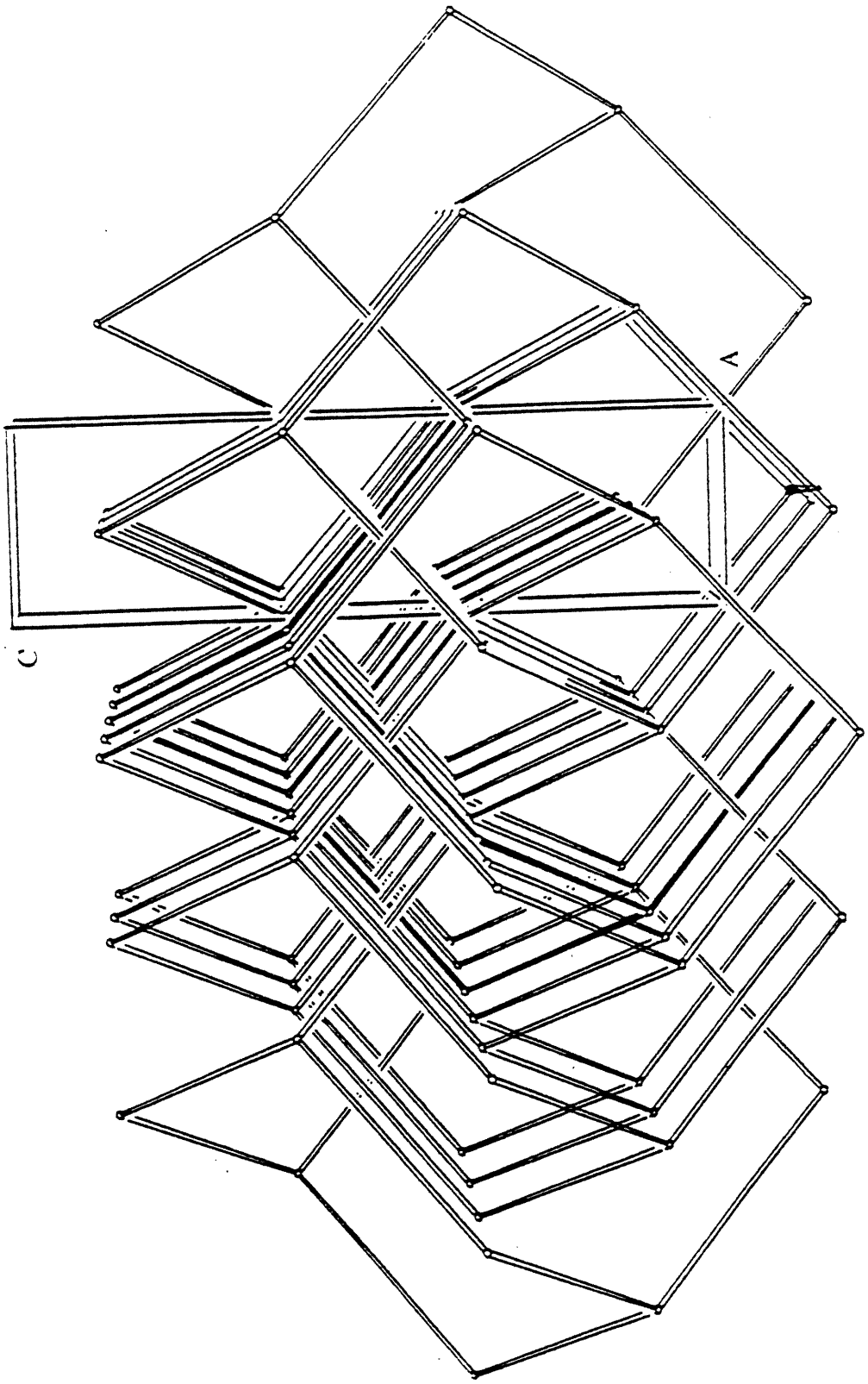

Figure 63. Channels defined by the diamondoid networks viewed along the **b** axis in the crystal of tecton **XVIII**.

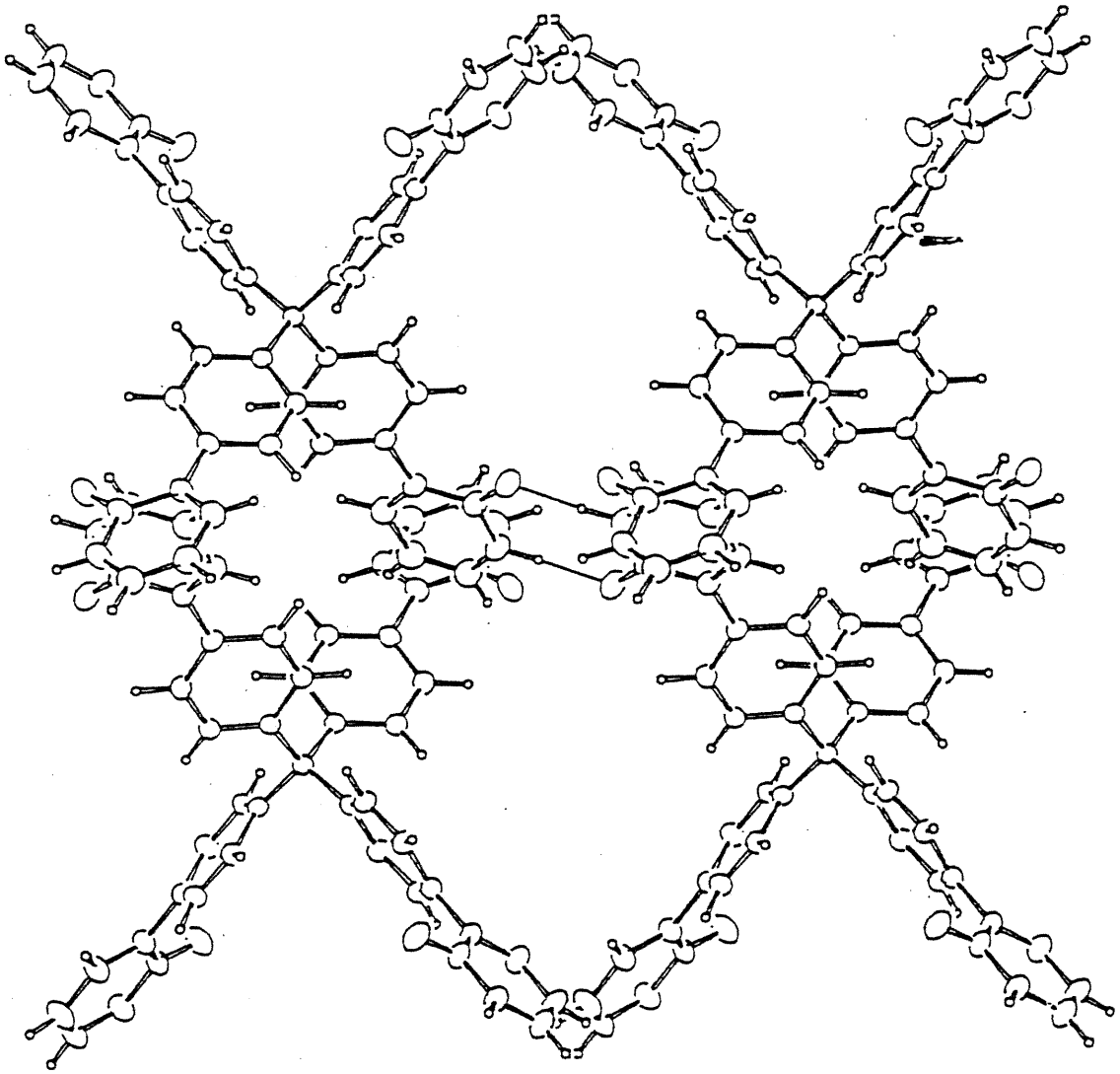

Figure 64. View (down the **b** axis) of two adjacent four-sided channels constructed from four hydrogen-bonded tectons **XVIII**, which are cut out of diamondoid lattices in the crystal of tecton **XVIII**•4DMF.

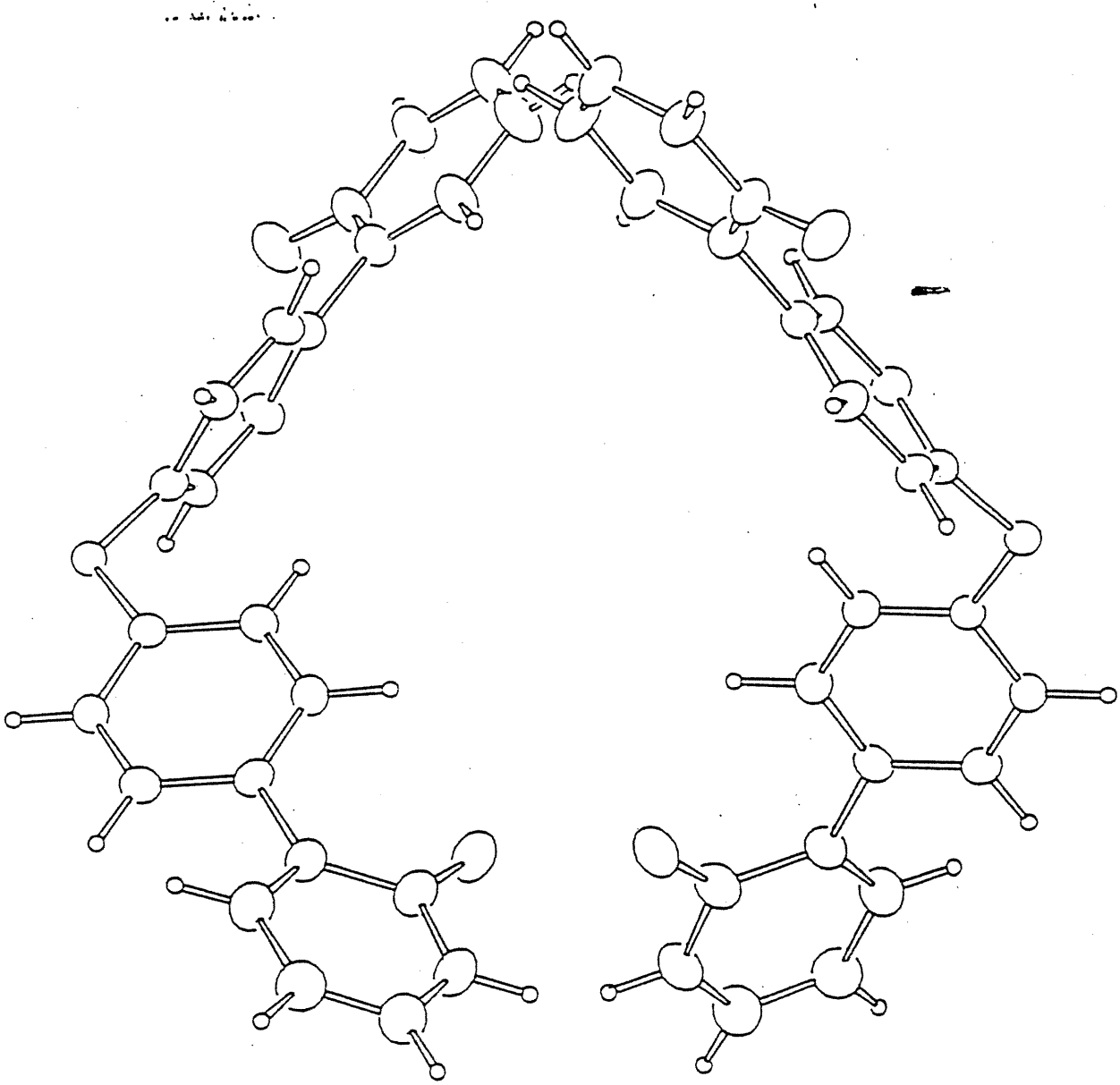

Figure 65. View (down the **b** axis) of an individual four-sided channel cut out of diamondoid networks in the crystal of tecton **XVIII**•4DMF.

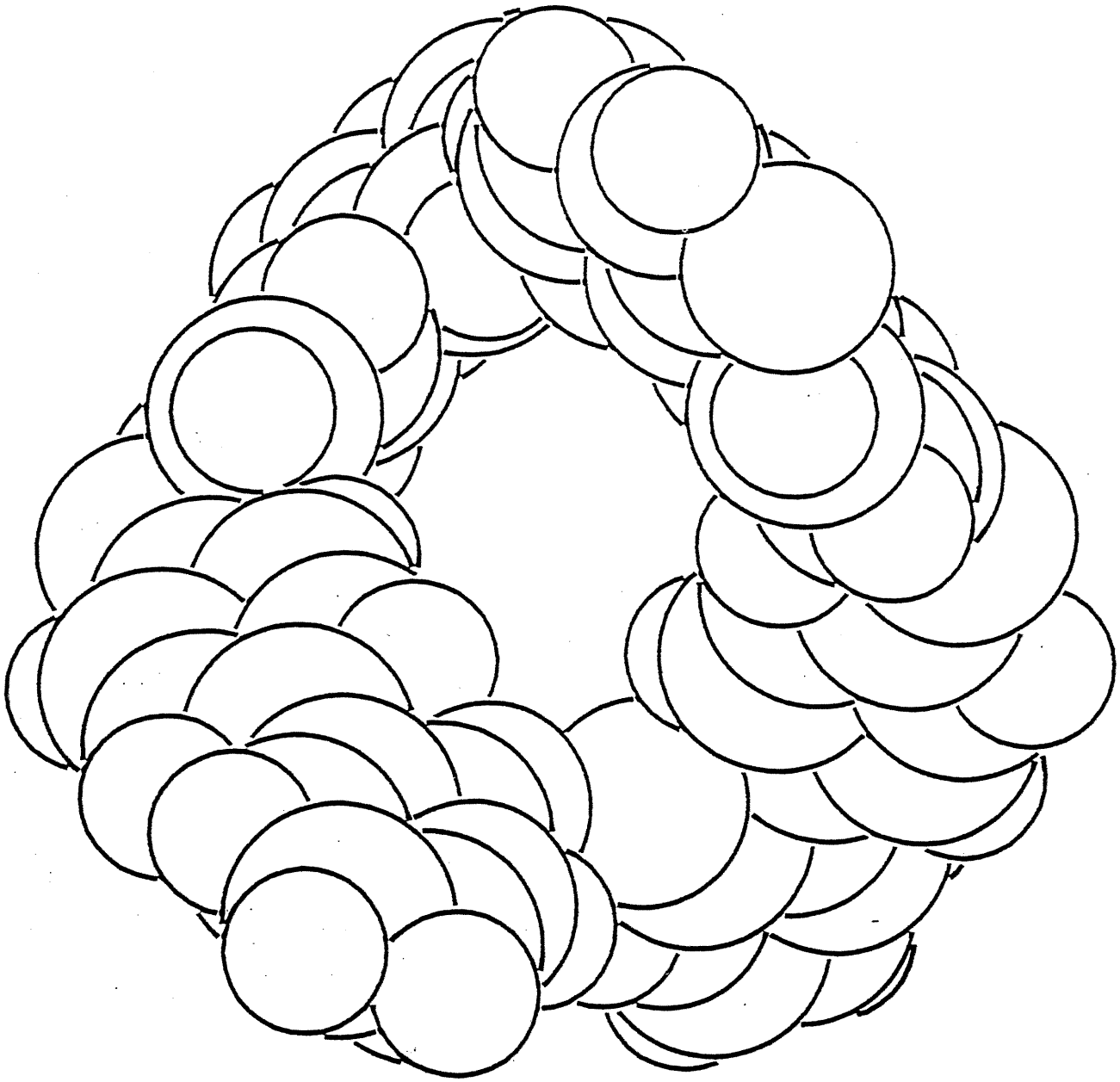

Figure 66. Space-filling view (down the **b** axis) of an individual four-sided channel cut out of diamondoid networks in the crystal of tecton **XVIII**•4DMF with diameter 6.0 Å x 4.7 Å.

can see that the pattern of interpenetration in the present crystal should define channels along the **a** and **b** axes. In Figure 63, channels defined by the diamondoid networks are shown. Two adjacent channels constructed from four hydrogen-bonded tectons **XVIII** are shown in Figure 64. In Figures 65 and 66, an individual four-sided channel constructed with two hydrogen-bonded tectons **XVIII** is presented in both cylinder-ball and space-filling stereoview with diameter 6.0 Å x 4.7 Å.

CHAPTER 6

CONCLUSIONS

In general, the prediction of the detailed crystal structures of unknown materials is currently extremely difficult or even impossible. However, the phenomena observed during the course of our work indicate that the strategy of molecular tectonics is an effective method for building solids with a high degree of predictability. Specifically, tectons that incorporate four tetrahedrally oriented 2-pyridone subunits have a strong tendency to self-associate by using intermolecular hydrogen bonding to generate diamondoid networks with large cavities. To avoid the severe hollowness defined by the network, independent diamondoid networks interpenetrate each other to various degrees, and channels defined by the networks are filled with enclathrated guest molecules.

Ermer and co-workers[13] tried several ways to lower the degree of interpenetration in the packing of tectons derived from 1,3,5,7-adamantanetetracarboxylic acid and related molecules in order to obtain novel types of solid host-guest inclusion compounds with more voluminous cavities. Their efforts and our own efforts to create tectons able to construct diamondoid networks with much larger chambers have not been notably successful. In part, this might be because too high degrees of interpenetration cause strain which disfavors crystallization of large diamondoid networks. To avoid this problem, we

designed and synthesized tecton **XVII** with an angular geometry and found that it crystallizes to form a three-dimensional hydrogen-bonded network not based on diamond but with channels whose diameters are nanosized (14 Å x 4 Å). In this case, despite the elongated intertectonic distance (23 Å), interpenetration is avoided in the crystal packing and increased porosity in the solid state of tectons is achieved. From this important achievement we can deduce that ingeniously designed tectons may give chemist innumerable ways to build ordered three-dimensional hydrogen-bonded networks with chambers of various sizes and shapes.

To introduce functional groups into tectons, we designed and synthesized tetrapyridines **78a-b**. Unfortunately, we were not able to find a method for deprotecting compounds **78a-b** and converting them into tecton **VI**. This is an important area for further work in the field of molecular tectonics, since the functional groups introduced could not only endow tectons with specific physical and chemical properties, but also assist predisposed 2-pyridone subunits to construct much more durable three-dimensional networks with larger cavities.

To amplify intertectonic adhesion, we designed and synthesized a series of tetrakis(dipyridine) compounds **44**, **50** and **57**. Our most important achievement is that we finally obtained tetrakis(dipyridine) **57** which may lead to tecton **IV** after a more careful and intensive investigation of methods of deprotection is completed. We believe that tectons with the geometry and adhesive properties of tecton **IV** should be able to self-associate by intermolecular hydrogen bonding to create novel solid organic materials which are porous, robust, and functional enough to be used in the fields of the design of new catalysts, new separating materials, and even new optical and electronic materials.

From our observations, we can conclude that clever application of the strategy of molecular tectonics can be employed as a routine crystal-engineering method to build a wide range of ordered three-dimensional organic networks with specific physical and chemical properties.

CHAPTER 7

EXPERIMENTAL SECTION

General

Melting points (**mp**) were determined on a Thomas-Hoover capillary melting point apparatus. All melting points are uncorrected.

Infrared (**IR**) spectra were obtained on a Perkin Elmer 1600 FTIR spectrophotometer. The infrared spectra for solids were recorded either as KBr pellets or as a film made by the evaporation of a concentrated solution in chloroform between sodium chloride plates.

Nuclear magnetic resonance (**NMR**) spectra for both ^{1}H and ^{13}C were recorded on Varian VXR-300 (300 MHz) or Bruker AMX-300 (300 MHz), or Bruker AMR-400 (400 MHz) spectrometers. Chemical shifts are reported in parts per million (δ scale) relative to tetramethylsilane (TMS). The coupling constants (J) are expressed in Hertz (Hz). The abbreviations used for the description of multiplicities of the peaks are as follow: (s)-- singlet; (d)-- doublet; (t)-- triplet; (q)-- quartet; (dd)-- doublet of doublets; (dt)-- doublet of triplets; (m)-- multiplet. All chemical shifts are measured at the center of the peak and unresolved multiples are given as a range.

High resolution mass spectra (**HRMS**) were obtained on an AEIMS-902 Kratos MS-50 TCSA (electron impact and FAB) mass spectrometer.

Tetrahydrofuran (THF) was freshly distilled from the sodium ketyl of benzophenone. Triethylamine was distilled from calcium hydride and was stored over KOH under an atmosphere of dry nitrogen. Dichloromethane was freshly distilled from calcium hydride. In all cases, the distillation was carried out under an atmosphere of nitrogen, and the solvents were refluxed with drying agents at least overnight before distillation. Tetrakis(triphenylphosphine)palladium (0) was prepared as described by Coulson[45]. It was stored in the dark under an atmosphere of dry nitrogen. All other reagents and solvents were reagent grade and were used without further purification.

Flash chromatography was accomplished according to the literature[46] procedure using Kieselgel 60 (230-400 mesh) silica gel (E. Merch).

Preparation of bis(triphenylphosphine)palladium dichloride.

To a solution of potassium chloride (2.7 g, 36 mmol) in 200 ml of water was added palladium dichloride (3.0 g, 17 mmol) to form a dark brown suspension. It was heated to 70-80°C to provide a clear solution. After stirring was continued at this temperature for 30 min, the solution was cooled to room temperature and then was poured into 700 ml of ethanol. K_2PdCl_2 was obtained as a olive precipitate. It was separated from the solution by centrifugation and dried in vacuo.

To a solution of triphenylphosphine (6.4 g, 24 mmol) in 200 ml of ethanol at 80°C was added K_2PdCl_2 (2.7 g, 8.2 mmol) to give rise to an olive suspension. After stirring was continued at 80°C for 3 hr, the mixture was cooled to room temperature and then was filtered to give crude product as a olive solid. It was washed with water, ethanol and pentane and dried in vacuo. The dry crude product was dissolved in about 250 ml of hot chloroform to form an olive brown solution. The resulting solution was filtered to afford a clear orange solution. On cooling, nice needle-like orange crystals separated out from

solution. Finally, bis(triphenylphosphine)palladium dichloride was provided as orange crystals in 83% yield.

Preparation of tetrakis(4-iodophenyl)methane (30)

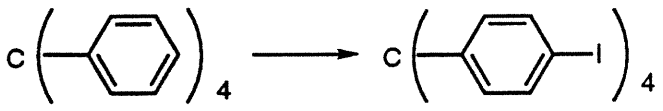

30

A suspension of tetraphenylmethane[17] (4.02 g, 12.5 mmol), iodobenzene bis(trifluoroacetate)[18] (14.4 g, 33.5 mmol), and iodine (6.36 g, 25.0 mmol) in 90 ml of CCl_4 was stirred at 50-60°C until the color of iodine disappeared. CCl_4 was removed by rotary evaporation. The residue was washed with ethanol and acetone and purified by recrystallization from THF to yield 6.43 g (63%) of compound **30** as a white crystalline solid.

mp	did not melt below 355°C
^{1}H NMR	($CDCl_3$) δ 7.58 (8H, d, J=8.6 Hz), 6.88 (8H, d, J=8.6 Hz)
^{13}C NMR	(THF-d_8) δ 143.23, 135.54, 131.14, 90.52, 62.54
IR (KBr)	3055 (w), 1565(w), 1475 (s), 800(s)
MS (EI)	m/z 824 (M^+), 697, 621, 239
Analysis	Calcd for $C_{25}H_{16}I_4$: C, 36.44; H, 1.96. Found: C, 36.41; H, 2.27

Preparation of 2,2',2'',2'''-[methanetetrayltetrakis(4,1-phenylene-2,1-ethynediyl)]tetrakis[6-(phenylmethoxy)pyridine] (31)

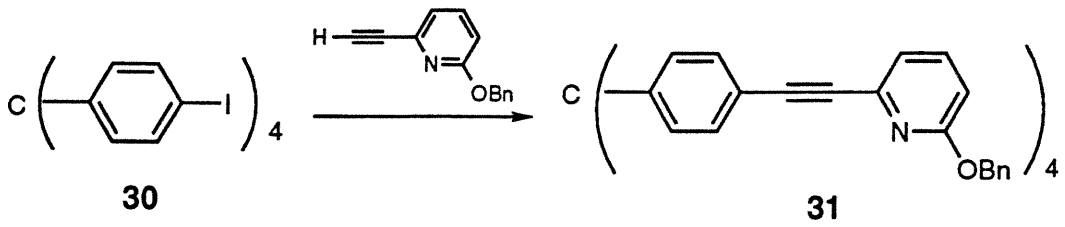

30 **31**

General Procedure I

To a suspension of tetrakis(4-iodophenyl)methane (**30**, 0.76 g, 0.93 mmol), bis(triphenylphosphine) palladium dichloride (0.11 g, 0.15 mmol), and copper iodide (54 mg, 0.28 mmol) in 8 ml of dry triethylamine was added a solution of 6-ethynyl-2-(phenylmethoxy)pyridine[10g] (1.0 g, 4.8 mmol) in 24 ml dry THF. The resulting mixture was refluxed overnight. The solvents were removed by rotary evaporation. The residue was diluted with 60 ml of chloroform, and the organic phase was washed with water and brine, dried over anhydrous magnesium sulfate, filtered, and evaporated to dryness in vacuo. The resulting residue was purified by flash chromatography on silica gel using a gradient of hexane and ethyl acetate as eluent, followed by rinsing with a mixed solvent of hexane and chloroform, to afford tetrapyridine **31** in 44% yield (0.47 g) as a white solid. The sample submitted for analysis was crystallized from chloroform and hexane as pale yellow crystals.

mp 144-146°C

^{1}H NMR ($CDCl_3$) δ 7.57 (4H, dd, J=7.3 and 8.4 Hz), 7.54 (8H, d, J=8.6 Hz), 7.5-7.3 (20H, m), 7.22 (8H, d, J=8.6 Hz), 7.16 (4H, dd, J=0.8 and 7.3 Hz), 6.78 (4H, dd, J=0.8 and 8.4 Hz), 5.42 (8H, s)

^{13}C NMR ($CDCl_3$) δ 163.32, 146.23, 140.08, 138.59, 137.01, 131.50, 130.83, 128.42, 128.18, 127.86, 120.95, 120.61, 111.41, 89.24, 88.11, 67.87, 64.95

IR (KBr) 2200 (w),1590 (s) 1570 (s), 1500 (m) 1440 (s), 1250 (s), 1015 (m)

MS (FAB) m/z 1149 (M^+)

Analysis Calcd for $C_{81}H_{56}N_4O_4$•0.5 $CHCl_3$: C, 80.96; H, 4.71. Found: C, 79.86; H, 5.06

Preparation of 6,6',6'',6'''-[methanetetrayltetrakis(4,1-phenylene-2,1-ethynediyl)]tetrakis[2(1H)-pyridinone] (tecton I)

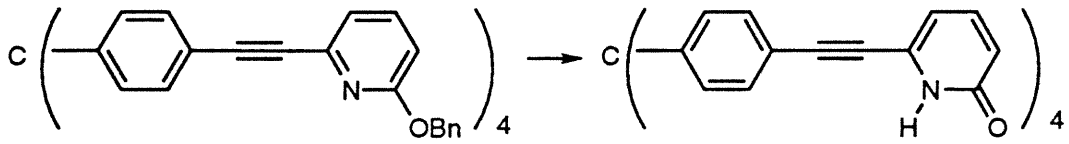

31 **Tecton I**

General Procedure II

A solution of tetrapyridine **31** (0.47 g, 4.1 mmol) in 17 ml of trifluoroacetic acid was heated at 60°C for about 6 hours. TFA was removed by rotary evaporation. The resulting residue was freed of traces of TFA by three treatments with benzene, each suspension being evaporated under vacuum. After the residue was rinsed with triethylamine, filtered and washed with acetone, tecton **I** was obtained in quantitative yield (0.33 g) as a pale yellow solid.

mp did not melt below 330°C

^{1}H NMR (DMSO-d_6) δ 11.96 (4H, s), 7.58 (8H, d, J=8.4 Hz), 7.46 (4H, dd, J=6.9 and 9.0 Hz), 7.25 (8H, d, J=8.4 Hz), 6.58 (4H, d, J=6.9 Hz) 6.45 (4H, d, J=9.0 Hz)

^{13}C NMR (DMSO-d_6) δ 162.59, 146.63, 140.41, 131.66, 130.87, 130.30, 119.80, 119.18, 111.93, 91.78, 84.29, 64.81

IR (KBr) 2200 (w), 1650(s), 1590(s)

MS (FAB) m/z 789 (M+1)

Analysis Calcd for $C_{53}H_{32}N_4O_4$: C, 80.69; H, 4.10. Found: C, 79.56; H, 3.45

Preparation of 3,3',3'',3'''-[methanetetrayltetrakis(4,1-phenylene-2,1-ethynediyl)]tetrakis[2-(phenylmethoxyl)pyridine] (82)

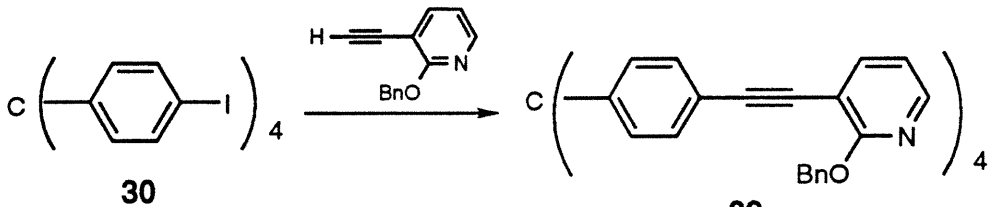

Tetrapyridine **82** was synthesized by the coupling reaction of tetrakis(4-iodophenyl)methane (**30**) and 3-ethynyl-2-(phenylmethoxy)pyridine[10g] according to general procedure I. It was obtained as a white solid in the yield of 42%. Crystallization of it from a mixed solvent of hexane and chloroform gave pale yellow needle-shaped crystals.

mp 158.5°-160°C

^{1}H NMR ($CDCl_3$) δ 8.13 (4H, dd, J=1.9 and 5.0 Hz), 7.77 (4H, dd, J=1.9 and 7.4 Hz), 7.45 (8H, d, J=8.4 Hz), 7.41-7.27 (20H, m), 7.20 (8H, d, J=8.4), 6.90 (4H, dd, J=5.0 and 7.4 Hz), 5.50 (8H, s)

^{13}C NMR ($CDCl_3$) δ 163.38, 146.53, 146.31, 141.71, 137.63, 131.42, 131.16, 128.64, 127.87, 127.52, 121.57, 116.89, 108.00, 94.77, 84.91, 67.96, 65.20

IR (KBr) 3031 (w), 2944 (w), 2218 (w), 1570 (s), 1428 (s), 1230 (s), 1018 (m)

MS (FAB) m/z 1149 (M^+)

Analysis Calcd for $C_{81}H_{56}N_4O_4 \cdot 0.5\ CHCl_3$: C, 80.96; H, 4.71. Found: C, 80.33; H, 4.91

Preparation of 3,3',3'',3'''-[methanetetrayltetrakis(4,1-phenylene-2,1-ethynediyl)]tetrakis[2(1H)-pyridinone] (tecton VIII)

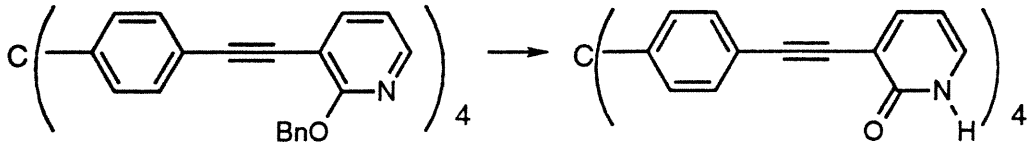

82 **Tecton VIII**

General Procedure III

To a solution of tetrapyridine **82** (0.12 g, 0.10 mmol) in 6 ml of dry dichloromethane was added 80 ml of iodotrimethylsilane (0.11 g, 0.55 mmol). The resulting solution was stirred at room temperature overnight. The reaction mixture was poured into 20 ml of methanol, filtered, washed with methanol, chloroform, and acetone sequentially, and dried in vacuo. Tecton **VIII** was provided quantitatively as a light yellow solid (78 mg).

mp 239.5-241°C

^{1}H NMR (DMSO-d_6) δ 12.02 (4H, s), 7.72 (4H, dd, J=2.3 and 6.9 Hz), 7.47 (8H, d, J=8.6 Hz), 7.46 (2H, dd, J=2.3 and 5.9 Hz), 7.16 (8H, d, J=8.6 Hz), 6.22 (4H, t, J=6.9 Hz)

^{13}C NMR (DMSO-d_6) δ 162.08, 146.54, 145.37, 137.30, 131.85, 131.60, 121.69, 115.27, 106.03, 93.64, 87.75, 65.28

IR (KBr) 3150(m), 2203 (w), 1642 (s) 1605(s), 1550 (s), 1500 (s), 1474 (m)

HRMS (FAB) calcd for $C_{53}H_{33}N_4O_4$ (M+1) 789.2502, found 789.2567

MS (FAB) m/z 789 (M+1)

Preparation of 5,5',5'',5'''-[methanetetrayltetrakis(4,1-phenylene-2,1-ethynediyl)]tetrakis[2-(phenylmethoxy)pyridine] (84)

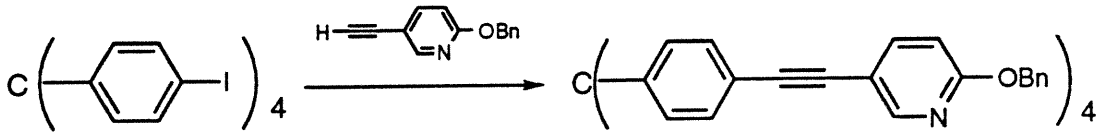

30 **84**

Tetrapyridine **84** was made by the coupling reaction of tetrakis(4-iodophenyl)methane and 5-ethynyl-2-(phenylmethoxy)pyridine[10h] according to general procedure I in 50% yield as a light yellow solid. Crystallization of it from a mixed solvent of hexane and chloroform provided tetrapyridine **84** as yellow needle-like crystals.

mp 219-221°C

^{1}H NMR ($CDCl_3$) δ 8.36 (4H, d, J=2.3 Hz), 7.70 (4H, dd, J=2.3 and 8.6 Hz), 7.5-7.3 (28H, m), 7.21 (8H, d, J=8.4 Hz), 6.80 (4H, d, J=8.6 Hz), 5.41 (8H, s)

^{13}C NMR ($CDCl_3$) δ 162.80, 149.68, 145.87, 141.22, 136.86, 130.98, 130.84, 128.45, 127.99, 127.93, 121.12, 113.20, 111.00, 90.34, 86.68, 67.91, 64.82

IR (KBr) 2217 (w), 1595 (s), 1503 (s), 1483 (s), 1282 (s), 1126 (m), 1019 (m), 825 (s), 733 (m), 696 (m)

MS(FAB) m/z 1149 (M^+)

Analysis Calcd for $C_{81}H_{56}N_4O_4$: C, 84.65; H, 4.91. Found: C, 83.93; H, 5.95

Preparation of 5,5',5'',5'''-[methanetetrayltetrakis(4,1-phenylene-2,1-ethynediyl)]tetrakis[2(1H)-pyridinone] (tecton IX)

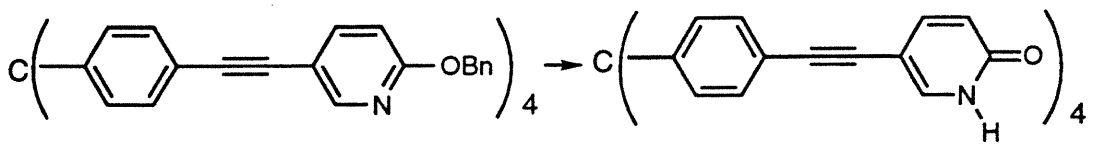

84 **Tecton IX**

Tecton **IX** was prepared by deprotection reaction of tetrapyridine **84** with TMSI according to general procedure III in a yield of 95% as a pale yellow solid.

mp did not melt below 355°C

^{1}H NMR (DMSO-d_6) δ 7.73 (4H, d, J=2.4 Hz), 7.50 (4H, dd, J=2.4 and 9.5 Hz), 7.45 (8H, d, J=8.4 Hz), 7.13 (8H, d, J=8.4 Hz), 6.36 (4H, d, J=9.5 Hz)

^{13}C NMR (DMSO-d_6) δ 161.16, 145.53, 142.60, 139.90, 130.84, 130.65, 120.67, 120.18, 100.30, 88.57, 86.39, 64,37

IR (KBr) 3422 (w, broad),2217 (w), 1655 (s), 1611 (s), 1542 (m), 1501 (m), 1425 (m), 1249 (m), 1132 (m), 837 (m)

HRMS (FAB) cald for $C_{53}H_{33}N_4O_4$ 789.2502, found 789.2534

MS (FAB) m/z 789 (M+1)

Preparation of 5,5',5'',5'''-[methanetetrayltetrakis(4,1-phenylene)]-tetrakis[2-(phenylmethoxy)pyridine] (105)

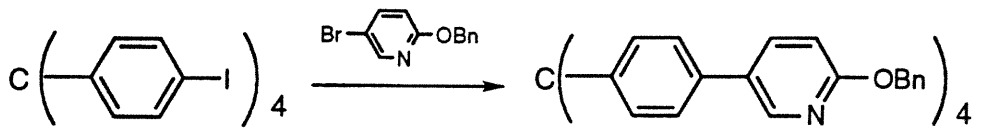

30 **105**

General Procedure IV

To a solution of 5-bromo-2-(phenylmethoxy)pyridine[10h] (1.7 g, 6.3 mmol) in dry THF (30 ml) was added 4.8 ml butyllithium (1.36 M in hexane) dropwise at -100°C. The resulting suspension was stirred at -100°C for 30 min., and was then treated with a solution of zinc chloride (0.88 g, 6.5 mmol) in dry THF (10 ml). It was warmed up to room temperature and maintained at this temperature for 1 hour. The resulting suspension was transferred to a flask which was charged with tetrakis(4-iodophenyl)methane (0.87 g, 1.1 mmol) and bis(triphenylphosphine)palladium dichloride (0.14 g, 0.20 mmol). The mixture was refluxed overnight. It was diluted with benzene, washed with 5% aqueous sodium bicarbonate solution and water, dried over anhydrous magnesium sulfate and filtered. Evaporation in vacuo gave a dark oil which was purified by flash chromatography on silica gel with hexane, ethyl acetate, and chloroform (80:10:10) as eluents and then rinsed with a mixed solvent of hexane and ethyl acetate to afford tetrapyridine **105** in 25% yield (0.27 g) as a light yellow solid. Crystallization of it from a mixed solvent of hexane and chloroform gave yellow needle-shaped crystals.

mp 218.5-220°C

^{1}H NMR ($CDCl_3$) δ 8.44 (4H, d, J=2.5 Hz), 7.84 (4H, dd, J=2.5 and 8.6 Hz), 7.52-7.30 (36H, m), 6.89 (4H, d, J=8.6 Hz), 5.43 (8H, s)

^{13}C NMR ($CDCl_3$) δ 162.51, 145.12, 144.12, 136.90, 136.65, 134.95, 131.09, 129.08, 127.95, 127.44, 127.36, 125.30, 110.71, 67.32, 63.59

IR (KBr) 1658 (s), 1600 (s), 1508 (m), 1428 (m), 1224 (m), 819 (s)

HRMS (FAB) calcd for $C_{73}H_{57}Br_2N_4O_4$ (M+1) 1053.4380, found 1053.4312

MS (FAB) m/z 1053 (M+1)

Analysis Calcd for $C_{73}H_{56}N_4O_4$: C, 83.25; H, 5.36. Found: C, 82.38; H, 5.57

Preparation of 5,5',5'',5'''-[methanetetrayltetrakis(4,1-phenylene)]-tetrakis[2(1H)-pyridinone] (tecton XIX)

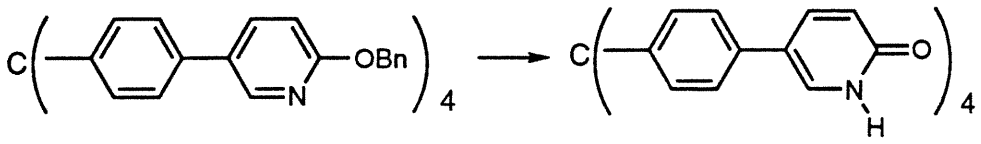

105 **Tecton XIX**

Tecton **XIX** was prepared by the deprotection of tetrapyridine **105** in TFA according to general procedure II in a yield of 95% as a light yellow solid.

mp did not melt below 355°C

^{1}H NMR (DMSO-d_6) δ 11.81 (4H, s), 7.82 (4H, d, J=9.6 Hz), 7.70 (4H, s), 7.52 (8H, d, J=8.0 Hz), 7.21 (8H, d, J=8.0 Hz), 6.41 (4H, d, J=9.6 Hz)

^{13}C NMR (DMSO-d_6) δ 161.83, 144.72, 139.91, 133.85, 132.84, 130.95, 124.67, 120.16, 117.22, 64.32

IR (KBr) 1658 (s), 1600 (s), 1508 (s), 1428 (s), 1224 (m), 1011 (m), 819 (s)

HRMS (FAB) calcd for $C_{45}H_{33}N_4O_4$ (M+1) 693.2502, found 693.2470

Preparation of 3,3',3'',3'''-[methanetetrayltetrakis(4,1-phenylene)]-tetrakis[2-(phenylmethoxy)pyridine] (104)

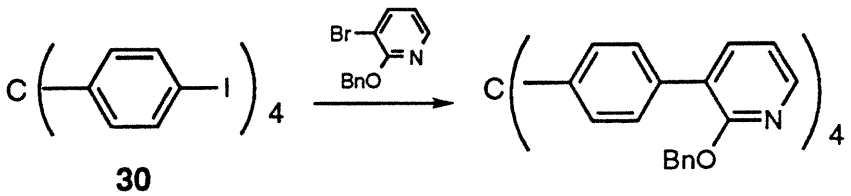

Tetrapyridine **104** was made by the coupling reaction of tetrakis(4-iodophenyl)methane and 3-bromo-2-(phenylmethoxy)pyridine[10g] according to general procedure IV in a yield of 58% as a white solid. Crystallization of it from a mixed solvent of hexane and chloroform gave white needles.

mp did not melt below 355°C

^{1}H NMR ($CDCl_3$) δ 8.17 (4H, dd, J=1.9 and 5.0 Hz), 7.76 (4H, dd, J=1.9 and 7.4 Hz), 7.57 (8H, d, J=8.6 Hz), 7.43 (8H, d, J=8.6 Hz), 7.4-7.1 (20H, m), 7.01 (4H, dd, J=5.0 and 7.4 Hz), 5.49 (8H, s)

^{13}C NMR ($CDCl_3$) δ 160.17, 145.82, 145.52, 138.52, 137.52, 134.10, 130.80, 128.36, 128.15, 127.22, 126.97, 124.23, 117.29, 67.28, 64.35

IR (KBr) 1579 (s), 1497 (m), 1446 (m), 1431 (m), 1246 (s), 1001 (s), 792 (s), 732 (s), 696 (s)

HRMS (FAB) calcd for $C_{73}H_{57}Br_2N_4O_4$ (M+1) 1053.4380, found 1053.4323

MS (FAB) m/z 1053 (M+1)

Preparation of 3,3',3'',3'''-[methanetetrayltetrakis(4,1-phenylene)]-tetrakis[2(1H)-pyridinone] (tecton XVIII)

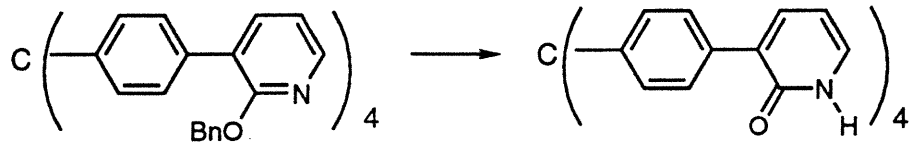

104 **Tecton XV**

Tecton **XVIII** was made by deprotection of tetrapyridine **104** in TFA according to general procedure II in quantitative yield as a white solid.

mp did not melt below 355°C

^{1}H NMR (DMSO-d_6) δ 11.78 (4H, s), 7.68 (8H, d, J=8.6 Hz), 7.65 (4H, d, J=2.1 Hz), 7.36 (4H, d, J=5.1 Hz), 7.28 (8H, d, J=8.6 Hz), 6.26 (4H, t, J=6.7 Hz)

^{13}C NMR (DMSO-d_6) δ 161.32, 145.51, 138.74, 134.72, 134.42, 129.99, 129.50, 127.68, 105.50, 64.05

IR 1638(s), 1607 (s), 1556 (m), 1504 (m), 1460 (m), 1425 (m), 1238 (m), 1002 (m), 828 (m), 764 (m)

HRMS (FAB) calcd for $C_{45}H_{33}N_4O_4$ (M+1) 693.2502, found 693.2457

Preparation of tetrakis[4-(2-trimethylsilylethynyl)phenyl]methane (45)

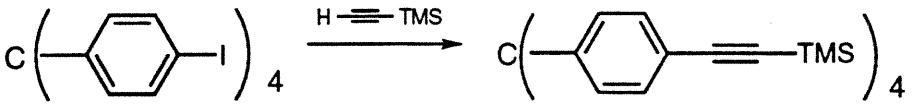

30 **45**

To a suspension of tetrakis(4-iodophenyl)methane (0.54 g, 0.65 mmol), bis(triphenylphosphine)palladium dichloride (64 mg, 0.091 mmol), and copper iodide (56 mg, 0.29 mmol) in 12 ml of dry triethylamine was added 0.75 ml of trimethylsilylacetylene

(0.51 g, 5.2 mmol). The resulting mixture was heated at 60° for 6 hours. After triethylamine was removed by rotary evaporation, the residue was extracted with hot benzene. The filtrate was concentrated under reduced pressure, and the residue was washed sequentially with ethanol (50 ml) and hot ethanol (30 ml) to afford a white solid in 97% yield (0.45 g). Compound **45** was crystallized from a mixed solvent of chloroform and hexane as white needle-like crystals.

mp	did not melt below 330°C
^{1}H NMR	($CDCl_3$) δ 7.33 (d, 8H, J=8.5 Hz), 7.04 (d, 8H, J=8.5 Hz), 0.23 (s, 36H)
^{13}C NMR	($CDCl_3$) δ 145.86, 131.24, 130.59, 121.08, 104.47, 94.63, 64.63, 0.09
IR (KBr)	2957 (m), 2161 (s), 1496 (s), 1406 (m), 1249 (s), 864 (s)
MS (FAB)	m/z 705 (M+1)

Preparation of tetrakis(4-ethynylphenyl)methane (46)

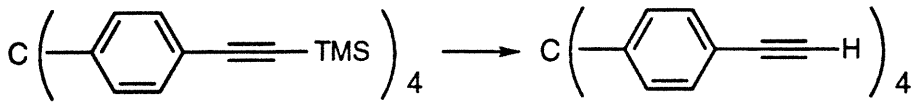

45 **46**

To a solution of tetrakis[4-(2-trimethylsilylethynyl)phenyl]methane (0.94 g, 1.3 mmol) in 20 ml of dichloromethane was added 10.ml of tetrabutylammonium fluoride in THF (1.0 M). After being stirred at room temperature for 30 min., the mixture was treated with 15 ml of methanol and 15 ml of 1 N KOH aqueous solution and stirred at room temperature for another 40 min. The reaction mixture was treated with 7 ml of 3 N HCl aqueous solution and concentrated under reduced pressure. The residue was diluted with 20 ml of water, neutralized with solid K_2CO_3, and extracted with dichloromethane. The extracts were dried over anhydrous $MgSO_4$, filtered, and evaporated to dryness. The

resulting light brown solid was further purified by chromatography on silica gel with hexane and ethyl acetate as eluents. Tetraphenylacetylene **46** was afforded in 84% (0.47 g) as a white solid.

mp	darkened above 260°C, but did not melt bellow 300°C
^{1}H NMR	($CDCl_3$) δ 7.39 (8H, d, J=8.6 Hz), 7.12 (8H, d, J=8.6 Hz), 3.07 (4H, s)
^{13}C NMR	($CDCl_3$) δ 146.12, 131.59, 130.67, 120.19, 83.10, 77.61, 64.72
IR (KBr)	3285 (s), 3025 (w), 2105(m), 1605 (w), 1500 (s), 825 (s)
MS (EI)	m/z 416 (M^+), 315, 213

Preparation of tetrakis[4-(2-iodoethynyl)phenyl]methane (86)

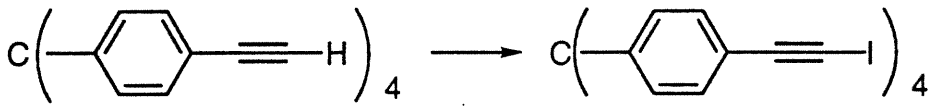

46 **86**

To a solution of 0.31 g tetrakis(4-ethynylphenyl)methane (0.31 g, 0.73 mmol) in 50 ml of dry THF was added 3.2 ml of butyllithium in hexane (1.0 M) at -70°C. The mixture was maintained at this temperature for 3.5 hours, then warmed up to -60°C and treated with iodine (0.99 g, 3.9 mmol) and stirred at this temperature for 2 hours. It was treated with 50 ml of 10% aqueous sodium persulfate solution and extracted with dichloromethane. The extracts were dried over anhydrous $MgSO_4$, filtered, and evaporated to dryness in vacuo. The resulting residue was purified by a short dry column with hexane and ethyl acetate (80:20) as eluents and recrystallized from THF to afford iodoacetylene **86** in 48% yield (0.32 g) as a very light yellow crystalline solid.

^{1}H NMR ($CDCl_3$) δ 7.32 (d, 8H, J=8.4 Hz), 7.07 (d, 8H, J=8.4 Hz)

IR 3025(w), 2255 (w), 1495(s), 1015(m), 825(s)

Preparation of 6-(cis-4-methoxy-3-buten-1-ynyl)-2-(phenylmethoxy)-pyridine (87).

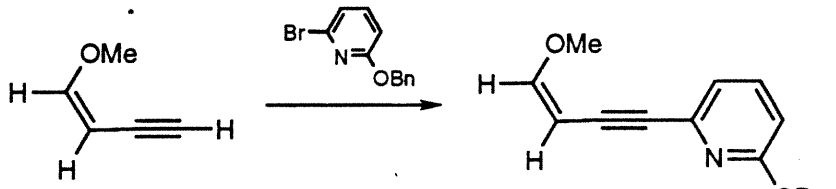

87

General Procedure V

In a 25 ml flask was placed 6-bromo-2-(phenylmethoxy)pyridine[10g] (0.61 g, 2.3 mmol), cis-1-methoxy-1-buten-3-yne (0.27 g, 3.3 mmol), bis(triphenylphosphine)-palladium dichloride (34 mg, 0.048 mmol), and copper iodide (12 mg, 0.063 mmol) and 10 ml dry triethylamine. The mixture was stirred at 70°C overnight. The reaction mixture was quenched with 25 ml of water and extracted with ether. The ether extracts were dried over anhydrous calcium chloride and potassium carbonate and were then evaporated to dryness. The resulting crude compound was purified by chromatography on silica gel, being eluted with hexane and ethyl acetate (85:15 and 80:20). Compound **87** was provided in 79% yield (0.49 g) as a yellow oil. Its proton NMR spectrum was taken immediately without further purification.

^{1}H NMR ($CDCl_3$) δ 7.51 (1H, dd, J=7.3 and 8.3 Hz), 7.5-7.3 (5H, m), 7.08 (1H, dd, J=0.68 and 7.3 Hz), 6.72 (1H, dd, J=0.68 and 8.3 Hz), 6.40 (1H, d, J=6.5 Hz), 5.39 (2H, s), 4.78 (1H, d, 6.5 Hz), 3.85 (3H, s)

Preparation of 2,2',2'',2'''-[methanetetrayltetrakis(4,1-phenylene-4,1-butadiynediyl)]tetrakis[6-(phenylmethoxy)pyridine] (85).

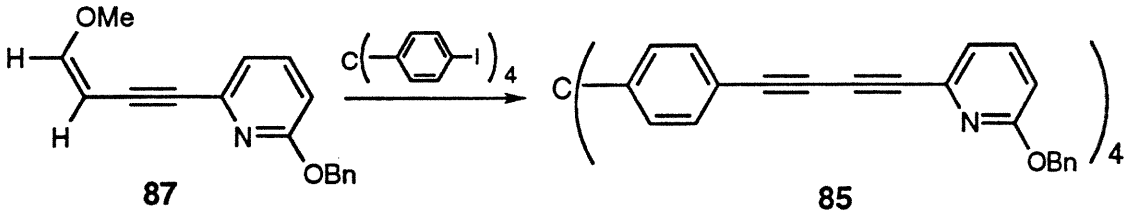

To a solution of freshly made compound **87** (2.4 g, 8.9 mmol) in 50 ml of dry THF was added a freshly made solution of LDA (18 mmol, 0.88M) in THF at -50°C. After being stirred at -50°C for 2 hours, the resulting mixture was treated with a solution of zinc chloride (1.2 g, 8.9 mmol) in 15 ml of dry THF at -40°C, warmed up to room temperature and maintained at that temperature for an hour. Then it was transferred into a 200 ml flask which was charged with tetrakis(4-iodophenyl)methane (1.1 g 1.3 mmol) and bis(triphenylphosphine)palladium dichloride (0.20 g, 0.28 mmol). The mixture was heated at a reflux overnight. Volatiles were removed by evaporation, and the crude product was purified by flash chromatography on silica gel with hexane and ethyl acetate (80:20) as eluent to afford tetrapyridine **85** in 46% (0.77 g) as a brown solid. A light brown solid was obtained after further purification on a preparative TLC plate (2mm thickness). A fine light brown precipitate was afford when tetrapyridine **85** was crystallized from a mixed solvent of chloroform and hexane.

mp No sharp melting point was observed

^{1}H NMR ($CDCl_3$) δ 7.56 (4H, dd, J=7.0 and 8.3 Hz), 7.5-7.3 (28H, m), 7.18 (8H, d, J=8.6 Hz), 7.14 (4H, d, J=7.0 Hz), 6.82 (4H, d, J=8.3 Hz), 5.40 (8H, s)

^{13}C NMR ($CDCl_3$) δ 163.34, 146.54, 138.80, 138.58, 136.88, 132.30, 130.76, 128.43, 128.15, 127.90, 122.00, 119.79, 112.56, 81.79, 80.74, 74.30, 73.08, 67.91, 65.15

IR (KBr) 2218 (m), 1584 (s), 1566 (s), 1489 (m), 1441 (s), 1343 (s), 1295 (s), 1260 (s), 1017 (s), 982 (m), 824 (s), 801 (s), 754 (s), 697 (s)

Preparation of 6,6',6'',6'''-[methanetetrayltetrakis(4,1-phenylene-4,1-butadiynediyl)]tetrakis[2(1H)-pyridinone] (XI).

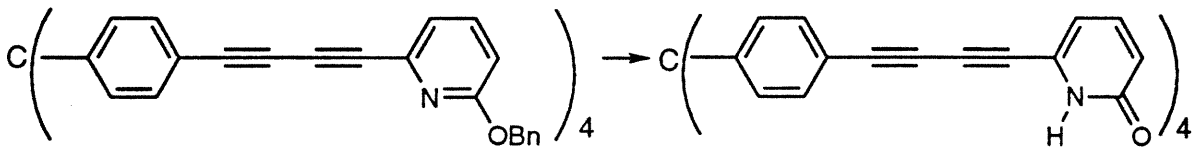

85 **Tecton XI**

Tecton **XI** was made by deprotection of compound **85** in TFA according to general procedure II in a yield of 79% as a brown solid.

mp did not melt below 330°C

^{1}H NMR ($DMSO\text{-}d_6$) δ 11.91 (4H, s), 7.62 (8H, d, J=8.4 Hz), 7.47 (4H, dd, J=6.6 and 8.9 Hz), 7.25 (8H, d, J=8.4 Hz), 6.74 (4H, d, J=6.6 Hz), 6.53 (4H, d, J=8.9 Hz)

^{13}C NMR ($DMSO\text{-}d_6$) δ 163.26, 147.96, 141.03, 133.57, 131.61, 130.15, 121.74, 118.88, 119.65, 84.41, 77.11, 76.72, 74.00, 65.93

IR (KBr) 2210 (m), 1648 (s), 1597 (s), 1542 (m), 1498 (m), 1449 (m), 1156 (m), 1016 (m), 987 (m), 823 (m), 800 (m), 715 (w)

MS (FAB) m/z 391, 307, 289, 154, 136

Preparation of 6-(4-bromophenyl)ethynyl-2-(phenylmethoxy)pyridine (92a)

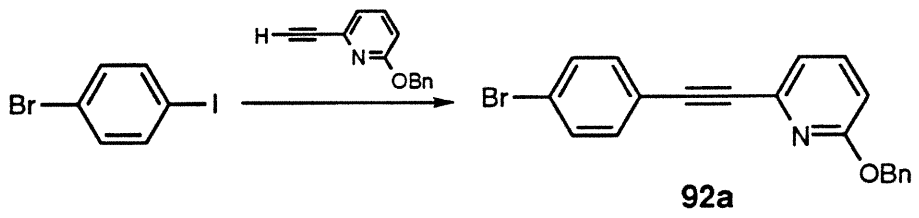

92a

Compound **92a** was made by the coupling reaction of 1-bromo-4-iodobenzene and 6-ethynyl-2-(phenylmethoxy)pyridine[10d] in general procedure V in 75% yield as a white crystalline solid. It was crystallized from a mixed solvent of chloroform and hexane as fine needle-shaped crystals.

mp 117-118°C

^{1}H NMR ($CDCl_3$) δ 7.58 (1H, dd, J=7.3 and 8.4 Hz), 7.54-7.34 (9H, m), 7.17 (1H, dd, J=0.8 and 7.3 Hz), 6.81 (1H, dd, J=0.8 and 8.4 Hz), 5.44 (2H, s)

^{13}C NMR ($CDCl_3$) δ 163.38, 139.88, 138.60, 136.97, 133.35, 131.60, 128.41, 128.12, 127.87, 123.15, 121.37, 120.96, 111.59, 89.77, 87.40, 67.88

IR (KBr) 2216(w), 1562(m), 1488(m), 1437 (s), 1329 (m), 1259 (s), 1026 (m), 806 (s), 731 (m), 694 (m)

HRMS (FAB) calcd for $C_{20}H_{15}BrNO$ (M+1) 364.0337, found 364.0350

MS (FAB) m/z 364 (M+1)

Analysis Calcd for $C_{20}H_{14}BrNO$: C, 65.95; H, 3.87. Found: C, 66.06; H, 3.91

Preparation of 5-(3-bromophenyl)-2-(phenylmethoxy)pyridine (100)

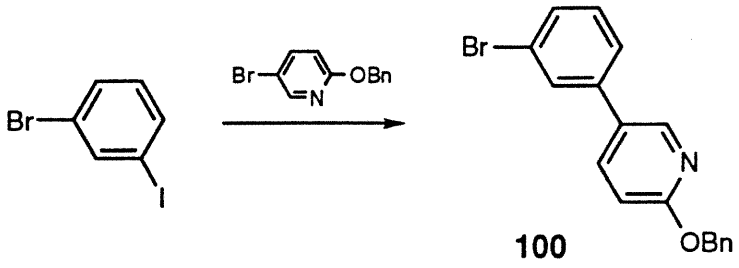

100

General Procedure VI

To a solution of 5-bromo-2-(phenylmethoxy)pyridine[10h] (2.6 g, 9.9 mmol) in dry THF (25 ml) was added 7.0 ml of butyllithium (1.4 M in hexane) at -78°C. The resultant suspension was stirred at -78°C for an hour, followed by treatment with a solution of zinc chloride (1.4 g, 10 mmol) in 10 ml of dry THF. The mixture was warmed up to room temperature and maintained at the temperature for an hour. The resulting solution was transferred to a flask which was charged with 1-bromo-3-iodobenzene (2.4 g, 8.6 mmol) and bis(triphenylphosphine)palladium dichloride (0.35 g, 0.50 mmol). The resulting mixture was refluxed overnight. After being cooled, it was quenched with 50 ml of 5% aqueous sodium bicarbonate solution. Extraction (ethyl ether) and evaporation of the dried (anhydrous magnesium sulfate) extracts gave a residue of orange oil, which was purified by flash chromatography on silica gel with hexane and ethyl acetate as eluents and then further purified by recrystallization from hexane and ether to afford compound **100** in 48% yield as a white crystalline solid.

mp 93-94.5°C

^{1}H NMR ($CDCl_3$) δ 8.38 (1H, d, J=2.0 Hz), 7.78 (1H, dd, J= 2.6 and 8.6 Hz), 7.69 (1H, t, J=2.0 Hz), 7.52-7.27 (8H, m), 6.90 (1H, dd, J=0.50 and 8.6 Hz) 5.45 (2H, s)

^{13}C NMR ($CDCl_3$) δ 163.34, 144.93, 139.96, 137.42, 137.09, 130.40, 130.21, 129.64, 128.83, 128.43, 127.95, 127.85, 125.20, 123.02, 111.28, 67.83

IR (KBr) 1603(s), 1569(m), 1498(s), 1468(m), 1283(s), 1008(s), 783(s), 735(s), 690(s)

HRMS (FAB) calcd for $C_{18}H_{14}BrNO$ (M+2) 341.0387, found 341.0415

MS (FAB) m/z 340 (M+1)

Preparation of 5-(3-iodophenyl)-2-(phenylmethoxy)pyridine (100a)

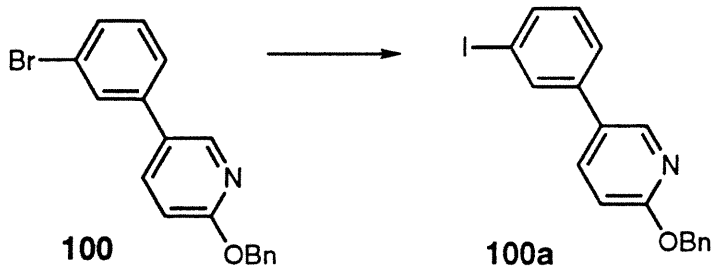

General Procedure VII

To a solution of compound **100** (1.2 g, 3.6 mmol) was added 2.6 ml of butyllithium (1.44 M, in hexane) dropwise at -78°C. After addition the mixture was stirred at -78°C for 1 hour, followed by treatment with solid iodine (0.93 g, 3.7 mmol). The mixture was warmed up to room temperature and stirred at that temperature overnight. The resulting mixture was diluted with 80 ml of ether and washed with 10% aqueous sodium persulfate solution (2x20 ml) and water (20 ml). The ethereal phase was dried over anhydrous magnesium sulfate and then filtered. Removal of solvents gave compound **100a** in a quantitative yield as a light color oil. It was employed without further purification.

^{1}H NMR ($CDCl_3$) δ 8.37 (1H, dd, J=0.6 and 2.6 Hz), 7.89 (1H, t, J=1.7 Hz), 7.77 (1H, dd, J=2.6 and 8.6 Hz), 7.70 (1H, dq, J=1.0, 1.7 and 7.8 Hz), 7.52-7.34 (6H, m), 7.19 (1H, t, J=7.8 Hz), 6.90 (1H, d, J=0.6 and 8.6 Hz), 5.45 (2H, s)

^{13}C NMR ($CDCl_3$) δ 163.29, 144.87, 140.04, 137.43, 137.08, 136.19, 135.60, 130.52, 128.74, 128.43, 127.93, 127.85, 125.84, 111.26, 94.86, 67.64

Preparation of 2-(phenylmethoxy)-5-[3-(trimethylsilylethynyl)phenyl]-pyridine (101)

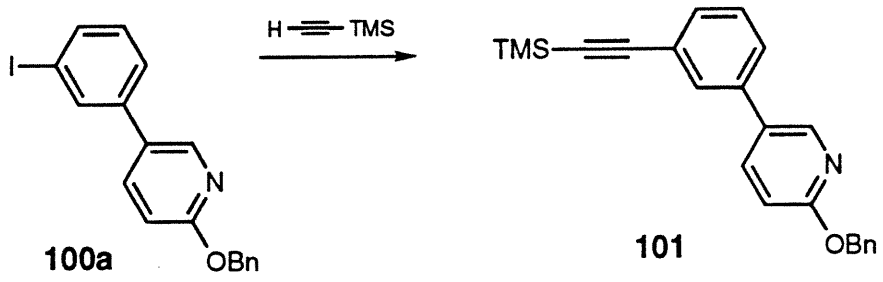

Compound **101** was made by the coupling reaction of compound **100a** and trimethylsilylacetylene according to general procedure V in 85% as a white crystalline solid. Crystallization of compound **101** from methanol gave white needles.

mp 100.5-102.5°C

^{1}H NMR ($CDCl_3$) δ 8.40 (1H, dd, J=0.7 and 2.6 Hz), 7.81 (1H, dd, J=2.6 and 8.6 Hz) 7.66 (1H, t, J=1.7 Hz), 7.52-7.34 (8H, m), 6.89 (1H, dd, J=0.7 and 8.6 Hz), 5.45 (2H, s), 0.29 (9H, s)

^{13}C NMR ($CDCl_3$) δ 163.19, 144.88, 137.92, 137.43, 137.18, 130.69, 130.14, 129.40, 128.81, 128.42, 127.93, 127.82, 126.71, 123.77, 111.15, 104.71, 94.62, 67.76, -0.10

IR (KBr) 2958 (m), 2157 (m), 1604 (s), 1497 (s), 1473 (s), 1421 (m), 1353 (s), 1249 (s), 1013 (m), 887 (s), 843 (s), 696 (s)

HRMS (FAB) calcd for $C_{23}H_{24}NOSi$ (M+1) 358.1627, found 358.1634

MS (FAB) m/z 358 (M+1)

Preparation of 5-(3-ethynylphenyl)-2-(phenylmethoxy)pyridine (102)

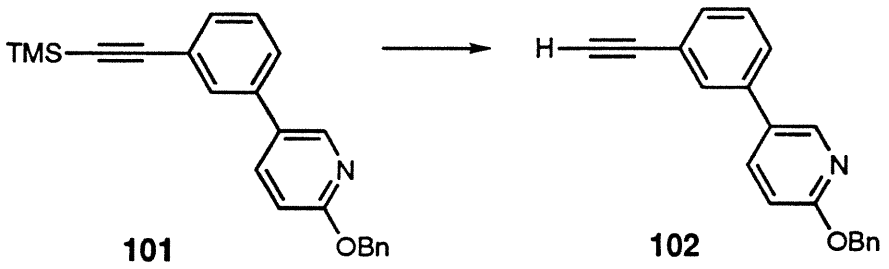

101 102

General Procedure VIII

To a solution of compound **101** (1.0 g, 2.9 mmol) in 6 ml of methanol and 6 ml of dichloromethane was sequentially added 6 ml of a 1 N aqueous solution of potassium hydroxide and tetrabutylammonium bromide (94 mg, 0.29 mmol). The resulting mixture was stirred at room temperature for 1 hour. It was quenched with a 3 N aqueous solution of hydrochloric acid and concentrated under reduced pressure. The residue was diluted with 30 ml of water and made alkaline with solid potassium carbonate. Extraction (diethyl ether) and evaporation of dry (magnesium sulfate) ethereal phases gave compound **102** in a quantitative yield as a light yellow crystalline solid. Crystallization of **102** from a mixed solvent of chloroform and hexane afforded an ivory crystalline solid.

mp 83.5-84.5°C

^{1}H NMR ($CDCl_3$) δ 8.39 (1H, d, J=2.6 Hz), 7.80 (1H, dq, J=1.0, 2.6 and 8.6 Hz), 7.67 (1H, s), 7.53-7.34 (8H, m), 6.90 (1H, d, J=8.6 Hz), 5.44 (2H, s), 3.13 (1H, s)

^{13}C NMR ($CDCl_3$) δ 163.23, 144.88, 138.06, 137.45, 137.15, 130.89, 130.27, 129.21, 128.95, 128.44, 127.94, 127.85, 127.06, 122.79, 111.24, 83.33, 77.55, 67.82

IR (KBr) 3294 (s), 2109 (w), 1604 (s), 1578 (m), 1497 (s), 1473 (s), 1353 (s), 1285 (s), 1248 (s), 1014 (m), 831 (m), 795 (s), 695 (s)

HRMS (FAB) calcd for $C_{20}H_{16}NO$ (M+1) 286.1232, found 286.1242

MS (FAB) m/z 285 (m^+)

Preparation of 5,5',5'',5'''-[methanetetrayltetrakis(4,1-phenylene-2,1-ethynediyl-3,1-phenylene)]tetrakis[2-(phenylmethoxy)pyridine] (103)

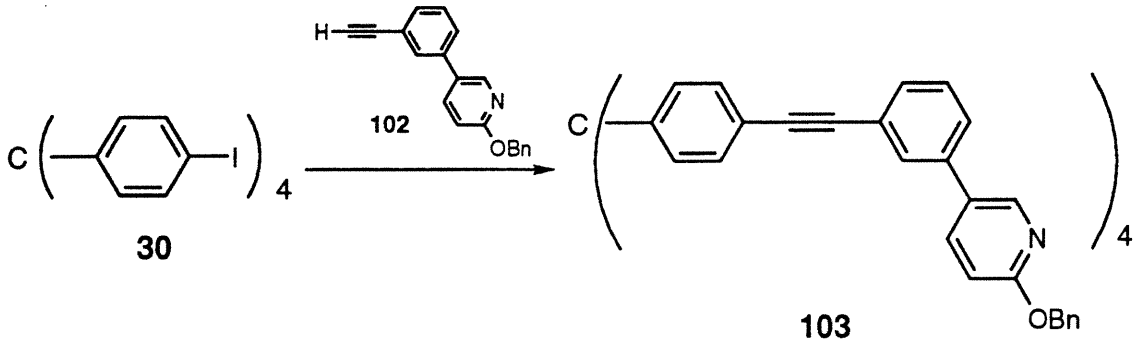

Compound **103** was made by the coupling reaction of tetrakis(4-iodophenyl)methane (**30**) and 5-(3-ethynylphenyl)-2-(phenylmethoxy)pyridine (**102**) according to general procedure I in 87% yield as a pale yellow solid. It was crystallized from a mixed solvent of chloroform and hexane as a very fine pale yellow crystalline solid.

mp 194-196°C

^{1}H NMR ($CDCl_3$) δ 8.42 (4H, d, J=2.5 Hz), 7.83 (4H, dd, J=2.5, 8.6 Hz), 7.71 (4H, s), 7.50 (16H, d, J=8.3 Hz), 7.54-7.28 (28H, m), 7.25 (4H, d, J=8.5 Hz), 6.90 (4H, d, J=8.6 Hz), 5.45 (8H, s)

^{13}C NMR ($CDCl_3$) δ 163.20, 145.93, 144.89, 138.08, 137.44, 137.15, 131.08, 130.85, 130.37, 129.74, 129.42, 128.95, 128.40, 127.90, 127.79, 126.57, 123.82, 121.18, 111.18, 89.51, 89.29, 67.76, 64.85

IR (KBr) 3031 (w), 2222 (w), 1603 (s), 1496 (s), 1473 (s), 1421 (m), 1286 (s), 1245 (m), 1018 (m), 825 (m), 793 (m), 695 (m)

MS (FAB) m/z 1454 (M^+)

Preparation of 5,5',5'',5'''-[methanetetrayltetrakis(4,1-phenylene-2,1-ethynediyl-3,1-phenylene)]tetrakis[2(1H)-pyridone] (tecton XVII)

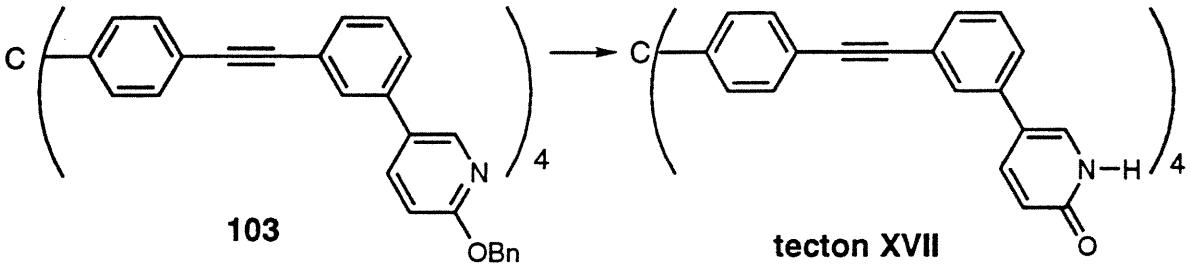

103 **tecton XVII**

Tecton **XVII** was made by the deprotection of tetrapyridine **103** with TMSI according to general procedure III in 90% yield as pale yellow solid. It was crystallized from DMF as pale yellow needle-shaped crystals.

mp did not melt below 355°C

^{1}H NMR ($DMSO-d_6$) δ 7.93 (4H, dd, J=2.5 and 9.5 Hz), 7.86 (4H, d, J=2.5 Hz), 7.75 (4H, s), 7.63-7.60 (4H, m), 7.57 (8H, d, J=8.4 Hz), 7.45 (8H, d, J=4.5 Hz), 7.22 (8H, d, J=8.4 Hz), 6.48 (4H, d, J=9.5 Hz)

^{13}C NMR ($DMSO-d_6$) δ 161.78, 145.95, 140.43, 136.70, 133.61, 131.30, 130.83, 129.83, 129.54, 128.16, 126.23, 122.91, 120.52, 119.77, 117.64, 89.86, 89.18, 64.82

IR (KBr) 3059 (m), 2218 (w), 1659 (s), 1594 (s), 1502 (m), 1420 (m), 1219 (m), 996 (m) 823(s) 793 (m), 693 (m)

MS (FAB) m/z 1093 (M+1)

Preparation of 3-(4-bromophenyl)-2-(phenylmethoxy)pyridine (94a)

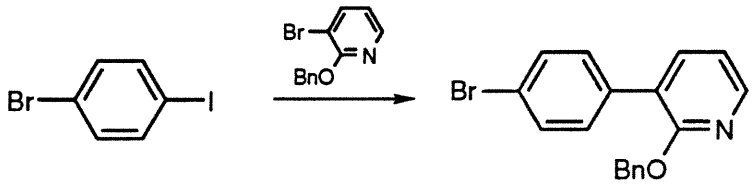

94a

Compound **94a** was synthesized by the coupling reaction of 1-bromo-4-iodobenzene and 3-bromo-2-(phenylmethoxy)pyridine[10d] according to general procedure VI. Recrystallization of the crude product from methanol gave the bromopyridine in 60% yield as a white crystalline solid.

mp 81.5-82.5°C

^{1}H NMR ($CDCl_3$) δ 8.41 (1H, dd, J=1.9 and 5.0 Hz), 7.63 (1H, dd, J=1.9 and 7.3 Hz), 7.54 (2H, d, J=8.6 Hz), 7.47 (2H, d, J=8.6 Hz), 7.4-7.3 (5H, m), 7.01 (1H, dd, J=5.0 and 7.3 Hz), 5.47 (2H, s)

^{13}C NMR ($CDCl_3$) δ 159.88, 145.84, 138.55, 137.19, 135.37, 131.20, 130.72, 128.27, 127.48, 127.28, 123.47, 121.62, 117.31, 67.64

IR (KBr) 1580 (s), 1558 (s), 1496 (m), 1450 (m), 1436 (s), 1359 (s), 1254 (s), 1018 (s), 834 (s), 790 (s), 732 (s), 696 (m)

HRMS (FAB) calcd for $C_{18}H_{15}BrNO$ (M+1) 340.0337, found 340.0309

MS (FAB) m/z 340 (M+1)

Analysis Calcd for $C_{18}H_{14}BrNO$: C, 63.55; H, 4.15. Found: C, 63.63; H, 4.28.

Preparation of 6-(4-bromophenyl)-2-(phenylmethoxy)pyridine (53)

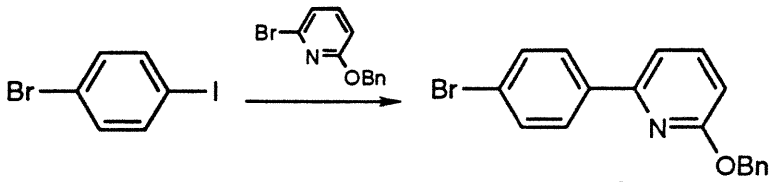

53

Compound **53** was made by the coupling reaction of 1-bromo-4-iodobenzene and 6-bromo-2-(phenylmethoxy)pyridine[10g] according to general procedure VI and crystallized from a mixed solvent of chloroform and hexane in 59% yield as a white crystalline solid.

mp 94.5-96°C

^{1}H NMR ($CDCl_3$) δ 7.91 (2H, d, J=8.6 Hz), 7.65 (1H, t, J=7.4 Hz), 7.59 (2H, d, J=8.6 Hz), 7.54-7.30 (6H, m), 6.78 (1H, d, J=8.2 Hz), 5.51 (2H, s)

^{13}C NMR ($CDCl_3$) δ 163.08, 153.26, 139.28, 137.77, 137.40, 131.58, 128.34, 128.13, 127.91, 127.69, 123.04, 112.72, 109.96, 67.38

IR (KBr) 1594 (s), 1574 (s), 1496 (m), 1445 (s), 1321 (s), 1252 (s), 1010 (m), 841 (m), 803 (s), 757 (s), 698 (s)

HRMS (FAB) calcd for $C_{18}H_{15}BrNO$ (M+1) 340.0337, found 340.0320

MS (FAB) m/z 340 (M+1)

Preparation of 6-(4-iodophenyl)-2-(phenylmethoxy)pyridine (96)

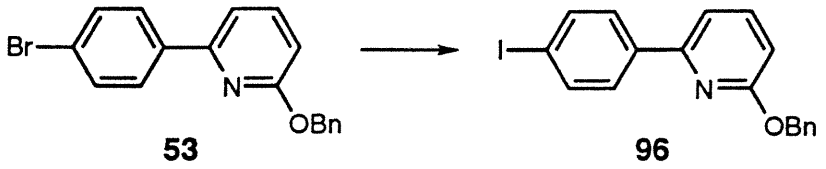

53 96

Compound **96** was made by metallation of aryl bromide **53** followed by treatment with solid iodine according to general procedure VII in quantitative yield as a light colored solid. Compound **96** was used as starting material without further purification.

^{1}H NMR ($CDCl_3$) δ 7.78 (4H, d, J=2.9 Hz), 7.65 (1H, dd, J=7.5 and 8.2 Hz), 7.5-7.3 (5H, m), 7.33 (1H, dd, J=0.7 and 7.5 Hz), 6.78 (1H, d, J=8.2 Hz), 5.50 (2H, s)

^{13}C NMR ($CDCl_3$) δ 163.05, 140.97, 139.25, 137.54, 137.38, 131.56, 128.31, 128.10, 127.89, 127.65, 123.02, 112.69, 109.94, 67.36

IR (KBr) 1585 (s), 1566 (s), 1483 (m), 1445 (s), 1325 (s), 1254 (s), 1015 (s)

Preparation of 2-(phenylmethoxy)-6-[4-(trimethylsilylethynyl)phenyl]-pyridine (97)

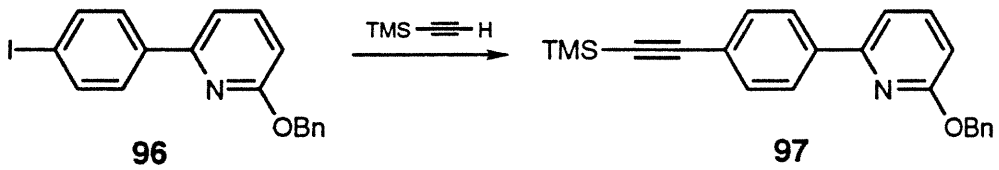

96 97

Compound **97** was made by the coupling reaction of compound **96** and trimethylsilylacetylene according to general procedure V in 93% yield as a light colored solid. It was crystallized from a mixed solvent of chloroform and hexane as white crystals.

mp 81.5-83°C

^{1}H NMR ($CDCl_3$) δ 7.98 (2H, d, J=7.9 Hz), 7.65 (1H, t, J=8.3 Hz), 7.55 (2H, d, J=8.3 Hz), 7.5-7.3 (6H, m), 6.76 (1H, d, J=8.3 Hz), 5.51 (2H, s), 0.28 (9H, s)

^{13}C NMR ($CDCl_3$) δ 163.13, 153.53, 139.28, 138.77, 137.50, 132.16, 128.40, 129.04, 127.75, 126.33, 123.40, 113.12, 110.01, 104.94, 95.37, 67.47, -0.07

IR (KBr) 2957 (m), 2156 (s), 1594 (s), 1573 (s), 1442 (s), 1323 (m), 1251 (s), 987 (m), 863 (s), 844 (s), 759 (s), 695 (m)

MS(FAB) m/z 358 (M+1)

Preparation of 2-(4-ethynylphenyl)-6-(phenylmethoxy)pyridine (98)

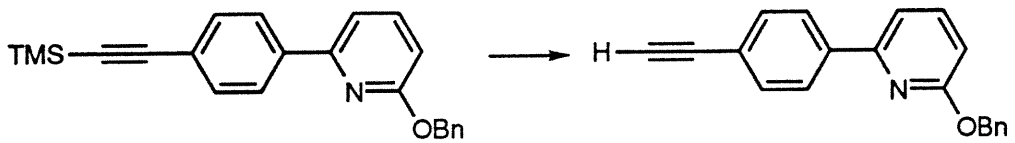

97 **98**

Compound **98** was made by the desilylation of compound **97** according to general procedure VIII and then crystallized from a mixed solvent of chloroform and hexane in a yield of 58% as a white crystalline solid.

mp 78.5-80°C

^{1}H NMR ($CDCl_3$) δ 8.02 (2H, d, J=8.5 Hz), 7.66 (1H, dd, J=7.5 and 8.2 Hz), 7.61 (2H, d, J=8.5 Hz), 7.56-7.30 (5H, m), 7.36 (1H, d, J=4.3 Hz), 6.79 (1H, d, J=8.2 Hz), 5.54 (2H, s), 3.19 (1H, s)

^{13}C NMR ($CDCl_3$) δ 163.08, 153.38, 139.23, 139.11, 147.41, 132.26, 128.33, 127.94, 127.69, 126.39, 122.28, 113.09, 110.56, 83.48, 78.13, 67.38

IR (KBr) 3290 (m), 2106 (w), 1573 (s), 1441 (s), 1323 (s), 1253 (s), 797 (s)

HRMS (FAB) calcd for $C_{20}H_{16}NO$ 286.1232, found 286.1244

MS (FAB) m/z 286 (M+1)

Analysis Calcd for $C_{20}H_{16}NOSi$: C, 84.19; H, 5.30. Found: C, 82.09; H, 5.57

Preparation of 2,2',2'',2'''-[methanetetrayltetrakis(4,1-phenylene-2,1-ethynediyl-4,1-phenylene)]tetrakis[6-(phenylmethoxy)pyridine] (99)

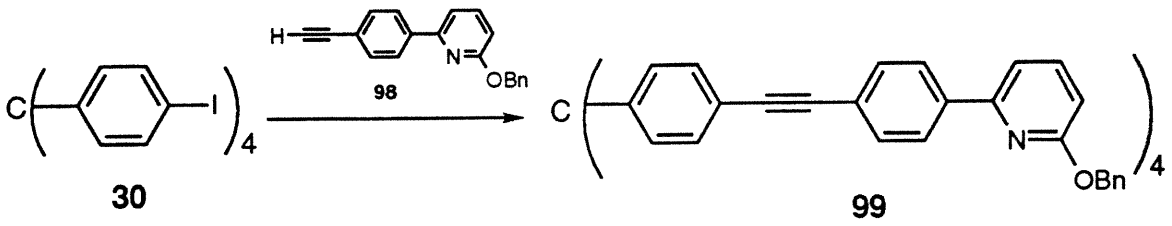

Compound **99** was synthesized by the coupling reaction of tetrakis(4-iodophenyl)methane (**30**) and aryl acetylene **96** according to general procedure II in 39% yield as a light brown solid. It was afforded as a fine pale yellow precipitate when it was crystallized from a mixed solvent of chloroform and hexane.

mp 242-244°C

^{1}H NMR ($CDCl_3$) δ 8.05 (8H, d, J=8.6 Hz), 7.67 (4H, dd, J=7.5, 8.2 Hz), 7.63 (8H, d, J=8.6 Hz), 7.51 (8H, d, J=8.5 Hz), 7.6-7.3 (24H, m), 7.26 (8H, d, J=8.5 Hz), 6.78 (4H, dd J=0.56, 8.2 Hz), 5.54 (8H, s)

^{13}C NMR ($CDCl_3$) δ 163.17, 153.61, 145.93, 139.29, 138.70, 137.54, 131.83, 131.08, 130.88, 128.40, 128.02, 127.74, 126.52, 123.50, 121.30, 113.11, 110.02, 90.12, 89.84, 67.45, 64.83

IR (KBr) 2214 (w), 1593 (s), 1573 (s), 1515 (m), 1496 (m), 1441 (s), 1400 (m), 1323 (s), 1253 (s), 1018 (m), 822 (m), 797 (s), 754 (s), 697 (s)

MS (FAB) m/z 1454 (M^+)

Preparation of 6,6',6'',6'''-[methanetetrayltetrakis(4,1-phenylene-2,1-ethynediyl-4,1-phenylene)]tetrakis[2(1H)-pyridinone] (tecton XVI)

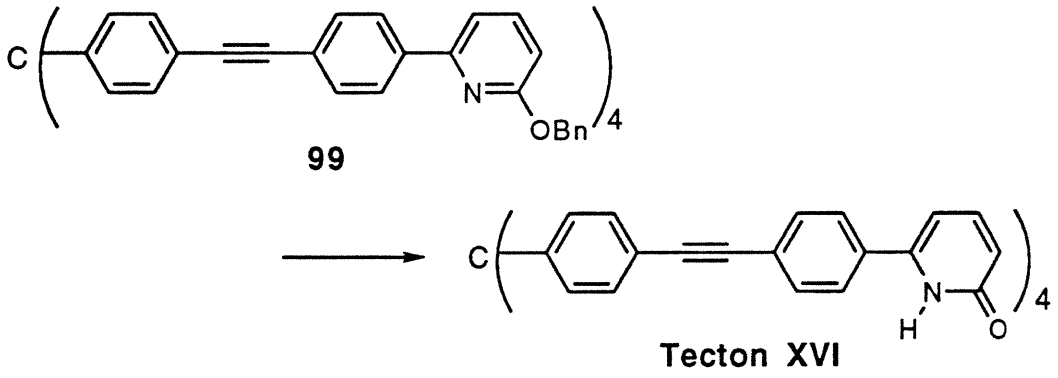

Tecton **XVI** was made by deprotecting tetrapyridine **99** with TMSI according to general procedure III in 85% yield as a brown solid.

mp did not melt below 355°C

^{1}H NMR (DMSO-d_6) 11.50 (4H, s, broad), 7.88 (8H, d, J=8.0 Hz), 7.64-7.50 (20H, m), 7.24 (8H, d, J=8.0 Hz), 6.85 (4H, d, broad), 6.44 (4H, d, J=8.7 Hz)

^{13}C NMR (DMSO-d_6) 163.23, 148.26, 146.02, 140.74, 135.05, 131.75, 131.31, 130.77, 127.02, 123.12, 120.35, 115.76, 106.80, 90.50, 89.42, 64.60

IR (KBr) 3388 (m, broad), 2211 (w), 1648 (s), 1606 (s), 1550 (m), 1514 (s), 1442 (m), 991 (m), 821 (s), 797 (s)

MS (FAB) m/z 1093 (M+1)

Preparation of 1,4-bis(trimethylsilylethynyl)benzene (88)

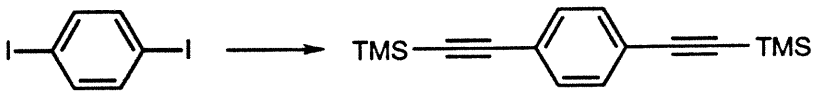

88

In a 50 ml dry flask charged with a stirring bar were placed 1,4-diiodobenzene (1.1 g, 3.5 mmol), bis(triphenylphosphine)palladium dichloride (0.16 g, 0.22 mmol), copper iodide (77 mg, 0.41 mmol), and 15 ml of dry triethylamine. To the mixture was added 1.2 ml of trimethylsilylacetylene (0.82 g, 8.3 mmol), and the resulting mixture was stirred at room temperature overnight. The reaction mixture was concentrated by rotary evaporation and then extracted with 100 ml of benzene. The resulting suspension was filtered, and the filtrate was evaporated to dryness. The crude product was purified by a short silica gel column with hexane and ethyl acetate as eluent (90:10), and then recrystallized from hexane. Compound **88** was obtained as a white crystalline solid in 96% yield (0.90 g).

mp 121-122°C

^{1}H NMR ($CDCl_3$) δ 7.39 (4H, s), 0.25 (18 H, s)

^{13}C NMR ($CDCl_3$) δ 131.20, 122.59, 104.02, 95.73, -0.62

IR (KBr) 2964 (m), 2156 (s), 1504 (m), 1492 (s), 845 (s)

HRMS (FAB) calcd for $C_{16}H_{23}Si_2$ (M+1) 271.1334, found 271.1321

MS (FAB) m/z 270 (M^+), 255, 241

Preparation of 2-phenylmethoxy-6-[4-(trimethylsilylethynyl)phenyl]-ethynylpyridine (89)

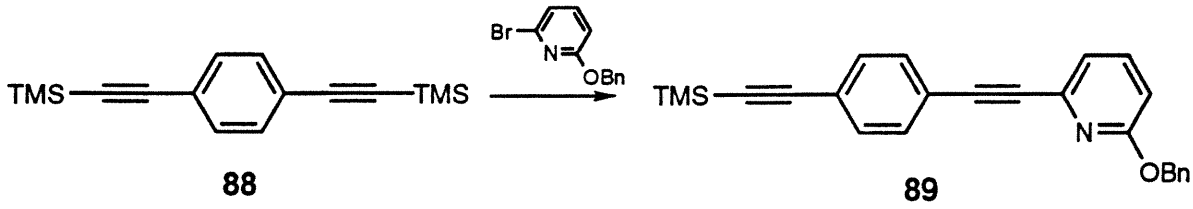

88 **89**

To a light yellow solution of 1,4-bis(trimethylsilylethynyl)benzene (**88**) (0.53 g, 1.9 mmol) in 12 ml of dry THF was added 1.9 mmol of butyllithium (1.03 M in hexane) over 25 min. at 0°C. The resulting mixture was warmed up to room temperature and stirred at that temperature for 4 hours, and was then treated with a solution of zinc chloride (0.27 g, 2.0 mmol) in 5 ml of dry THF. After stirring was continued for another hour, a solution of 6-bromo-2-(phenylmethoxy)pyridine[10d] (0.62 g, 2.4 mmol) in dry THF (5 ml) and a suspension of tetrakis(triphenylphosphine)palladium (0.2 g, 0.17 mmol) in dry THF (5 ml) were added respectively. The resulting mixture was refluxed overnight. On cooling, the reaction mixture was quenched with 35 ml of 5% sodium bicarbonate aqueous solution. Extraction (diethyl ether) and evaporation of dried extracts (anhydrous magnesium sulfate) gave a residue which was purified by flash chromatography on silica gel with hexane and chloroform as eluents to provide compound **89** in 52% yield (0.38 g) as a light brown solid. It was crystallized from a mixed solvent of chloroform and methanol as long white needles.

mp 109°C

^{1}H NMR ($CDCl_3$) δ 7.58 (1H, dd, J=7.3 and 8.3 Hz), 7.54 (2H, d, J=8.4 Hz), 7.5-7.3 (7H, m), 7.17 (1H, d, J=7.3 Hz), 6.79 (1H, d, J=8.3 Hz), 0.26 (9H, s)

^{13}C NMR ($CDCl_3$) δ 163.34, 139.90, 138.63, 136.96, 131.82, 131.76, 128.43, 128.15, 127.89, 123.47, 122.38, 121.00, 111.56, 104.43, 96.61, 90.46, 88.15, 67.91, -0.15

IR (KBr) 2958 (m), 2213 (w), 2156 (m), 1586 (s), 1568 (s), 1498 (m), 1454 (m), 1441 (s), 1328 (s), 1250 (s), 1010 (m), 863 (s), 841 (s), 760 (m), 698 (m)

HRMS (FAB) calcd for $C_{25}H_{24}NOSi$ (M+1) 382.1627, found 382.1609

MS (FAB) m/z 382 (M+1), 366, 275

Analysis Calcd for $C_{25}H_{23}NOSi$: C, 78.70; H, 6.08. Found: C, 78.29; H, 6.28

Preparation of 6-(4-ethynylphenyl)ethynyl-2-(phenylmethoxy)pyridine (90)

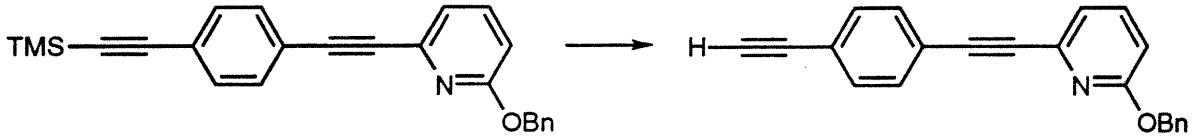

89 **90**

A mixture of compound **89** (0.88 g, 2.3 mmol), 15 ml of 1N KOH aqueous solution, 2 ml of tetrabutylammonium fluoride (1.1 M in THF), 10 ml dichloromethane and 10 ml methanol was stirred at room temperature for 50 min, followed by addition of 6 ml of 3N HCl. The resulting mixture was concentrated under reduced pressure. The residue was diluted with 20 ml of water and neutralized with solid K_2CO_3. Extraction (diethyl ether) and evaporation of the dried (anhydrous. $MgSO_4$) extracts gave a residue which was purified by recrystallization from ether and hexane to provide compound **90** in 68% yield as a light yellow crystalline solid.

mp 108.5-110°C

^{1}H NMR ($CDCl_3$) δ 7.58 (1H, dd, J=7.3 and 8.3 Hz), 7.57 (2H, d, J=8.8 Hz), 7.44-7.30 (7H, m), 7.18 (1H, d, J=7.3 Hz), 6.80 (1H, d, J=8.3 Hz), 5.43 (2H, s), 3.20 (1H, s)

^{13}C NMR ($CDCl_3$) δ 163.36, 139.87, 138.64, 136.94, 132.02, 131.85, 128.45, 128.16, 127.91, 122.84, 122.46, 121.06, 111.63, 90.57, 87.92, 83.11, 79.24, 67.92

IR (KBr) 3260 (s), 2200 (w), 1588 (s), 1565 (s), 1495 (m), 1435 (s), 1255 (s), 1100 (s), 900 (m), 830 (s), 795 (s), 730 (s), 690 (s)

HRMS (FAB) calcd for $C_{22}H_{16}NO$ (M+1) 310.1232, found 310.1245

MS (FAB) m/z 310 (M+1)

Preparation of 2,2',2'',2'''-[methanetetrayltetrakis(4,1-phenylene-2,1-ethynediyl-4,1-phenylene-2,1-ethynediyl)]tetrakis[6-(phenylmethoxy)-pyridine] (91)

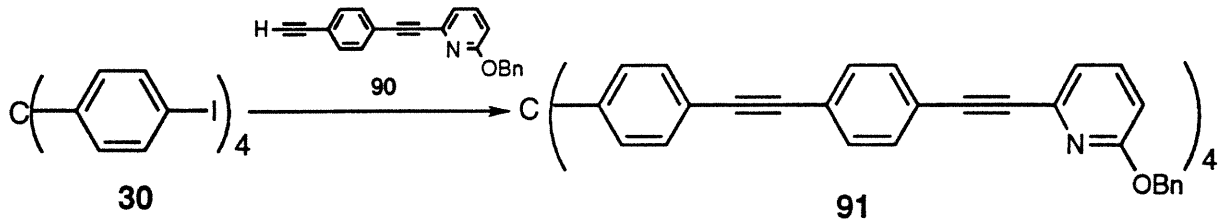

Tetrapyridine **91** was made by the coupling reaction of tetrakis(4-iodophenyl)methane (**30**) with compound **90** according to the general procedure II in 45% yield as a brown solid. Crystallization of tetrapyridine **91** from a mixed solvent of chloroform and hexane gave a yellow crystalline solid.

mp 232.5-234°C

^{1}H NMR ($CDCl_3$) δ 7.61-7.52 (20H, m), 7.47 (8H, d, J=8.6 Hz), 7.54-7.30 (20H, m), 7.23 (8H, d, J=8.6 Hz), 7.18 (4H, d, J=7.2 Hz), 6.80 (4H, d, J=8.3 Hz), 5.44 (8H, s)

^{13}C NMR ($CDCl_3$) δ 163.29, 145.94, 139.88, 138.55, 136.91, 132.30, 131.85, 131.42, 131.05, 130.79, 128.36, 128.08, 127.82, 123.49, 122.18, 120.86, 111.49, 91.00, 90.44, 89.38, 88.14, 67.85, 64.82

IR (KBr) 2209 (w), 1585 (m), 1567 (s), 1512 (m), 1440 (s), 1328 (m), 1256 (m), 1018 (m), 836 (m), 800 (s), 696 (m)

MS (FAB) m/z 1550 (M^+)

Preparation of 6,6',6'',6'''-[methanetetrayltetrakis(4,1-phenylene-2,1-ethynediyl-4,1-phenylene-2,1-ethynediyl)]tetrakis[2(1H)-pyridinone] (tecton XII)

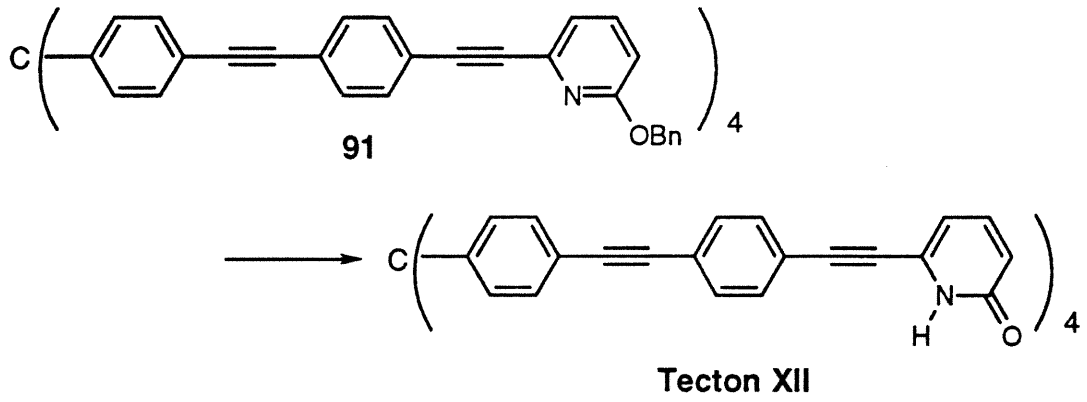

Tecton **XII** was made by deprotecting tetrapyridine **91** with TMSI according to general procedure III in quantitative yield as a brown solid.

mp did not melt below 355°C

signals missing peaks

^{1}H NMR (DMSO-d_6) δ 7.61 (16H, s), 7.60 (8H, d, J=8.5 Hz), 7.47 (4H, dd, J=6.9 and 9.1 Hz), 7.23 (8H, d, J=8.5 Hz), 6.61 (4H, d, J=6.9 Hz), 6.45 (4H, d, J=9.1 Hz)

^{13}C NMR (DMSO-d_6) δ 162.54, 146.20, 140.45, 132.98, 132.07, 131.90, 131.43, 130.81, 128.33, 123.45, 121.10, 120.20, 112.11, 91.82, 91.55, 89.26, 85.78, 64.69

IR (KBr) 3410 (w, broad), 2213 (m), 1649 (s), 1598 (s), 1443(m), 1276 (m), 1157 (m), 1006 (m), 826 (m), 800 (m)

MS (FAB) m/z 1189 (M+1)

Preparation of 4-amino-6-bromo-2-(phenylmethoxy)pyridine (75a)

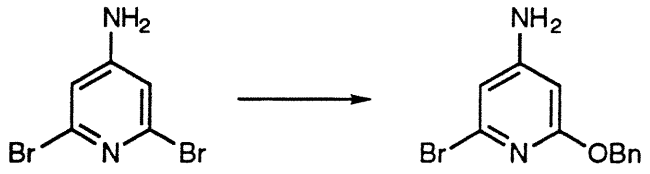

75a

In a 50 ml dry flask, which was equipped with a Dean-Stark trap, were placed 4-amino-2,6-dibromopyridine[37a-b] (1.1 g, 4.5 mmol), benzyl alcohol (0.49 g, 4.5 mmol), crushed potassium hydroxide (0.53 g, 9.4 mmol), dibenzyl-18-crown-6 (84 mg, 0.23 mmol), and 35 ml of dry toluene. The mixture was stirred at a reflux for 6 hours. On cooling, it was quenched with 35 ml of water. Extraction (toluene) and evaporation of the dried (anhydrous potassium carbonate) extracts gave a brown oil which was purified by flash chromatography on silica gel with hexane and ethyl acetate as eluents to afford compound **75a** as a pink oil in 69% yield.

^{1}H NMR (DMSO-d$_6$) δ 7.41-7.30 (5H, m), 6.39 (1H, dd, J=1.5, 3.0 Hz), 6.30 (2H, s), 5.86 (1H, dd, J=1.5, 3.0 Hz), 5.18 (2H, s)

^{13}C NMR (DMSO-d$_6$) δ 163.59, 158.77, 138.31, 137.32, 128.42, 128.01, 127.82, 107.11, 91.21, 67.14

IR (KBr) 3482 (m), 3389 (m), 3217 (m), 1625 (s), 1599 (s), 1549 (s), 1454 (m), 1434 (s), 1345 (m), 1198 (s), 1026 (m), 979 (m), 826 (s), 737 (s), 697 (s)

Preparation of 4-amino-6-bromo-2-methoxypyridine (75b)

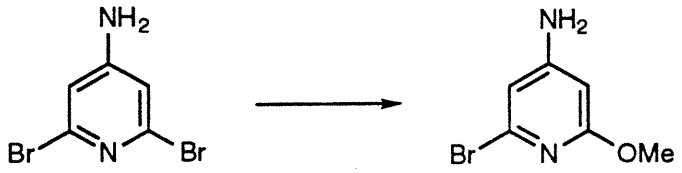

75b

To a solution of 4-amino-2,6-dibromopyridine[37a-b] (0.64 g, 2.5 mmol) in 10 ml of 2,4,6-collidine was added 0.60 ml of sodium methoxide in methanol (25%). The mixture was refluxed overnight. It was quenched with 25 ml of water and extracted with chloroform. The extracts were dried over anhydrous magnesium sulfate, and chloroform was removed by rotary evaporation while collidine was removed by bubble-to-bubble distillation under vacuum at about 80°C to afford compound **75b** in 85% yield as a light brown solid. It was crystallized from chloroform as light brown crystals.

mp 115-117°C

^{1}H NMR (CDCl$_3$) δ 6.41 (1H, d, J=1.7 Hz), 5.87 (1H, d, J=1.7 Hz), 4.12 (2H, s), 3.88 (3H, s)

^{13}C NMR (CDCl$_3$) δ 164.75, 156.07, 139.27, 107.76, 92.53, 53.79

IR (KBr) 3422 (m), 3321 (m), 3198 (m), 1638 (s), 1596 (s), 1549 (s), 1472 (s), 1417 (s), 1222 (s), 1054 (s)

HRMS (EI) Calcd for $C_6H_7BrN_2O$ (M-1) 200.9664, found 200.9676

Preparation of 4-amino-6-ethynyl-2-(phenylmethoxy)pyridine (77a)

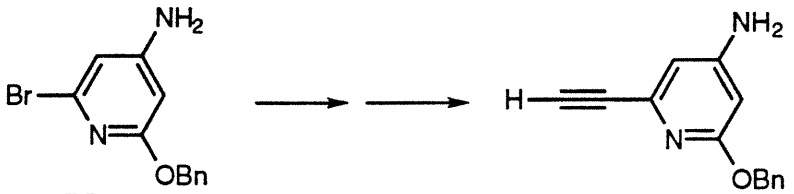

75a **77a**

Compound **77a** was made by the coupling reaction of 4-amino-6-bromo-2-(phenylmethoxy)pyridine (**75a**) with trimethylsilylacetylene in general procedure V without any other purification except for filtration through a short dry silica gel column with hexane and ethyl acetate (80:20) as eluents. The crude product was desilylated according to general procedure VIII to give a brown oil which was purified by flash chromatography on silica gel with hexane and ethyl acetate as eluents to provide compound **77a** in 83% yield as a light yellow oil.

^{1}H NMR ($CDCl_3$) δ 7.5-7.3 (5H, m) 6.49 (1H, d, J=1.9 Hz), 6.00 (1H, d, J=1.9 Hz), 5.35 (2H, s), 4.10 (2H, s), 3.05 (1H, s)

^{13}C NMR ($CDCl_3$) δ 164.85, 154.84, 139.25, 137.32, 128.35, 128.01, 127.71, 109.99, 94.76, 83.14, 75.45, 67.68

IR (KBr) 3478 (m), 3388 (m), 3285 (m), 2110 (w), 1626 (s), 1600 (s), 1563 (s), 1440 (s), 1201 (s),1042 (m)

HRMS (FAB) Calcd for $C_{14}H_{13}N_2O$ (M+1) 225.1028, found 225.1034

MS (FAB) m/z 225 (M+1)

Preparation of 4-amino-6-ethynyl-2-methoxypyridine (77b)

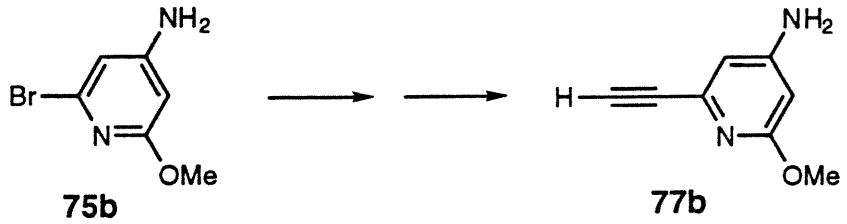

Compound **77b** was synthesized by the coupling reaction of 4-amino-6-bromo-2-methoxypyridine (**75b**) and trimethylsilylacetylene according to general procedure V without purification. The resulting crude compound was desilylated according to general procedure VIII to afford a brown oil which was purified by flash chromatography on silica gel with hexane, ethyl acetate, and chloroform as eluents. Compound **77b** was obtained in 83% yield as a light colored solid. It was crystallized from a mixed solvent of chloroform and hexane as an ivory crystalline solid.

mp 92-93.5°C

^{1}H NMR ($CDCl_3$) δ 6.47 (1H, d, J=1.9 Hz), 5.93 (1H, d, J=1.9 Hz), 4.27 (2H, s), 3.87 (3H, s), 3.01 (1H, s)

^{13}C NMR ($CDCl_3$) δ 165.27, 154.86, 139.16, 109.80, 94.22, 83.13, 75.28, 53.37

IR (KBr) 3470 (m), 3380 (m), 3286 (s), 2107 (w), 1628 (s), 1601 (s), 1563 (s), 1461 (s), 1430 (m), 1371 (s), 1297 (m), 1211 (s), 836 (m)

HRMS (EI) calcd for $C_8H_8N_2O$ 148.0367, found 148.0642

Preparation of 2,2',2'',2'''-[methanetetrayltetrakis(4,1-phenylene-2,1-ethynediyl)]tetrakis[4-amino-6-(phenylmethoxy)pyridine] (78a)

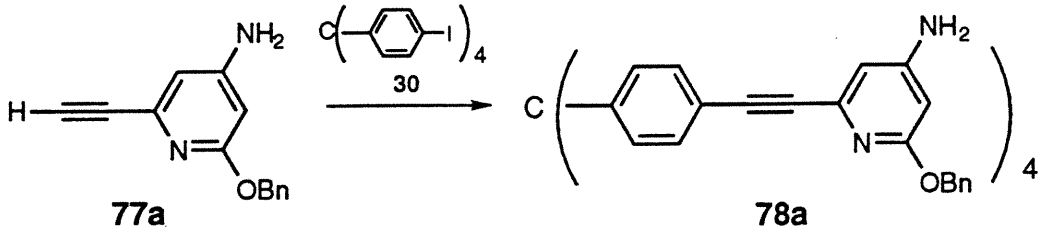

Tetrapyridine **78a** was made by the coupling reaction of tetrakis(4-iodophenyl)methane (**30**) and 4-amino-6-ethynyl-2-(phenylmethoxy)pyridine (**77a**) according to general procedure II as a light pale yellow solid in 80% yield. It was provided as fine ivory precipitate when we tried to crystallize it from a mixed solvent of chloroform and hexane.

mp 134-136°C

^{1}H NMR ($CDCl_3$) δ 7.51 (8H, d, J=8.6 Hz), 7.5-7.3 (20H, m), 7.18 (8H, d, J=8.6 Hz), 6.54 (4H, d, J=1.9 Hz), 5.99 (4H, d, J=1.9 Hz), 5.38 (8H, s), 4.08 (8H, s)

^{13}C NMR (DMSO-d_6) δ 165.05, 157.90, 146.93, 139.57, 138.51, 132.31, 131.62, 129.21, 128.66, 128.49, 120.87, 110.35, 93.24, 90.58, 86.83, 67.47, 65.43

IR (KBr) 3474 (m), 3386 (m), 3216 (w), 2212 (w), 1623 (s), 1597 (s), 1561 (s), 1499 (m), 1446 (s), 1356 (s), 1194 (s), 1020 (m), 826 (s)

MS (FAB) m/z 1209 (M+1)

Preparation of 2,2',2'',2'''-[methanetetrayltetrakis(4,1-phenylene-2,1-ethynediyl)]tetrakis(4-amino-6-methoxypyridine) (78b)

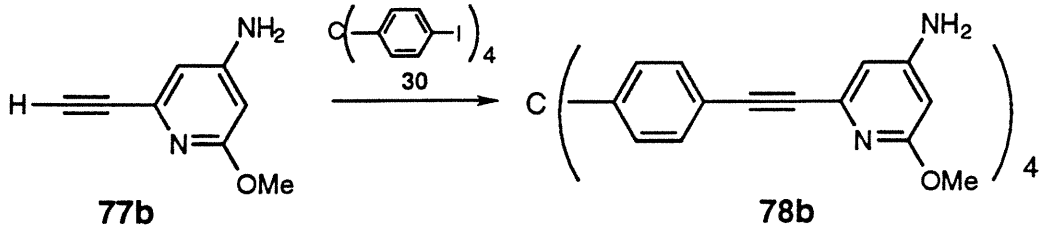

Tetrapyridine **78b** was made by the coupling reaction of tetrakis(4-iodophenyl)methane (**30**) and compound **77b** according to general procedure II in 81% yield as a light brown solid. A light brown precipitate was obtained when tetrapyridine was crystallized from chloroform and hexane.

mp No sharp melting point was observed

^{1}H NMR (DMSO-d_6) δ 7.55 (8H, d, J=8.4 Hz), 7.20 (8H, d, J=8.4 Hz), 6.47 (4H, d, J=1.4 Hz), 6.09 (8H, s), 5.83 (4H, d, J=1.4 Hz), 3.73 (12H, s)

^{13}C NMR (DMSO-d_6) δ 165.67, 157.67, 146.88, 139.77, 132.28, 131.61, 120.94, 110.24, 93.01, 91.09, 86.61, 65.41, 53.72

IR (KBr) 3473 (m), 3385 (m), 3218 (m), 2212 (w), 1624 (s), 1597 (s), 1561 (s), 1459 (s), 1437 (m), 1205 (s), 826 (s)

MS (FAB) m/z 905 (M+1)

Preparation of 3,5-dibromo-2-(phenylmethoxy)-6-(trimethylsilylethynyl)-pyridine (79)

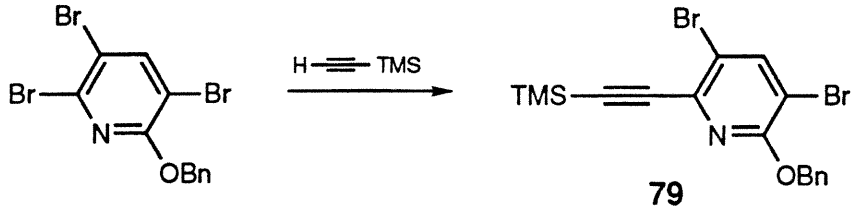

In a 25 ml dry flask which was charged with 2-phenylmethoxy-3,5,6-tribromopyridine[26] (0.45 g, 1.1 mmol), bis(triphenylphosphine)palladium dichloride (16 mg, 0.023 mmol), copper iodide (6.1 mg, 0.033 mmol), and 12 ml of dry triethylamine, was added 0.16 ml of trimethylsilylacetylene (0.11 g, 1.1 mmol). The mixture was stirred at room temperature for 6 hours. Triethylamine was removed by rotary evaporation. The residue was treated with water (30 ml), and then extracted with ether (3x60 ml). Evaporation of the dry ethereal phase (anhydrous magnesium sulfate) under reduced pressure gave a brown oil which was purified by flash chromatography on silica gel with hexane and chloroform as eluent to afford compound **79** in a yield of 44% as a light colored oil.

^{1}H NMR ($CDCl_3$) δ 7.99 (1H, s), 7.52-7.30 (5H, m), 5.44 (2H, s), 0.31 (9H, s)

^{13}C NMR ($CDCl_3$) δ 157.91, 144.17, 138.17, 136.19, 128.36, 127.87, 127.68, 115.24, 107.78, 101.37, 101.12, 69.02, -0.43

IR (KBr) 2959 (m), 2164 (w), 1553 (m), 1539 (m), 1454 (m), 1419 (s), 1356 (s), 1249 (s), 1028 (w), 826 (s)

HRMS (FAB) calcd for $C_{17}H_{18}Br_2NOSi$ (M+1) 437.95244, found 437.9508

MS (FAB) m/z 440 (M+1)

Preparation of 3,5-dibromo-6-ethynyl-2-(phenylmethoxy)pyridine (80)

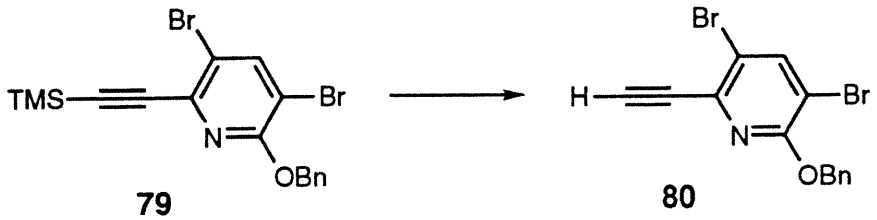

79 **80**

Compound **80** was made by the desilylation reaction of compound **79** according to general procedure VIII. The crude product was purified by a short dry silica gel column with hexane and ethyl acetate (80:20) as eluent, and then was crystallized from a mixed solvent of chloroform and methanol to provide compound **80** in 93% yield as a pale yellow crystalline solid.

mp 81-82.5°C

^{1}H NMR ($CDCl_3$) δ 8.02 (1H, s), 7.52-7.30 (5H, m), 5.44 (2H, s), 3.46 (1H, s)

^{13}C NMR ($CDCl_3$) δ 158.09, 144.35, 137.40, 136.04, 128.43, 127.98, 127.73, 114.99, 108.62, 82.04, 80.65, 69.11

IR (KBr) 3287 (m), 2115 (w), 1554 (m), 1454 (m), 1420 (s), 1357 (s), 1290 (m), 1246 (m), 1055 (s), 1016 (w)

HRMS (FAB) calcd for $C_{14}H_{10}Br_2NO$ (M+1) 365.9129, found 365.9148

MS (FAB) m/z 368 (M+1)

Analysis Calcd for $C_{14}H_{19}Br_2NO$: C, 45.81; H, 2.47. Found: C, 45.31; H, 2.51

Preparation of 2,2',2'',2'''-[methanetetrayltetrakis(4,1-phenylene-2,1-ethynediyl)]tetrakis[3,5-dibromo-6-(phenylmethoxy)pyridine] (81)

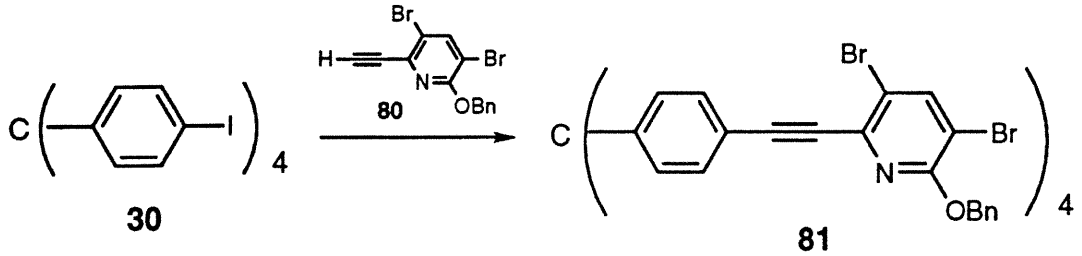

Tetrapyridine **81** was made by the coupling reaction of tetrakis(4-iodophenyl)methane (**30**) and 3,5-dibromo-6-ethynyl-2-(phenylmethoxy)pyridine (**81**) according to general procedure II in 73% yield as a brown solid.

^{1}H NMR ($CDCl_3$) δ 8.03 (4H, s), 7.60-7.20 (36H, m), 5.47 (8H, s)

^{13}C NMR ($CDCl_3$) δ 158.08, 146.59, 144.21, 138.47, 136.20, 131.71, 130.80, 128.39, 127.91, 127.69, 120.20, 115.07, 107.60, 93.78, 87.60, 69.02, 65.15

IR (KBr) 2216 (s), 1732 (s), 1550 (s), 1498 (m), 1454 (m), 1417 (s), 1356 (s), 1242 (s), 1053 (s), 1026 (m), 904 (m), 826 (s), 743 (s), 695 (s)

Preparation of 6-(2-phenylmethoxy-3-pyridyl)ethynyl-2-(phenylmethoxy)-3-(trimethylsilylethynyl)pyridine (42)

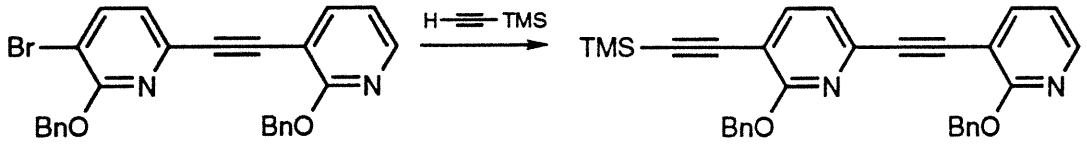

41 **42**

Compound **42** was made by the coupling reaction of dipyridine **41**[26] and trimethylsilylacetylene according to procedure V in a yield of 85% as a pale yellow oil.

^{1}H NMR ($CDCl_3$) δ 8.18 (1H, dd, J=1.9 and 5.0 Hz), 7.85 (1H, dd, J=1.9 and 7.4 Hz), 7.67 (1H, d, J=7.6 Hz), 7.58-7.28 (10H, m), 7.10 (1H, d, J=7.6 Hz), 6.93 (1H, dd, J=5.0 and 7.4 Hz), 5.53 (2H, s), 5.49 (2H, s), 0.27 (9H, s)

^{13}C NMR ($CDCl_3$) δ 163.38, 163.14, 146.98, 141.85, 141.41, 139.27, 137.17, 137.07, 128.28, 128.18, 127.55, 127.42, 127.21, 127.03, 120.48, 116.56, 107.62, 106.80, 102.30, 99.24, 94.0, 85.30, 67.79, 67.79, -0.24

IR (KBr) 2957 (m), 2214 (w), 2156 (m), 1572 (s), 1552 (s), 1498 (m), 1456 (s), 1420 (s), 1410 (s), 1358 (s), 1250 (s), 1236 (s), 1018 (m), 863 (s), 843 (s), 766 (m), 733 (m), 696 (m)

HRMS (FAB) calcd for $C_{31}H_{29}N_2O_2Si$ (M+1) 489.1998, found 489.2019

MS (FAB) m/z 489 (M+1)

Preparation of 3-ethynyl-6-(2-phenylmethoxy-3-pyridyl)ethynyl-2-(phenylmethoxy)pyridine (43)

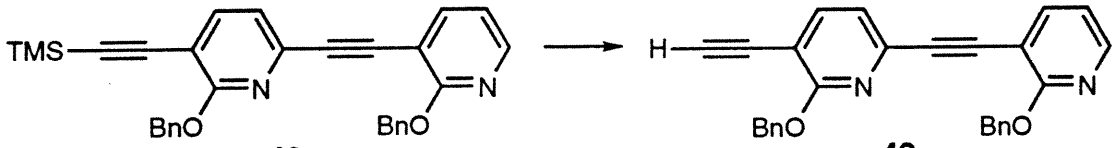

42 **43**

Compound **43** was synthesized by desilylation of compound **42** according to general procedure V and crystallized from a mixed solvent of chloroform and methanol in 90% yield as an ivory crystalline solid.

mp 98.5-100°C

^{1}H NMR ($CDCl_3$) δ 8.18 (1H, dd, J=1.9 and 5.0 Hz), 7.85 (1H, dd, J=1.9 and 7.4 Hz), 7.70 (1H, d, J=7.6 Hz), 7.58-7.28 (10H, m), 7.11 (1H, d, J=7.7 Hz), 6.93 (1H, dd, J=5.0 and 7.4 Hz), 5.53 (2H, s), 5.52 (2H, s), 3.41 (1H, s)

^{13}C NMR ($CDCl_3$) δ 163.40, 163.17, 147.08, 142.23, 141.89, 139.73, 137.17, 136.89, 128.30, 128.30, 127.66, 127.66, 127.57, 127.24, 120.44, 116.47, 106.72, 106.45, 93.83, 85.31, 84.10, 78.22, 68.04, 67.76

IR 3197 (s, HC≡C), 2216 (w, C≡C)

HRMS (FAB) calcd for $C_{28}H_{21}N_2O_2$ (M+1) 417.1603, found 417.1618.

m/z (FAB) 417 (M+1)

Preparation of 3,3',3'',3'''-{methanetetrayltetrakis(4,1-phenylene-2,1-ethynediyl-2,5-[6-(phenylmethoxy)pyridylene]-2,1-ethynediyl)}tetrakis[2-(phenyl-methoxy)pyridine] (44)

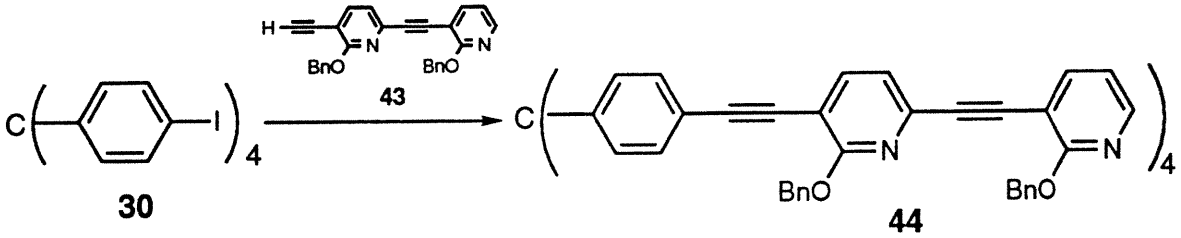

Tetrakis(dipyridine) **44** was made by the coupling reaction of tetrakis(4-iodophenyl)methane (**30**) and compound **43** according to general procedure II in 34% yield as a brown solid.

mp 106.5-108°C

^{1}H NMR ($CDCl_3$) δ 8.18 (4H, dd, J=1.9 and 5.0 Hz), 7.86 (4H, dd, J=1.9 and 7.4 Hz), 7.73 (4H, d, J=7.7 Hz), 7.45 (8H, d, J=8.4 Hz), 7.6-7.3 (40H, m), 7.20 (8H, d, J=8.4 Hz), 7.14 (4H, d, J=7.7 Hz), 6.94 (4H, dd, J=5.0 and 7.4 Hz), 5.53 (16H, s)

^{13}C NMR ($CDCl_3$) δ 163.38, 162.71, 146.95, 146.07, 141.87, 141.04, 139.13, 137.19, 137.09, 131.13, 130.84, 128.30, 128.30, 127.61, 127.56,

127.46 127.24, 121.17, 120.66, 116.57, 107.72, 106.87, 96.05, 94.14, 85.23, 84.77, 67.98, 67.80, 64.94

IR (KBr) 2215.9 (w, C≡C)

m/z (FAB) 1978 (M^{+})

Preparation of 3-bromo-6-(trimethylsilyl)ethynyl-2-(phenylmethoxy)-pyridine (47)

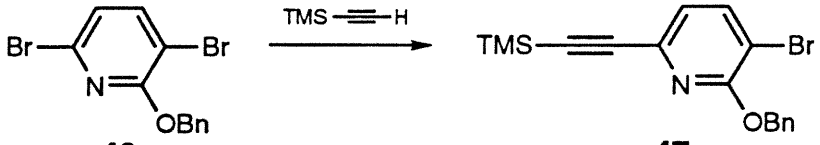

40 **47**

An ice-cooled solution of 3,6-dibromo-2-(phenylmethoxy)pyridine[26] (**40**) (2.2 g, 6.3 mmol), and 1.0 ml of trimethylsilylacetylene (0.68 g, 6.9 mmol) in 10 ml of dry triethylamine was transferred to a 50 ml flask charged with bis(triphenylphosphine)palladium dichloride (91 mg, 0.13 mmol), copper iodide (28 mg, 0.15 mmol), and 10 ml of dry triethylamine at 0°C. The mixture was stirred at 0°C for 2 hours, and then the ice bath was removed and stirring was continued at room temperature overnight. The resulting mixture was diluted with 200 ml of ether and then was washed with water and brine. Evaporation of the dried organic phase (anhydrous magnesium sulfate) in vacuo gave a residue of brown oil which was purified by flash chromatography on silica gel with hexane and benzene as eluents to provide compound **47** as a colorless oil in a yield of 69%.

^{1}H NMR ($CDCl_3$) δ 7.76 (1H, d, J=7.8 Hz), 7.54-7.30 (5H, m), 6.98 (1H, d, J=7.8 Hz), 5.47 (2H, s), 0.29 (9H, s)

^{13}C NMR ($CDCl_3$) δ 158.98, 141.49, 138.56, 136.63, 128.32, 127.71, 127.58, 122.02, 107.67, 102.99, 95.23, 68.58, -0.33

IR (KBr) 2958 (s, CH_3), 2158 (m, C≡C)

HRMS (FAB) Calcd for $C_{17}H_{18}BrNOSi$ 360.0419, found 360.0429.

m/z (FAB) 360 (M^+)

Preparation of 3-(6-phenylmethoxy-2-pyridyl)ethynyl-2-(phenylmethoxy)-6-(trimethylsilylethynyl)pyridine (48)

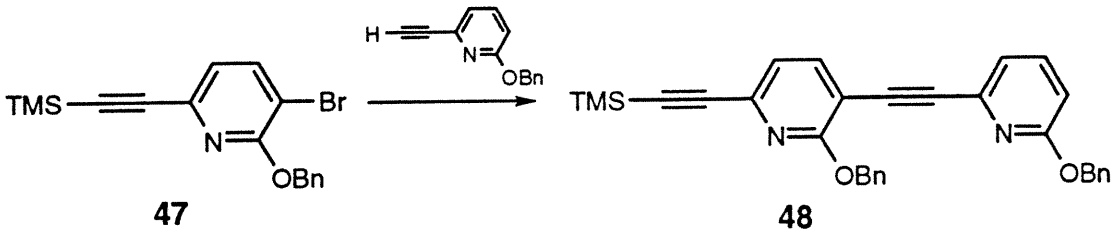

47 **48**

Compound **48** was made by the coupling reaction of compound **47** and 6-ethynyl-2-(phenylmethoxy)pyridine[10a] in general procedure V in 87% yield as a yellow oil.

^{1}H NMR ($CDCl_3$) δ 7.79 (1H, d, J=7.7 Hz), 7.60-7.28 (11H, m), 7.13 (1H, d, J=7.3 Hz), 7.12 (1H, d, J=7.7 Hz), 6.79 (1H, d, J=8.4 Hz), 5.43 (2H, s), 5.41 (2H, s), 0.30 (9H, s)

^{13}C NMR ($CDCl_3$) δ 163.26, 162.87, 141.45, 139.84, 139.84, 139.39, 138.47, 136.98, 136.95, 128.35, 128.34, 127.80, 127.49, 127.37, 121.01, 120.81, 111.57, 107.16, 103.54, 96.47, 95.50, 83.20, 68.01, 67.77, -0.36

IR (KBr) 2957 (m), 2213 (w), 2155 (w), 1587 (s), 1567 (s), 1448 (s), 1407 (m), 1357 (s), 1332 (s), 1252 (s), 1011 (s), 983 (m), 843 (s), 800 (s), 731 (s), 696 (s)

HRMS (EI) calcd for $C_{31}H_{28}N_2O_2Si$ 488.1920, found 488.1935

MS (EI) m/z 488 (M^+)

Preparation of 6-ethynyl-3-(6-phenylmethoxy-2-pyridyl)ethynyl-2-(phenylmethoxy)pyridine (49)

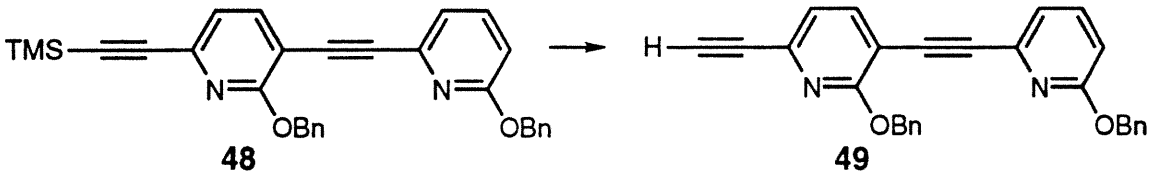

48 **49**

Compound **49** was made by desilylation of compound **48** according to general procedure VIII in 91% yield as a pale yellow oil.

^{1}H NMR ($CDCl_3$) δ 7.81 (1H, d, J=7.6 Hz), 7.56 (1H, dd, J=7.3 and 8.3 Hz), 7.56-7.28 (10H, m), 7.15 (1H, d, J=7.6 Hz), 7.14 (1H, dd, J=0.74 and 7.3 Hz), 6.79 (1H, dd, J=0.74 and 8.3 Hz), 5.53 (2H, s), 5.41 (2H, s), 3.26 (1H, s)

^{13}C NMR ($CDCl_3$) δ 163.25, 163.02, 141.60, 139.72, 139.72, 138.56, 138.56, 136.90, 136.84, 128.34, 128.23, 128.12, 127.83, 127.56, 127.37, 121.07, 120.71, 111.66, 107.76, 95.58, 82.57, 78.31, 68.07, 67.85

IR (KBr) 3281 (m), 2213 (w), 2108 (w), 1587 (s), 1566 (s), 1498 (m), 1449 (s), 1410 (m), 1357 (s), 1255 (s), 1008 (s), 984 (m), 801 (s), 734 (s), 696 (s)

HRMS (EI) calcd for $C_{28}H_{20}N_2O_2$ 416.1525, found 416.1496

MS (EI) m/z 416 (M^+)

Preparation of 6,6',6'',6'''-{methanetetrayltetrakis(4,1-phenylene-2,1-ethynediyl-3,6-[2-(phenylmethoxy)pyridylene]-2,1-ethynediyl)}tetrakis[2-(phenylmethoxy)pyridine] (50)

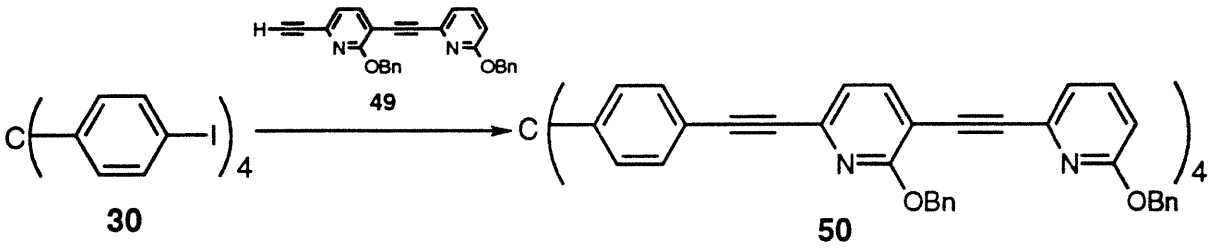

Tetrakis(dipyridine) **50** was made by the coupling reaction of tetrakis(4-iodophenyl)methane (**30**) and compound **49** according to general procedure II in 41% yield as a brown solid.

^{1}H NMR ($CDCl_3$) δ 7.83 (4H, d, J=7.7 Hz), 7.60-7.21 (60H, m), 7.18 (4H, d, J=7.7 Hz), 7.14 (4H, d, J=7.3 Hz), 6.78 (4H, d, J=8.4 Hz), 5.57 (8H, s), 5.42, (8H, s)

^{13}C NMR ($CDCl_3$) δ 163.27, 163.00, 146.36, 141.52, 139.87, 139.68, 138.48, 136.98, 136.95, 131.55, 130.80, 130.72, 128.35, 128.22, 128.13, 127.80, 127.52, 127.39, 121.03, 120.54, 120.41, 106.93, 95.55, 89.21, 83.29, 77.09, 68.01, 67.78, 64.32

IR (KBr) 2207 (m), 1567 (s), 1499 (m), 1452 (s), 1410 (m), 1357 (s), 1254 (s), 1006 (m), 827 (m), 801 (s), 734 (s), 696 (s)

Preparation of 5-bromo-3-iodo-2(1H)-pyridone (57)

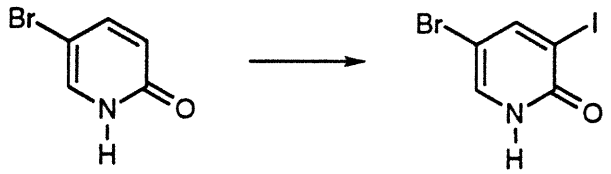

57

In a 100 ml three-necked flask equipped with a stirring bar, a condenser and a dropping funnel was placed a suspension of 5-bromo-2(1H)-pyridone[28] (0.81 g, 3.7 mmol) in 30 ml of 20% sulfuric acid. After it was heated to reflux, a suspension of potassium iodate (1.5 g, 8.8 mmol) in 10 ml of water was added. After 10 min, a solution of potassium iodide (1.46 g, 8.8 mmol) in 15 ml of water was added during a period of 1.5 hours, which caused precipitation of a yellow solid. On cooling, the mixture was diluted with water and filtered. The resulting solid was washed with water, 5% sodium bisulfate aqueous solution and then more water to afford compound **57** in 64% yield as a light gray solid.

mp 217.5-219.5°C

^{1}H NMR (DMSO-d_6) δ 13.0-11.0 (1H, s, broad), 8.19 (1H, dd, J=0.7, 2.6 Hz), 7.71 (1H, dd, J=0.7, 2.6 Hz)

^{13}C NMR (DMSO-d_6) δ 159.07, 150.78, 136.97, 97.24, 93.67

IR (KBr) 3416 (w, broad), 1656 (s), 1635 (s), 1599 (s), 1236 (m)

HRMS (FAB) calcd for C_5H_4BrINO (M+1) 299.8529, found 299.8521

MS (FAB) m/z 300 (M^+)

Preparation of 5-bromo-2-methoxy-3-[4-(6-phenylmethoxy-2-pyridyl)-phenyl]pyridine (54)

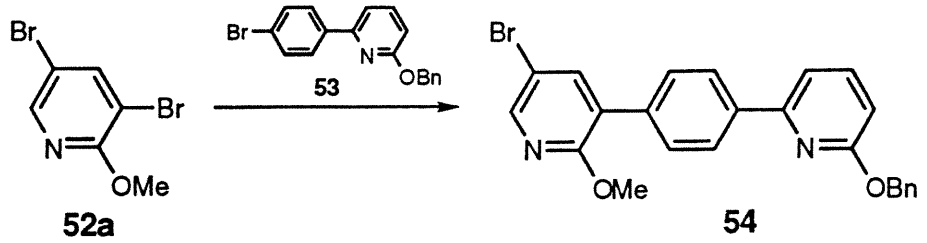

Compound **54** was made by the coupling reaction of 3,5-dibromo-2-methoxypyridine (**52a**)[27] or 5-bromo-3-iodo-2-methoxypyridine (**52b**) and compound (**53**) in general procedure VI in 47% yield as a colorless oil.

^{1}H NMR ($CDCl_3$) δ 8.22 (1H, d, J=2.5 Hz), 8.11 (2H, d, J=8.6 Hz), 7.79 (1H, d, J=2.5 Hz), 7.68 (1H, dd, J=7.5 and 8.2 Hz), 7.65 (2H, d, J=8.6 Hz), 7.41 (1H, dd, J=0.6 and 7.5 Hz), 7.60-7.30 (5H, m), 6.79 (1H, dd, J=0.6 and 8.2 Hz), 5.55 (2H, s), 3.99 (3H, s)

^{13}C NMR ($CDCl_3$) δ 163.18, 159.75, 153.92, 146.10, 140.47, 139.28, 138.69, 137.59, 135.71, 129.27, 128.40, 128.03, 127.73, 126.60, 125.91, 113.07, 111.93, 109.89, 67.41, 53.91

IR (KBr) 1595 (s), 1577 (s), 1464 (s), 1448 (s), 1398 (s), 1370 (s), 1256 (s), 1005 (s), 904 (m), 795 (s), 740 (s), 693 (s)

HRMS (FAB) calcd for $C_{24}H_{21}BrN_2O_2$ (M+2) 488.0760, found 488.0735

MS (FAB) m/z 487 (M+1)

Preparation of 5-(trimethylsilylethynyl)-2-methoxy-3-[4-(6-phenylmethoxy-2-pyridyl)phenyl]pyridine (55)

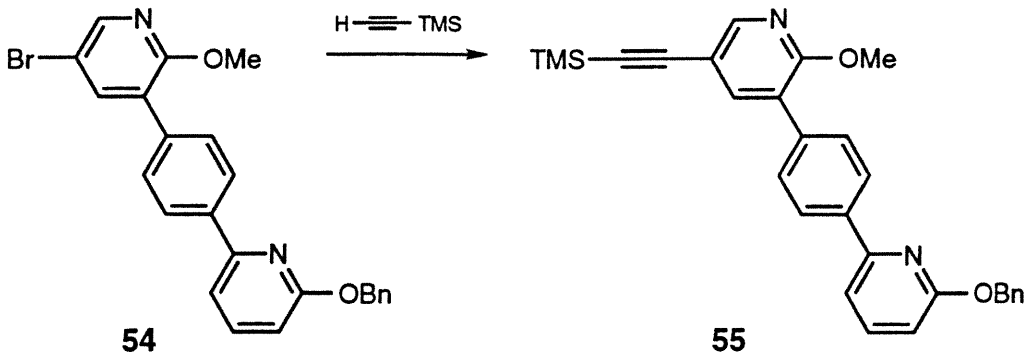

54 55

Compound **55** was made by the coupling reaction of compound **54** and trimethylsilylacetylene according to general procedure V in a yield of 82% as a colorless thick oil.

^{1}H NMR ($CDCl_3$) δ 8.30 (1H, dd, J=1.0, 2.2 Hz), 8.10 (2H, d, J=8.2 Hz), 7.76 (1H, dd, J=1.0, 2.2 Hz), 7.67 (1H, dd, J=7.5, 8.2 Hz), 7.65 (2H, d, J=8.2 Hz), 7.55-7.34 (6H, m), 6.78 (1H, d, J=8.2), 5.55 (2H, s), 4.02 (3H, s)

^{13}C NMR ($CDCl_3$) δ 163.17, 160.28, 154.05, 149.15, 141.22, 139.25, 138.43, 137.63, 136.19, 129.31, 128.39, 128.02, 127.71, 126.61, 123.76, 113.48, 113.02, 109.79, 101.75, 95.98, 67.38, 53.88, -0.12

IR (KBr) 2953 (m), 2157 (m), 1594 (s), 1574 (s), 1469 (s), 1443 (s), 1394 (s), 1250 (s), 1015 (s), 845 (s)

Preparation of 5-ethynyl-2-methoxy-3-[4-(6-phenylmethoxy-2-pyridyl)-phenyl]pyridine (56)

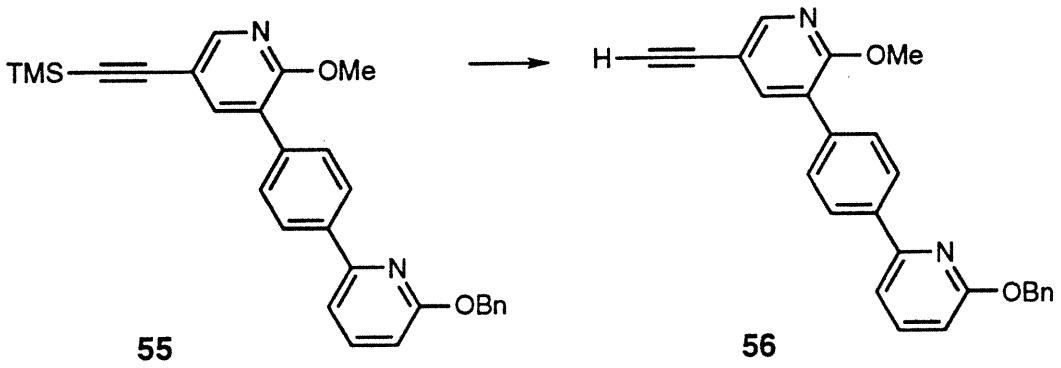

55 56

Compound **56** was made by the desilylation of compound **55** according to general procedure VIII and crystallized from a mixed solvent of chloroform and methanol in a yield of 93% as a white crystalline solid.

^{1}H NMR ($CDCl_3$) δ 8.34 (1H, d, J=2.2 Hz), 8.11 (2H, d, J=8.6 Hz), 7.78 (1H, d, J=2.2 Hz), 7.68 (1H, dd, J=7.6 and 8.1 Hz), 7.66 (2H, d, J=8.6 Hz), 7.60-7.30 (6H, m), 6.79 (1H, dd, J=0.40 and 8.1 Hz), 5.55 (2H, s), 4.03 (3H, s), 3.16 (1H, s)

^{13}C NMR ($CDCl_3$) δ 163.12, 160.51, 153.95, 149.34, 141.19, 139.22, 138.47, 137.54, 136.00, 129.26, 128.35, 127.98, 127.68, 126.51, 123.88, 113.00, 112.32, 109.78, 80.46, 78.73, 67.35, 53.88

IR (KBr) 3303 (m), 2108 (w), 1597 (s), 1576 (s), 1463 (s), 1448 (s), 1396 (s), 1256 (s), 1015 (s), 792 (s)

HRMS (FAB) calcd for $C_{26}H_{21}N_2O_2$ (M+1) 493.1603, found 493.1623

MS (FAB) m/z 493 (M+1)

Preparation of 6,6',6'',6'''-{methanetetrayltetrakis[4,1-phenylene-2,1-ethynediyl-3,5-(2-methoxypyridylene)-4,1-phenylene]}tetrakis[2-(phenylmethoxy)pyridine] (57)

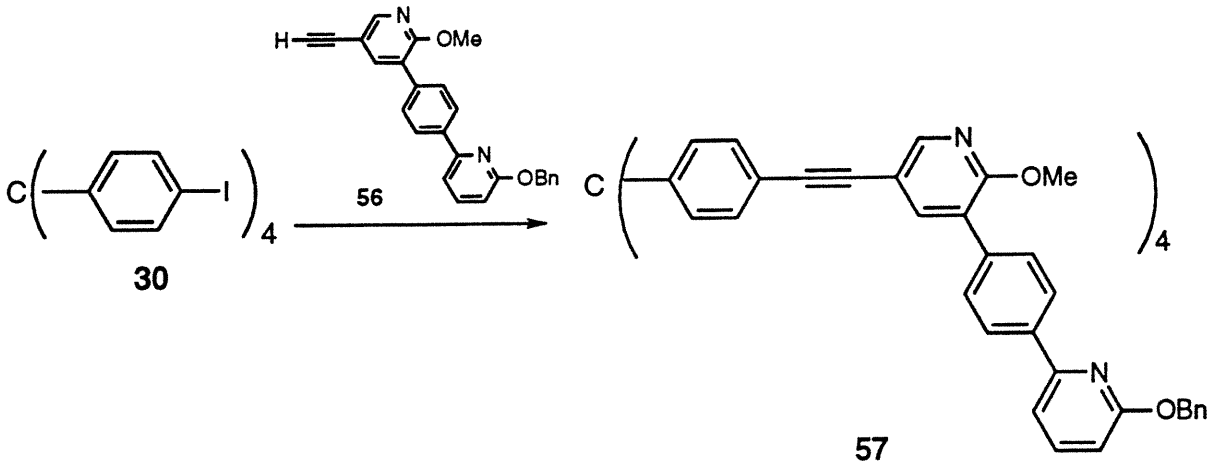

Tetrakis(dipyridine) **57** was made by the coupling reaction of tetrakis(4-iodophenyl)methane (**30**) and compound **56** according to general procedure II in a yield of 86% as a light yellow solid.

mp No sharp melting point was observed

^{1}H NMR ($CDCl_3$) δ 8.36 (4H, d, J=2.2 Hz), 8.11 (8H, d, J=8.4 Hz), 7.81 (4H, d, J=2.2 Hz), 7.676 (4H, t, J=7.8 Hz), 7.679 (8H, d, J=8.4 Hz), 7.53 (4H, d, J=7.0 Hz), 7.49 (8H, d, J=8.5 Hz), 7.42-7.33 (20H, m), 7.24 (8H, d, J=8.5 Hz), 6.78 (4H, d, J=8.2 Hz), 5.55 (8H, s), 4.04 (12H, s)

^{13}C NMR ($CDCl_3$) δ 163.17, 160.30, 154.02, 148.73, 145.90, 140.77, 139.26, 138.48, 137.60, 136.21, 130.99, 130.87, 129.34, 128.39, 128.03, 127.72, 126.56, 123.96, 121.13, 113.48, 113.04, 109.81, 90.46, 86.61, 67.40, 53.92

IR (KBr) 3031 (w), 2950 (m), 2210 (w), 1593 (s), 1574 (s), 1502 (m), 1470 (s), 1443 (s), 1395(s), 1298(s), 1253 (s), 1016 (s), 798 (s)

MS (FAB) m/z 1882 (M^+)

Preparation of 3-[4-(2-phenylmethoxy-3-pyridyl)-2-bromophenyl]-1,1-diethyltriazene (69)

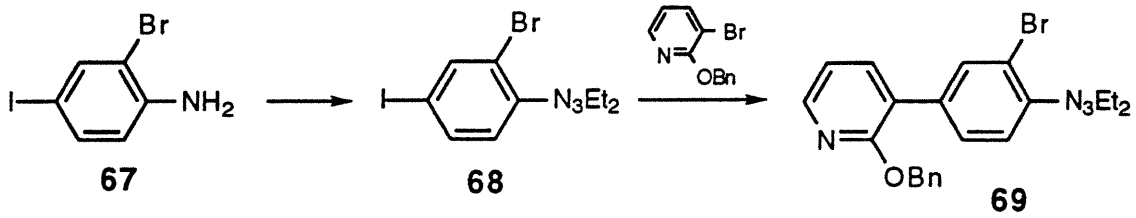

To a solution of 2-bromo-4-iodoaniline[31b, 34] (1.4 g, 5.5 mmol) in a mixture of concentrated hydrochloric acid (6.4 ml) and water (6.4 ml) was added dropwise a solution of sodium nitrite (0.59 g, 8.6 mmol) in water (6 ml) at 0°C. Stirring was continued for an additional 40 min. at 0°C. Then the mixture was transferred into a solution of potassium carbonate (5.4 g, 39 mmol) and diethylamine (4.1 ml, 39 mmol) in 80 ml of ice water. The resulting mixture was extracted with ether, and the combined ethereal phases were washed with water and dried over anhydrous magnesium sulfate. The dry extract was evaporated to dryness under reduced pressure to provide compound **68** in 92% yield as an orange oil. Without further purification, **68** was coupled with 3-bromo-2-(phenylmethoxy)-pyridine[10d] according to general procedure VI to provide compound **69** in a yield of 57% as a light orange oil.

^{1}H NMR ($CDCl_3$) δ 8.16 (1H, dd, J=1.9 and 5.0 Hz), 7.90 (1H, d, J=1.8 Hz), 7.66 (1H, dd, J=1.9 and 7.3 Hz), 7.50 (1H, dd, J=1.9 and 8.4 Hz), 7.38-7.28 (6H, m), 6.99 (1H, dd, J=5.0 and 7.3 Hz), 5.48 (2H, s), 3.82 (4H, q, J=7.2 and 14.3 Hz), 1.33 (6H, s, broad)

^{13}C NMR ($CDCl_3$) δ 160.09, 147.60, 145.67, 138.31, 137.38, 134.24, 133.85, 128.56, 128.34, 127.38, 127.23, 123.29, 119.41, 117.86, 117.32, 67.51, 49.23, 41.97, 14.55, 10.90

Preparation of 3-(3-bromo-4-iodophenyl)-2(1H)-pyridone (70b)

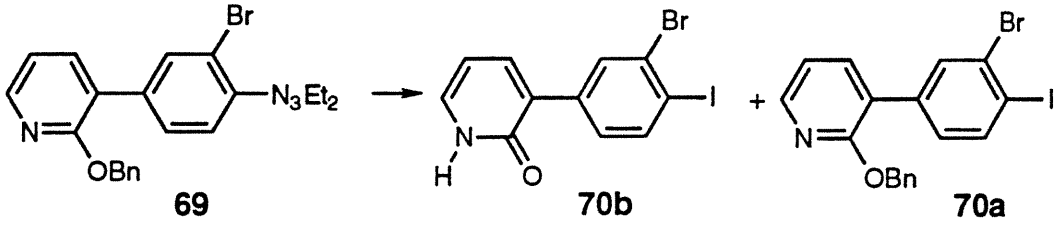

To a pale yellow solution of diethyltriazene **69** (0.21 g, 4.8 mmol) and sodium iodide (0.16 g, 1.1 mmol) in 5 ml of acetonitrile was added 0.12 ml of trimethylsilyl chloride (0.93 mmol). A white precipitate formed immediately and the color of the mixture turned to light brown. The mixture was stirred at 60°C for about 30 min. It was quenched with 5% aqueous sodium bicarbonate solution and extracted with ether. The combined ethereal phases were washed with 10% aqueous sodium persulfate solution and water. Evaporation of the dry (anhydrous magnesium sulfate) extracts gave a reddish orange solid which was a mixture of compound **70b** (major) and **70a** (minor). It was rinsed with a mixed solvent of hexane and ethyl acetate (80/20) for a while and then filtered to provide compound **70b** (64 mg) as a light pink solid.

mp 230-232°C

^{1}H NMR (DMSO-d_6) δ 11.94 (1H, s), 8.18 (1H, d, J=1.6 Hz), 7.92 (1H, d, J=8.3 Hz), 7.76 (1H, dd, J=1.6 and 7.0 Hz),7.45-7.42 (2H, overlapped), 6.30 (1H, t, J=6.7 Hz)

^{13}C NMR (DMSO-d_6) δ 160.86, 139.69, 139.44, 138.51, 135.82, 131.81, 128.63, 128.47, 126.99, 105.54, 100.05

IR (KBr) 3456 (broad),3253 (m), 1644 (s), 1632 (s), 1610 (s), 1556 (s), 1475 (m), 870 (m), 762 (s)

HRMS (EI) calcd for $C_{11}H_8BrINO$ (M+1) 375.8834, found 375.8815

MS (EI) m/z 375 (M^+)

Preparation of 3-(4-bromo-2-iodophenyl)-1,1-diethyltriazene (60)

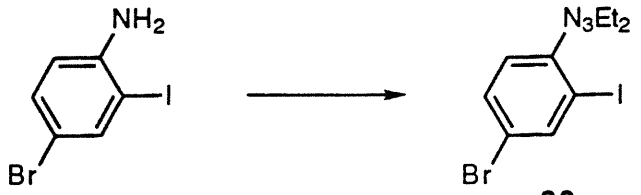

59 **60**

A cooled mixture of 4 ml of concentrated hydrochloric acid and 4 ml of water was transferred into a flask which was charged with 4-bromo-2-iodoaniline[34, 31b] (0.80 g, 2.7 mmol) and sodium nitrite (0.30 g, 4.3 mmol) at 0°C. The resulting mixture was stirred at 0°C for 1 hour. It was then transferred into a solution of potassium carbonate (3.4 g, 25 mmol) and diethylamine (2.6 ml, 25 mmol) in 90 ml of ice water. Extraction (diethyl ether) and evaporation of the dry (anhydrous magnesium sulfate) extracts provided compound **60** as an orange oil in 96% yield.

1H NMR ($CDCl_3$) δ 7.97 (1H, dd, J=1.1, 2.1 Hz), 7.39 (1H, dd, J=2.1, 8.6 Hz), 7.25 (1H, dd, J=1.1, 15.0 Hz), 3.81 (4H, q, J=7.2, 14.3 Hz), x.xx (6H, t, J=x.x Hz)

^{13}C NMR ($CDCl_3$) δ 149.46, 140.63, 131.47, 118.12, 118.07, 96.75, 49.23, 42.19, 14.39, 10.81

IR (KBr) 2973 (m), 2932 (m), 2128 (w), 2099 (m), 1611 (broad, w), 1565 (m), 1449 (s), 1409 (s), 1391 (s), 1373 (s), 1339 (s), 1247 (m), 1108 (s), 1076 (s), 1025 (s), 868 (m), 819 (s)

HRMS (EI) calcd for $C_{10}H_{13}BrIN_3$ (M+1) 381.94126, found 381.9396

MS (EI) m/z 381 (M^+)

References

(1) (a) Lehn, J. M. *Angew. Chem., Int. Ed. Engl.* **1988**, *27*, 89; (b) Lehn, J. M. *Angew. Chem., Int. Ed. Engl.* **1990**, *29*, 130; (c) Desiraju, G. R. *Crystal Engineering: The Design of Organic Solids* Elsevier, Amsterdan, **1989**

(2) (a) Dauber, P. A.; Hagler, A. T. *Acc. Chem. Res.* **1980**, *13*, 105; (b) Leiserowitz, L.; Schmidt, G. M. J. *J. Chem. Soc. (A)* **1969**, 2372. (c) Leiserowitz, L. *Acta Crystallogr.* **1976**, *B32*, 775. (d) Hagler, A. T.; Leiserowitz, L. *J. Am. Chem. Soc.* **1978**, *100*, 5879. (e) Berkovitch-Yellin, Z.; Leiserowitz, L. *J. Am. Chem. Soc.* **1980**, *102*, 7677. (f) Berkovitch-Yellin, Z.; Leiserowitz, L. *J. Am. Chem. Soc.* **1982**, *102*, 4052. (g) Weinstein, S.; Leiserowitz, L.; Gil-Av, E. *J. Am. Chem. Soc.* **1980**, *102*, 2768. (h) Leiserowitz, L.; Hagler, A. T. *Proc. R. Soc. London*, **1983**, *A388*, 133. (i) Leiserowitz, L.; Nader, J. *Acta Crystallogr.* **1977**, *B33*, 2719. (j) Berkovitch-Yellin, Z.; Ariel, S.; Leiserowitz, L. *J. Am. Chem. Soc.* **1983**, *105*, 765.

(3) (a) Etter, M. C.; Ranawake, G. *J. Am. Chem. Soc.* **1992**, *114*, 4430. (b) Etter, M. C. *Acc. Chem. Res.* **1990**, *23*, 120. (c) Etter, M. C.; MacDonald, J. C.; Bernstein, J. *Acta Crystallogr.* **1990**, *B46*, 256. (d) Reutzei, S. M.; Etter, M. C. *J. Phys. Org. Chem.* **1992**, *5*, 44. (d) Etter, M. C.; Adsmond, D. A. *J. Chem. Soc., Chem. Commun.* **1990**, 589. (e) Etter, M. C.; Urbanczyk-Lipkowska, Z.; Zia-Ebrahimi, M.; Panunto, T. W. *J. Am. Chem. Soc.* **1990**, *112*, 8415. (f) Etter, M. C. *J. Phys. Chem.* **1991**, *95*, 4601.

(4) (a) Zhao, X.; Chang, Y.-L.; Fowler, F. W.; Lauher, J. W. *J. Am. Chem. Soc.* **1990**, *112*, 6627. (b) Lauher, J. W.; Chang, Y.-L.; Fowler, J. W. *Mol. Cryst. Liq. Cryst.* **1992**, *211*, 99. (c) Chang, Y.-L.; West, M.-A.; Fowler, F. W.; Lauher, J. W. *J. Am. Chem. Soc.* **1993**, *11 5*, 5991.

(5) (a) Zerkowski, J. A.; Seto, C. T.; Wierda, D. A.; Whitesides, G. M. *J. Am. Chem. Soc.* **1990**, *112*, 9025. (b) Seto, C. T.; Whitesides, G. M. *J. Am. Chem. Soc.* **1990**, *112*, 6409. (c) Seto, C. T.; Whitesides, G. M. *J. Am. Chem. Soc.* **1991**, *113*, 712. (d)

Zerkowski, J. A.; Seto, C. T.; Wierda, D. A.; Whitesides, G. M. *J. Am. Chem. Soc.* **1992**, *114*, 5473. (e) Seto, C. T.; Whitesides, G. M. *J. Am. Chem. Soc.* **1993**, *115*, 905. (f) Seto, C. T.; Mathias, J. P.; Whitesides, G. M. *J. Am. Chem. Soc.* **1993**, *115*, 1321. (g) Zerkowski, J. A.; Mathias, J. P.; Whitesides, G. M. *J. Am. Chem. Soc.* **1994**, *116*, 4305. (f) Zerkowski, J. A.; Whitesides, G. M. *J. Am. Chem. Soc.* **1994**, *116*, 4298.

(6) (a) Lehn, J.-M.; Mascal, M.; DeCian, A.; Fischer, J. *J. Chem. Soc., Chem. Commun.* **1990**, 479. (b) Drain, C. M.; Fischer, R.; Nolen, E. G.; Lehn, J.-M. *J. Chem. Soc., Chem. Commun.* **1993**, 243. (c) Lehn, J.-M. *Angew. Chem., Int. Ed. Engl.* **1990**, *29* , 1304. (d) Lehn, J.-M.; Mascal, M.; DeCian, A.; Fischer, J. *J. Chem. Soc., Perkin Trans. 2* **1992**, 461. (e) Kotera, M.; Lehn, J.-M.; Vigneron, J.-P. *J. Chem. Soc., Chem. Commun.* **1994**, 197.

(7) (a) Rebek, J. Jr *Angew. Chem.* **1990**, *102*, 261. (b) Blake, J. F.; Jorgensen, W. L.; *J. Am. Chem. Soc.* **1990**, *112*, 7278. (c) Diederich, F. *Angew. Chem., Int. Ed. Engl.* **1988**, *27*, 362. (d) Friedrichsen, B. P.; Powell, D. R.; Whitlock, H. W. *J. Am. Chem. Soc.* **1990**, *112*, 8931. (e) Hamilton, A. D.; Pant, N.; Muehkdorf, A. *Pure Appl. Chem.* **1988**, *60*, 533. (f) Tecilla, P.; Chang, S.-K.; Hamilton, A. D. *J. Am. Chem. Soc.* **1990**, *112*, 9586. (g) Zimmerman, S. C.; Wu, W. J. *J. Am. Chem. Soc.* **1989**, *111*, 8054. (h) Kelly, T. R.; Maguire, M. P. *J. Am. Chem. Soc.* **1987**, *109*, 6549. (i) Kelly, T. R.; Bridger, G. J. *J. Am. Chem. Soc.* **1990**, *112*, 8024. (j) Bell, T. W.; Liu, J. *J. Am. Chem. Soc.* **1988**, *110*, 3673. (k) Nowick, J. S.; Powell, N. A.; Martinez, E. J.; Smith, E. M.; Noronha, G. *J. Org. Chem.* **1992**, *57*, 3763.

(8) (a) Garcia-Tellado, F.; Geib, S. J.; Goswami, S.; Hamilton, A. D. *J. Am. Chem. Soc.* **1991**, *113*, 9265. (b) Fan, E.; Arman, S. A. Kincaid, V.; S.; Hamilton, A. D. *J. Am. Chem. Soc.* **1993**, *115*, 369. (c) Yang, J.; Fan, E.; Geib, S. J.; Hamilton, A. D. *J. Am. Chem. Soc.* **1993** *115*, 5314. (d) Geib, S. J.; Vicent, C.; Fan, E.; Hamilton, A. D. *Angew. Chem., Int. Ed. Engl.* **1993**, *32*, 119.

(9) (a) Nethaji, M.; Pattabi, V. *Acta Crystallogr.* **1989**, *C45*, 509. (b) Low, J. N.; Wilson, C. C. *Acta Crystallogr.* **1983**, *C39* , 1688. (c) Kadooka, M. M.; Chang, M. Y. ; Fukami, H.; Scheuer, P. J.; Solheim, B. A.; Springer, J. P. *Tetrahedron* **1976**, *32*, 919. (d) Kvick, A.; Booles, S. S. *Acta Crystallogr.*, **1972**, *B28*, 3405.

(10) (a) Su, D.; Wang, X.; Simard, M.; Wuest, J. D. *Supramolecular Chemistry*, in press. (b) Wang, X.; Simard, M.; Wuest, J. D. *J. Am. Chem. Soc.* **1994**, *116*, 12119. (c) Wuest, J. D. In *Mesomolecules: From Molecules to Materials* eds. Mendenhall, G. D.; Greenberg, A.; Liebman, J. F.; Chapman & Hall, New York, in press. (d) Persico, F.; Wuest, J. D. *J. Org. Chem.* **1993**, *58*, 95. (e) Simard, M.; Su, D.; Wuest, J. D. *J. Am. Chem. Soc.* **1991**, *113*, 4696. (f) Gallant, M.; Phan Viet, M. T.; Wuest, J. D. *J. Org. Chem.* **1991**, *56*, 2284. (g) Ducharme, Y., Wuest, J. D. *J. Org. Chem.* **1988**, *53*, 5787.

(11) Ducharme, Y.; Wuest, J. D., unpublished results.

(12) Wang, X.; Wuest, J. D., unpublished results.

(13) For related work, see: (a) Ermer, O. *J. Am. Chem. Soc.* **1988**, *110*, 3747. (b) Ermer, O.; Lindenberg, L. *Helv. Chim. Acta* **1988**, *71*, 1084. (c) Ermer, O.; Eling, A. *Angew. Chem., Int. Ed. Engl.* **1988**, *27*, 829. (d) Ermer, O.; Lindenberg, L. *Chem. Ber.* **1990**, *123*, 1111. (e) Ermer, O.; Lindenberg, L. *Helv. Chim. Acta* **1991**, *74*, 825.

(14) For discussions of related hydrogen-bonded clathrates, see: (a)Weber, E.; Czugler, M. *Top. Curr. Chem.* **1988**, *149*, 45. (b) Weber, E. *Top. Curr. Chem.* **1987**, *140*, 1.

(15) (a) Pauling, L. *The Nature of the Chemical Bond* 2nd Edn., Cornell University Press, **1948**. (b) Endo, S.; Tsuboi, T.; Koto, K. *Nature* **1989**, *340*, 452.

(16) For other recent references describing molecules designed to participate in complex networks of hydrogen bonds, see: (a) Hanessian, S.; Gomtsyan, A.; Simard, M.; Roelens, S. *J. Am. Chem. Soc.* **1994**, *116*, 4395. (b) Russell, V. A.; Etter, M.C.; Ward, M.D. *J. Am. Chem. Soc.* **1994**, *116*, 1941. (c) Bfanda, N.; Wuler, R.; Rebek, J., Jr. *Science* **1994**, *263*, 1267. (d) Yang, J.; Marendaz, J.-L.; Geib, S. J.; Hamilton, A. D. *Tetrahedron Lett.* **1994**, *35*, 3665-3668.

(17) Neugebauer, F. A.; Fischer, H.; Bernhardt, R. *Chem. Ber.* **1976**, *109*, 2389.

(18) Merkushev, E. B.; Simakhina, N. D.; Koveshnikova, G. M. *Synthesis* **1980**, 486.

(19) Sakamoto, T.; Shiraiwa, M.; Yamanaka, H. *Synthesis* **1983**, 312.

(20) Marsh, J. P.; Goodman, L. *J. Org. Chem.* **1965**, *30*, 2491.

(21) (a) Gavezzotti, A.; Filippini, G. *Mol. Cryst. Liq. Cryst.* **1993**, *235*, 225. (b) Gavezzotti, A. *J. Am. Chem. Soc.* **1991**, *113*, 4622.

(22) (a) Kitaigorodsky, A. I. *Molecular Crystals and Molecules* Academic Press, **1973**. (b) Pertsin, A. J.; Kitaigorodsky, A. I. *The Atom-Atom Potential Method* Springer-Verlag, **1987**.

(23) Herbstein, F. H. *Topics in Current Chemistry* **1987**, *140*, 107, ed. Weber, E. (Springer-Verlag)

(24) (a) Hunter, C. A. *Chem. Soc. Rev.* **1994**, 101-109 and the references therein. (b) Hunter, C. A. *Angew. Chem., Int. Ed. Engl.* **1993**, *32*, 1584. (c) Hunter, C. A., Sanders, J. K. M. *J. Am. Chem. Soc.* **1990**, *112*, 5525.

(25) For π-π interactions in combination with hydrogen bonding see (a) Bisson, A. P.; Carver, F. J.; Hunter, C. A.; Waltho, J. P. *J. Am. Chem. Soc.* **1994**, *116*, 10292 and the references therein . (b) Gunter, M. J.; Hockless, D. C. R.; Johnston, M. R.; Skelton, B. W.; White, A. H. *J. Am. Chem. Soc.* **1994**, *116*, 4810 and the references therein. (c) Beeson, J. C.; Fitzgerald, L. J.; Gallucci, J. C.; Gerkin, E. R.; Rademacher, J. T.; Czarnik, A. W. *J. Am. Chem. Soc.* **1994**, *116*, 4621 and the references therein.

(26) Richard, L.; Wuest, J. D., unpublished results.

(27) Bargar, T. M.; Wilson, T.; Daniel, J. K. *J. Heterocyclic Chem.* **1985**, *22*, 1583.

(28) Tee, O. S.; Paventi, M. *J. Am. Chem. Soc.* **1982**, *104*, 4142.

(29) *Chemical Abstracts* **1970**, *72*, 21574s

(30) Shiao, M.-J.; Tarng, K.-Y. *Heterocycles* **1990**, *31*, 819.

(31) (a) Kajigaeshi, S.; Kakinami, T.; Inoue, K.; Kondo; M. Nakamura, H.; Fujikawa, M.; Okamoto, T. *Bull. Chem. Soc. Jpn.* **1988**, *61*, 597. (b) Kajigaeshi, S.; Kakinami,

T.; Yamasaki, H.; Fujisaki, S.; Okamoto, T. *Bull. Chem. Soc. Jpn.* **1988**, *61*, 600. (c) Kajigaeshi, S.; Kakinami, T.; Yamasaki, H.; Fujisaki, S.; Okamoto, T. *Bull. Chem. Soc. Jpn.* **1988**, *61*, 2681.

(32) (a) Satyamurthy, N.; Barrio, J. R. *J. Org. Chem.* **1983**, *48*, 4394. (b) Ku, H.; Barrio, J. R. *J. Org. Chem.* **1981**, *46*, 5239.

(33) Moore, J. S.; Weinstein, E. J.; Wu, Z. *Tetrahedron Lett.* **1991**, *32*, 2465.

(34) Berthelot, J.; Guette, C.; Essayegh, M.; Desbene, P. L.; Basselier, J. J. *Synth. Commun* . **1986**, *16*, 1641.

(35) (a) Fujimoto, A.; Inuzuka, K. *Bull. Chem. Soc. Jpn.* **1990**, *63*, 2292. (b) Adamo, C.; Barone, v.; Loison, S.; Minichino, C. *J. Chem. Soc., Perkin Trans. 2* **1993**, 697. (c) Bordwell, F. G.; Singer, D. L., Satish, A. V. *J. Am. Chem. Soc.* **1993**, *115*, 3543. (d) Parchment, G. O.; Burton, N. A.; Hillier, I. H. *Chem. Phys. Lett.* **1993**, 46. (e) Parchment, G. O.; Burton, N. A.; Hillier, I. H. *J. Chem. Soc., Perkin Trans. 2* **1993**, 861. (f) Doig, J. A.; Williams, D. H. *J. Am. Chem. Soc.* **1992**, *114*, 338.

(36) (a) Beak, P.; Covington, J. B.; Smith, S. G.; White, J. M.; Zeigler, J. M. *J. Org. Chem.* **1980**, *45*, 1354. (b) Beak, P. *Acc. Chem. Res.*, **1977**, *10*, 186. (c) Beak, P.; Covington, J. B.; Smith, S. G. *J. Am. Chem. Soc.* **1976**, *98*, 186.

(37) (a) Rousseau, R. J.; Robins, R. K. *J. Heterocyclic Chem.* **1965**, *2*, 196. (b) Daisley, R. W.; Hanbali, J. R. *Org. Prep. Proced. Int.* **1983**, *15*, 280. (c) Cummins, C. H. *Tetrahedron Lett.* **1994**, *35*, 857.

(38) Negishi, E.; Okukado, N.; Lovich, S. F.; Luo, F.-T. *J. Org. Chem.* **1984**, *49*, 2629.

(39) (a) Holmes, A. B.; James, G. E. *Tetrahedron Lett.* **1980**, *21*, 3111-3112. (b) Holmes, A. B.; Jennings-White, C. L. D.; Schulthess, A. H. *J. Chem. Soc., Chem. Commun.* **1979**, 840.

(40) Wityak, J. *Synth. Comm.* **1991**, *21*, 977.

(41) Miller, J. A.; Zweifel, G. *Synthesis* **1983**, 128.

(42) Aakeröy, C. B.; Seddon, K. R. *Chem. Soc. Rev.* **1993**, 397.

(43) (a) Gavezzotti, A.; Filippini, G. *J. Phys. Chem.* **1994**, 4831. (b) Filippini, G.; Gavezzotti, A. *Acta Crystallogr.* **1993**, *B49*, 868. (c) Gavezzotti, A.; Filippini, G. *Acta Crystallogr.* **1992**, *B48*, 537. (d) Gavezzotti, A *J. Am. Chem. Soc.* **1989**, *111*, 1835. (e) Gavezzotti, A.; Filippini, G. *Synthetic Metals* **1991**, *40*, 257.

(44) Michopoulos, Y.; Adam, C. D. *Mol. Phys.* **1991**, *72*, 899.

(45) Coulson, D.R. *Inorg. Synth.* **1972**, *13*, 121.

(46) Still, W. C.; Khan, M.; Mitra, A. *J. Org. Chem.* **1978**, *43*, 2923.

APPENDIX 1

CRYSTAL AND MOLECULAR STRUCTURE OF

TECTON I·8 $CH_3CH_2CO_2H$

Crystallographic report for TECTON **I**·8 $CH_3CH_2CO_2H$

$C_{53}H_{32}N_4O_4.8C_3H_6O_2$	FW = 1381.50	T_m = 200K
Tetragonal	$P4_2/n$	Z = 2
a = b = 21.977(2)	c = 7.7866(9)Å	V = 3760.7(6)Å^3
d_c = 1.220 Mg m^{-3}	μ = 6.94 cm^{-1}	λ(CuKα) = 1.54178Å

Crystal size = 0.17 x 0.27 x 0.27 mm^3

Crystals suitable for X-ray diffraction obtained from a Propionic acid/hexane mixture (1:1). Crystal bounded by {110}, {1$\bar{1}$0}, {10$\bar{1}$}; dimensions 0.17 x 0.27 x 0.27mm. Unit cell from 25 well-centered reflections in the range $20 \leq \theta \leq 22°$. Nonius CAD-4 diffractometer, graphite monochromatized CuK$\bar{\alpha}$ radiation, ω scan technique, $\Delta\omega = (1.00 + 0.14 \tan\theta)°$, $2\theta_{max} = 140.0°$ ($0 \leq h \leq 26$, $0 \leq k \leq 26$, $0 \leq \ell \leq 9$). Orientation monitored every 200 measurements, intensity checked every hour using 5 standard reflections, largest intensity fluctuation ±0.8%. A set of 3765 independent reflections was collected at 200K of which 2460, such that $I \geq 1.96\sigma(I)$, were retained for structure determination and refinement. Lp corrections, no absorption correction.

The structure was solved by direct-methods (SHELXS-86)* and difference Fourier synthesis (SHELX-76). Molecule found on the $\bar{4}$ symmetry equipoint

*The programs used here are modified versions of NRC-2, data reduction, NRC-10, bond distances and angles and NRC-22, mean planes (Ahmed, Hall, Pippy and Huber, 1973); SHELXS-86, multisolution program (Sheldrick, 1986); SHELX-76, program for structure determination (Sheldrick, 1976) and ORTEP, stereodrawings (Johnson, 1965).

corresponding to 1/4 of the molecule par asymmetric unit. Full-matrix least-squares refinement based on F's, all non-hydrogen atoms anisotropic, hydrogen atoms initially calculated at idealized positions refined in the last cycles.

Function minimized: $\Sigma w(|Fo| - |Fc|)^2$. Final R=0.057, wR=0.048 (weights derived from the counting statistics $w=1/\sigma^2(F)$) and S=2.46 for 308 refined parameters. Maximum $(\Delta/\sigma)=0.47$, average $(\Delta/\sigma)=0.03$; in the final difference Fourier synthesis, general background in the range -0.23,+0.22, e/Å^3.

The scattering curves for the nonhydrogen atoms were taken from Cromer and Mann (1968) and those for the H-atoms from Stewart, Davidson, and Simpson (1965).

Table I. Atomic coordinates (x 10^5) and equivalent isotropic temperature factors (x 10^3) for the non-hydrogen atoms of TECTON I·8 $CH_3CH_2CO_2H$

ATOM	X	Y	Z	U_{eq}
O(14)	7343(9)	60591(9)	-8626(24)	71
N(14)	7894(9)	50774(10)	54(27)	49
C(1)	25000	25000	75000	34
C(2)	20870(10)	28684(10)	62783(27)	36
C(3)	17515(11)	25571(11)	50324(31)	44
C(4)	14260(11)	28619(12)	37906(31)	47
C(5)	14257(11)	34922(11)	37376(30)	43
C(6)	17507(13)	38074(12)	49746(34)	52
C(7)	20749(12)	34975(11)	62211(32)	47
C(8)	11400(11)	38181(12)	23566(33)	52
C(9)	9453(12)	40972(12)	11733(33)	54
C(10)	7610(11)	44614(12)	-2579(32)	48
C(11)	5935(13)	42447(13)	-18122(35)	58
C(12)	4750(13)	46630(14)	-31384(35)	62
C(13)	5159(13)	52697(13)	-28706(35)	58
C(14)	6786(11)	55002(12)	-12320(36)	53
O(211)	4397(15)	70531(10)	-26170(32)	128
O(212)	1601(11)	65425(9)	-49136(27)	84
C(21)	2640(15)	70148(15)	-42244(43)	75
C(22)	1990(19)	76240(15)	-50495(52)	100
C(23)	277(20)	75921(18)	-68790(54)	108
O(311)	13419(11)	64703(11)	18575(33)	100
O(312)	12115(11)	55659(12)	30605(28)	95
C(31)	14086(16)	60666(21)	31115(48)	88
C(32)	17828(21)	62608(23)	46850(58)	125
C(33)	20293(30)	68315(36)	45304(71)	198

Table II. Distances and angles.

Bond	Distances (esd's), Å	Bonds	Angles (esd's), deg
C(1)-C(2)	1.544(2)	C(2)-C(1)-C(2)[a]	103.94(11)
C(2)-C(3)	1.397(3)	C(2)-C(1)-C(2)[b]	112.31(11)
C(2)-C(7)	1.384(3)	C(1)-C(2)-C(3)	118.8(2)
C(3)-C(4)	1.377(4)	C(1)-C(2)-C(7)	123.7(2)
C(4)-C(5)	1.386(4)	C(2)-C(3)-C(4)	121.6(2)
C(5)-C(6)	1.385(4)	C(3)-C(4)-C(5)	120.5(2)
C(5)-C(8)	1.436(4)	C(4)-C(5)-C(6)	118.6(2)
C(6)-C(7)	1.383(4)	C(5)-C(6)-C(7)	120.5(2)
C(8)-C(9)	1.187(4)	C(6)-C(7)-C(2)	121.6(2)
C(9)-C(10)	1.431(4)	C(7)-C(2)-C(3)	117.2(2)
C(10)-C(11)	1.352(4)	C(4)-C(5)-C(8)	121.4(2)
C(10)-N(14)	1.371(3)	C(6)-C(5)-C(8)	119.8(2)
C(11)-C(12)	1.407(4)	C(5)-C(8)-C(9)	175.2(3)
C(12)-C(13)	1.352(4)	C(8)-C(9)-C(10)	174.9(3)
C(13)-C(14)	1.419(4)	C(9)-C(10)-C(11)	125.3(2)
C(14)-N(14)	1.360(4)	C(9)-C(10)-N(14)	115.0(2)
C(14)-O(14)	1.267(3)	C(10)-C(11)-C(12)	118.5(3)
		C(11)-C(12)-C(13)	121.2(3)
		C(12)-C(13)-C(14)	120.5(3)
		C(13)-C(14)-N(14)	116.0(2)
		C(14)-N(14)-C(10)	124.1(2)
		N(14)-C(10)-C(11)	119.6(2)
		C(13)-C(14)-O(14)	125.1(2)
		N(14)-C(14)-O(14)	118.9(2)
C(21)-O(211)	1.312(4)	O(211)-C(21)-O(212)	122.8(3)
C(21)-O(212)	1.191(4)	O(211)-C(21)-C(22)	112.4(3)
C(21)-C(22)	1.492(5)	O(212)-C(21)-C(22)	124.7(3)
C(22)-C(23)	1.475(6)	C(21)-C(22)-C(23)	113.4(3)
C(31)-O(311)	1.327(5)	O(311)-C(31)-O(312)	123.8(4)
C(31)-O(312)	1.183(5)	O(311)-C(31)-C(32)	117.4(3)
C(31)-C(32)	1.536(6)	O(312)-C(31)-C(32)	118.8(4)
C(32)-C(33)	1.372(9)	C(31)-C(32)-C(33)	113.3(4)

a: 1/2-x, 1/2-y, z b: either y, 1/2-x, 3/2-z or 1/2-y, x, 3/2-z

Table III. Bond distances (Å) and angles (deg) related to the hydrogen bonding.

Bond (A-H···B)	Distances (esd's) A-B	A-H	H-B	Angles (esd's) A-H-B
N(14)-H(14)···O(312)	2.770(3)	0.92(2)	1.86(2)	173(2)
O(211)-H(211)···O(14)	2.657(3)	1.10(3)	1.67(2)	164(2)
O(311)-H(311)···O(14)	2.662(3)	0.97(2)	1.70(2)	170(2)

Bonds	Angles (esd's), deg	Bonds	Angles (esd's), deg
C(10)-N(14)···O(312)	121.8(2)	C(10)-N(14)-H(14)	123.6(12)
C(14)-N(14)···O(312)	113.8(2)	C(14)-N(14)-H(14)	112.3(12)
C(31)-O(312)···N(14)	120.8(2)	C(31)-O(312)···H(14)	120.7(7)
C(21)-O(211)···O(14)	120.6(2)	C(21)-O(211)-H(211)	110.7(14)
C(14)-O(14)···O(211)	131.0(2)	C(14)-O(14)···H(211)	125.0(9)
C(31)-O(311)···O(14)	114.4(2)	C(31)-O(311)-H(311)	116.7(15)
C(14)-O(14)···O(311)	123.9(2)	C(14)-O(14)···H(311)	126.4(8)

Table IV. Anisotropic temperature factors (x 10^4).

ATOM	U11	U22	U33	U12	U13	U23
O(14)	913(12)	544(10)	659(11)	-29(10)	-204(10)	75(10)
N(14)	503(11)	571(12)	406(10)	30(10)	-102(10)	41(10)
C(1)	375(12)	375(12)	264(16)	0	0	0
C(2)	384(11)	400(11)	286(10)	33(9)	24(10)	1(10)
C(3)	540(12)	402(11)	379(11)	33(11)	-89(11)	-11(11)
C(4)	544(13)	506(13)	365(11)	19(11)	-105(11)	-21(11)
C(5)	449(12)	513(12)	340(11)	83(11)	3(11)	44(11)
C(6)	686(14)	402(12)	483(12)	88(12)	-51(12)	23(12)
C(7)	596(13)	418(12)	383(11)	33(11)	-93(11)	-43(11)
C(8)	522(13)	579(13)	451(12)	100(11)	13(12)	49(12)
C(9)	520(13)	583(13)	509(13)	100(12)	-20(12)	72(12)
C(10)	465(12)	537(13)	444(12)	55(11)	-70(11)	72(11)
C(11)	689(14)	527(13)	518(13)	50(12)	-143(12)	40(12)
C(12)	710(15)	661(15)	504(13)	65(13)	-220(13)	4(13)
C(13)	654(14)	617(14)	479(13)	2(12)	-190(12)	88(12)
C(14)	506(13)	560(13)	526(13)	-2(12)	-88(12)	102(12)
O(211)	2321(18)	575(12)	933(14)	-9(14)	-633(15)	50(12)
O(212)	1157(14)	564(11)	800(12)	-25(11)	-141(12)	49(11)
C(21)	877(16)	568(14)	816(16)	-13(14)	-146(15)	72(14)
C(22)	1289(19)	592(15)	1107(18)	32(16)	-296(17)	263(15)
C(23)	1239(19)	842(17)	1170(18)	62(16)	-346(17)	350(16)
O(311)	1135(15)	945(14)	916(14)	-156(12)	-215(13)	-192(13)
O(312)	1150(15)	1092(14)	595(12)	6(13)	-168(12)	-134(12)
C(31)	785(16)	1170(18)	680(16)	104(16)	-71(15)	-198(17)
C(32)	1220(19)	1276(19)	1261(19)	-174(18)	-313(18)	-428(18)
C(33)	2163(21)	2244(21)	1528(20)	-378(21)	-491(20)	167(21)

Table V. Refined hydrogen coordinates (x 10^4) and refined isotropic temperature factors (x 10^3) for TECTON I·8 $CH_3CH_2CO_2H$

ATOM	X	Y	Z	U_{iso}
H(3)	1773(9)	2115(9)	5042(17)	50(2)
H(4)	1199(9)	2647(9)	3000(18)	51(2)
H(6)	1738(10)	4234(10)	4919(18)	66(2)
H(7)	2303(9)	3725(9)	6991(18)	48(2)
H(11)	567(10)	3787(10)	-2006(18)	76(2)
H(12)	367(10)	4472(10)	-4217(18)	73(2)
H(13)	476(10)	5590(10)	-3771(19)	81(2)
H(14)	900(10)	5251(10)	1029(18)	67(2)
H(211)	520(13)	6636(13)	-2127(20)	140(2)
H(221)	632(13)	7857(12)	-4960(20)	141(2)
H(222)	-97(13)	7836(14)	-4473(20)	154(2)
H(231)	23(12)	8046(12)	-7395(20)	128(2)
H(232)	-273(14)	7304(14)	-7100(21)	167(2)
H(233)	403(14)	7385(14)	-7498(20)	163(2)
H(311)	1085(13)	6351(13)	896(20)	130(2)
H(321)	2170(13)	5939(13)	4880(20)	146(2)
H(322)	1511(13)	6241(13)	5856(20)	138(2)
H(331)	2288(15)	6940(15)	5530(21)	200(2)
H(332)	1684(15)	7127(15)	4366(21)	179(2)
H(333)	2307(14)	6836(15)	3389(20)	185(2)

Table VI. Distances and angles related to the refined hydrogen atoms.

Bond	Distances (esd's), Å	Bonds	Angles (esd's), deg
C(3)-H(3)	0.97(2)	C(2)-C(3)-H(3)	117.3(11)
		C(4)-C(3)-H(3)	121.1(11)
C(4)-H(4)	0.92(2)	C(3)-C(4)-H(4)	120.0(11)
		C(5)-C(4)-H(4)	119.4(11)
C(6)-H(6)	0.94(2)	C(5)-C(6)-H(6)	116.9(12)
		C(7)-C(6)-H(6)	122.6(12)
C(7)-H(7)	0.93(2)	C(6)-C(7)-H(7)	117.8(11)
		C(2)-C(7)-H(7)	120.5(11)
C(11)-H(11)	1.02(2)	C(10)-C(11)-H(11)	119.7(12)
		C(12)-C(11)-H(11)	121.7(12)
C(12)-H(12)	0.97(2)	C(11)-C(12)-H(12)	113.5(12)
		C(13)-C(12)-H(12)	125.3(12)
C(13)-H(13)	1.00(2)	C(12)-C(13)-H(13)	125.6(12)
		C(14)-C(13)-H(13)	113.7(12)
C(22)-H(221)	1.08(3)	C(21)-C(22)-H(221)	108(1)
C(22)-H(222)	0.92(3)	C(21)-C(22)-H(222)	108(2)
		C(23)-C(22)-H(221)	108(1)
		C(23)-C(22)-H(222)	108(2)
		H(221)-C(22)-H(222)	111(2)
C(23)-H(231)	1.08(3)	C(22)-C(23)-H(231)	109(1)
C(23)-H(232)	0.93(3)	C(22)-C(23)-H(232)	113(2)
C(23)-H(233)	1.06(3)	C(22)-C(23)-H(233)	105(1)
		H(231)-C(23)-H(232)	124(2)
		H(231)-C(23)-H(233)	104(2)
		H(232)-C(23)-H(233)	100(2)

Table VI. (continued)

Bond	Distances (esd's), Å	Bonds	Angles (esd's), deg
C(32)-H(321)	1.12(3)	C(31)-C(32)-H(321)	110(1)
C(32)-H(322)	1.09(2)	C(31)-C(32)-H(322)	111(1)
		C(33)-C(32)-H(321)	107(1)
		C(33)-C(32)-H(322)	109(1)
		H(321)-C(32)-H(322)	106(2)
C(33)-H(331)	0.99(2)	C(32)-C(33)-H(331)	112(2)
C(33)-H(332)	1.01(3)	C(32)-C(33)-H(332)	108(2)
C(33)-H(333)	1.08(2)	C(32)-C(33)-H(333)	108(2)
		H(331)-C(33)-H(332)	112(2)
		H(331)-C(33)-H(333)	109(2)
		H(332)-C(33)-H(333)	108(2)

Table VII. Distances to the weighted least-squares planes.

Distances to the plane (esd's), Å

Phenyl plane

C(2)*	0.004(2)	C(5)*	0.006(2)
C(3)*	-.001(2)	C(6)*	-.003(3)
C(4)*	-.005(2)	C(7)*	-.004(3)
C(1)	0.172(2)	C(8)	0.137(2)
C(9)	0.338(3)	C(10)	0.670(2)

Pyridone plane

C(10)*	-.006(2)	C(13)*	-.001(3)
C(11)*	0.013(2)	C(14)*	0.006(3)
C(12)*	-.010(3)	N(14)*	0.000(2)
C(5)	0.627(2)	C(8)	0.296(2)
C(9)	0.119(3)	C(10)	0.019(2)

Propionic acid planes

Acid(2xx)

O(211)*	0.007(3)	O(212)*	-.003(2)
C(21)*	0.002(3)	C(22)*	-.028(4)
C(23)*	0.024(4)		

Acid(3xx)

O(311)*	-.001(2)	O(312)*	0.008(2)
C(31)*	-.019(4)	C(32)*	-.028(5)
C(33)*	0.056(7)		

* Atoms used in the plane calculation

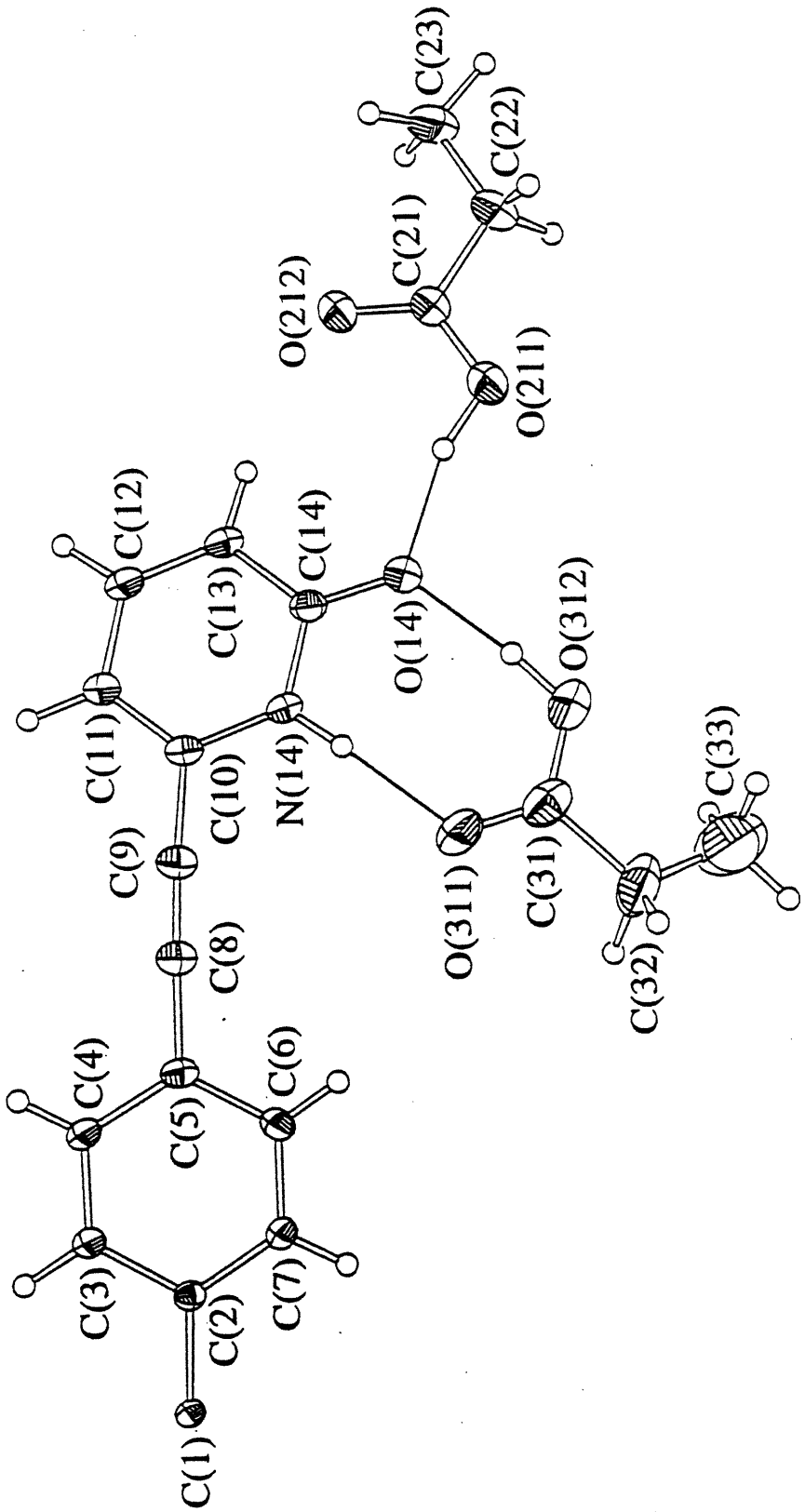
C(23)
C(22)
C(21)
O(212)
O(211)
C(12)
C(14)
C(13)
O(14)
O(312)
C(11)
C(10)
N(14)
C(9)
O(311)
C(31)
C(33)
C(8)
C(32)
C(4)
C(6)
C(5)
C(3)
C(7)
C(2)
C(1)

Figure 1

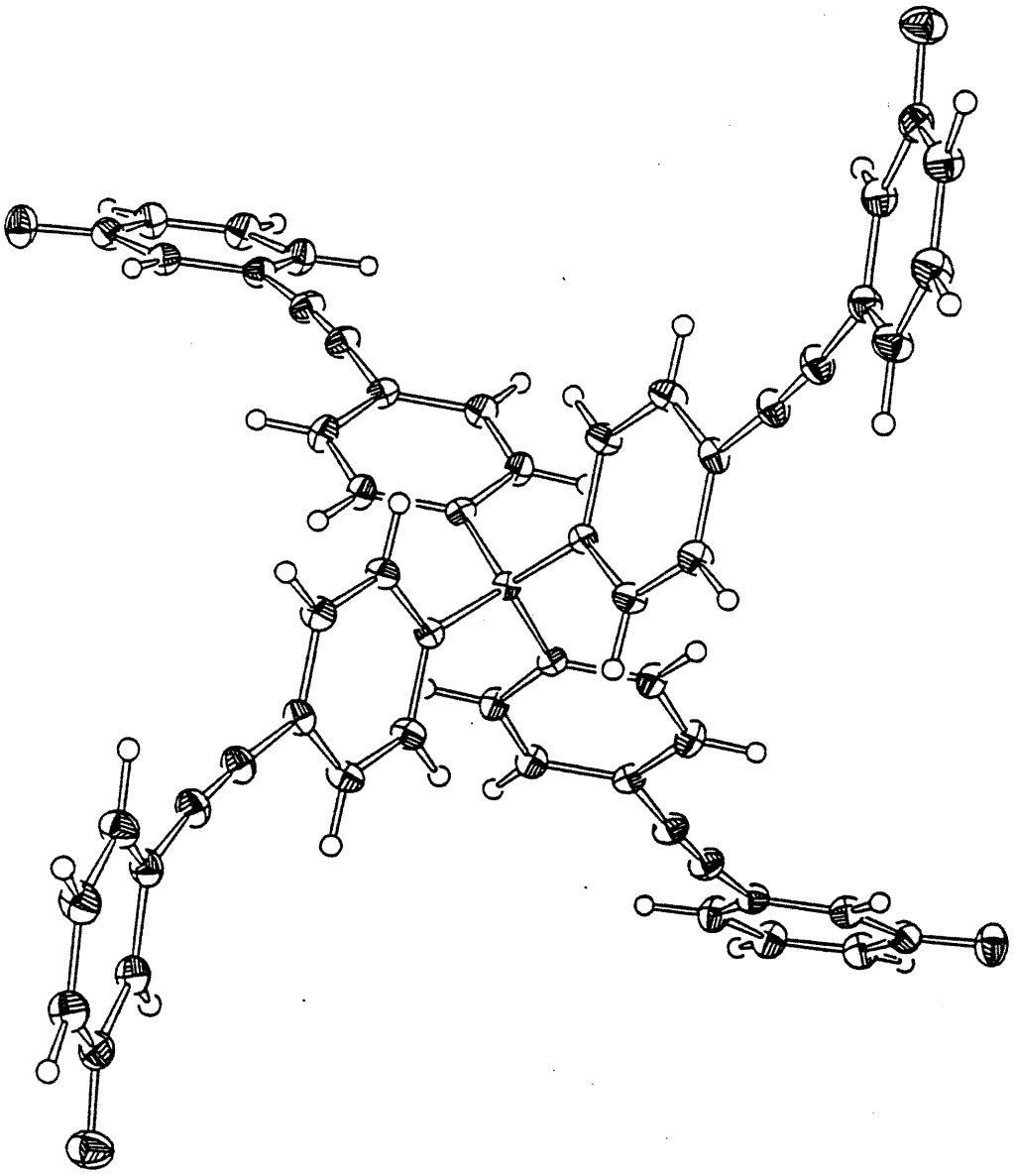

Figure 2

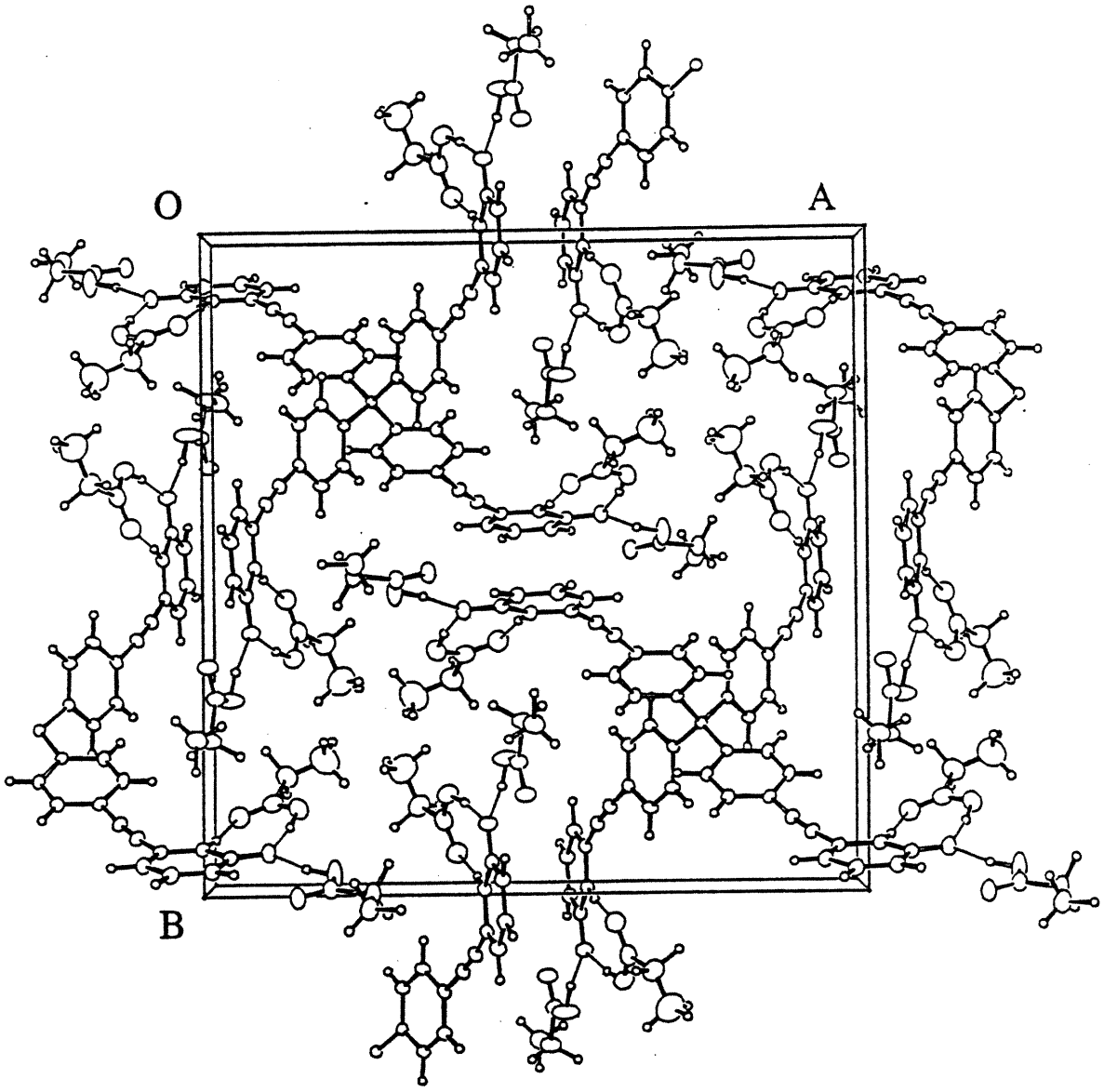

Figure 3

CAPTIONS

Figure 1. Asymmetric unit for TECTON I·8 $CH_3CH_2CO_2H$. Non-hydrogen atoms represented at 50% probability level, hydrogens by spheres of arbitrary size.

Figure 2. Complete molecule shown down the $\bar{4}$ axis.

Figure 3. ORTEP view of the cell down c axis showing the packing arrangement.

APPENDIX 2

CRYSTAL AND MOLECULAR STRUCTURE OF

TECTON I·2 $CH_3CH_2CH_2CO_2H$

Crystallographic report for TECTON I·2 $CH_3CH_2CH_2CO_2H$

$C_{53}H_{32}N_4O_4.2C_4H_8O_2$	FW = 965.07	T_m = 180 K
Monoclinic	C2/c	Z = 4
a = 31.249(7)	b = 7.350(4)	c = 23.145(6)Å
β = 104.69(2)°	V = 5142(3)Å^3	d_c = 1.247 Mg m^{-3}
μ = 6.36 cm^{-1}	λ(CuKα) = 1.54178Å	

Crystal size = 0.08 x 0.14 x 0.32 mm^3

Crystals suitable for X-ray diffraction obtained directly from a Butanoic acid solution of the pyridone. Crystal bounded by {10$\bar{1}$}, {100}, {010}; dimensions 0.08 x 0.14 x 0.32mm. Unit cell from 25 well-centered reflections in the range 41 ≤ 2θ ≤ 49°. Nonius CAD-4 diffractometer, graphite monochromatized CuKᾱ radiation, ω/2θ scan technique, $\Delta\omega = (0.80 + 0.14 \tan\theta)°$, $2\theta_{max}$ = 140.0° (limiting indices -38≤h≤38, -8≤k≤8, -28≤ℓ≤28), 22077 reflections was collected at 200K. Orientation monitored every 200 measurements, intensity checked every hour using 6 standard reflections, largest intensity fluctuation ±3.8%. A set of 4874 independent reflections was obtained after averaging to 2/m Laue symmetry of which 1880, such that I≥1.96σ(I), were retained for structure determination and refinement. Lp corrections, no absorption correction.

The structure was solved by direct-methods (SHELXS-86)* and difference

*The programs used here are modified versions of NRC-2, data reduction, NRC-10, bond distances and angles and NRC-22, mean planes (Ahmed, Hall, Pippy and Huber, 1973); SHELXS-86, multisolution program (Sheldrick, 1986); SHELX-76, program for structure determination (Sheldrick, 1976) and ORTEP, stereodrawings (Johnson, 1965).

Fourier synthesis (SHELX-76). Full-matrix least-squares refinement based on F's, all non-hydrogen atoms of the pyridone molecule anisotropic, hydrogen atoms calculated at idealized positions not refined. Molecules found on the two-fold axis equipoint corresponding to 1/2 of the pyridone molecule par asymmetric unit. Solvent molecules found included in the canal largely desordered. Major desorder resolved with acid molecules presenting two acid ends. Minor desorder not resolved but introduced to lower the R factor and permitting to get a much refined model for the adamantanoid cage. Solvent refined isotropically. Minor desorder introduced with common isotropic temperature factor, initially refined, then fixed at the end of the refinement. Occupancies of the minor unresolved model refined. All minor desorder introduced as carbon type atoms.

Function minimized: $\Sigma w(|Fo| - |Fc|)^2$. Final R=0.060, wR=0.058 (weights derived from the counting statistics $w^{-1} = \sigma^2(F) + 0.0001F^2$) and S=1.86 for 336 refined parameters. Maximum (Δ/σ)=0.54, average (Δ/σ)=0.02; in the final difference Fourier synthesis, general background in the range -0.21,+0.16, e/Å^3.

The scattering curves for the nonhydrogen atoms were taken from Cromer and Mann (1968) and those for the H-atoms from Stewart, Davidson, and Simpson (1965).

Table I. Atomic coordinates (x 10^4; C(4X), × 10^3) and equivalent isotropic temperature factors (x 10^3) for the non-hydrogen atoms of TECTON I· 2 $CH_3CH_2CH_2CO_2H$.

ATOM	X	Y	Z	U_{eq}
O(114)	2816(1)	19498(5)	5081(2)	105
O(214)	381(1)	-1155(6)	-297(2)	97
N(114)	2241(1)	18707(6)	4323(2)	79
N(214)	457(1)	1675(7)	127(2)	79
C(1)	0	11145(10)	2500	70
C(12)	392(2)	12421(7)	2753(2)	68
C(13)	502(2)	13721(8)	2387(2)	80
C(14)	824(2)	14979(8)	2579(2)	80
C(15)	1060(2)	14972(8)	3185(2)	74
C(16)	952(2)	13690(8)	3556(2)	81
C(17)	626(2)	12437(8)	3358(2)	77
C(18)	1375(2)	16347(9)	3392(2)	85
C(19)	1617(2)	17581(10)	3561(2)	89
C(110)	1922(2)	19038(10)	3795(3)	87
C(111)	1903(2)	20710(10)	3555(3)	111
C(112)	2211(3)	22048(9)	3824(3)	123
C(113)	2529(2)	21671(9)	4333(3)	110
C(114)	2549(2)	19949(9)	4605(3)	88
C(22)	97(2)	9860(8)	2019(2)	73
C(23)	487(2)	9899(8)	1837(2)	82
C(24)	566(2)	8600(8)	1433(2)	82
C(25)	266(2)	7249(8)	1218(2)	73
C(26)	-136(2)	7220(8)	1388(2)	78

Table I. (continued)

ATOM	X	Y	Z	U_{eq}
C(27)	-211(2)	8513(8)	1785(2)	77
C(28)	373(2)	5831(9)	857(2)	83
C(29)	482(2)	4639(9)	592(2)	85
C(210)	672(2)	3271(10)	283(2)	89
C(211)	1072(2)	3558(10)	155(2)	117
C(212)	1245(2)	2083(11)	-113(3)	122
C(213)	1035(2)	501(10)	-254(2)	104
C(214)	605(2)	225(10)	-155(2)	85
O(311)	3276(7)	4975(31)	8013(10)	227
O(312)	3015(8)	4500(32)	8773(10)	262
O(341)	3304(8)	-1487(35)	8620(11)	294
O(342)	2894(8)	-1180(34)	7684(12)	285
C(31)	3191(7)	3906(28)	8380(9)	235
C(32)	3040(5)	2190(21)	8419(6)	213
C(33)	3302(5)	1358(26)	8172(8)	240
C(34)	3228(6)	-590(26)	8150(8)	231
C(41)[a]	302(1)	99(4)	776(1)	
C(42)[a]	326(1)	579(4)	870(1)	
C(43)[a]	329(1)	-205(4)	793(1)	
C(44)[a]	274(1)	391(5)	801(2)	
C(45)[a]	345(2)	328(6)	814(2)	
C(46)[a]	285(2)	582(5)	783(2)	
C(47)[a]	264(2)	201(6)	776(3)	

a: Atoms introduced with fixed isotropic temperature (U_{eq} = 0.30) corresponding to the unresolved desorder found in the canal.

Table II. Distances and angles for the resolved part.

Bond	Distances (esd's), Å	Bonds	Angles (esd's), deg
C(1)-C(12)	1.536(7)	C(12)-C(1)-C(22)	111.4(4)
C(12)-C(13)	1.377(7)	C(12)-C(1)-C(12)[a]	104.7(4)
C(12)-C(17)	1.406(6)	C(12)-C(1)-C(22)[a]	112.4(4)
C(13)-C(14)	1.356(8)	C(1)-C(12)-C(13)	119.2(4)
C(14)-C(15)	1.409(7)	C(1)-C(12)-C(17)	123.2(4)
C(15)-C(16)	1.373(8)	C(12)-C(13)-C(14)	123.5(5)
C(15)-C(18)	1.407(9)	C(13)-C(14)-C(15)	118.8(5)
C(16)-C(17)	1.364(8)	C(14)-C(15)-C(16)	118.4(5)
C(18)-C(19)	1.182(9)	C(15)-C(16)-C(17)	122.3(5)
C(19)-C(110)	1.445(10)	C(16)-C(17)-C(12)	119.7(5)
C(110)-C(111)	1.344(10)	C(17)-C(12)-C(13)	117.3(4)
C(110)-N(114)	1.389(7)	C(14)-C(15)-C(18)	118.7(5)
C(111)-C(112)	1.406(10)	C(16)-C(15)-C(18)	122.8(5)
C(112)-C(113)	1.363(10)	C(15)-C(18)-C(19)	175.6(7)
C(113)-C(114)	1.408(9)	C(18)-C(19)-C(110)	177.1(7)
C(114)-N(114)	1.366(8)	C(19)-C(110)-C(111)	124.6(6)
C(114)-O(114)	1.246(8)	C(19)-C(110)-N(114)	117.3(5)
		C(110)-C(111)-C(112)	120.2(6)
		C(111)-C(112)-C(113)	120.5(6)
		C(112)-C(113)-C(114)	120.6(6)
		C(113)-C(114)-N(114)	116.2(6)
		C(114)-N(114)-C(110)	124.4(5)
		N(114)-C(110)-C(111)	118.1(6)
		C(113)-C(114)-O(114)	125.3(6)
		N(114)-C(114)-O(114)	118.5(6)
C(1)-C(22)	1.547(7)	C(22)-C(1)-C(12)[a]	112.4(4)
C(22)-C(23)	1.387(8)	C(22)-C(1)-C(22)[a]	104.8(4)
C(22)-C(27)	1.391(8)	C(22)[a]-C(1)-C(12)[a]	111.4(4)
C(23)-C(24)	1.401(7)	C(1)-C(22)-C(23)	123.6(4)
C(24)-C(25)	1.370(8)	C(1)-C(22)-C(27)	118.2(4)
C(25)-C(26)	1.409(8)	C(22)-C(23)-C(24)	120.4(5)
C(25)-C(28)	1.428(8)	C(23)-C(24)-C(25)	121.1(5)
C(26)-C(27)	1.383(7)	C(24)-C(25)-C(26)	119.1(5)

Table II. (continued)

Bond	Distances (esd's), Å	Bonds	Angles (esd's), deg
C(28)-C(29)	1.169(8)	C(25)-C(26)-C(27)	119.3(5)
C(29)-C(210)	1.446(9)	C(26)-C(27)-C(22)	122.1(5)
C(210)-C(211)	1.372(10)	C(27)-C(22)-C(23)	118.1(5)
C(210)-N(214)	1.354(9)	C(24)-C(25)-C(28)	120.1(5)
C(211)-C(212)	1.422(10)	C(26)-C(25)-C(28)	120.7(5)
C(212)-C(213)	1.334(10)	C(25)-C(28)-C(29)	175.7(6)
C(213)-C(214)	1.434(9)	C(28)-C(29)-C(210)	172.7(6)
C(214)-N(214)	1.389(8)	C(29)-C(210)-C(211)	120.7(6)
C(214)-O(214)	1.229(8)	C(29)-C(210)-N(214)	119.7(5)
		C(210)-C(211)-C(212)	116.4(6)
		C(211)-C(212)-C(213)	123.6(6)
		C(212)-C(213)-C(214)	120.5(6)
		C(213)-C(214)-N(214)	113.8(5)
		C(214)-N(214)-C(210)	126.0(5)
		N(214)-C(210)-C(211)	119.5(6)
		C(213)-C(214)-O(214)	124.6(6)
		N(214)-C(214)-O(214)	121.6(6)
C(31)-O(311)	1.23(3)	O(311)-C(31)-O(312)	119.(2)
C(31)-O(312)	1.25(3)	O(311)-C(31)-C(32)	141.(2)
C(31)-C(32)	1.36(3)	O(312)-C(31)-C(32)	93.(2)
C(32)-C(33)	1.27(3)	C(31)-C(32)-C(33)	98.(2)
C(33)-C(34)	1.45(3)	C(32)-C(33)-C(34)	112.(2)
C(34)-O(341)	1.22(3)	O(341)-C(34)-O(342)	117.(2)
C(34)-O(342)	1.37(3)	O(341)-C(34)-C(33)	120.(2)
		O(342)-C(34)-C(33)	115.(2)

a: -x, y, 1/2 - z

Table III. Bond distances (Å) and angles (deg) related to the hydrogen bonding.

Bond (A-H···B)	Distances (esd's) A-B	A-H	H-B	Angles (esd's) A-H-B
N(114)-H(114)···O(114)[a]	2.758(6)	0.95(-)	1.82(-)	169(-)
N(214)-H(214)···O(214)[b]	2.771(6)	0.95(-)	1.83(-)	173(-)
O(311)-H(×)···O(341)[c]	2.95(3)			

Bonds	Angles (esd's), deg	Bonds	Angles (esd's), deg
C(110)-N(114)···O(114)[a]	117.8(4)	C(110)-N(114)-H(114)	118(-)
C(114)-N(114)···O(114)[a]	117.3(4)	C(114)-N(114)-H(114)	118(-)
C(114)-O(114)···N(114)[a]	123.8(4)	C(114)-O(114)···H(114)[a]	124(-)
C(210)-N(214)···O(214)[a]	120.3(4)	C(210)-N(214)-H(214)	117(-)
C(214)-N(214)···O(214)[a]	113.6(4)	C(214)-N(214)-H(214)	117(-)
C(214)-O(214)···N(214)[a]	124.8(4)	C(214)-O(214)···H(214)[a]	126(-)
C(31)-O(311)···O(341)[c]	102.7(16)	C(34)-O(341)···O(311)[d]	94.3(16)

a: 1/2-x, 7/2-y, 1-z
b: -x, -y, -z
c: x, 1+y, z
d: x, -1+y, z

Table IV. Anisotropic temperature factors (x 10^3).

ATOM	U11	U22	U33	U12	U13	U23
O(114)	99(3)	96(3)	107(3)	-15(2)	1(2)	-13(2)
O(214)	106(3)	117(3)	78(2)	-16(3)	39(2)	-19(2)
N(114)	74(3)	80(3)	80(3)	-4(3)	16(2)	-6(3)
N(214)	86(3)	107(4)	46(2)	-9(3)	19(2)	-7(3)
C(1)	76(4)	91(5)	44(3)	0	15(3)	0
C(12)	66(3)	93(4)	43(2)	-1(3)	8(2)	-4(3)
C(13)	83(3)	106(4)	47(3)	-9(3)	9(3)	2(3)
C(14)	79(3)	111(4)	46(3)	-11(3)	8(2)	2(3)
C(15)	64(3)	90(4)	64(3)	-10(3)	10(3)	-12(3)
C(16)	77(3)	111(4)	48(3)	-3(3)	2(3)	-4(3)
C(17)	77(3)	104(4)	45(2)	2(3)	7(2)	2(3)
C(18)	88(4)	101(4)	64(3)	-1(4)	17(3)	-5(3)
C(19)	92(4)	106(4)	71(3)	-3(4)	22(3)	-12(3)
C(110)	95(4)	99(4)	72(3)	6(4)	32(3)	0(4)
C(111)	120(4)	119(5)	93(4)	4(4)	25(3)	7(4)
C(112)	175(5)	97(5)	104(4)	-1(4)	51(4)	20(4)
C(113)	146(5)	84(4)	108(4)	-14(4)	45(4)	-3(4)
C(114)	86(4)	81(4)	99(4)	-15(4)	27(3)	-20(4)
C(22)	68(3)	109(4)	39(2)	-8(3)	10(2)	-3(3)
C(23)	79(3)	112(4)	51(3)	-11(3)	11(3)	-7(3)
C(24)	82(3)	114(4)	50(3)	-15(4)	18(3)	-8(3)
C(25)	89(4)	90(4)	40(2)	-1(3)	18(3)	-3(3)
C(26)	81(3)	103(4)	45(3)	-11(3)	7(3)	0(3)
C(27)	81(3)	103(4)	47(3)	-4(3)	19(3)	-5(3)

Table IV. (continued)

ATOM	U11	U22	U33	U12	U13	U23
C(28)	97(4)	97(4)	52(3)	-4(3)	15(3)	-5(3)
C(29)	97(4)	98(4)	58(3)	1(4)	17(3)	-8(3)
C(210)	89(4)	123(5)	54(3)	-19(4)	18(3)	-7(3)
C(211)	102(4)	171(5)	84(3)	-37(4)	35(3)	-37(4)
C(212)	90(4)	190(5)	96(4)	-31(4)	43(3)	-50(4)
C(213)	82(4)	151(5)	83(3)	-17(4)	29(3)	-39(4)
C(214)	96(4)	112(5)	51(3)	-2(4)	25(3)	-9(3)
O(311)[a]	227(6)					
O(312)[a]	262(6)					
O(341)[a]	294(6)					
O(342)[a]	285(6)					
C(31)[a]	235(5)					
C(32)[a]	213(5)					
C(33)[a]	240(5)					
C(34)[a]	231(5)					

a: Refined isotropically.

Table V. Calculated hydrogen coordinates (x 10^4) for TECTON **I**·2 CH_3CH_2-CH_2CO_2H.

ATOM	X	Y	Z
H(13)	344	13737	1978
H(14)	890	15848	2310
H(16)	1111	13676	3965
H(17)	558	11578	3627
H(111)	1681	20989	3202
H(112)	2197	23225	3650
H(113)	2740	22578	4505
H(114)	2244	17541	4501
H(23)	701	10811	1987
H(24)	832	8657	1307
H(26)	-353	6322	1232
H(27)	-481	8480	1901
H(211)	1226	4681	241
H(212)	1525	2232	-197
H(213)	1171	-450	-421
H(214)	179	1535	218
H(311)	3025	4732	8554
H(312)	3156	4211	7972
H(313)	3494	3979	8586
H(321)	2739	2053	8208
H(322)	3078	1821	8822
H(331)	3257	1802	7776
H(332)	3598	1587	8389
H(341)	3429	-1154	7959
H(342)	2933	-840	7930
H(343)	3273	-1055	8544

Table VI. Distances and angles related to the unresolved desorder.

Bond	Distances (esd's), Å	Bonds	Angles (esd's), deg
C(41)-C(34)	1.51(4)	C(34)-C(41)-C(47)	130.(3)
C(41)-C(47)	1.40(7)	O(312)-C(42)-C(31)	52.(2)
C(42)-O(312)	1.26(4)	O(341)-C(43)-C(34)	49.(2)
C(42)-C(31)	1.56(4)	C(31)-C(44)-C(46)	85.(3)
C(43)-O(341)	1.39(4)	C(31)-C(44)-C(47)	107.(4)
C(43)-C(34)	1.38(4)	C(46)-C(44)-C(47)	141.(4)
C(44)-C(31)	1.45(5)	O(311)-C(45)-C(33)	140.(4)
C(44)-C(47)	1.51(6)		
C(44)-C(46)	1.53(6)		
C(45)-O(311)	1.36(5)		
C(45)-C(33)	1.49(5)		
C(46)-O(311)	1.43(6)		

Table VII. Distances to the weighted least-squares planes.

Distances to the plane (esd's), Å

Phenyl plane 1

$\chi^2 = 2.50$

C(12)*	0.005(5)	C(15)*	0.002(6)
C(13)*	-.002(6)	C(16)*	-.002(6)
C(14)*	-.002(5)	C(17)*	-.005(5)
C(1)	-.096(5)	C(18)	-.081(6)
C(19)	-.236(7)	C(110)	-.406(7)

Pyridone plane 1

$\chi^2 = 14.09$

C(110)*	0.017(6)	C(113)*	0.011(7)
C(111)*	-.010(7)	C(114)*	-.002(6)
C(112)*	-.006(8)	N(114)*	-.005(4)
C(15)	-.157(5)	C(18)	-.042(6)
C(19)	-.010(6)	O(114)	-.038(4)

Phenyl plane 2

$\chi^2 = 19.40$

C(22)*	-.008(5)	C(25)*	-.016(5)
C(23)*	0.002(5)	C(26)*	0.007(5)
C(24)*	0.010(5)	C(27)*	0.004(5)
C(1)	-.131(4)	C(28)	-.148(6)
C(29)	-.334(6)	C(210)	-.589(6)

Table VII. (continued)

Pyridone plane 2

$\chi^2 = 55.32$

C(210)*	-.014(5)	C(213)*	-.019(5)
C(211)*	0.021(6)	C(214)*	0.025(5)
C(212)*	-.001(6)	N(214)*	-.004(4)
C(25)	-.397(5)	C(28)	-.182(5)
C(29)	-.086(5)	O(214)	0.074(4)

Butyric acid planes

End O(31x)

$\chi^2 = 56.90$

O(311)*	0.07(2)	O(312)*	0.04(2)
C(31)*	-.14(2)	C(32)*	0.02(2)

End O(34x)

$\chi^2 = 81.91$

O(341)*	-.09(3)	O(342)*	-.09(3)
C(33)*	-.04(2)	C(34)*	0.14(2)

Full plane

$\chi^2 = 289.53$

O(311)*	0.14(2)	O(312)*	-.15(2)
C(31)*	-.10(2)	C(32)*	0.16(2)
C(33)*	-.15(2)	C(34)*	0.01(2)
O(341)	-.71(2)	O(342)	1.28(3)

* Atoms used in the plane calculation

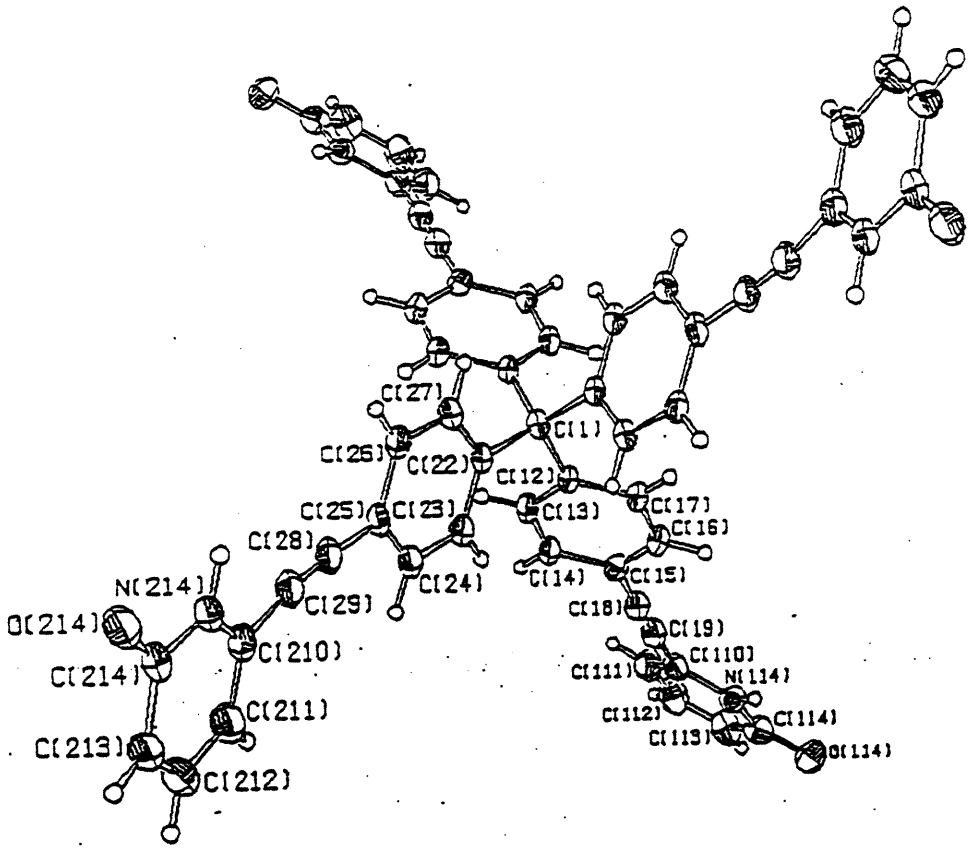
C(27)
C(1)
C(26)
C(22)
C(12)
C(25)
C(23)
C(13)
C(17)
C(16)
C(28)
C(24)
C(14)
C(15)
N(214)
C(18)
O(214)
C(29)
C(19)
C(210)
C(110)
C(214)
C(111)
N(114)
C(211)
C(112)
C(114)
C(213)
C(113)
O(114)
C(212)

Figure 1

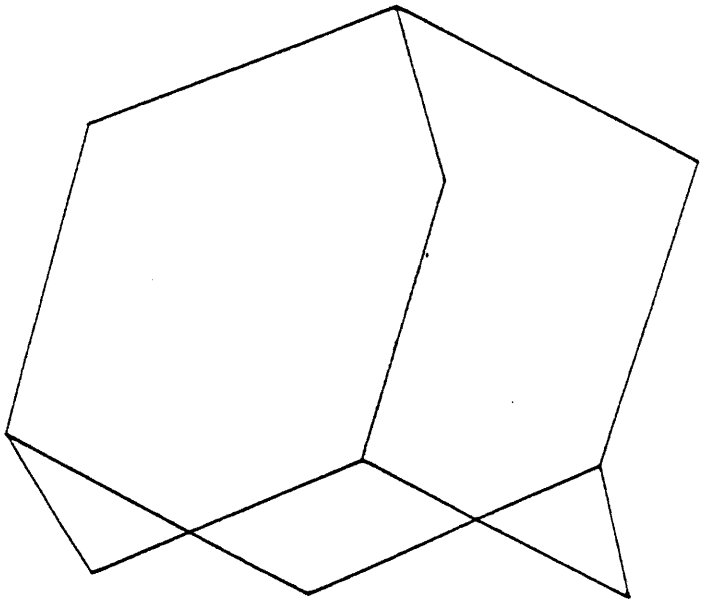

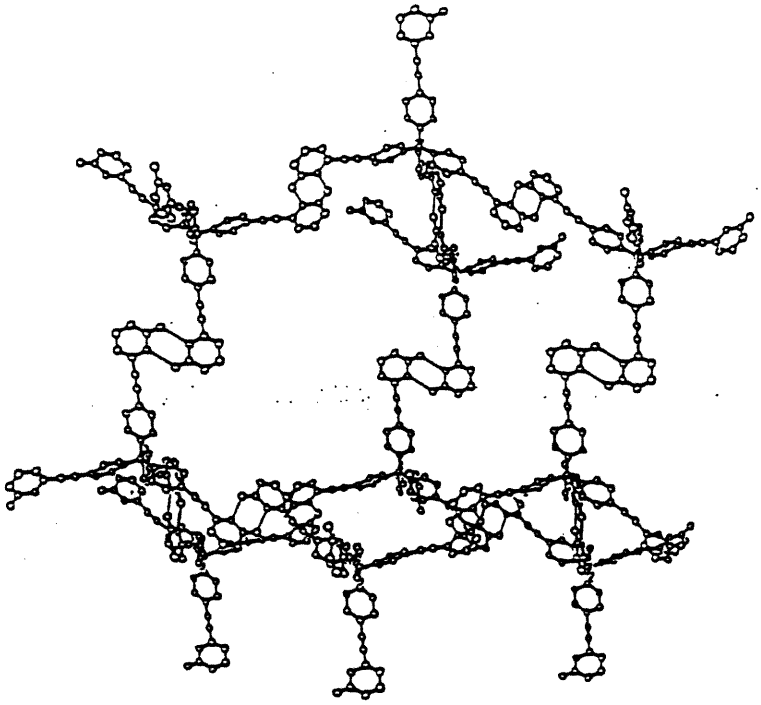

Figure 2

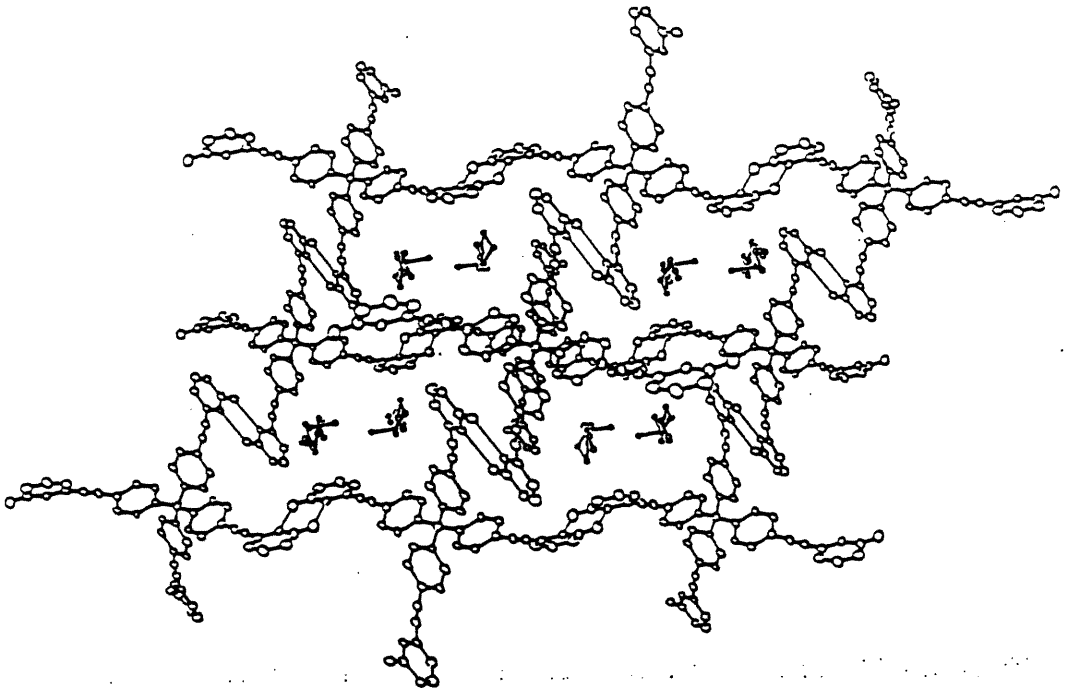

Figure 3

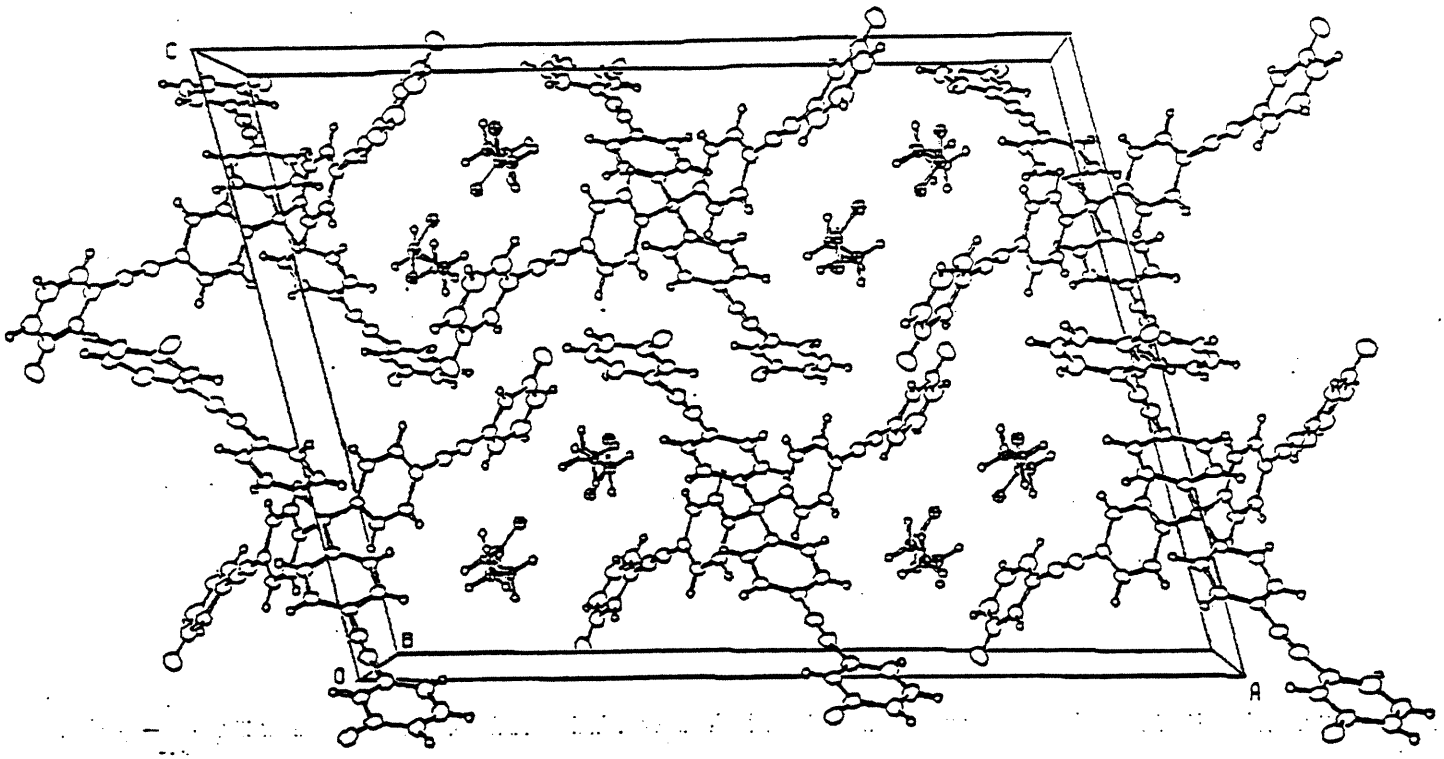

Figure 4

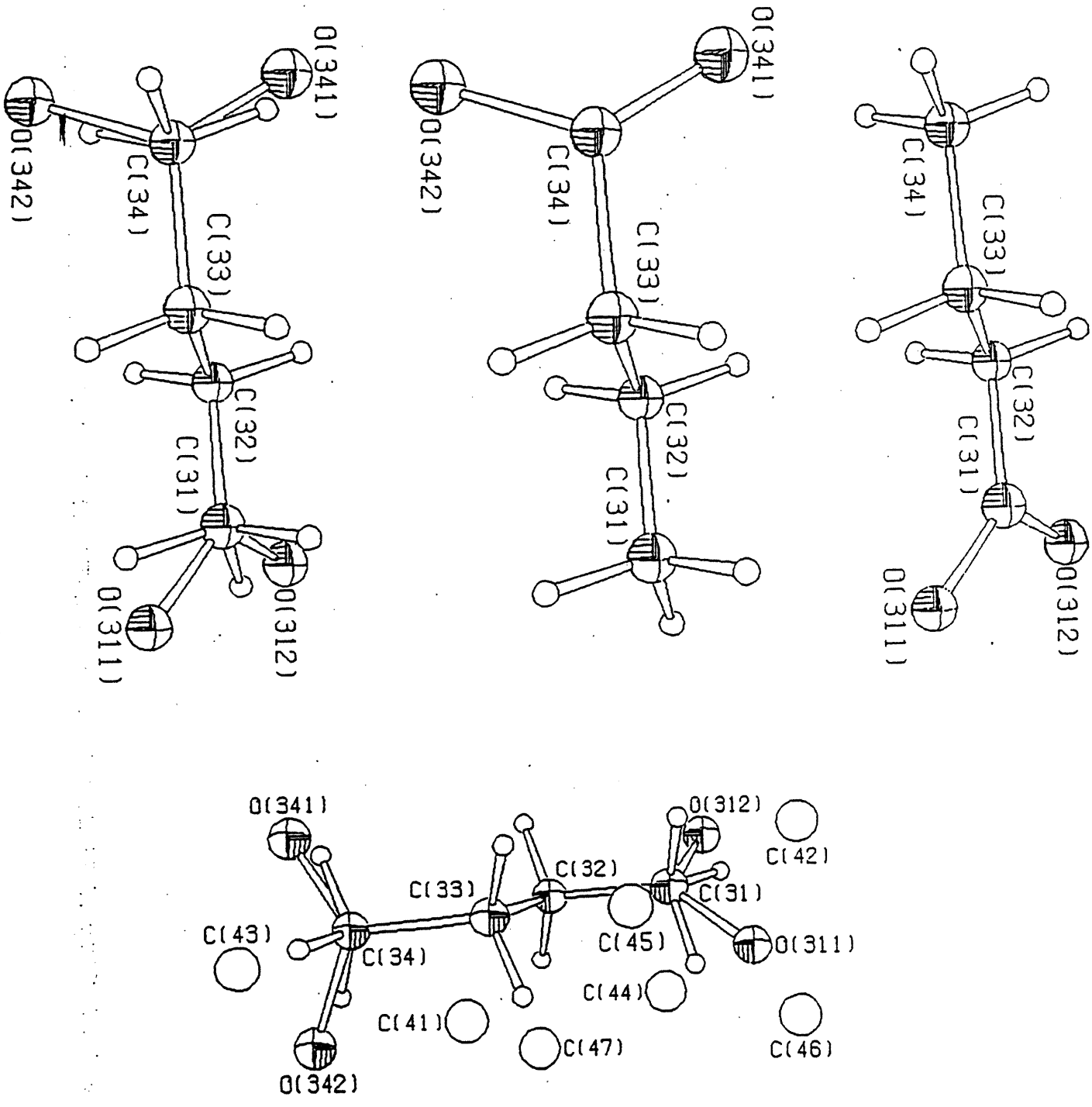

Figure 5

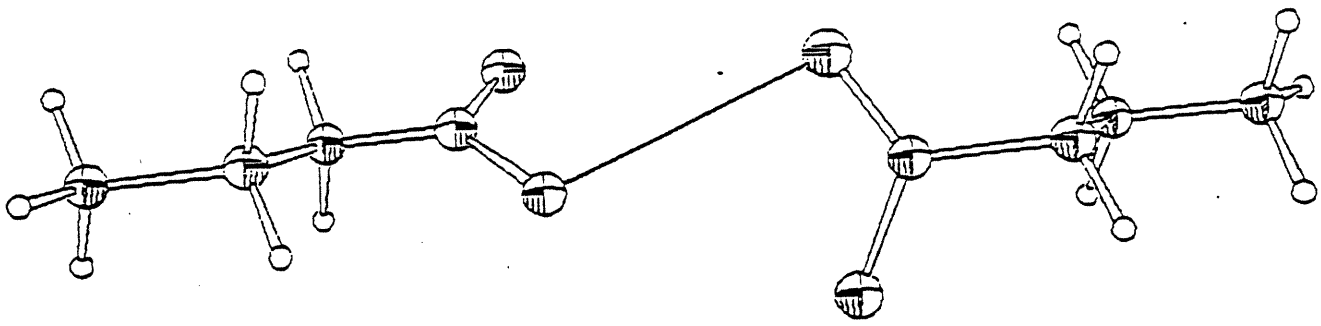

Figure 6

CAPTIONS

Figure 1. Pyridone molecule with numbering scheme for TECTON I·2 CH_2CH_2-CH_2CO_2H. Non-hydrogen atoms represented at 50% probability level, hydrogens by spheres of arbitrary size.

Figure 2. Adamantanoid cage formed by the linked pyridone molecules. Acid molecules not included for clarity. Orientation of the adamantane model showed on the top side.

Figure 3. View of the packing canal arrangement down b axis. The canals are occupied by the desordered acid molecules. Only the major occupancy model resolved is presented (arbitrary spheres), pyridone showed at 30% probality level.

Figure 4. Stereoview of the unit cell. Arbitrary spheres used for the acid moiety.

Figure 5. Butyric acid molecule found in the canal. a) Major model with end O(31x); b) Major model with end O(34x); c) Major model complete; and d) Minor model included.

Figure 6. Hydrogen bonding association found as the link between two resolved butyric acid molecules placed in the canal in a successive arrangement.

APPENDIX 3

CRYSTAL AND MOLECULAR STRUCTURE OF

TECTON **XVII**·4 DMF

Crystallographic report for TECTON **XVII**·4 DMF

Space Group and Cell Dimensions

Monoclinic	C2/c	
a = 46.338(16)	b = 7.344(2)	c = 22.072(8)Å
β = 98.72(3)°	Volume = 7424(4)Å^3	

Empirical formula : $C_{89}H_{76}N_8O_8$

Cell dimensions were obtained from 25 reflections, 2θ angle in the range 40 - 45°

Crystal dimensions : 0.17 {001} × 0.31 {100} × 0.76 {010} mm

FW = 1385.58	Z = 4	F(000) = 2920
Dcalc = 1.240 Mg.m^{-3}	μ = 0.64 mm^{-1}	λ = 1.54056Å
$2\theta_{max}$ = 140.0°	T = 215K	

The intensity data were collected on a Nonius diffractometer using the ω/2θ scan mode {Δω = (0.80 + 0.14 tanθ)°}, graphite monochromatized CuKα radiation and scan rate of 16.5°min^{-1}. Orientation monitored every 400 measurements, intensity checked every hour using 5 standard reflections, largest intensity fluctuation: ±6.9%.

The h,k,l ranges are : -55 55, 0 8, 0 26

Octants measured: all Laue sphere, ±h±k±ℓ

No. of reflections measured	32921
No. of unique reflections (R_{merge} = 0.078)	7017
No. of reflections with $I_{net} > 2.00\ \sigma(I_{net})$	4371

Lp correction done. No absorption correction was applied.

The structure was solved by direct method using SHELXS-86[1] (Sheldrick, 1990) and difference Fourier synthesis using NRCVAX (Gabe, 1989) and SHELXL-93 (Sheldrick, 1994). Full-matrix least-squares refinement based on F^2 using all reflections, all non-hydrogen atoms of the tetrapyridone anisotropic, hydrogen atoms isotropic. Hydrogen atoms introduced at idealized positions with U(iso) adjusted to 20% higher value compared to the bonded atom. Very high disorder observed for the DMF solvent molecules included in the channels, not resolved. 25 peaks included to take into account solvent contribution refined as carbon atoms with common B_{iso} and occupancies factors allowed to refined (total occ. = 6.7 carbon atoms corresponding to 40.3 electrons; B_{iso} = 0.15Å^2). No hydrogen included in the final model at the DMF positions.

The last least squares cycle was calculated with 479 parameters and 6800 reflections. A very large number of 217 reflections located at low angle in the h0ℓ plane were found to suffer an extremely large extinction and were discarded.

Weights based on counting-statistics were used. Function minimized: $\Sigma w(Fo^2-Fc^2)$ $w = 1/[\sigma^2(Fo^2)+(0.1625P)^2]$ where $P=(Fo^2+2Fc^2)/3$.

The residuals are as follows :

For significant reflections,	R1 = 0.0783	*w*R2 = 0.2158	GoF = 1.122
For all reflections,	R1 = 0.1041	*w*R2 = 0.2325	GoF = 0.939

where $R1 = \Sigma(\|\,|Fo| - |Fc|\,\|)/\Sigma(|Fo|)$,
$wR2 = [\Sigma[w(Fo^2-Fc^2)^2]/\Sigma[w(Fo^2)^2]]^{1/2}$ and
$GoF = [\Sigma[w(Fo^2-Fc^2)^2]/(\text{No. of reflns - No. of params.})]^{1/2}$

The maximum shift/σ ratio was 0.156.

In the last ΔF map, the deepest hole was -0.33 e/Å^3,
and the highest peak 0.23 e/Å^3.

Secondary extinction coefficient not refined. The scattering curves and anomalous dispersion contribution (df' and df") for all atoms were from International Tables Vol C.

---

[1]The programs used here are SHELXS-86, multisolution program (Sheldrick, 1986); NRCVAX, program system for structure analysis (Gabe, LePage, Charland and Lee, 1989); SHELXL-93, program for structure refinement (Sheldrick, 1995) and ORTEP, stereodrawings (Johnson, 1965).

Table I. Atomic coordinates and equivalent isotropic temperature factor for the non-hydrogen atoms of TECTON **XVII**·4 DMF

ATOM	X	Y	Z	U_{eq}
O(120)	0.28692(5)	-0.9526(3)	0.4131(2)	0.1067(10)
O(220)	0.20608(4)	1.0564(3)	0.0678(2)	0.1071(10)
N(120)	0.32502(5)	-0.7585(3)	0.4364(2)	0.0839(9)
N(220)	0.24585(3)	1.2395(2)	0.07723(12)	0.0841(9)
C(1)	0.5000	0.2749(4)	0.2500	0.0445(7)
C(12)	0.48866(5)	0.1455(3)	0.29621(11)	0.0435(5)
C(13)	0.45996(5)	0.1389(3)	0.30750(12)	0.0495(6)
C(14)	0.45100(5)	0.0055(3)	0.34455(12)	0.0536(6)
C(15)	0.47018(5)	-0.1266(3)	0.37162(12)	0.0494(6)
C(16)	0.49922(5)	-0.1185(3)	0.36117(12)	0.0493(6)
C(17)	0.50817(5)	0.0145(3)	0.32497(12)	0.0478(6)
C(18)	0.46086(5)	-0.2774(3)	0.40432(13)	0.0536(6)
C(19)	0.45390(5)	-0.4152(3)	0.42815(13)	0.0551(6)
C(110)	0.44524(5)	-0.5861(3)	0.45162(13)	0.0533(6)
C(111)	0.41556(5)	-0.6309(3)	0.44232(14)	0.0569(6)
C(112)	0.40613(5)	-0.7993(3)	0.46140(13)	0.0563(6)
C(113)	0.42710(6)	-0.9211(3)	0.48906(14)	0.0600(7)

Table I. (continued)

ATOM	X	Y	Z	U_{eq}
C(114)	0.45627(6)	-0.8771(4)	0.49817(14)	0.0598(7)
C(115)	0.46555(6)	-0.7095(3)	0.47907(13)	0.0586(7)
C(116)	0.35373(6)	-0.7176(4)	0.4482(2)	0.0722(9)
C(117)	0.37465(6)	-0.8462(3)	0.4503(2)	0.0630(7)
C(118)	0.36444(6)	-1.0279(4)	0.4392(2)	0.0770(10)
C(119)	0.33571(7)	-1.0685(4)	0.4280(2)	0.0828(10)
C(120)	0.31392(6)	-0.9307(4)	0.4254(2)	0.0848(11)
C(22)	0.47576(4)	0.4033(3)	0.21845(12)	0.0437(5)
C(23)	0.46380(5)	0.5283(3)	0.25511(13)	0.0525(6)
C(24)	0.44288(5)	0.6521(3)	0.22985(14)	0.0565(7)
C(25)	0.43329(5)	0.6557(3)	0.16708(13)	0.0500(6)
C(26)	0.44556(5)	0.5339(3)	0.13057(12)	0.0491(6)
C(27)	0.46633(5)	0.4091(3)	0.15580(12)	0.0463(5)
C(28)	0.41233(5)	0.7902(3)	0.14243(14)	0.0562(6)
C(29)	0.39510(5)	0.9072(3)	0.12456(14)	0.0590(7)
C(210)	0.37532(5)	1.0521(3)	0.1043(2)	0.0604(7)
C(211)	0.34526(5)	1.0251(3)	0.0978(2)	0.0644(8)
C(212)	0.32575(5)	1.1649(3)	0.0786(2)	0.0680(8)

Table I. (continued)

ATOM	X	Y	Z	U_{eq}
C(213)	0.33711(6)	1.3341(4)	0.0656(2)	0.0839(11)
C(214)	0.36663(7)	1.3624(4)	0.0729(2)	0.0844(11)
C(215)	0.38611(6)	1.2226(4)	0.0916(2)	0.0733(9)
C(216)	0.27486(6)	1.2696(4)	0.0806(2)	0.0797(10)
C(217)	0.29374(6)	1.1332(4)	0.0734(2)	0.0716(9)
C(218)	0.28139(6)	0.9575(4)	0.0633(2)	0.0861(11)
C(219)	0.25256(3)	0.9263(2)	0.06135(12)	0.0948(13)
C(220)	0.23282(3)	1.0715(2)	0.06893(12)	0.0853(11)

ATOM	X	Y	Z	Occ.
CX(1)	0.8649(3)	0.108(2)	0.3538(7)	0.75(2)
CX(2)	0.8027(3)	0.136(2)	0.1563(6)	0.74(2)
CX(3)	0.8840(9)	-0.194(6)	0.280(3)	0.20(2)
CX(4)	0.7801(7)	0.155(3)	0.1758(10)	0.36(1)
CX(5)	0.8491(5)	0.046(3)	0.1908(11)	0.30(1)
CX(6)	0.8223(7)	0.103(3)	0.1667(10)	0.37(2)
CX(7)	0.7741(7)	0.266(6)	0.219(2)	0.27(2)
CX(8)	0.8539(5)	-0.104(4)	0.2800(13)	0.32(1)
CX(9)	0.8506(6)	-0.110(5)	0.220(2)	0.31(2)

Table I. (continued)

ATOM	X	Y	Z	Occ.
CX(10)	0.8272(5)	-0.230(3)	0.2469(10)	0.32(1)
CX(11)	0.8825(10)	0.182(6)	0.338(2)	0.21(2)
CX(12)	0.8470(8)	0.015(5)	0.324(2)	0.23(1)
CX(13)	0.8079(7)	0.415(4)	0.2494(14)	0.24(1)
CX(14)	0.8429(8)	0.340(5)	0.297(2)	0.20(1)
CX(15)	0.8610(7)	0.020(5)	0.261(2)	0.24(1)
CX(16)	0.8412(10)	0.174(6)	0.333(2)	0.17(1)
CX(17)	0.7966(10)	0.293(6)	0.282(2)	0.15(1)
CX(18)	0.7580(13)	0.157(6)	0.181(2)	0.16(1)
CX(19)	0.7756(14)	0.139(10)	0.244(3)	0.11(1)
CX(20)	0.8803(6)	-0.149(3)	0.248(2)	0.36(2)
CX(21)	0.7404(11)	0.325(6)	0.217(2)	0.15(1)
CX(22)	0.8025(14)	0.200(8)	0.196(3)	0.14(2)
CX(23)	0.7819(14)	0.379(10)	0.230(3)	0.14(2)
CX(24)	0.8685(13)	0.116(7)	0.317(3)	0.18(2)
CX(25)	0.857(2)	-0.201(15)	0.242(4)	0.10(2)

$B_{iso} = 0.15 Å^2$ for all CX(n) atoms introduced as model for the disordered DMF solvent

U(eq) is defined as one third of the trace of the orthogonalized Uij tensor.

Table II. Distances and angles.

Bond	Distances (esd's), Å	Bond	Distances (esd's), Å
C(1)-C(12)	1.543(3)	C(1)-C(12)[a]	1.543(3)
C(1)-C(22)	1.549(3)	C(1)-C(22)[a]	1.549(3)
C(12)-C(13)	1.391(3)	C(22)-C(27)	1.386(4)
C(12)-C(17)	1.404(3)	C(22)-C(23)	1.393(3)
C(13)-C(14)	1.379(3)	C(23)-C(24)	1.383(3)
C(14)-C(15)	1.389(3)	C(24)-C(25)	1.390(4)
C(15)-C(16)	1.401(3)	C(25)-C(26)	1.383(4)
C(15)-C(18)	1.424(3)	C(25)-C(28)	1.433(3)
C(16)-C(17)	1.366(3)	C(26)-C(27)	1.384(3)
C(18)-C(19)	1.206(3)	C(28)-C(29)	1.198(3)
C(19)-C(110)	1.438(3)	C(29)-C(210)	1.431(3)
C(110)-C(115)	1.379(4)	C(210)-C(211)	1.392(3)
C(110)-C(111)	1.398(3)	C(210)-C(215)	1.393(4)
C(111)-C(112)	1.398(3)	C(211)-C(212)	1.391(3)
C(112)-C(113)	1.392(4)	C(212)-C(213)	1.396(4)
C(112)-C(117)	1.483(3)	C(212)-C(217)	1.489(4)
C(113)-C(114)	1.375(4)	C(213)-C(214)	1.369(4)
C(114)-C(115)	1.390(4)	C(214)-C(215)	1.387(4)
C(116)-C(117)	1.349(4)	C(216)-N(220)	1.353(3)
C(116)-N(120)	1.350(3)	C(216)-C(217)	1.355(4)
C(117)-C(118)	1.424(4)	C(217)-C(218)	1.416(4)
C(118)-C(119)	1.350(4)	C(218)-C(219)	1.350(3)
C(119)-C(120)	1.425(4)	C(219)-C(220)	1.431(4)
C(120)-O(120)	1.249(4)	C(220)-O(220)	1.240(3)
C(120)-N(120)	1.372(3)	C(220)-N(220)	1.374(3)

Bonds	Angles (esd's), deg	Bonds	Angles (esd's), deg
C(116)-N(120)-C(120)	124.8(3)	C(216)-N(220)-C(220)	124.54(14)
C(12)-C(1)-C(12)[a]	104.0(2)	C(12)-C(1)-C(22)[a]	111.96(12)
C(12)[a]-C(1)-C(22)[a]	112.06(11)	C(12)-C(1)-C(22)	112.06(11)
C(12)[a]-C(1)-C(22)	111.95(12)	C(22)[a]-C(1)-C(22)	105.0(2)
C(13)-C(12)-C(17)	117.5(2)	C(27)-C(22)-C(23)	117.8(2)
C(13)-C(12)-C(1)	124.8(2)	C(27)-C(22)-C(1)	124.4(2)
C(17)-C(12)-C(1)	117.4(2)	C(23)-C(22)-C(1)	117.7(2)

Table II. (contimued)

Bonds	Angles (esd's), deg	Bonds	Angles (esd's), deg
C(14)-C(13)-C(12)	120.9(2)	C(24)-C(23)-C(22)	121.0(2)
C(13)-C(14)-C(15)	121.4(2)	C(23)-C(24)-C(25)	120.9(2)
C(14)-C(15)-C(16)	117.9(2)	C(26)-C(25)-C(24)	118.1(2)
C(14)-C(15)-C(18)	122.6(2)	C(26)-C(25)-C(28)	122.6(3)
C(16)-C(15)-C(18)	119.3(2)	C(24)-C(25)-C(28)	119.2(2)
C(17)-C(16)-C(15)	120.8(2)	C(25)-C(26)-C(27)	121.1(2)
C(16)-C(17)-C(12)	121.5(2)	C(26)-C(27)-C(22)	121.1(2)
C(19)-C(18)-C(15)	174.0(3)	C(29)-C(28)-C(25)	176.7(3)
C(18)-C(19)-C(110)	175.3(3)	C(28)-C(29)-C(210)	177.8(3)
C(115)-C(110)-C(111)	120.0(2)	C(211)-C(210)-C(215)	119.4(2)
C(115)-C(110)-C(19)	121.5(2)	C(211)-C(210)-C(29)	120.6(2)
C(111)-C(110)-C(19)	118.3(2)	C(215)-C(210)-C(29)	119.9(2)
C(110)-C(111)-C(112)	120.6(2)	C(212)-C(211)-C(210)	121.3(2)
C(113)-C(112)-C(111)	118.1(2)	C(211)-C(212)-C(213)	118.2(2)
C(113)-C(112)-C(117)	121.8(2)	C(211)-C(212)-C(217)	120.1(2)
C(111)-C(112)-C(117)	120.0(2)	C(213)-C(212)-C(217)	121.7(2)
C(114)-C(113)-C(112)	121.3(2)	C(214)-C(213)-C(212)	120.8(2)
C(113)-C(114)-C(115)	120.4(2)	C(213)-C(214)-C(215)	121.1(3)
C(110)-C(115)-C(114)	119.6(2)	C(214)-C(215)-C(210)	119.2(2)
C(117)-C(116)-N(120)	122.2(2)	N(220)-C(216)-C(217)	121.8(2)
C(116)-C(117)-C(118)	115.6(2)	C(216)-C(217)-C(218)	116.1(2)
C(116)-C(117)-C(112)	121.8(2)	C(216)-C(217)-C(212)	121.9(2)
C(118)-C(117)-C(112)	122.6(2)	C(218)-C(217)-C(212)	121.9(2)
C(119)-C(118)-C(117)	122.1(3)	C(219)-C(218)-C(217)	122.3(2)
C(118)-C(119)-C(120)	121.6(3)	C(218)-C(219)-C(220)	121.15(14)
O(120)-C(120)-N(120)	119.6(3)	O(220)-C(220)-N(220)	120.03(13)
O(120)-C(120)-C(119)	126.7(3)	O(220)-C(220)-C(219)	125.83(13)
N(120)-C(120)-C(119)	113.7(3)	N(220)-C(220)-C(219)	114.1(2)

a: 1-x, y, 1/2-z

Table III. Bond distances (Å) and angles (deg) related to the hydrogen bonding.

Bond (A-H···B)	Distances (esd's) A-B	A-H	H-B	Angles (esd's) A-H-B
N(120)-HN(120)...O(220)[a]	2.720(3)	0.87	1.87	166.3
N(220)-HN(220)...O(120)[b]	2.750(3)	0.87	1.88	175.4

Bonds	Angles (esd's), deg	Bonds	Angles (esd's), deg
C(116)-N(120)...O(220)[a]	108.6(2)	C(116)-N(120)-HN(120)	117.6
C(120)-N(120)...O(220)[a]	126.5(2)	C(120)-N(120)-HN(120)	117.6
N(120)...O(220)[a]-C(220)[a]	126.8(2)	HN(120)...O(220)[a]-C(220)[a]	122.5
C(216)-N(220)...O(120)[b]	114.6(2)	C(216)-N(220)-HN(220)	117.7
C(220)-N(220)...O(120)[b]	120.80(6)	C(220)-N(220)-HN(220)	117.7
N(220)...O(120)[b]-C(120)[b]	129.5(2)	HN(220)...O(120)[b]-C(120)[b]	128.2

a: 1/2-x, -3/2+y, 1/2-z
b: 1/2-x, 5/2+y, 1/2-z

Table IV. Anisotropic temperature factors.

ATOM	U11	U22	U33	U12	U13	U23
O(120)	0.0486(11)	0.0585(13)	0.211(3)	-0.001(2)	0.013(2)	-0.0156(10)
N(120)	0.0484(12)	0.0468(13)	0.157(3)	-0.0079(14)	0.019(2)	-0.0097(10)
O(220)	0.0423(10)	0.0555(12)	0.220(3)	0.011(2)	0.0077(14)	0.0058(9)
N(220)	0.0399(11)	0.0451(12)	0.163(3)	0.0044(14)	0.0029(14)	0.0086(9)
C(1)	0.0368(14)	0.0262(13)	0.069(2)	0.000	0.0027(13)	0.000
C(12)	0.0371(10)	0.0269(9)	0.0656(14)	-0.0049(9)	0.0052(9)	-0.0016(8)
C(13)	0.0389(11)	0.0369(11)	0.072(2)	-0.0012(11)	0.0064(10)	0.0025(9)
C(14)	0.0377(11)	0.0477(13)	0.077(2)	-0.0024(12)	0.0123(11)	-0.0027(10)
C(15)	0.0492(12)	0.0347(11)	0.066(2)	-0.0048(10)	0.0137(11)	-0.0068(9)
C(16)	0.0450(12)	0.0312(10)	0.071(2)	0.0028(10)	0.0080(11)	0.0029(9)
C(17)	0.0363(10)	0.0326(10)	0.075(2)	0.0022(10)	0.0088(10)	0.0008(8)
C(18)	0.0508(13)	0.0447(13)	0.066(2)	-0.0015(11)	0.0125(11)	-0.0062(10)
C(19)	0.0511(13)	0.0470(13)	0.070(2)	-0.0014(12)	0.0190(12)	-0.0082(11)
C(110)	0.0506(13)	0.0433(12)	0.068(2)	-0.0021(11)	0.0143(11)	-0.0098(10)
C(111)	0.0478(13)	0.0425(12)	0.082(2)	0.0009(12)	0.0150(12)	-0.0052(10)
C(112)	0.0493(13)	0.0406(12)	0.081(2)	-0.0028(12)	0.0180(12)	-0.0087(10)
C(113)	0.059(2)	0.0404(12)	0.083(2)	0.0018(12)	0.0181(13)	-0.0045(11)
C(114)	0.0558(14)	0.0466(13)	0.077(2)	0.0020(12)	0.0100(12)	0.0015(11)

Table IV. (continued)

ATOM	U11	U22	U33	U12	U13	U23
C(115)	0.0482(13)	0.0497(14)	0.079(2)	-0.0028(12)	0.0128(12)	-0.0067(11)
C(116)	0.0498(14)	0.0434(14)	0.126(3)	-0.006(2)	0.020(2)	-0.0111(11)
C(117)	0.0490(14)	0.0430(13)	0.098(2)	0.0000(13)	0.0135(13)	-0.0101(11)
C(118)	0.053(2)	0.0417(14)	0.135(3)	-0.002(2)	0.011(2)	-0.0068(11)
C(119)	0.058(2)	0.0428(14)	0.148(3)	-0.003(2)	0.015(2)	-0.0128(12)
C(120)	0.049(2)	0.049(2)	0.155(3)	-0.002(2)	0.013(2)	-0.0146(12)
C(22)	0.0357(10)	0.0239(9)	0.070(2)	-0.0008(9)	0.0029(10)	-0.0023(8)
C(23)	0.0495(12)	0.0350(11)	0.070(2)	-0.0055(10)	0.0006(11)	0.0070(9)
C(24)	0.0489(13)	0.0337(11)	0.085(2)	-0.0081(11)	0.0044(12)	0.0081(9)
C(25)	0.0337(10)	0.0321(11)	0.082(2)	0.0037(11)	0.0009(10)	-0.0001(8)
C(26)	0.0391(11)	0.0374(11)	0.068(2)	0.0028(10)	0.0001(10)	-0.0042(9)
C(27)	0.0393(10)	0.0291(10)	0.070(2)	-0.0005(10)	0.0052(10)	-0.0003(8)
C(28)	0.0360(11)	0.0402(12)	0.091(2)	0.0005(12)	0.0043(11)	0.0010(9)
C(29)	0.0376(11)	0.0459(13)	0.090(2)	0.0037(13)	0.0001(12)	0.0049(10)
C(210)	0.0401(12)	0.0414(12)	0.097(2)	0.0013(12)	0.0004(12)	0.0074(10)
C(211)	0.0425(12)	0.0394(12)	0.108(2)	0.0036(13)	0.0009(13)	0.0037(10)
C(212)	0.0392(12)	0.0435(13)	0.118(2)	-0.0014(14)	0.0013(14)	0.0043(10)
C(213)	0.0471(14)	0.0426(14)	0.156(3)	0.011(2)	-0.005(2)	0.0070(11)

Table IV. (continued)

ATOM	U11	U22	U33	U12	U13	U23
C(214)	0.055(2)	0.0409(14)	0.151(3)	0.013(2)	-0.004(2)	-0.0012(12)
C(215)	0.0398(12)	0.0467(14)	0.130(3)	0.004(2)	0.0020(14)	0.0002(11)
C(216)	0.0442(13)	0.0429(14)	0.146(3)	0.002(2)	-0.006(2)	0.0053(11)
C(217)	0.0383(13)	0.0447(13)	0.127(3)	0.000(2)	-0.0031(14)	0.0049(10)
C(218)	0.0444(14)	0.0442(14)	0.166(4)	-0.007(2)	0.003(2)	0.0055(11)
C(219)	0.0456(14)	0.045(2)	0.190(4)	-0.007(2)	0.006(2)	0.0017(12)
C(220)	0.0401(13)	0.050(2)	0.161(4)	0.007(2)	-0.001(2)	0.0041(12)

The anisotropic displacement factor exponent takes the form:

$$-2\pi^2 [h^2 a^{*2} U11 + ... + 2 h k a^* b^* U12]$$

Table V. Calculated hydrogen coordinates and temperature factors for TECTON **XVII**·4 DMF

ATOM	X	Y	Z	B_{iso}
H(13)	0.44648(5)	0.2264(3)	0.28966(12)	0.059
H(14)	0.43150(5)	0.0041(3)	0.35161(12)	0.064
H(16)	0.51271(5)	-0.2056(3)	0.37929(12)	0.059
H(17)	0.52785(5)	0.0185(3)	0.31918(12)	0.057
H(111)	0.40183(5)	-0.5470(3)	0.42306(14)	0.068
H(113)	0.42121(6)	-1.0356(3)	0.50175(14)	0.072
H(114)	0.47003(6)	-0.9609(4)	0.51742(14)	0.072
H(115)	0.48554(6)	-0.6805(3)	0.48484(13)	0.070
H(116)	0.35932(6)	-0.5955(4)	0.4551(2)	0.087
H(118)	0.37814(6)	-1.1225(4)	0.4397(2)	0.092
H(119)	0.32994(7)	-1.1906(4)	0.4217(2)	0.099
HN(120)	0.31265(5)	-0.6692(3)	0.4356(2)	0.101
H(23)	0.47004(5)	0.5286(3)	0.29766(13)	0.063
H(24)	0.43505(5)	0.7348(3)	0.25549(14)	0.068
H(26)	0.43970(5)	0.5360(3)	0.08789(12)	0.059
H(27)	0.47418(5)	0.3268(3)	0.13003(12)	0.056
H(211)	0.33801(5)	0.9101(3)	0.1067(2)	0.077

Table V. (continued)

ATOM	X	Y	Z	B_{iso}
H(213)	0.32434(6)	1.4297(4)	0.0516(2)	0.101
H(214)	0.37383(7)	1.4784(4)	0.0652(2)	0.101
H(215)	0.40634(6)	1.2428(4)	0.0956(2)	0.088
H(216)	0.28212(6)	1.3883(4)	0.0882(2)	0.096
H(218)	0.29369(6)	0.8591(4)	0.0577(2)	0.103
H(219)	0.24532(3)	0.8072(2)	0.05492(12)	0.114
HN(220)	0.23467(3)	1.3330(2)	0.08053(12)	0.101

Table VI. Distances to the weighted least-squares planes.

Plane no. 1

*	-0.011 (0.002)	C(12)
*	0.003 (0.002)	C(13)
*	0.007 (0.002)	C(14)
*	-0.008 (0.002)	C(15)
*	0.000 (0.002)	C(16)
*	0.010 (0.002)	C(17)
	-0.176 (0.003)	C(1)
	-0.156 (0.004)	C(18)
	-0.387 (0.005)	C(19)
	-0.776 (0.006)	C(110)

Rms deviation of fitted atoms = 0.007

Plane no. 2

*	0.004 (0.002)	C(110)
*	-0.003 (0.002)	C(111)
*	0.002 (0.002)	C(112)
*	-0.002 (0.002)	C(113)
*	0.003 (0.002)	C(114)
*	-0.003 (0.002)	C(115)
	-0.570 (0.007)	C(15)
	-0.239 (0.006)	C(18)
	-0.076 (0.004)	C(19)
	-0.028 (0.005)	C(117)

Rms deviation of fitted atoms = 0.003

Plane no. 3

*	0.000 (0.003)	N(120)
*	0.002 (0.003)	C(116)
*	0.001 (0.003)	C(117)
*	-0.004 (0.003)	C(118)
*	0.006 (0.003)	C(119)

Table VI. (continued)

Plane no. 3 (continued)

*	-0.003 (0.003)	C(120)
	-0.045 (0.006)	O(120)
	-0.040 (0.005)	C(112)

Rms deviation of fitted atoms = 0.003

Plane no. 4

*	-0.006 (0.001)	C(22)
*	0.005 (0.002)	C(23)
*	0.002 (0.002)	C(24)
*	-0.008 (0.002)	C(25)
*	0.007 (0.002)	C(26)
*	0.000 (0.001)	C(27)
	0.060 (0.003)	C(1)
	0.036 (0.004)	C(28)
	0.091 (0.004)	C(29)
	0.204 (0.006)	C(210)

Rms deviation of fitted atoms = 0.005

Plane no. 5

*	-0.004 (0.002)	C(210)
*	0.004 (0.002)	C(211)
*	0.003 (0.003)	C(212)
*	-0.009 (0.003)	C(213)
*	0.009 (0.003)	C(214)
*	-0.003 (0.003)	C(215)
	0.155 (0.009)	C(25)
	0.039 (0.007)	C(28)
	0.007 (0.006)	C(29)
	0.040 (0.006)	C(217)

Rms deviation of fitted atoms = 0.006

Table VI. (continued)

Plane no. 6

*	-0.014 (0.002)	N(220)
*	0.009 (0.002)	C(216)
*	0.001 (0.003)	C(217)
*	-0.007 (0.003)	C(218)
*	0.002 (0.002)	C(219)
*	0.008 (0.001)	C(220)
	0.014 (0.006)	O(220)
	0.060 (0.006)	C(212)

Rms deviation of fitted atoms = 0.008

* indicates atoms used to define plane

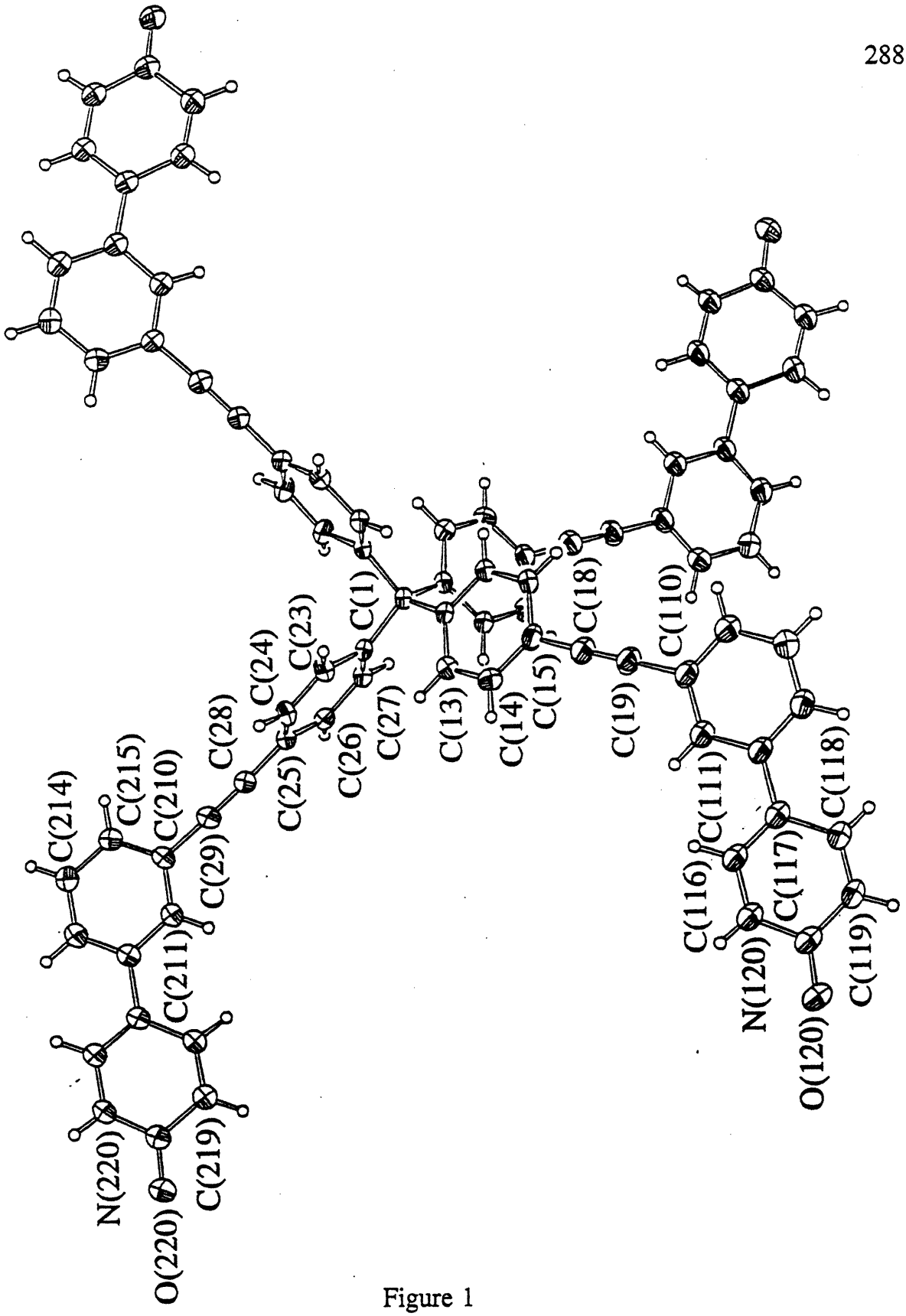
C(1)
C(13)
C(14)
C(15)
C(18)
C(19)
C(110)
C(111)
C(116)
C(117)
C(118)
C(119)
N(120)
O(120)
C(23)
C(24)
C(25)
C(26)
C(27)
C(28)
C(29)
C(210)
C(211)
C(214)
C(215)
C(219)
N(220)
O(220)

Figure 1

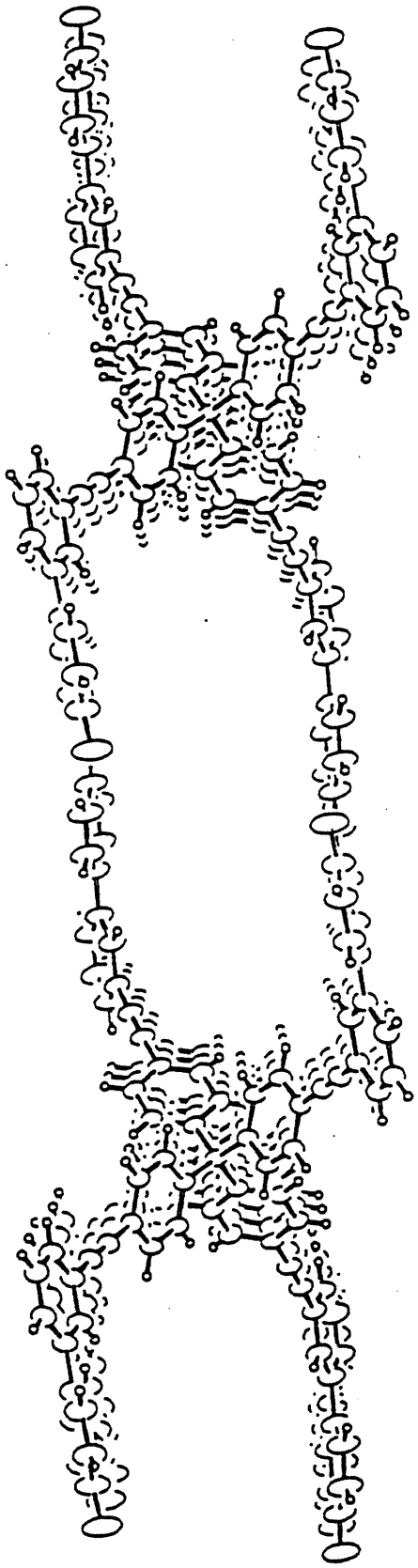

Figure 2

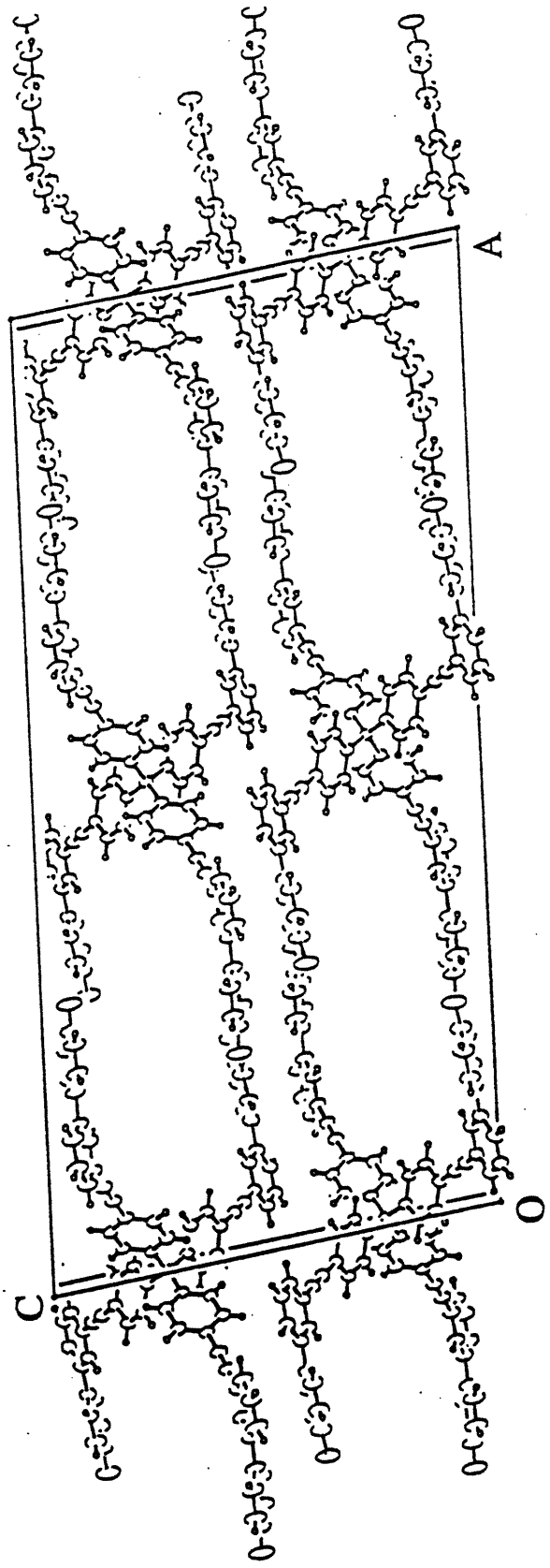

Figure 3

CAPTIONS

Figure 1 ORTEP view of TECTON **XVII**·4 DMF with the numbering scheme adopted. Ellipsoids drawn at 40% probality level. Hydrogens represented by spheres of arbitrary size.

Figure 2 ORTEP view of the very large canal down b axis shown without the disordered DMF solvent. Hydrogen bonding represented using thin bonds.

Figure 3. ORTEP view of the cell down b axis.

APPENDIX 4

CRYSTAL AND MOLECULAR STRUCTURE OF

TECTON XVIII·4 DMF

Crystallographic report for TECTON **XVIII**·4 DMF

Space Group and Cell Dimensions

Tetragonal	$I4_1/a$
a = b = 11.523(2)	c = 40.421(9)Å
Volume = 5367.1(15)Å^3	

Empirical formula : $C_{57}H_{60}N_8O_8$

Cell dimensions were obtained from 25 reflections, 2θ angle in the range 40 - 45°

Crystal dimensions : 0.08 {100} × 0.42 {010,1$\bar{1}$0} × 0.44 {001} mm

FW = 985.15	Z = 4	F(000) = 2088
Dcalc = 1.219 Mg.m^{-3}	μ = 0.63 mm^{-1}	λ = 1.54056Å
$2\theta_{max}$ = 120.0°	T = 210K	

The intensity data were collected on a Nonius diffractometer using the ω/2θ scan mode {Δω = (0.80 + 0.14 tanθ)°}, graphite monochromatized CuKα radiation and scan rate of 16.5°min^{-1}. Orientation monitored every 400 measurements, intensity checked every hour using 5 standard reflections, largest intensity fluctuation: ±6.5%.

The h,k,l ranges are : 0 12, 0 12, 0 45

Octants measured: all Laue sphere, ±h±k±ℓ

No. of reflections measured	15426
No. of unique reflections (R_{merge} = 0.062)	1994
No. of reflections with $I_{net} > 2.00\ \sigma(I_{net})$	957

Lp correction done. No absorption correction was applied.

The structure was solved by direct method using SHELXS-86[1] (Sheldrick, 1990) and difference Fourier synthesis using NRCVAX (Gabe, 1989) and SHELXL-93 (Sheldrick, 1994). Full-matrix least-squares refinement based on F^2 using all reflections, all non-hydrogen atoms of the tetrapyridone anisotropic, hydrogen atoms isotropic. Hydrogen atoms introduced at idealized positions with U(iso) adjusted to 20% higher value compared to the bonded atom. Very high disorder observed for the DMF solvant molecules included in the channels, not resolved. 11 peaks included to take into account solvant contribution refined as carbon atoms with common B_{iso} and occupancies factors allowed to refined (total occ. = 6.1 carbon atoms; B_{iso} = 0.28Å^2). No hydrogen included in the final model at the DMF positions.

The last least squares cycle was calculated with 166 parameters and 1994 reflections.

Weights based on counting-statistics were used. Function minimized: $\Sigma w(Fo^2-Fc^2)$ $w = 1/[\sigma^2(Fo^2)+(0.0942P)^2]$ where $P=(Fo^2+2Fc^2)/3$.

The residuals are as follows :

For significant reflections,	R1 = 0.0671	*w*R2 = 0.1714	GoF = 1.180
For all reflections,	R1 = 0.1207	*w*R2 = 0.1882	GoF = 0.863

where $R1 = \Sigma(\|Fo\| - |Fc\|)/\Sigma(|Fo|)$,
$wR2 = [\Sigma[w(Fo^2-Fc^2)^2]/\Sigma[w(Fo^2)^2]]^{1/2}$ and
GoF = $[\Sigma[w(Fo^2-Fc^2)^2]/$(No. of reflns - No. of params.)$]^{1/2}$

The maximum shift/σ ratio was 0.096.

In the last ΔF map, the deepest hole was -0.18 e/Å^3, and the highest peak 0.21 e/Å^3.

Secondary extinction coefficient refined: 0.0009(2)

The scattering curves and anomalous dispersion contribution (df' and df'') for all atoms were taken from International Tables Vol C.

---

[1]The programs used here are SHELXS-86, multisolution program (Sheldrick, 1986); NRCVAX, program system for structure analysis (Gabe, LePage, Charland and Lee, 1989); SHELXL-93, program for structure refinement (Sheldrick, 1995) and ORTEP, stereodrawings (Johnson, 1965).

Table I. Atomic coordinates and equivalent isotropic temperature factor for the non-hydrogen atoms of TECTON **XVIII**·4 DMF

ATOM	X	Y	Z	U_{eq}
O(8)	0.0986(2)	0.5459(2)	0.02916(7)	0.0916(10)
N(8)	0.1220(3)	0.3953(3)	-0.00649(8)	0.0834(11)
C(1)	0.5000	0.7500	0.1250	0.051(2)
C(2)	0.4388(3)	0.6625(3)	0.10202(8)	0.0526(9)
C(3)	0.5024(3)	0.6117(3)	0.07644(8)	0.0591(10)
C(4)	0.4504(3)	0.5396(3)	0.05355(8)	0.0628(10)
C(5)	0.3326(3)	0.5146(3)	0.05512(8)	0.0581(9)
C(6)	0.2709(3)	0.5631(3)	0.08083(9)	0.0639(10)
C(7)	0.3232(3)	0.6351(3)	0.10366(8)	0.0593(10)
C(8)	0.1632(4)	0.4657(3)	0.01798(10)	0.0746(12)
C(9)	0.2800(3)	0.4407(3)	0.02920(9)	0.0665(11)
C(10)	0.3377(4)	0.3504(3)	0.01524(10)	0.0834(13)
C(11)	0.2882(4)	0.2826(4)	-0.00988(11)	0.094(2)
C(12)	0.1799(4)	0.3071(4)	-0.02038(11)	0.0898(14)

ATOM	X	Y	Z	Occ.
CX(1)	0.930(2)	0.160(2)	0.1805(4)	0.91(2)
CX(2)	0.858(3)	0.016(3)	0.1815(7)	0.58(2)

Table I. (continued)

ATOM	X	Y	Z	Occ.
CX(3)	0.929(5)	0.049(4)	0.1634(13)	0.42(2)
CX(4)	1.078(2)	-0.101(2)	0.1071(6)	0.53(2)
CX(5)	1.015(2)	-0.2022(13)	0.1246(4)	0.87(2)
CX(6)	1.032(3)	0.214(3)	0.1700(5)	0.52(2)
CX(7)	0.818(3)	0.113(2)	0.1656(6)	0.56(2)
CX(8)	1.018(5)	0.035(4)	0.1422(13)	0.28(2)
CX(9)	0.983(3)	-0.200(3)	0.1653(6)	0.49(2)
CX(10)	0.965(2)	-0.082(3)	0.1534(7)	0.51(2)
CX(11)	1.028(3)	-0.201(3)	0.0845(6)	0.44(2)

$B_{iso} = 0.28\text{Å}^2$ for all CX(n) atoms introduced as model for the disordered DMF solvent

U(eq) is defined as one third of the trace of the orthogonalized Uij tensor.

Table II. Distances and angles.

Bond	Distances (esd's), Å	Bond	Distances (esd's), Å
O(8)-C(8)	1.270(4)	N(8)-C(12)	1.339(4)
N(8)-C(8)	1.365(4)	C(1)-C(2)	1.542(3)
C(2)-C(7)	1.371(4)	C(2)-C(3)	1.396(4)
C(3)-C(4)	1.381(4)	C(4)-C(5)	1.389(5)
C(5)-C(6)	1.377(4)	C(5)-C(9)	1.480(4)
C(6)-C(7)	1.379(4)	C(8)-C(9)	1.449(5)
C(9)-C(10)	1.358(5)	C(10)-C(11)	1.402(5)
C(11)-C(12)	1.348(5)		

Bonds	Angles (esd's), deg	Bonds	Angles (esd's), deg
C(12)-N(8)-C(8)	125.5(4)	$C(2)^a$-C(1)-$C(2)^b$	111.29(12)
$C(2)^a$-C(1)-C(2)	105.9(2)	$C(2)^b$-C(1)-C(2)	111.29(12)
$C(2)^a$-C(1)-$C(2)^c$	111.28(12)	$C(2)^b$-C(1)-$C(2)^c$	105.9(2)
C(2)-C(1)-$C(2)^c$	111.29(12)	C(7)-C(2)-C(3)	116.7(3)
C(7)-C(2)-C(1)	124.4(3)	C(3)-C(2)-C(1)	118.7(3)
C(4)-C(3)-C(2)	121.4(3)	C(3)-C(4)-C(5)	121.2(3)
C(6)-C(5)-C(4)	117.0(3)	C(6)-C(5)-C(9)	123.8(3)
C(4)-C(5)-C(9)	119.1(3)	C(5)-C(6)-C(7)	121.6(3)
C(2)-C(7)-C(6)	122.0(3)	O(8)-C(8)-N(8)	119.1(4)
O(8)-C(8)-C(9)	125.3(3)	N(8)-C(8)-C(9)	115.6(4)
C(10)-C(9)-C(8)	118.5(3)	C(10)-C(9)-C(5)	122.3(4)
C(8)-C(9)-C(5)	119.2(3)	C(9)-C(10)-C(11)	121.9(4)
C(12)-C(11)-C(10)	119.2(4)	N(8)-C(12)-C(11)	119.2(4)

a: 1-x, 3/2-y, z
b: -1/4+y, 5/4-x, 1/4-z
c: 5/4-y, 1/4+x, 1/4-z

Table III. Bond distances (Å) and angles (deg) related to the hydrogen bonding.

Bond (A-H···B)	Distances (esd's) A-B	A-H	H-B	Angles (esd's) A-H-B
N(8)-HN(8)...O(8)[a]	2.785(4)	0.87	1.92	174.5

Bonds	Angles (esd's), deg	Bonds	Angles (esd's), deg
C(8)-N(8)...O(8)[a]	114.3(3)	C(8)-N(8)-HN(8)	117.2
C(12)-N(8)...O(8)[a]	120.1(3)	C(12)-N(8)-HN(8)	117.2
N(8)...O(8)[a]-C(8)[a]	126.5(2)	HN(8)...O(8)[a]-C(8)[a]	127.8

a: -x, 1-y, -z

Table IV. Anisotropic temperature factors.

ATOM	U11	U22	U33	U12	U13	U23
O(8)	0.085(2)	0.086(2)	0.104(2)	-0.033(2)	-0.024(2)	0.012(2)
N(8)	0.083(2)	0.078(2)	0.089(2)	-0.023(2)	-0.020(2)	0.000(2)
C(1)	0.049(2)	0.049(2)	0.054(4)	0.000	0.000	0.000
C(2)	0.055(2)	0.053(2)	0.049(2)	0.004(2)	-0.003(2)	0.002(2)
C(3)	0.055(2)	0.064(2)	0.058(2)	-0.005(2)	0.000(2)	-0.001(2)
C(4)	0.067(3)	0.064(2)	0.058(2)	-0.007(2)	0.003(2)	0.005(2)
C(5)	0.062(2)	0.053(2)	0.059(2)	-0.002(2)	-0.008(2)	-0.001(2)
C(6)	0.056(2)	0.070(3)	0.066(2)	-0.007(2)	0.000(2)	-0.004(2)
C(7)	0.060(2)	0.061(2)	0.056(2)	-0.008(2)	0.003(2)	-0.001(2)
C(8)	0.081(3)	0.061(3)	0.082(3)	-0.020(2)	-0.015(2)	-0.001(2)
C(9)	0.066(3)	0.063(2)	0.071(2)	-0.013(2)	-0.008(2)	0.001(2)
C(10)	0.080(3)	0.075(3)	0.095(3)	-0.025(2)	-0.005(2)	0.001(2)
C(11)	0.099(4)	0.084(3)	0.100(3)	-0.038(3)	0.000(3)	0.012(3)
C(12)	0.093(3)	0.078(3)	0.099(3)	-0.032(3)	-0.009(3)	0.003(3)

The anisotropic displacement factor exponent takes the form:

$$-2\pi^2 [h^2 a^{*2} U11 + ... + 2 h k a^* b^* U12]$$

Table V. Calculated hydrogen coordinates and temperature factors for TECTON **XVIII**·4 DMF

ATOM	X	Y	Z	B_{iso}
HN(8)	0.0521	0.4088	-0.01366	0.100
H(3)	0.5823	0.6269	0.07477	0.071
H(4)	0.4955	0.5068	0.03658	0.075
H(6)	0.1913	0.5468	0.08286	0.077
H(7)	0.2781	0.6664	0.12088	0.071
H(10)	0.4130	0.3328	0.02263	0.100
H(11)	0.3301	0.2208	-0.01929	0.113
H(12)	0.1455	0.2628	-0.03726	0.108

Table VI. Distances to the weighted least-squares planes.

Plane no. 1

*	0.010 (0.002)	C(2)
*	-0.005 (0.002)	C(3)
*	-0.004 (0.002)	C(4)
*	0.009 (0.002)	C(5)
*	-0.004 (0.002)	C(6)
*	-0.005 (0.002)	C(7)
	0.126 (0.004)	C(1)
	1.451 (0.006)	O(8)
	0.857 (0.007)	N(8)
	0.830 (0.006)	C(8)
	0.065 (0.005)	C(9)
	-0.567 (0.006)	C(10)
	-0.481 (0.008)	C(11)
	0.242 (0.009)	C(12)

Rms deviation of fitted atoms = 0.007

Plane no. 2

*	-0.001 (0.003)	N(8)
*	-0.003 (0.003)	C(8)
*	0.006 (0.003)	C(9)
*	-0.004 (0.003)	C(10)
*	-0.001 (0.003)	C(11)
*	0.003 (0.003)	C(12)
	0.490 (0.012)	C(1)
	0.242 (0.010)	C(2)
	0.865 (0.009)	C(3)
	0.764 (0.007)	C(4)
	0.037 (0.006)	C(5)
	-0.597 (0.007)	C(6)
	-0.495 (0.009)	C(7)
	-0.018 (0.006)	O(8)

Rms deviation of fitted atoms = 0.003

* indicates atom used to define plane

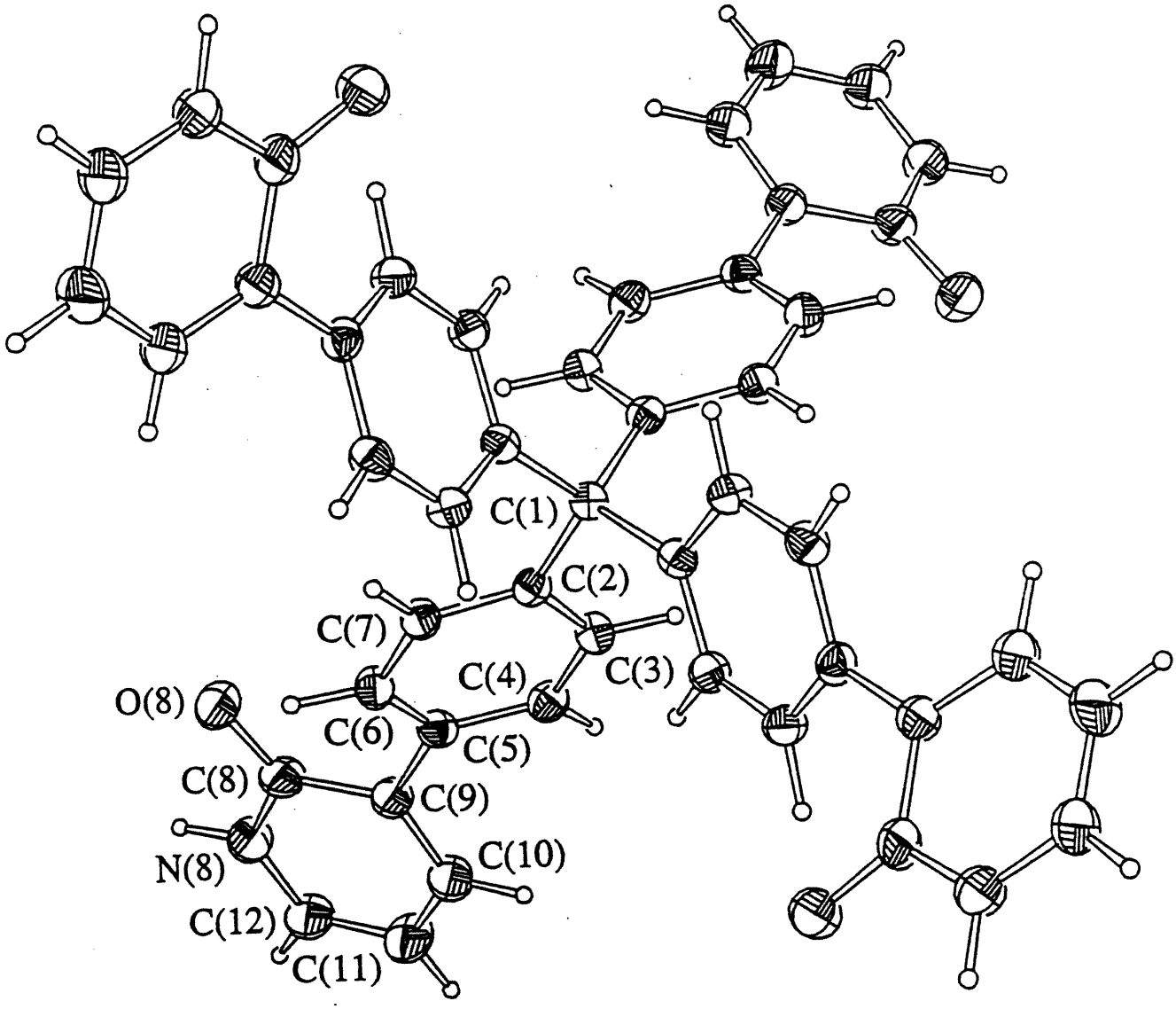

Figure 1

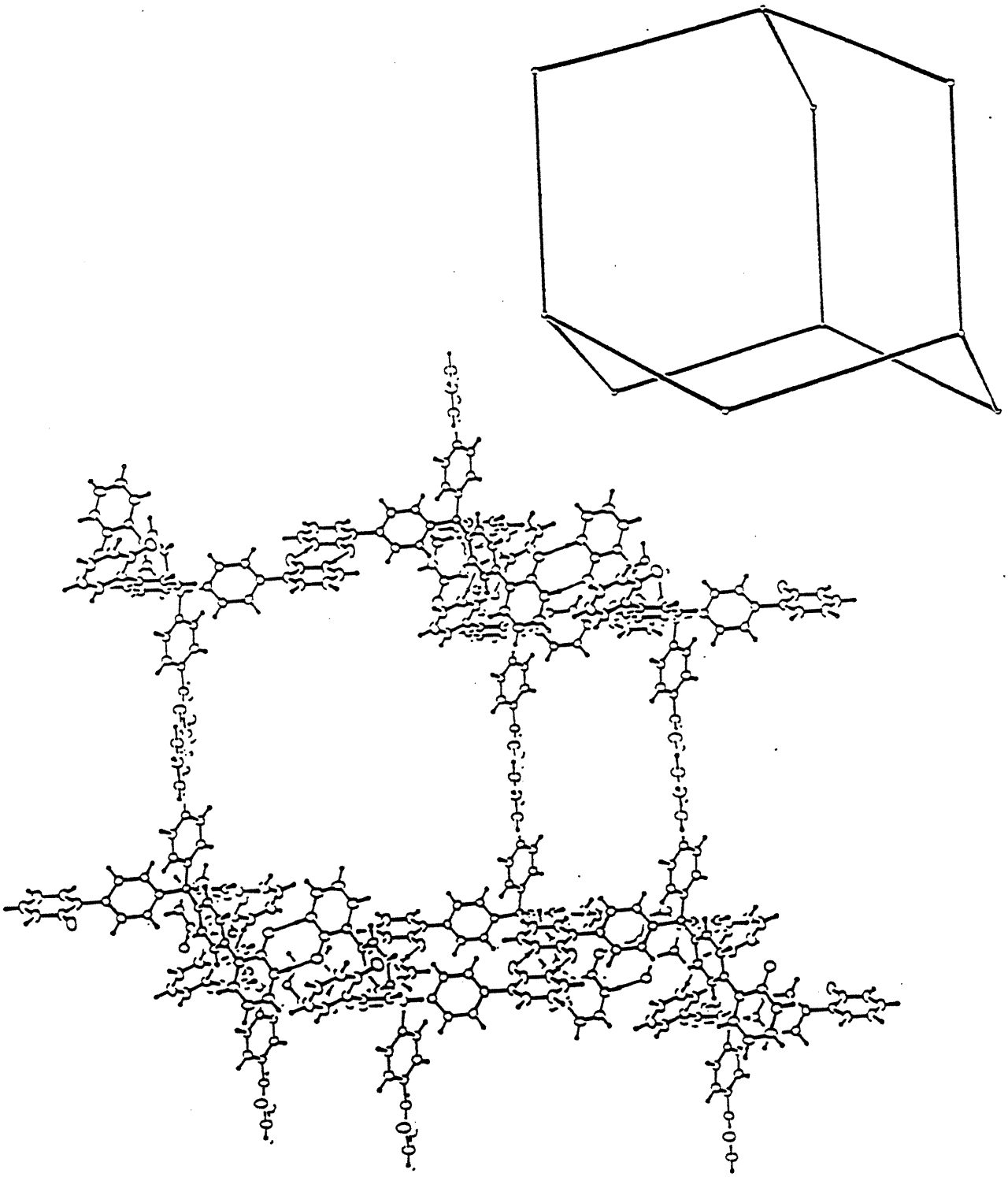

Figure 2

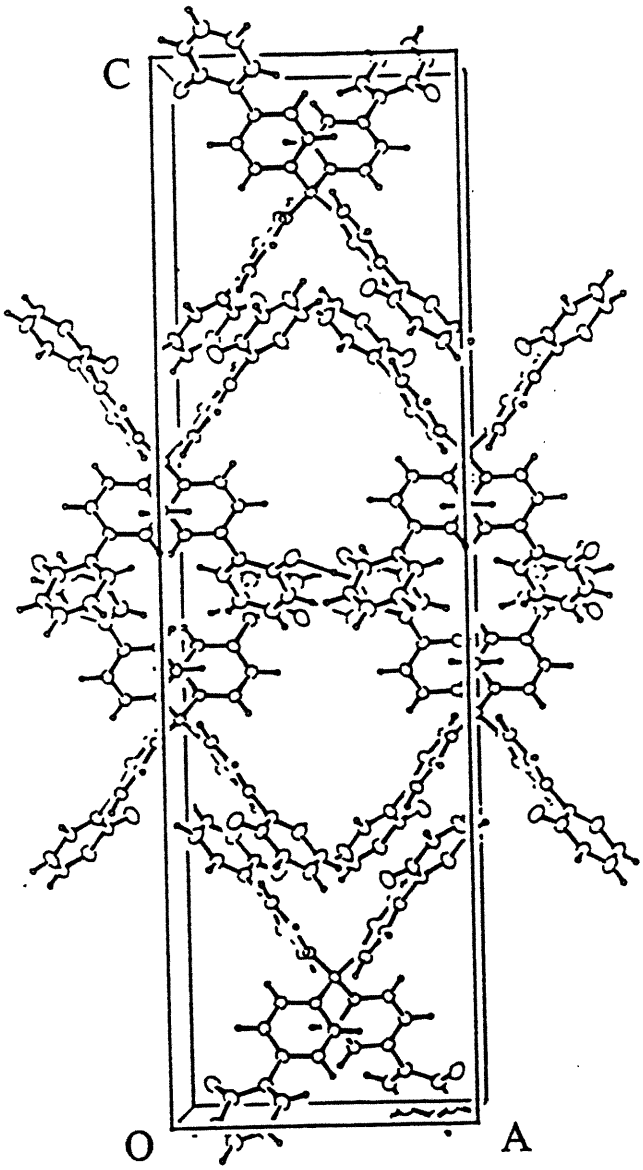

Figure 3

CAPTIONS

Figure 1 ORTEP view of TECTON **XVIII**·4 DMF with the numbering scheme adopted. Ellipsoids drawn at 40% probality level. Hydrogens represented by spheres of arbitrary size.

Figure 2 Adamantane type hydrogen bonding network propagation shown without the disordered DMF solvent. Hydrogen bonding represented using thin bonds.

Figure 3 ORTEP view of the cell down b axis.